Herstellung und Charakterisierung Artifizieller Assemblierungsmorphologien und Komposit-Materialien aus Rekombinanten Spinnenseidenproteinen

Dissertation

Zur Erlangung des Grades

Doktor rerum naturalium

(Dr. rer. nat.)

im Promotionsprogramm „Molekulare Biowissenschaften“ der
Bayreuther Graduiertenschule für Mathematik und Naturwissenschaften
(BayNAT)

vorgelegt von

Elena Doblhofer M.Sc.

Juni 2016

Die vorliegende Arbeit wurde von August 2011 bis Juni 2016 am Lehrstuhl Biomaterialien, Fakultät für Ingenieurwissenschaften, Universität Bayreuth, unter Betreuung von Herrn Prof. Dr. Thomas Scheibel angefertigt.

Vollständiger Abdruck der von der Bayreuther Graduiertenschule für Mathematik und Naturwissenschaften (BayNAT) der Universität Bayreuth genehmigten Dissertation zur Erlangung des Grades eines Doktors der Naturwissenschaften (Dr. rer. nat.)

Dissertation eingereicht am: 01.07.2016

Zulassung durch das Leitungsgremium: 12.07.2016

Wissenschaftliches Kolloquium: 17.01.2017

Amtierender Direktor der BayNAT: Prof. Dr. Stephan Kümmel

Prüfungsausschuss:

Prof. Dr. Thomas Scheibel (Erstgutachter)

Prof. Dr. Josef Breu (Zweitgutachter)

Prof. Dr. Hans-Werner Schmidt (Vorsitz)

Prof. Dr. Andreas Möglich

Two roads diverged in a wood, and I —

I took the one less traveled by,

And that has made all the difference.

Robert Frost (1874–1963).
Mountain Interval, 1920

INHALTSVERZEICHNIS

ZUSAMMENFASSUNG

In den letzten Jahrzehnten waren vor allem Kunststoffe aus synthetischen Polymeren für den enormen technischen und medizinischen Fortschritt der Menschheit verantwortlich. Dabei zeigte sich aber schon bald nach ihrer Kommerzialisierung auch die Kehrseite dieser vielseitigen und kostengünstigen Materialien. Das Auffinden von Plastikteilen in verendeten Seevögeln und Mikroplastik in marinen Habitaten, sowie den damit verbundenen Folgen bewegte Wissenschaftler dazu, Alternativen zu petrochemisch hergestellten und nicht bioabbaubaren Stoffen zu finden. In diesem Zusammenhang rückten bioabbaubare Materialien aus nachwachsenden Rohstoffen zwar bereits in den Fokus der Wissenschaft, konnten jedoch bisher nur wenige kommerzielle Anwendungen finden. Die Gründe dafür waren meist die teure Produktion und nur geringe Verfügbarkeit in ausreichender Qualität.

Eine Materialklasse, die als Ersatz für synthetische Polymere fungieren kann, sind Proteine. Sie sind bioabbaubar und stellen eine Vielzahl an funktionellen Gruppen zur Modifikation zur Verfügung. Rekombinante Spinnenseidenproteine bieten aufgrund biotechnologischer Herstellung eine einfache Möglichkeit zur Modifikation der Primärstruktur auf Basis einer Änderung der Gensequenz und gewährleisten zusätzlich hohe Reinheit. Spinnenseidenproteine sind außerdem nur wenig immunogen, nicht toxisch und Materialien daraus weisen eine gute mechanische Belastbarkeit auf. In den letzten Jahren wurde daher vor allem das anionische, rekombinante Spinnenseidenprotein eADF4(C16) aus der Konsensussequenz der repetitiven Kerndomäne des *Dragline*-Seidenproteins ADF4 (*Araneus diadematus* Fibroin) der europäischen Gartenkreuzspinne abgeleitet und etabliert. Dieses eignete sich aufgrund seiner negativen Nettoladung vor allem für Wechselwirkungen mit positiv geladenen Substanzen, sowie für Anwendungen in denen nur geringe Interaktion zwischen Zellen und Proteinoberfläche gewünscht ist (z.B. Beschichtungen für Implantate). Um eine Erweiterung der Anwendbarkeit von rekombinanten Spinnenseidenproteinen zu erreichen, lag der Fokus der vorliegenden Dissertation in der Entwicklung eines polykationischen, rekombinanten Spinnenseidenproteins, eADF4(κ16) genannt. Hierfür wurde die Aminosäure L-Glutaminsäure (bei pH 7 negativ geladen) in jedem C-Modul von eADF4(C16), gegen die Aminosäure L-Lysin (bei pH 7 positiv geladen) ausgetauscht. Nach erfolgreicher

Herstellung und Reinigung dieses Proteins wurde dessen Anwendung in Form zweier verschiedener Assemblierungsmorphologien getestet.

Im ersten Teil konnte gezeigt werden, dass aus eADF4(κ16) sphärische Partikel durch Präzipitation mittels kosmotroper Salze hergestellt werden konnten, die als Wirkstofftransportsysteme Anwendung finden. Analysen der Interaktion der eADF4(κ16) Partikel mit niedermolekularen Modellwirkstoffen ergaben daraufhin, dass zwar negativ geladene Modellwirkstoffe in den Spinnenseidenproteinpartikeln aufgenommen werden konnten, diese aber nur eine geringe elektrostatische Interaktion zwischen den Modellsubstanzen und der Proteinmatrix aufwiesen. So führte eine Inkubation der beladenen Partikel unter physiologischen Bedingungen zur Freisetzung der Modellsubstanz innerhalb von einigen Minuten. Ein anschließender Versuch durch Einkapseln der Modellsubstanz mittels *Layer-by-Layer*-Technik, bei der das entgegengesetzt geladene Spinnenseidenprotein eADF4(C16) für die Hülle verwendet wurde, führte entgegen der Erwartungen nicht zu einer Verzögerung der Substanzfreisetzung.

Im Gegensatz zu niedermolekularen Modellsubstanzen zeigten größere Moleküle mit negativer Ladung, wie zum Beispiel kurze DNA-Stränge, die als Modell für siRNA fungieren können, eine verlangsamte Diffusion unter physiologischen Bedingungen. So konnte eine retardierte Freisetzung beobachtet werden, wodurch sich Partikel aus eADF4(κ16) als potentielles Transportsystem zur systemischen Applikation von gentherapeutischen Medikationen unter Nutzung des EPR (engl. *enhanced permeability and retention* = erhöhte Permeabilität und Retention) -Effekts qualifizierten.

Da gentherapeutische Medikamente nach Erreichen des Zielgewebes vor allem intrazellulär wirken, wurde in einem zweiten Teil dieser Arbeit die Auswirkung der Beladung der eADF4(κ16) Partikel mit kurzen DNA-Strängen auf die Aufnahme in eukaryotischen Zellen analysiert. Während die Partikel ohne Cargo aufgrund guter elektrostatischer Wechselwirkungen zwischen Zellwand und Partikel in hohem Maß von HeLa-Zellen aufgenommen wurden, führte die Beladung der Partikel mit einzelsträngigen, fluoreszenz-markierten DNA-Molekülen zu einer stark verringerten Aufnahme. Die Annahme einer veränderten zellulären Aufnahme aufgrund einer Veränderung der elektroosmotischen Eigenschaften der Partikel durch Ablage der DNA-Moleküle auf der Partikeloberfläche konnte jedoch nicht experimentell bestätigt werden, wodurch die Ursache ungeklärt blieb. Eine erneute Beschichtung durch Inkubation der beladenen

Partikel in einer eADF4(κ16)-Lösung konnte den Effekt auf die Aufnahme der Partikel durch die Beladung revidieren.

Um aus rekombinanten Spinnenseidenproteinen hergestellte Partikel industriell für Arzneimittelformulierungen produzieren zu können, müssen Kontrollmethoden für eine gleichbleibende Qualität etabliert werden. Hierfür wurde in dieser Arbeit die Kombination aus elektroosmotischen und kolloidalen Eigenschaften der Partikel analysiert. Dabei konnte gezeigt werden, dass sich die betreffenden Materialparameter in den unterschiedlichen Herstellungschargen innerhalb der gleichen Partikelart stark unterscheiden. Abweichungen sind wahrscheinlich auf Unterschiede in den Dichteprofilen der Partikel zurückzuführen, die aus geringen Modifikationen der Produktionsparameter bei manueller Herstellung der Partikel mittels Salzfällung resultieren. Die Bestimmung der elektrophoretischen Mobilität von Partikeln aus rekombinanten Spinnenseidenproteinen bei niedrigen Salzkonzentrationen bietet daher eine direkte Möglichkeit die Oberfläche der Partikel effektiv zu analysieren und somit die Gleichheit verschiedener Partikelchargen zu garantieren.

In einem zweiten Teil der vorliegenden Dissertation wurde die Verwendung von Filmen des neu entwickelten rekombinanten Spinnenseidenproteins im technischen Anwendungsbereich analysiert. Dabei wurde beispielhaft ein Nanokomposit aus dem synthetischen Schichtsilikat Natrium-Hektorit und dem Spinnenseidenprotein eADF4(κ16) entwickelt, welches durch Aufbringen auf eine PET (Polyethylentherephthalat)-Folie deren Permeabilität um das 600-fache verringern konnte. Diese Werte übersteigen die Leistungsfähigkeit häufig verwendeter Verpackungsmaterialien in der Lebensmittelindustrie, wie z.B. PVDC (Polyvinylidenchlorid), um das 60-fache. Die Herstellung der genannten Beschichtung verlief dabei in einem einfachen, wasserbasierten Prozess ohne Additive und unter Verwendung von umweltfreundlichen, bioabbaubaren und nachhaltigen Materialien. Eine einzigartige Kombination von chemischer und mechanischer Stabilität mit hoher Sauerstoff- und Wasserdampfbarriere sowie einer wasserbasierten Herstellung machen die hier gezeigte Beschichtung geeignet für die Verwendung in Lebensmittelverpackungen.

SUMMARY

Over the last few decades, plastics made of synthetic polymers were in the focus of scientific research and their use resulted in enormous medical and technical advances of mankind. However, shortly after industrial production of plastics, negative influences of this material on nature became apparent: Plastic fragments were found in perished sea birds and micro plastic was spotted in remote marine habitats. These occurrences and the consequences thereof encouraged scientists to look for non-petrochemical and biodegradable materials which can still be used in a great variety of applications. One class of material that can be used as a substitute for synthetic polymers is the class of proteins. Protein materials are biodegradable and provide a large variety of functional groups for modification. In contrast to most other proteins, recombinantly produced spider silk proteins offer the possibility for modification of the primary structure as well as high purity, due to their biotechnological production. Recombinant spider silk proteins, furthermore, have low-immunogenicity, are non-toxic and morphologies made of these proteins exhibit high mechanical stability. Recently, the anionic recombinant spider silk protein eADF4(C16) was designed based on the repetitive core of the natural spider silk protein ADF4 (*Araneus diadematus* fibroin 4) which can be found in the dragline silk of the European garden spider. Due to its negative net charge eADF4(C16) is especially suitable for applications in which good interactions with positively charged substances, as well as no interactions between cells and protein surfaces are required. For an extended application range of recombinant spider silk proteins, this work focused on the development of a new and positively charged variant of eADF4 and its medical and technical applications. Therefore, every codon for L-glutamic acid (negatively charged at pH 7) of in the DNA template of eADF4(C16) was exchanged by a codon for L-lysine (positively charged at pH 7). The resulting protein was named eADF4(κ16) and exhibits 16 positive net charges. After successful production and purification, this protein was tested for its possible applications in two different assembly morphologies.

In a first part of this work, spherical particles made of eADF4(κ16) were produced and analyzed for their suitability as drug delivery vehicles. The resulting cationic particles were loaded with negatively charged small model substances by electrostatic interactions in a salt-free environment. However, the interactions of the particle matrix and the model

substances were weak, and a rapid release of the cargo (in the range of a few minutes) was observed under physiological conditions. A layer-by-layer approach to encapsulate the loaded particles with the oppositely charged eADF4(C16) did not lead to a retardation of the model substance release.

Unlike small model substances, larger molecules with a high negative net charge, like short DNA strands that can be used as model for siRNA, showed a slower release profile. In this case, continuous, retarded release could be detected. These findings qualified eADF4(κ16) particles as suitable carriers to be used in gene therapy utilizing the EPR (enhanced permeability and retention)-Effect.

Since drugs used in gene therapy operate in an intracellular environment after reaching the target tissue, the cellular uptake efficiency of eADF4(κ16) particles carrying DNA cargo were tested in a further study. Therein it was shown that eADF4(κ16) particles without cargo were taken up by HeLa cells with high efficiency, whereas DNA loaded particles were not. It is possible that the decreased uptake was due to changed electroosmotic properties, because of deposition of the DNA strands on the particle's surface, however, this could not be proofed. Therefore, the mechanism behind the obtained decreased uptake remained unclear. By coating the loaded eADF4(κ16) particles, the uptake rate was returned to a value similar to unloaded particles and the particles were again proven suitable to carry large negatively charged model substances into eukaryotic cells.

To use the described particles made of recombinant spider silk protein commercially in drug formulations, their consistent quality must be guaranteed. Therefore, analysis of electroosmotic and colloidal properties was established to examine the similarity of different particle batches. From this analysis, it could be shown that there is a large variability between the single batches. This could be due to divergence of production parameters, due to a manually performed production process. Nevertheless, this study showed that analysis of the electroosmotic and colloidal properties of the particles provide the opportunity to validate the similarity of different particle batches.

In a second part of this dissertation, the use of the newly developed cationic recombinant spider silk protein eADF4(κ16) in technical applications was tested. As an example, a nanocomposite made of the synthetic layered silicate sodium hectorite as filler and the biodegradable biopolymer eADF4(κ16) matrix was developed. This nanocomposite was produced in a fully aqueous process without any additives by a simple

drop casting method. Drop casting of this composite on a PET-foil resulted in a 600-fold reduction of the permeability of the foil. Surprisingly, this nanocomposite coating was, though produced in an all aqueous process, completely water insoluble, which is yet to be accomplished by any other biodegradable, water-based barrier nanocomposite developed in the past. Additionally, the resulting coated PET-foil permeability performance even surpassed other commercially used packaging materials in food industry a 60-fold (e.g. PVDC (Polyvinylidenchlorid)). This unique combination of chemical and mechanical stability with high oxygen and water vapor barrier properties, produced in a fully aqueous production process, makes the coating suitable to develop sustainable packaging materials.

1 Einleitung

1.1 Kunststoffe

Die Entwicklung von synthetischen Polymeren trug im letzten Jahrhundert stark zum technischen und medizinischen Fortschritt der modernen Welt bei. Sie dienen zur Verbesserung der Lebensqualität in sehr unterschiedlichen Bereichen, von Verpackungsmaterialien, die Nahrungsmittel länger frisch halten, bis hin zu Wirkstofftransportsystemen, die therapeutische Vorteile durch kontrollierte Wirkstofffreisetzung liefern (*1, 2*). Die ersten Kunststoffe wurden zwar bereits Mitte des 19. Jahrhunderts entdeckt, doch erst ihre industrielle Herstellung in den 40er Jahren des 20. Jahrhunderts führte zu einem exponentiellen Anstieg der Kunststoffproduktion und Verwertung (Abbildung 1) (*3, 4*).

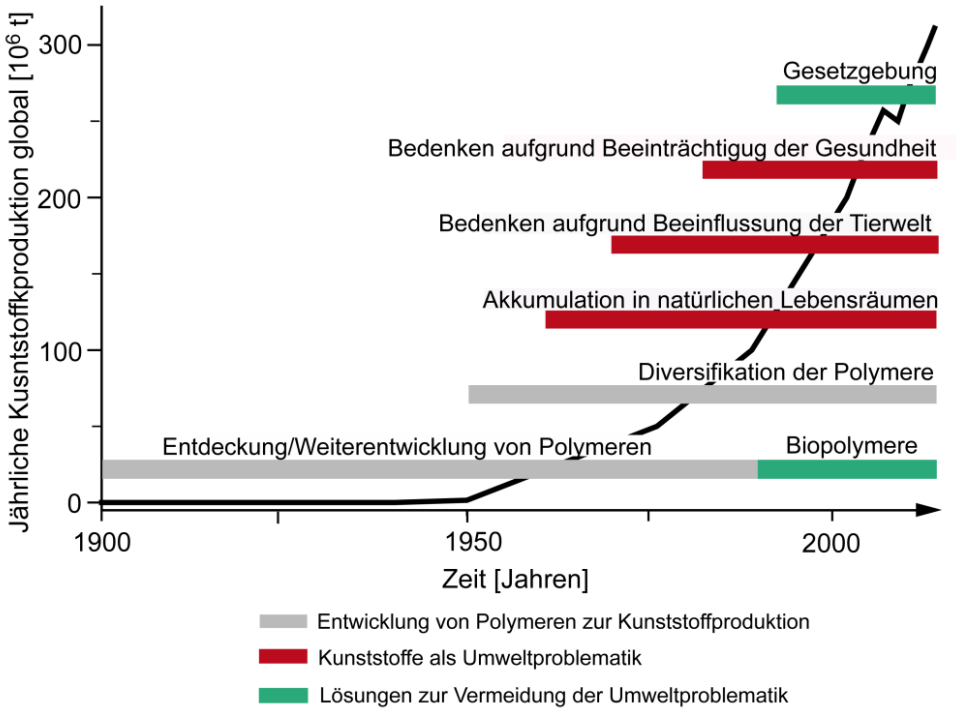

Abbildung 1: Zeitliche Einordnung der Kunststoffproduktion und ihre Folgen auf Mensch und Umwelt. Modifiziert nach (*4-6*).

Durch fortwährende Weiterentwicklung und Neuentdeckungen von Polymeren sind heute über 20 verschiedene Arten von synthetischen Polymeren im Einsatz, die kostengünstig zu leichten, stabilen und korrosionsresistenten Kunststoffen mit hoher elektrischer und thermischer Isolationseffizienz verarbeitet werden können (*7*). Kunststoffe sind daher vielseitige Materialien, die je nach Zusammensetzung und Verarbeitung

unterschiedliche mechanische, optische oder haptische Eigenschaften aufweisen können und in fast allen Bereichen unseres Lebens „von der Wiege bis zur Bahre“ Anwendung finden (*8*). So nützlich Kunststoffe für die Entwicklung der Menschheit waren und immer noch sind, so kurzfristig nach ihrer Kommerzialisierung konnten auch erste negative Aspekte festgestellt werden. Bereits 1960 wurden Kunststoffteile in den Eingeweiden von verendeten Seevögeln und Anfang der 1970er Jahre große Mengen an nicht biologisch abbaubaren Kunststofffragmenten in marinen Habitaten gefunden (*9, 10*). Kunststoffe bestehen außerdem nur selten aus reinem Polymer; bei der Herstellung werden in der Regel Additive und Weichmacher beigemischt, um ein geeignetes Materialverhalten für eine gezielte Anwendung zu erreichen. In diesem Zusammenhang wurden bereits 1972 erste Bedenken laut, dass die beigefügten Chemikalien aus den Kunststoffen ausbluten und der Gesundheit des Ökosystems, sowie dem menschlichen Körper schaden könnten (*1, 11*).

Im Jahr 2014 wurden weltweit insgesamt 311 Millionen Tonnen Kunststoff aus synthetischen Polymeren produziert, wobei in etwa die doppelte Menge an Rohöl verbraucht wird (*6, 12*). Alleine 40 % der jährlich produzierten synthetischen Polymere wurden für die Herstellung von Verpackungsmaterialien verwendet (*6*), die überwiegend Einwegwaren darstellen und somit nach Gebrauch in weniger als einem Jahr nach Produktion bereits entsorgt werden. Dabei bildet die Entsorgung von Kunststoffen einen großen umweltbelastenden Faktor. Etwa ein Drittel des kommunalen Feststoffabfalls besteht aus extrem haltbaren Verpackungskunststoffen, wobei Polyethylen (PE), Polypropylen (PP), Polyvinylchlorid (PVC), Polystyrol (PS) und Polyethylentherephthalat (PET) den größten Anteil ausmachen (*13, 14*). Diese klassischen synthetischen Polymere haben meist ein sehr hohes Molekulargewicht und sind nicht bioabbaubar. Für sie gibt es drei verschiedene Entsorgungswege: 29,7 % des Kunststoffmülls werden recycelt, 39,5 % zur Energiegewinnung verbrannt, und 30,8 % landen auf Mülldeponien (*6*). Jeder dieser Entsorgungswege birgt dabei jedoch seine Nachteile. So gibt es nur wenige Anwendungen für recycelte Kunststoffe, da durch die ursprüngliche Verarbeitung die verschiedenen Arten an Polymeren nur schlecht voneinander und von den darin enthaltenen Additiven getrennt werden können. Es kommt folglich bei einer Wiederverwertung zu Verunreinigungen und zu geringerer Leistungsfähigkeit des resultierenden Kunststoffs (*1*). Durch Verbrennung können neben großen Mengen CO_2 auch kanzerogene und toxische Gase, wie Dioxine, entstehen, die bei unsachgemäßer Filterung in die Umwelt gelangen

(*15*). Die Lagerung des Kunststoffmülls auf Deponien ist ebenfalls schwierig, da so sehr leicht Teile davon in die Umwelt gelangen und das Ökosystem belasten.

Heute sind synthetische Polymere auch in der medizinischen Anwendung die am meisten verwendete Materialklasse. Sie werden auf Grund ihrer überwiegend bioinerten Eigenschaften und ihrer Langlebigkeit für die Herstellung von chirurgischen Instrumenten, Kathetern, Stents, Herzschrittmachern oder Prothesen eingesetzt. Ein kleinerer Anteil an synthetischen Polymeren wird zudem als Träger von Wirkstoffen für Transport und kontrollierte Freisetzung im menschlichen Körper verwendet. Dabei spielen vor allem die bioabbaubaren Eigenschaften und die biologische Verträglichkeit des Materials eine große Rolle. Daher sind hier überwiegend bioabbaubare Polymere im Einsatz, um als mobile Wirkstofftransportsysteme zur systemischen Verteilung von Wirkstoffen über den Blutkreislauf zu fungieren. Die dafür eingesetzten Polymerpartikel haben bei intravenöser Verabreichung jedoch nur eine sehr geringe Zirkulationsdauer, da in den meisten Fällen eine schnelle Anlagerung von Opsoninen (Proteine des Immunsystems) oder Apolipoproteinen (Protein-Anteil der Lipoproteine im Blut) stattfindet, die dann zu einer schnellen Ausscheidung oder Akkumulation der Partikel in der Leber führen (*16*). Die am häufigsten für Wirkstofftransportsysteme verwendeten synthetischen Polymere kommen aus der Materialklasse der Polyester, Polyorthoester und Polyanhydride. Diese Polymere sind bioabbaubar und werden in wässrigem Milieu zu Carbonsäuren gespalten, was zu einem lokalen Ansäuern der Umgebung und daraus resultierenden Entzündungen im menschlichen Körper führen kann (*17*). Um einer schnellen Ausscheidung entgegenzuwirken kann durch Modifikation von Polymerpartikeln mit Poly(ethylenglycol) (PEG) eine „Tarnung“ der Partikel stattfinden, die Zirkulationszeit verlängert und der so genannte EPR-Effekt zur Therapie genutzt werden (genauer siehe Kapitel 1.3) (*16*). Durch die Verwendung des synthetischen Polymers PEG können jedoch weitere Komplikationen beobachtet werden: So ist es möglich, dass der Körper PEG-spezifische Antikörper bildet, was zu einer Sensibilisierung und bei erneuter Verabreichung zu einer schnellen Ausscheidung der PEG-modifizierten Wirkstofftransporter führt (*18, 19*). Eine weitere Problematik bei der Verwendung von PEG ist der bislang kaum aufgeklärte biologische Abbauweg dieses Polymers. Kleinere PEG-Moleküle (< 400 Da) können mit Hilfe der Alkoholdehydrogenase zu toxischen Disäure- und Hydroxycarbonsäure-Metaboliten oxidiert werden, wohingegen große PEG-Moleküle vor allem durch die Niere ausgeschieden werden müssen (*Molecular Weight Cutoff*: 30-50 kDa) (*20, 21*). Der

Verbleib noch größerer PEG-Moleküle und die daraus resultierenden Folgen sind bis heute nicht vollständig belegt.

Ein großer Teil der weltweit hergestellten Kunststoffe aus synthetischen Polymeren findet Anwendung in Verpackungen von Lebensmitteln, wobei ein großer Bedarf an Materialien mit guter Barrierewirkung gegen Sauerstoff und Wasserdampf vorherrscht. Etwa ein Drittel der industriell hergestellten Lebensmittel für den menschlichen Verzehr werden bereits auf dem Weg zum Verbraucher entsorgt. Dies entspricht 1,3 Milliarden Tonnen an Nahrungsmitteln jährlich. Beim Endverbraucher landen davon weitere 95 – 115 kg pro Jahr im Müll und sogar 13 % davon ohne überhaupt geöffnet zu werden, was in Deutschland einem Wert von etwa 300 € pro Kopf und Jahr bedeutet (*22, 23*). Die Ursache für diese enorme Verschwendung von Lebensmitteln und Ressourcen, die bei der Herstellung der Lebensmittel verwendet werden, liegt in der geringen Haltbarkeit einiger Produkte. Dabei könnte eine Verlängerung des Mindesthaltbarkeitsdatums der Lebensmittel zur Lösung dieses Problems beitragen. Die Haltbarkeit von Lebensmitteln wird im Grunde von der atmosphärischen Umgebung der Lebensmittel bestimmt. Sauerstoff und Wasserdampf führen darin zu Oxidation von Fettsäuren und Wassereinlagerungen, die das Produkt ungenießbar machen (*24, 25*).

Durch die Verwendung von Kunststoffen aus synthetischen Polymeren, wird den verpackten Lebensmitteln vor allem mechanischer, chemischer und mikrobieller Schutz gegenüber der Umgebung geboten und liefert zusätzlich für den Produzenten den Vorteil ausreichender Transparenz, um den Inhalt zu präsentieren. Die am häufigsten verwendeten Polymere sind dabei Polyethylen (PE, HD-PE: Milchflaschen und Tüten, LD-PE: Tabletts), Polypropylen (PP, Verpackungen geeignet zum Einfüllen heißer Flüssigkeiten), Polystyrol (PS, Styroporverpackungen), Polyvinylchlorid (PVC) und Polyethylentherephthalat (PET, Flaschen für Getränke mit Kohlensäure), die für verschiedenste Anwendungen geeignete Eigenschaften vorweisen (Abbildung 2: nicht abbaubare petrochemisch hergestellte Kunststoffe) (*26*). Dabei handelt es sich ausschließlich um langlebige Materialien, deren Einsatz für die kurzfristige Anwendung als Lebensmittelverpackung aufgrund der bereits beschriebenen Müllproblematik nur bedingt gerechtfertigt werden kann. Des Weiteren werden regelmäßig Studien veröffentlicht, die belegen, dass Additive und Nebenprodukte der Kunststoffherstellung aus den Verpackungsmaterialien in die Lebensmittel übergehen können (*27*). Der größte limitierende Faktor bei der Verwendung von synthetischen Polymeren zur Herstellung von

Lebensmittelverpackungen ist jedoch deren inhärente Durchlässigkeit (Permeabilität) für Gase und Dämpfe, wie zum Beispiel Sauerstoff, Kohlenstoffdioxid oder organische Moleküle (z.B. Aromastoffe) (*28*). Um die Permeabilität der Verpackungen zu verringern und geeignete Barriere-Eigenschaften zu erreichen, werden verschiedene Strategien angewendet. Am häufigsten sind dabei die Verwendung von Polymermischungen, Beschichtungen bestehender Verpackungsfolien mit Hochbarrierematerialien, wie zum Beispiel Aluminium, oder die Möglichkeit, Polymere mit Füllstoffen zu versehen und somit Komposite zu gestalten. Von besonderer Relevanz für industrielle Anwendungen sind dabei einfach durchzuführende Beschichtungsverfahren, d.h. das Veredeln eines preisgünstigen Substrats (*29*).

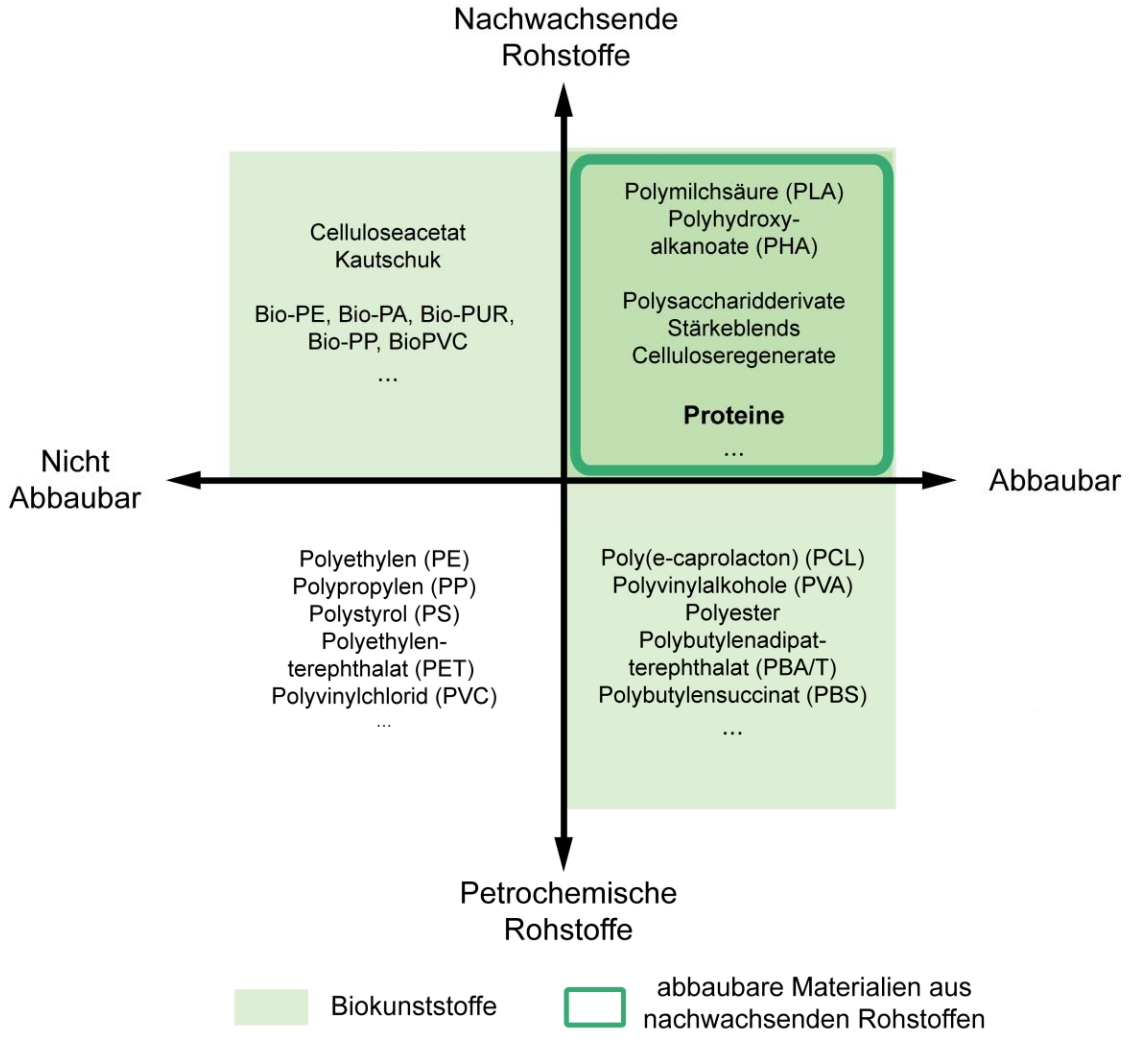

Abbildung 2: Einteilung von Kunststoffen anhand Ausgansmaterial und Abbaubarkeit (*29, 30*). Modifiziert nach (*30*) mit freundlicher Genehmigung aus H.-J. Endres, A. Siebert-Raths, Technische Biopolymere. *Rahmenbedingungen, Marktsituation, Herstellung, Aufbau und Eigenschaften. 1st ed. München: Hanser*, (2009).

Die Barrierebeschichtung mit Nanokompositen bietet hierfür alle Voraussetzungen. Dabei werden als nanopartikulärer Füllstoff häufig Schichtsilikate (siehe Abschnitt 1.4) verwendet, wobei das Einbringen dieser Partikel in eine Polymermatrix neben verbesserten Mechanik- und Hitzeschutz-Eigenschaften zu erhöhter Gasbarriere führen kann (*31*). Schichtsilikatplättchen selbst sind undurchlässig für jegliche Art von Gasen. Bei der Herstellung von Nanokomposit-Beschichtungen legen sich im optimalen Fall einzelne Plättchen wie eine Art Labyrinth in der Matrix ab und stellen so nur einen geschlängelten Pfad zur Diffusion von Gasmolekülen durch die Matrix zur Verfügung. Dabei wird die Zeit, die Gasmoleküle für die Diffusion benötigen, stark verlängert und somit länger vom Kontakt mit Lebensmitteln abgehalten (Abbildung 3) (*32*). Durch Laminieren von Verpackungsfolien mit diesen Nanokomposit-Beschichtungen entsteht die Möglichkeit, das Volumen der ursprünglichen Verpackungsmaterialien zu verringern und dabei eine gleichbleibende oder sogar erhöhte Barriere zu erreichen. Problematisch ist jedoch, dass als Matrix für die Herstellung solcher Nanokomposit-Beschichtung meist ebenfalls langlebige synthetische Polymere Verwendung finden, die nach Gebrauch nicht von den ursprünglichen Verpackungsfolien getrennt werden können und somit ein Recyceln der laminierten Verpackungsmaterialien unmöglich machen.

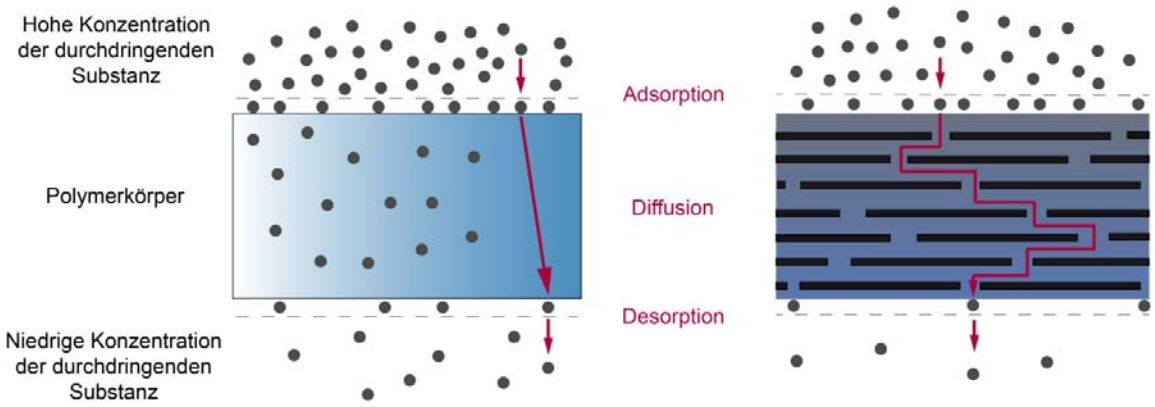

Abbildung 3: Änderung des Diffusionswegs einer polymerdurchdringenden Substanz durch Einbringen von Nanopartikeln.

Es gibt verschiedene Ansätze, für die beschriebene Problematik gut verträgliche und umweltfreundliche Lösungen zu finden. Dabei liegt ein großer Fokus der Forschung auch in der Verpackungsindustrie auf bioabbaubaren Materialien, wie Polymilchsäure (PLA = engl. *Poly lactic acid*), Polyfettsäuren (PHA = engl. *polyhydroxyalkanoate*), Stärke und Zellulose, die als Matrix für Nanokomposite dienen können. Jedoch ist die Nachfrage nach diesen Rohstoffen in der Kunststoffindustrie bisher aufgrund von hohen Preisen und

geringer Verfügbarkeit noch sehr verhalten. Zusätzlich stellen die hohe Wasserdampf- und Sauerstoffdurchlässigkeit eine große Herausforderung bei der Verarbeitung zu Verpackungen für Nahrungsmittel dar. Die Sensibilität von Stärke- und Cellulosefilmen gegenüber hohen Luftfeuchten bilden zudem einen großen Nachteil und limitieren die Haltbarkeit der Materialien (*33-35*).

1.2 Nachhaltige Lösungswege für den Ersatz synthetischer Polymere

In den 80er Jahren des 20. Jahrhunderts begann aufgrund der beschriebenen Problematik im technischen und medizinischen Anwendungsfeld die Suche nach Alternativen zu rohölbasierten Kunststoffen, die zusätzlich zur Überwindung der Rohstoffknappheit eine Lösung für das bestehende Müllproblem bieten (Abbildung 1). Das nachhaltige Ergebnis dieser Suche waren bioabbaubare Kunststoffe, hergestellt aus erneuerbaren Rohstoffquellen, wie sie aus Land- und Forstwirtschaft oder biogenen Abfallprodukten entstehen (abbaubare Materialien aus nachhaltigen Rohstoffen, Abbildung **2**) (*14*).

1.2.1 Proteinmaterialien

Eine Materialklasse, die seit den 1980er Jahren zur Herstellung von Biokunststoff immer mehr Beachtung findet, ist die Gruppe der Proteine (Abbildung 2) (*36*). Sie zeigen bei der Verarbeitung ähnliche Eigenschaften wie Polysaccharide, bieten allerdings eine erhöhte Diversität an funktionellen Gruppen und somit verschiedene Möglichkeiten zur Modifikation der Kunststoffoberfläche (*37*). Im Allgemeinen sind Proteine Heteropolymere, die aus 20 natürlichen Aminosäuren, mit unpolaren, ungeladenen polaren, positiv geladenen oder negativ geladenen (bei pH 7) Aminosäureresten, zusammengesetzt sind. Sie werden je nach Herkunft in pflanzliche (z.B. Soja- oder Weizenprotein, Tabelle 1) oder tierische Proteine (z.B. Gelatine, Casein oder Keratin, Tabelle 2) eingeteilt (*38*). Die meisten Proteine enthalten 100 bis 500 Aminosäuren (Primärstruktur), die durch intramolekulare Wechselwirkungen der Aminosäurereste elektrostatische, hydrophobe oder kovalente Wechselwirkungen/Bindungen eingehen können. Die so gebildeten Sekundärstrukturelemente können sich wiederum durch intramolekulare Wechselwirkungen zu einer Tertiärstruktur zusammenlagern, während intermolekulare Interaktionen von einzelnen Proteinmolekülen zur Quartärstruktur führen. Die makroskopischen Eigenschaften von proteinbasierten Materialien werden durch das Zusammenspiel dieser einzelnen hierarchischen Ebenen bestimmt (*39*). Bei der Verwendung von Proteinen als Biokunstoff spielt, wie bei klassischen Polymeren, die Verarbeitung des Materials eine große Rolle. So können einzelne Strukturelemente durch Beifügen von Chemikalien (Additiven), wie Glycerol oder Fettsäuren, oder durch Behandlung mit Hitze, mechanischer Beanspruchung oder Säuren und Basen variiert und somit Einfluss auf die makroskopischen Eigenschaften und die Haltbarkeit des resultierenden Kunststoffs genommen werden (Tabelle 1 und Tabelle 2). Durch die

mögliche Veränderung der Kunststoffeigenschaften ergibt sich auch für Proteinmaterialien eine große Vielfalt an Anwendungsmöglichkeiten (*38, 39*), wie zum Beispiel als Oberfläche zur Enzym-Immobilisierung, kontrollierbare Wirkstofftransporter, Absorptionsmaterialien für Flüssigkeiten oder Verpackungsmaterialien (Tabelle 1 und Tabelle 2) (*40, 41*). Der Abbau von Proteinen findet zwar im Gegensatz zu synthetischen Polymeren sehr schnell statt, führt jedoch zu Abbauprodukten, die der Körper wiederverwerten kann und sind somit besser verträglich (*42, 43*).

Die meisten zur Herstellung von Biokunststoffen untersuchten Proteine finden bisher nur wenig kommerzielle Anwendung, da eine petrochemische Herstellung von Kunststoffen bis heute kostengünstigere und stabilere Materialien liefert. Zusätzlich stellt vor allem die Gewinnung der Proteine ein großes Problem für die Leistungsfähigkeit der resultierenden Kunststoffe dar. Die meisten tierischen und pflanzlichen Proteine, die aus natürlichen Ressourcen gewonnen werden, bestehen aus einer Mischung von Proteinmolekülen verschiedener Länge und unterschiedlicher Löslichkeit. Eigenschaften, die sich mit jeder neuen Produktionscharge unterscheiden können. Eine Isolation eines definierten Moleküls aus dieser Mischung ist nur schwer möglich und sehr aufwändig, wodurch nur wenig Kontrolle über gleichbleibende Qualität des Rohstoffs und konstantes Materialverhalten bei der Verarbeitung verschiedener Rohstoff-Chargen ermöglicht wird (*44, 45*). Die meisten Proteinmaterialien sind zudem sehr spröde, weshalb bei ihrer Verarbeitung umweltschädliche Additive beigefügt werden müssen, um gewünschte Materialeigenschaften zu erreichen. Einige der pflanzlichen Proteine, wie z. B. Zein oder Gluten, können zusätzlich Allergien auslösen, während manche tierische Proteinmaterialien, die aus Schlachtabfällen stammen, die Gefahr beinhalten, virale Krankheiten zu übertragen, was auch die Anwendung in Wirkstofftransportsystemen negativ beeinflusst. Die am häufigsten verwendeten Proteine zur Biokunststoffherstellung, ihre potentiellen Anwendungen, beigefügte Additive und die Problematik bei der Verwendung der einzelnen Proteine sind in Tabelle 1 und Tabelle 2 zusammengefasst.

Tabelle 1: Übersicht pflanzlicher Proteine, die als grundlegendes Material zur Herstellung von Biokunststoffen geeignet sind.

Protein-material	**Potentielle Anwendung**	**Additive/Füllstoffe**	**Verarbeitungs-methoden**	**Vorteile**	**Nachteile**	**Quellen**
Soja-Protein	<u>Technisch:</u> - Klebstoff - Beschichtungen - Kompositmaterialien - Konstruktionswerkstoff - Ballistik - Feuerhemmendes Material - Verpackungen <u>Medizinisch:</u> - Wundverbände - Beschichtungen von Implantaten	<u>Weichmacher:</u> - Glycerol <u>Quervernetzer:</u> - Glutaraldehyd <u>Mischungen:</u> - Polyvinylalkohol - Phytagel® - Gellan - Fettsäuren - Polyphosphate - Zein <u>Kompositfüllstoffe:</u> - Natürliche Fasern (z.B. Jute, Flachs, Chinagras, etc.) - Halloysit Nanoröhrchen - Schichtsilikate - Nano- und Microcellulose	<u>Formteile:</u> - Formpressen <u>Partikel:</u> - Emulsions-fällung	<u>Technisch:</u> - Weltweit Verfügbar - Günstig - Komposite sind weniger entflammbar als Epoxide und Vinylester	<u>Technisch:</u> - Feuchtigkeits-empfindlich - Spröde - Stabil nur nach Quervernetzung <u>Medizinisch:</u> - Immunogen	(*46-61*)

Protein-material	**Potentielle Anwendung**	**Additive/Füllstoffe**	**Verarbeitungs-methoden**	**Vorteile**	**Nachteile**	**Quellen**
Weizen-Gluten	<u>Technisch:</u> - Klebstoff - Lösliche Verpackungen - Lebensmittel-verpackungen - Papierbeschichtungen - Beschichtungen <u>Medizinisch:</u> - Partikel für Wirkstofftransport - Gerüst für Gewebezüchtung	<u>Weichmacher:</u> - Glycerol - Polyole - Oligosaccharide - Milchsäure <u>Cysteinmodifikation:</u> - TCEP-HCl - N-Ethylenmaleimid <u>Quervernetzer:</u> - Polyvinylalkohol kombiniert mit 3-Mercaptopropionsäure - Polyacrylat <u>Mischungen:</u> - Polyphenole <u>Kompositfüllstoffe:</u> - Naturfasern - Chitin - Cellulose - Lignin - Nanoclays	<u>Formteile:</u> - Extrusion - Spritzguss - Thermoformen <u>Film/Beschichtung:</u> - Filmgießen - Rollpressen - Laminieren <u>Partikel:</u> - Emulsionsfällung <u>Fasern:</u> - Elektrostatisches Spinnen - Nassspinnen	<u>Technisch:</u> - Günstig - Flexibel - Widerstandsfähig - Heißsiegelfähig - Gute viscoelastische Eigenschaften - Transparent - Relativ undurchlässig für O_2 und CO_2 - Gut zugänglich - Natürliche Quervernetzung aufgrund hohem Cysteinanteil - Antibakteriell	<u>Technisch:</u> - Geringe Wasserbarriere-Eigenschaften - Spröde <u>Medizinisch:</u> - Allergien auslösend - Nicht Wasserlöslich	(*14, 41, 55, 62-72*)

Protein-material	Potentielle Anwendung	Additive/Füllstoffe	Verarbeitungs-methoden	Vorteile	Nachteile	Quellen
Zein	<u>Technisch:</u> - Celluloid-ähnliche Materialien - Ersatz für Schellack - Bodenlacke - Schutzbeschichtungen - Beschichtungen für „*quick-service*“-Verpackung - Textilfasern (Vicara) - Tinte - Holzkleber <u>Medizinisch:</u> - Beschichtungen von Tabletten - Kardiovaskulare Stents - Gerüst für Gewebe-züchtung (2D und 3D) - Hydrogele für Colon-spezifische Wirkstofffreisetzung - Mikro- und Nanopartikel für Wirkstofftransport - Wundauflagen	<u>Weichmacher:</u> - Glycerol (in Kombi-nation mit Polypropylen-glycol) - Polyethylenglycol <u>Quervernetzer:</u> - Formaldehyd - Dialdehydstärke <u>Mischungen:</u> - Wachse - Kolofonium - Sojaprotein <u>Komposit:</u> - Pektin - Hydroxyapatit	<u>Formteile:</u> - Formpressen <u>Faserherstellung:</u> - Trockenspinnen - Nassspinnen - Elektrostatisches Spinnen <u>Film/Beschichtung:</u> - Rollenpresse - Gießen - Ausrollen <u>Partikel:</u> - Emulsionsfällung - Phasenseparation	<u>Technisch:</u> - Fett- und Lösungsmittel-beständig - Mikrobielle Resistenz - Relativ undurchlässig für O_2 und CO_2 - Langsam aushärtend <u>Medizinisch:</u> - Hämokompatibel	<u>Technisch:</u> - Verarbeitung in organischen Lösungsmitteln - Hygroskopisch - Feuchtigkeits-empfindlich - Schnelle Fäulnis - Leichter Insektenbefall - Forminstabil bei hoher Luftfeuchte <u>Medizinisch:</u> - Allergien auslösend	(*44, 61, 68, 72-83*)

TECEP-HCl = tris(2-Carboxyethyl)phosphinhydrochlorid

Tabelle 2: Übersicht tierischer Proteine, die als grundlegendes Material zur Herstellung von Biokunststoffen geeignet sind.

Protein-material	Potentielle Anwendung	Additive/Füllstoffe	Verarbeitungs-methoden	Vorteile	Nachteile	Quellen
Kollagen/ Gelatine	Technisch: - Halogensilber-Emulsionen für Fotografie Medizinisch: - Partikel für Wirkstofftransport - Kapseln für Wirkstofftransport - Verdichtung von Gefäßprothesen - (Hämostatische) Wundauflagen - Gerüst für Gewebe-züchtung (3D)	Weichmacher: - Glycerol - Sorbit Quervernetzer: - Glutaraldehyd - Poly-L-Glutaminsäure - Diisocyanat - Carbodiimid - Carbonsäureazide - Polyepoxide - Genipin Mischungen: - Polycaprolacton Kompositfüllstoffe: - Chitosan - Hydroxyapatit - Gypsum (Calciumsulfat-Dihydrat) - Tricalciumphosphat - Stärke - Seidenfasern - Cellulose - Carbon-Nanoröhrchen	Formteile: - Formpressen Faserherstellung: - Trockenspinnen - Nassspinnen - Elektrostatisches Spinnen Film/Beschichtung: - Rollenpresse - Gießen - Ausrollen Partikel: - Emulsionsfällung - Phasenseparation Hydrogele: - Gelieren in wässrigen Lösungen	Technisch: - Gute optische Eigenschaften Medizinisch: - Nicht immunogen - In vivo resorbierbar	Technisch: - Wasserlöslich - Geringe mechanische Stabilität Medizinisch: - Risiko viraler tierischer Kontamination - Allergien auslösend - Kollagen toxisch bei intravenöser Applikation	(*30, 60, 84-98*)

Protein-material	Potentielle Anwendung	Additive/Füllstoffe	Verarbeitungs-methoden	Vorteile	Nachteile	Quellen
Keratin	Technisch: - Verpackungen - Essbare Filme - Papierbeschichtungen - Wasserfilter - Textilfasern Medizinisch: - Gerüst für Gewebe-züchtung (2D und 3D) - Beschichtungen - Nervregeneration - Wundauflagen - Wirkstoffträger-membranen	Weichmacher: - Glycerol Quervernetzer: - Formaldehyd - Methylacrylat - Methylmetacrylat - Natriumsulfit - Diethyltartrat - Polypropylenglycol - Ethylenglycol - SDS Cystein-Modifikation: - Iodacetamid - Iodessigsäure - Bromsuccinylsäure Kompositfüllstoffe. - Polyethylen (Matrix) - Chitosan - Silk fibroin Fasern - Polyethylenoxid - Polyamid 6 - Polyvenylalkohol - Hydroxyapatit	Formteile: - Formpressen - Filmgießen Faserherstellung: - Nassspinnen Film/Beschichtung: - Gießen Schäume: - Salt leaching - Gefriertrocknen	Technisch: - Mechanisch stabil (hohe Festigkeit und Steifigkeit) - Thermisch stabil - Natürliche Quervernetzung aufgrund des hohen Cysteinanteils - Langsam bioabbaubar Medizinisch - Antibakteriell - Antithrombogen	Technisch: - Schwierige Verarbeitung aufgrund eines hohen Cysteinanteils - Modifikation der Cysteine führt zu geringerer mechanischer Belastbarkeit	(*99-117*)

Protein-material	Potentielle Anwendung	Additive/Füllstoffe	Verarbeitungs-methoden	Vorteile	Nachteile	Quellen
Ovalbumin	Technisch: - Essbare Verpackungen Medizinisch: - Partikel für Wirkstofftransport	Weichmacher: - Glycerol - PEG - Sorbit Quervernetzer: - Glutaraldehyd	Film/Beschichtung: Abschöpfen Partikel: Präzipitation	Technisch: - Klar - Transparent - Antibakteriell	Technisch: - Feuchtigkeits-empfindlich - Spröde	(*85, 118, 119*)
Casein	Technisch: - Wasserbasierte Klebstoffe - Bindemittel für Anstrichfarben - Weichmacher für Beton - (Essbare) Verpackungen - Isolationsmatten - Kleinteile (Knöpfe, Griffe, Schnallen, Schmuck) - (geräuscharme) Stricknadeln Medizinisch: - Partikel für Wirkstoff-transport	Quervernetzung: - Formaldehyd	Formteile: - Formpressen Film/Beschichtung: - Abschöpfen	Technisch: - Schwer entflammbar - Hochglänzende Oberfläche	Technisch: - Wasserempfindlich - Forminstabil bei hoher Luftfeuchte	(*30, 84, 85, 120*)

1.2.2 Materialien aus Spinnenseidenproteinen

Neben den in Tabelle 1 und Tabelle 2 aufgelisteten Proteinen aus nachwachsenden Rohstoffen stellen Spinnenseidenproteine eine weitere Proteinklasse dar, die zur Herstellung von Biokunststoffen geeignet ist. Bereits seit Tausenden von Jahren fasziniert Spinnenseide die Menschheit durch ihre einzigartige Kombination aus Festigkeit und Elastizität (*121*). Die daraus resultierende außergewöhnliche Zähigkeit der Spinnenseidenfasern übertrifft die der meisten synthetischen Fasern, wie beispielsweise Kevlar (*122, 123*). Neben außerordentlichen mechanischen Eigenschaften zeigt Spinnenseide zudem eine gute Biokompatibilität und geringe Immunogenität (*124-126*).

Die Kombination aus mechanischer Stabilität, Bioabbaubarkeit und der Möglichkeit, die Proteine unter milden Bedingungen in wässrigen Prozessen und unter Verzicht auf toxische oder organische Lösungsmittel verarbeiten zu können, machen Produkte aus Spinnenseide interessant für eine Vielfalt von Anwendungen, beginnend bei der Entwicklung von Biomaterialien bis hin zu industriell gefertigten Hochleistungsfasern (*127, 128*). Inzwischen ist eine gute Verfügbarkeit dieses Materials durch biotechnologische Herstellung möglich, wodurch zusätzlich eine hohe Reinheit der Proteine und die Möglichkeit zur kontrollierten Modifikation und Verarbeitung geschaffen wurden. Aufgrund ihrer biologisch gut verträglichen Eigenschaften finden rekombinante Spinnenseidenproteine aktuell kommerzielle Anwendung in der Kosmetikindustrie, als funktionelle Inhaltsstoffe in Form von Mikropartikeln und Hydrogelen (*129*).

Um das Anwendungsspektrum von biotechnologisch gewonnenen Spinnenseidenproteinen weiter ausbauen zu können, beschäftigt sich diese Arbeit mit der Verarbeitung einer neuen, kationischen Variante von rekombinanten Spinnenseidenproteinen, die von der *Dragline*-Seide der Europäischen Gartenkreuzspinne *Araneus diadematus* abgeleitet ist und zu Materialien, die Verwendung als Träger von Wirkstoffen zur systemischen Anwendung im menschlichen Körper und als Beschichtungen in Verpackungsmaterialien finden können. In den folgenden Kapiteln soll daher genauer auf die Kriterien zur Herstellung von Trägern von Wirkstoffen und die Herstellung von Nanokompositmaterialien, die als Barriere-Beschichtungen fungieren können, sowie die Herkunft, die Herstellung und die Verarbeitungsmethoden rekombinanter Spinnenseidenproteine eingegangen werden.

1.3 Wirkstofftransport und Wirkstofffreisetzung

Kontrollierter Wirkstofftransport und gezielte Wirkstofffreisetzung sind wichtige Faktoren bei der medikamentösen Behandlung von Erkrankungen. Bei konventioneller Applikation werden Medikamente meist oral oder intravenös verabreicht, wobei Wirkstoffe durch Darm oder Blut aufgenommen und systemisch im Körper verteilt werden. Dadurch ergeben sich am Wirkort vergleichsweise geringe Konzentrationen, obwohl dort für eine wirksame Behandlung relativ hohe Wirkstoffkonzentrationen benötigt werden (therapeutisches Fenster, vgl. Abbildung 4) um die gewünschte Wirkung zu erzielen. Hierfür wird meist eine Verabreichung von hohen Dosen benötigt, um eine systemische Konzentration zu erreichen, die im therapeutischen Fenster liegt. Dies kann mit erhöhter Wahrscheinlichkeit zu unerwünschten (toxischen) Nebenwirkungen führen (Abbildung 4). Bei konventioneller Verabreichung von Medikamenten werden Wirkstoffe meist schnell metabolisiert und/oder ausgeschieden, wodurch eine Verabreichung in kurzen zeitlichen Abständen erforderlich wird, um die Wirkstoffkonzentration im therapeutischen Fenster aufrecht zu halten und so eine ausreichende Wirkung zu erzielen (Abbildung 4). Neben einer erhöhten Wahrscheinlichkeit von Nebenwirkungen kommt es dann auch zu weiteren Einschränkungen des Patienten im Alltag (*130*). Um diese Problematik zu umgehen, wurden in den 1970er Jahren die ersten kontrollierten Wirkstofftransportsysteme zur retardierten Wirkstofffreisetzung auf den Markt gebracht (*131*), und nicht einmal 20 Jahre später (1997) brachte der Vertrieb von modernen Wirkstofftransportsystemen allein in den USA über 14 Milliarden Dollar ein (*130, 132*). Diese schnelle Entwicklung ist vor allem auf die vielen Vorteile zurückzuführen, die Wirkstofftransportsysteme mit kontrollierter Wirkstofffreisetzung im Vergleich zu konventioneller Verabreichung aufweisen. So ergibt sich eine erhöhte Wirksamkeit und therapeutische Aktivität des Medikaments, da durch das schützende Trägermaterial keine sofortige Metabolisierung stattfinden kann. Außerdem kann durch die kontinuierliche Freisetzung die initiale Verabreichungsdosis reduziert werden, was zu verminderter Toxizität und somit zu einer geringeren Wahrscheinlichkeit des Eintretens von Nebenwirkungen führt. Des Weiteren wird durch eine kontinuierliche Wirkstofffreisetzung im therapeutischen Fenster die Patientenkonformität verbessert, da die Verabreichungsintervalle in geringeren zeitlichen Abständen stattfinden können. Dabei ist das Ziel von modernen Wirkstofftransportsystemen die zielgerichtete Steuerung eines

Wirkstoffs hin zum Wirkort und somit die generelle Verbesserung von medikamentösen Therapien (*133*). Wirkstofftransportsysteme werden dabei in zwei Arten eingeteilt:

a) Temporal kontrollierte Freisetzung

Bei einer temporal kontrollierten Freisetzung werden Wirkstoffe über einen ausgedehnten, definierten Zeitraum während der Behandlung freigesetzt. Dabei wird der verabreichte Wirkstoff immer noch systemisch im Körper verteilt, aber kontinuierlich freigesetzt, so dass die systemische Konzentration über einen gewünschten Zeitraum konstant und im therapeutischen Fenster liegt (Abbildung 4). Die Freisetzungsrate entspricht hier der Eliminierungsrate des Medikaments und ist somit die optimale Freisetzungsart für Wirkstoffe, die schnell metabolisert und ausgeschieden werden. Eine signifikante Verbesserung von Medikamententherapien wird vor allem für die Verabreichung von Schmerzmitteln für Tumorpatienten im Endstadium erreicht *(130)*.

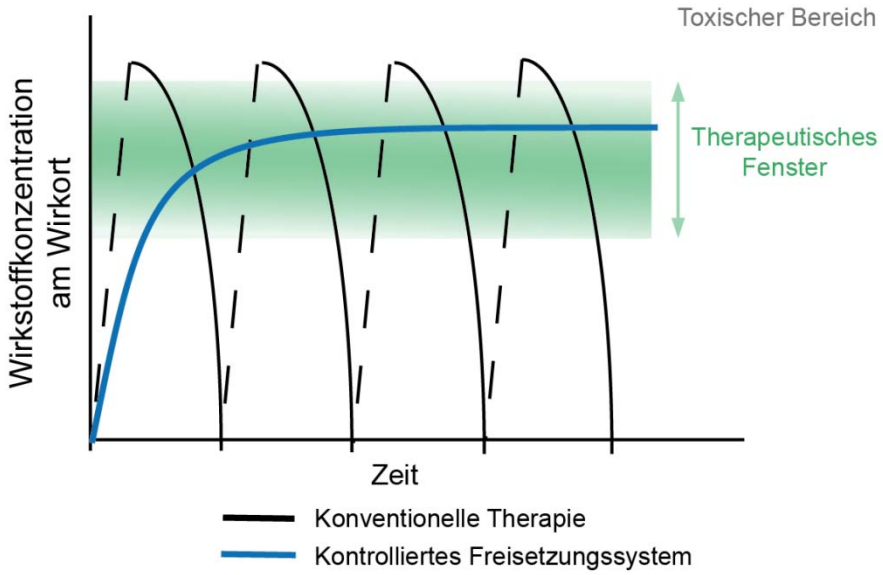

Abbildung 4: Temporal kontrollierte Wirkstofffreisetzung durch Verabreichung kontrollierter Wirkstofffreisetzungssysteme; Eine einmalige Medikamentenverabreichung kann die systemische Wirkstoffkonzentration im Körper über längeren Zeitraum im therapeutischen Fenster halten, während konventionelle Verabreichung nur kurze Zeit die benötigte Wirkstoffkonzentration liefert. Modifiziert nach (*130*) mit freundlicher Genehmigung der American Chemical Society aus K. E. Uhrich, S. M. Cannizzaro, R. S. Langer, K. M. Shakesheff, Polymeric systems for controlled drug release. *Chemical Reviews* **99**, 3181 (1999). Copyright (1999) American Chemical Society.

b) Verteilungskontrollierte Freisetzung

Bei der verteilungskontrollierten Freisetzung zielen Wirkstofftransportsysteme auf die Freisetzung von Substanzen an einem bestimmten Wirkort ab. Dies ist vor allem von Bedeutung, sobald konventionelle Applikationen dazu führen, dass Wirkstoffe auf gesundes Gewebe treffen und dort starke Nebenwirkungen verursachen und im

schlimmsten Fall einen Abbruch der Therapie erfordern (z.B. Abbruch der Chemotherapie bei Angriff der Zytotoxika auf die Knochenmarkzellen) (*130*). Eine weitere Indikation für verteilungskontrollierte Wirkstofffreisetzung liegt dann vor, wenn bei konventioneller Verabreichung durch die natürliche Verteilung des Wirkstoffs der Wirkort nicht erreicht werden kann (z.B. Moleküle, die an einem Rezeptor im Gehirn wirken, selbst aber die Blut-Hirn-Schranke nicht überschreiten können) (*134*). Dabei werden in der verteilungskontrollierten Freisetzung Wirkstofftransportsysteme gezielt an den Wirkort geleitet oder können nur dort die geladenen Substanzen freisetzen. Im restlichen Körper bleibt die Wirkstoffkonzentration dabei im optimalen Fall so gering, dass die systemische Wirkstoffkonzentration unterhalb der Konzentration bleibt, die Nebenwirkungen hervorruft (Abbildung 5) (*130*).

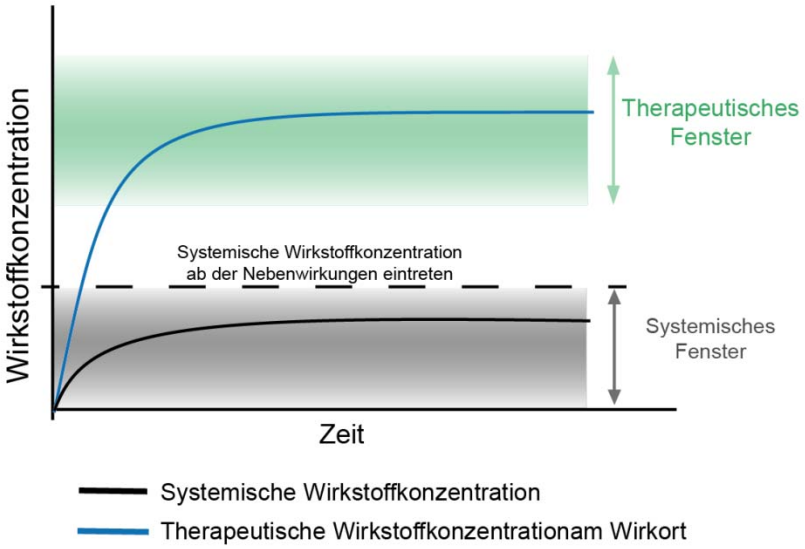

Abbildung 5: Verteilungskontrollierte Wirkstofffreisetzung; Durch eine Verabreichung des kontrollierten Wirktstofffreisetzungssystems wird der Wirkstoff nur am gewünschten Wirkort abgegeben während die systemische Konzentration gering bleibt. Modifiziert nach (*130*) mit freundlicher Genehmigung der American Chemical Society aus K. E. Uhrich, S. M. Cannizzaro, R. S. Langer, K. M. Shakesheff, Polymeric systems for controlled drug release. *Chemical Reviews* **99**, 3181 (1999). Copyright (1999) American Chemical Society.

Die einfachste Methode, um eine Freisetzung von Wirkstoffen direkt am Wirkort zu erreichen ist das Implantieren von stationären Wirkstoffcontainern (*135*). Dies ist jedoch nur dann von Vorteil, wenn der Wirkort leicht und ohne Risiko für den Patienten erreichbar ist und der Wirkstoff diesen nicht verlassen kann. Für die meisten Krankheiten muss jedoch ein System angewendet werden, bei dem der verwendete Wirkstofftransporter zu einem bestimmten Wirkort gelangen kann (*130*).

Sowohl in der temporal kontrollierten, als auch der verteilungskontrollierten Freisetzung werden häufig kolloidale Wirkstofftransportsysteme (Mikro- oder Nanopartikel) verwendet (*18*). Bei systemischer Verabreichung müssen Wirkstoffe durch das wässrige Milieu im Körper des Patienten diffundieren, um an den Wirkort zu gelangen und dort ihre Wirkung zu entfalten. Wirkstofftransporter können dabei Wirkstoffmoleküle schützen und zu einem längeren Verbleib im Körper führen (*136*). Hierfür können verschiedene Arten von Wirkstofftransportsystemen verwendet werden (Abbildung 6).

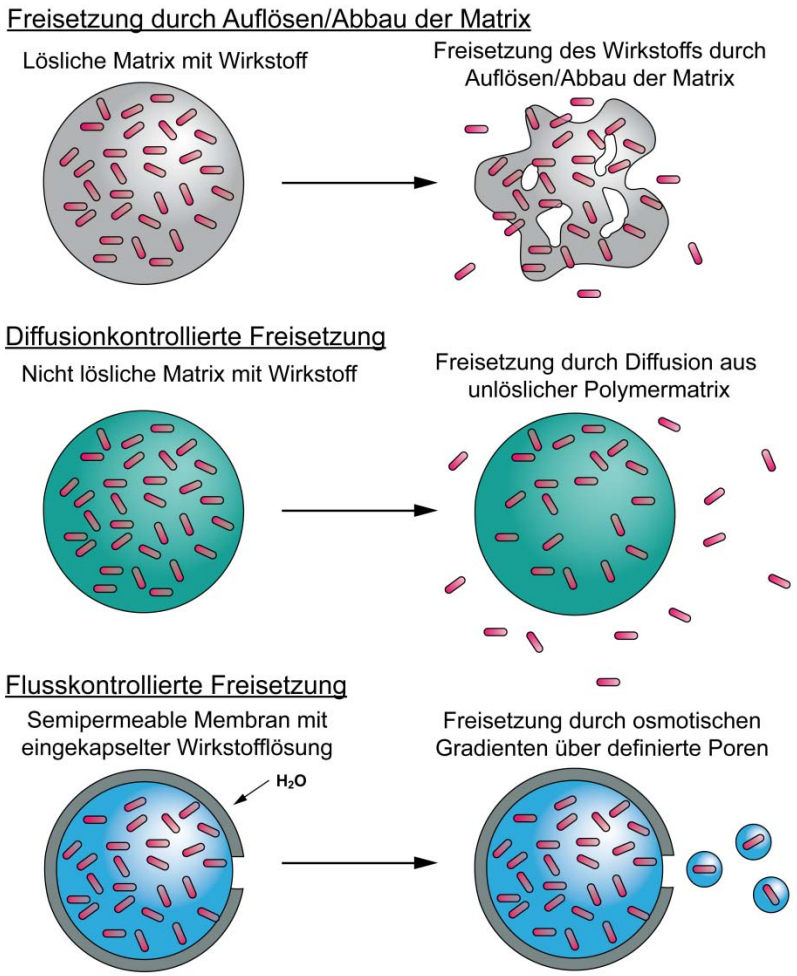

Abbildung 6: Arten von temporal kontrollierter Wirkstofffreisetzung bestimmt durch die verwendete Matrix. Modifiziert nach (*130*) mit freundlicher Genehmigung der American Chemical Society aus K. E. Uhrich, S. M. Cannizzaro, R. S. Langer, K. M. Shakesheff, Polymeric systems for controlled drug release. *Chemical Reviews* **99**, 3181 (1999). Copyright (1999) American Chemical Society

So kann zum einen eine Freisetzung des Wirkstoffs erst durch das Auflösen des Trägermaterials möglich sein. Die Freisetzung ist dann zeitlich durch den Degradationsprozess der Trägermatrix limitiert. Eine weitere Möglichkeit bietet die diffusionskontrollierte Freisetzung des Wirkstoffs, wobei sich das Trägermaterial nicht auflöst, sondern die Freisetzungsrate durch die Interaktion zwischen Wirkstoff und Matrix

bestimmt wird. Bei der flusskontrollierten Freisetzung wird ein Gradient von osmotischen Potentialen an einer semipermeablen Membran genutzt, um Wirkstofflösungen freizusetzen. Dabei wird durch die Diffusion von H_2O in eine Kapsel (den Wirkstoffträger) der Druck auf die Kapsel erhöht, wodurch die Lösung nach außen fließen kann. Durch die Größe der Poren wird dann die Flussrate und somit die Freisetzungsrate der Wirkstoffe bestimmt (Abbildung 6).

Für eine verteilungskontrollierte Wirkstofffreisetzung spielen noch zusätzliche Faktoren eine Rolle. So können Wirkstofftransporter sowohl durch passive, als auch durch aktive Signale am Wirkort akkumulieren (*drug targeting*). Beim passiven *drug targeting* werden die physiologischen Bedingungen des Körpers genutzt, um bestimmte Wirkorte zu erreichen. So zeigen zum Beispiel erkrankte Gewebe physiologische Veränderungen, die für eine Aufnahme von Wirkstofftransportern genutzt werden können. Eine dieser Veränderungen bildet eine unvollständig ausgebildete und löchrige Vaskularisation in entzündetem und tumorösem Gewebe, die es ermöglicht, partikuläre Transportsysteme durch die Wand der Blutgefäße in das erkrankte Gewebe zu schleusen. Dieses Phänomen der passiven Anreicherung von Makromolekülen, Liposomen oder Nanopartikeln wird als EPR-Effekt (engl. *enhanced permeability and retention* = „erhöhte Permeabilität und Retention“) bezeichnet. Um diesen Effekt für eine erfolgreiche Therapie zu nutzen, müssen Wirkstofftransportsysteme verschiedene Anforderungen erfüllen. So können nur Partikel mit einem maximalen Durchmesser von ca. 400 nm aus Blutgefäßen in tumoröses Gewebe geschleust werden (*137*), wobei der optimale Durchmesser für Wirkstofftransportsysteme von der jeweiligen Erkrankung und dem damit verbundenen Gewebe abhängt. Neben der Größe spielt auch die Oberflächenladung und Form der Transportsysteme eine große Rolle und bestimmt die Halbwertszeit, Zirkulationszeit und den Zeitraum, in dem die Partikel im Gewebe zurück gehalten werden. Die Oberflächenladung von Partikeln, die zum Wirkstofftransport verwendet werden, hat einen sehr starken Einfluss auf dessen Aufnahme in Zellen. Kationische Partikel haben dabei eine relativ geringe Halbwertszeit aufgrund von verstärkter Interaktion mit Proteinen im Blutstrom. Es wurde jedoch in vergangenen Studien gezeigt, dass generell Partikel mit Oberflächenpotentialen kleiner als 15 mV nur in geringen Maßen von Macrophagen aufgenommen werden und somit ausreichend lange Zirkulationszeiten im Körper aufweisen. Weitere Faktoren, wie Geometrie und Hydrophilie spielen eine weitere wichtige Rolle bei der Verteilung von Wirkstofftransportsystemen im Körper des Patienten (*18, 138, 139*).

Beim aktiven *drug targeting* bietet sich durch Modifikation und Funktionalisierung der Trägermatrix eines Wirkstofftransporters mit Peptiden, Antikörpern, Zuckern oder Lektinen die Möglichkeit, Rezeptoren von Zellen in einem bestimmten Gewebe direkt anzusteuern. Dabei sind vor allem Rezeptoren von großer Bedeutung, die in erkranktem Gewebe vermehrt produziert werden (*18*).

Zusätzlich zum EPR-Effekt können beim passiven *drug targeting* auch diverse interne Stimuli genutzt werden, wie zum Beispiel Unterschiede im pH und Redoxpotential (niedriger pH und hohe Glutathion-Konzentrationen in tumorösem Gewebe), um Wirkstoffe ausschließlich am Wirkort freizusetzen (*137, 140-142*).

Sobald ein Wirkstoff den Wirkort erreicht hat, kann dieser entweder intra- oder extrazellulär agieren. Bei intrazellulärer Wirksamkeit reicht es daher nicht, dass der Wirkstofftransporter ein spezifisches Gewebe erreicht. Für eine gezielte Freisetzung ins Cytosol können Modifikationen der Trägermatrix mit so genannten CPPs (engl. *Cell Penetrating Peptides* = zellmembrandurchdringende Peptide) genutzt werden (*143*). CPPs umfassen eine Klasse von meist kationischen Peptiden, die aus 5-30 Aminosäuren zusammengesetzt sind (*144-146*). Verschiedene Studien zeigten, dass für eine effektive Penetration der Zellen mindestens acht positive Ladungen benötigt werden (*147, 148*). Wobei für manche kationische CPPs, wie z.B. das R_8-Peptid, sogar Kernlokalisierungs-Eigenschaften beschrieben wurden (*148, 149*).

Generell werden positiv geladene Transportsysteme schneller in den Zellen aufgenommen als negativ geladene. Dies ist vor allem auf elektrostatische Wechselwirkungen mit den negativ geladenen Phospholipid-Kopfgruppen der Zellmembran zurückzuführen (*138, 150, 151*). Dennoch zeigen Partikel mit negativer Oberflächenladung eine erhöhte Aufnahmeeffizienz verglichen zu neutralen Partikeln (*18*). Neben CPPs oder positiv geladenen Gruppen kann auch die Peptidsequenz Arginin-Glycin-Asparaginsäure (RGD), ein Ligand des Zelladhäsionsproteins Integrin $\alpha v\beta 3$, zu erhöhter Effizienz von intrazellulärem Wirkstofftransport beitragen (*152, 153*).

Für die Anwendungen von Wirkstoffen der neuesten Generation, wie z.B. Peptide und siRNA, sind Wirkstofftransportsysteme unerlässlich, da diese Art von Biomakromolekülen bei konventioneller Anwendung vor Erreichen des Wirkorts abgebaut wird (*130*)

1.4 Nanokomposit-Materialien

Verbundwerkstoffe, so genannte Komposite, bestehen aus mindestens zwei verschiedenen Materialien, wobei eine der Komponenten die kontinuierliche Phase, auch Matrix genannt, und eine andere die diskontinuierliche Phase, Füllstoff genannt, darstellt (*154*). Die Bezeichnung Nanokomposite bezieht sich auf Verbundmaterialien, in denen mindestens eine Dimension der verwendeten Füllstoffpartikel weniger als 100 nm misst (so genannte Nanopartikel). Hierfür verwendete Nanopartikel sind zum Beispiel Carbon-Nanoröhrchen, Graphen oder auch Schichtsilikate (so genannte *Nanoclays*) (*26, 155*). Durch Einbringen von Nanopartikeln in eine Matrix können neue, verbesserte Materialbeschaffenheiten erreicht werden, die vor allem die mechanischen und thermostabilen Eigenschaften der einzelnen Komponenten weit übersteigen. Dabei ist der wichtigste Faktor für eine Verbesserung der jeweiligen Materialeigenschaften die Interaktion zwischen Nanopartikeln und Matrix, die im Belastungsfall für eine gute Kraftübertragung von der Matrix hin zum Füllstoff sorgt (*156*). Eine optimale Interaktion kann vor allem durch ein hohes Oberfläche-zu-Volumen-Verhältnis der Nanopartikel erreicht werden und starken Einfluss auf die makroskopischen Eigenschaften eines Materials nehmen (*156-158*). Um diese starke Interaktionen zwischen Füllstoff und Matrix ausbilden zu können, wird eine gute Mischbarkeit der beiden Komponenten vorausgesetzt, wobei vor allem ähnliche hydrophobe/hydrophile Eigenschaften von Füllstoff und Matrix ausschlaggebend sind. Für die Herstellung von Nanokompositen gibt es vier verschiedene Verfahren:

1. Mischen in Lösung: Dabei wird das Polymer in einem geeigneten Lösungsmittel zusammen mit den Nanopartikeln aufgenommen, die Dispersion auf eine Oberfläche aufgebracht und das Lösungsmittel verdampft.
2. Schmelzvermischen: Die Polymerschmelze wird direkt mit den Nanopartikeln vermischt und ausgehärtet.
3. *In situ* Polymerisation: Nanopartikel werden in flüssiger Monomerlösung dispergiert, anschließend wird die Polymerisation in Anwesenheit der Nanopartikel durchgeführt.
4. Templat-Synthese: Das Polymer wird hier als Templat verwendet, an dem die Nanopartikel aus einer *precursor*-Lösung synthetisiert werden.

Im Detail wird in dieser Arbeit allein auf die Herstellung durch Mischen in Lösung eingegangen. Dieses Verfahren bietet die Möglichkeit getrennt hergestellte Materialien in einem für die einzelnen Komponenten geeigneten Lösungsmittel zu kombinieren. Die Art des Lösungsmittels ist dabei essenziell, um vollständiges Dispergieren der Nanopartikel zu gewährleisten. Außerdem beeinflusst das Lösungsmittel auch Materialeigenschaften, Ausbildung von Oberflächenstrukturen, sowie das Quell- und Deformationsverhalten. Dieses Verfahren ist kostengünstig und zeitsparend (*159*).

Schichtsilikate sind eine Art von Tonmineralien, die in der Natur vorkommen, aber auch synthetisch hergestellt werden und einen tafeligen Habitus in schichtartigem Aufbau aufweisen (*160*). Sie werden seit den 1950er Jahren zur Herstellung von Kompositen verwendet (*161*). Einzelne Partikel, so genannte Taktoide, bestehen aus parallel gestapelten Silikatlamellen, wobei jede einzelne Lamelle aus einer Lage kantenverknüpfter Oktaeder, bestehend aus einem bivalenten Kation (Al^{3+} oder Mg^{2+}) umgeben von acht Sauerstoffatomen, und zwei Lagen eckenverknüpfter Tetraeder, bestehend aus einem Siliziumatom umgeben von vier Sauerstoffatomen, in Sandwich-Bauweise aufgebaut ist (Abbildung 7) (*164*).

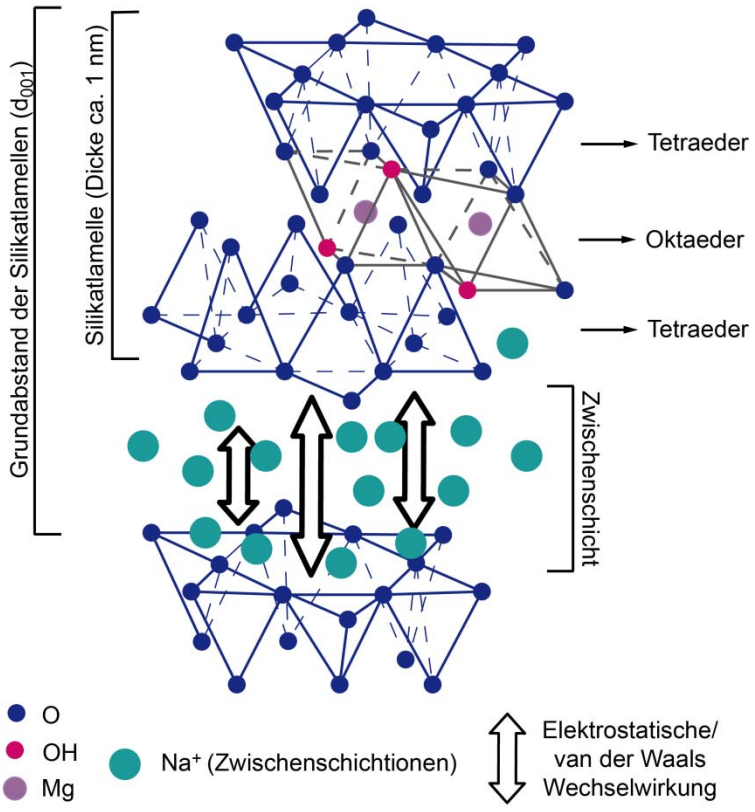

Abbildung 7: Aufbau eines Schichtsilikats. Modifiziert nach *(164)* mit freundlicher Genehmigung von © 2011 Olad A. Published in A. Olad, in *Advances in Diverse Industrial Applications of Nanocomposites,* D. B. Reddy, Ed. (2011) under CC BY-NC-SA 3.0 license. Available from: http://dx.doi.org/10.5772/14464.

Aufgrund ihres Aufbaus werden diese Tonmineralien auch als 2:1 Schichtsilikate bezeichnet, zu denen auch der in dieser Arbeit verwendete Natrium-Fluorohektorit (Na-hec) mit der Summenformel $[Na_{0.5}]^{IL}[Li_{0.5}Mg_{2.5}]^{OL}[Si_4]^{TL}O_{10}F_2$ gehört (*162, 163*).

Durch den Austausch von Kationen in der Tetraeder- und/oder Oktaeder-Schicht gegen niedervalente Kationen entsteht durch die vorgegebene Ladung des Anionengerüsts eine negative Überschussladung, die so genannte Schichtladung. Sie kann durch Interkalation von Zwischenschichtkationen kompensiert werden (Abbildung 7). Durch die Zwischenschichtkationen werden im Wesentlichen die physikochemischen Eigenschaften der Schichtsilikate bestimmt, denn diese hängen vor allem von der Schichtladung und der Art dieser Kationen ab. Sie bestimmen auch den Schichtabstand der Silikatlamellen und somit deren interlamellare Wechselwirkungen und Kohäsion (*165, 166*).

Die besonderen Merkmale von Schichtsilikaten beziehen sich vor allem auf ihr Quellverhalten und somit ihre interkristalline Reaktivität. Diese ist größtenteils auf eine hohe Hydratationsenthalpie der Zwischenschichtkationen zurückzuführen, an die bei erhöhter relativer Feuchte (r.H.) in der Umgebung eine vermehrte Anlagerung von Wassermolekülen stattfinden kann. Die Koordination von Wassermolekülen führt dann zu einer Aufweitung des Schichtabstands, dessen Grad durch ein kompetitives Gleichgewicht von attraktiven und repulsiven Kräften bestimmt wird (*167*). Während darin Coulombanziehung und van-der-Waals-Kräfte der Quellung entgegenwirken, wird diese durch eine hohe Hydratationsenthalpie stark begünstigt (*168*). Vor allem bei synthetischen Schichtsilikaten kann durch die geeignete Wahl von Schichtladung und Zwischenschichtkationen das Quellverhalten der Taktoide beeinflusst werden. So kann die Quellung so stark begünstigt sein, dass bei Kontakt mit deionisiertem Wasser die Kohäsion der Silikatlamellen überwunden wird und schließlich die Taktoide in einzelne Silikatlamellen delaminieren (*169*). Im Hinblick auf die Verwendung von Schichtsilikaten in Nanokomposit-Materialien ist das Erreichen dieses Zustands favorisiert, da interkalierte Wassermoleküle in den Zwischenschichten als Gleitfilm wirken können und somit im Nanokomposit das Material schwächen.

Um bei der Verwendung von Schichtsilikaten zur Herstellung von Nanokompositen optimale Ergebnisse in Hinsicht auf Mechanik, Hitzebeständigkeit und Barriereeigenschaften zu erhalten, müssen verschiedene Aspekte berücksichtigt werden. Es muss ein Verfahren entwickelt werden, das eine gute Kompatibilisierung von Matrix und Füllstoff an der Grenzfläche und eine gute Texturierung, d.h. parallele Orientierung der Plättchen zueinander in einer Ebene, gewährleistet. Dabei kann es helfen, eine

Modifikation der Schichtsilikate vorzunehmen. Wie bereits erwähnt spielt bei der Herstellung von Nanokompositen vor allem die Interaktion zwischen Matrix und Füllstoff eine bedeutende Rolle. Unter Verwendung von Schichtsilikaten kann jedoch eine intrinsische Inkompatibilität zwischen den verwendeten, meist hydrophoben Matrixpolymeren und den hydrophilen *Nanoclays* auftreten, die eine gute Mischbarkeit verhindern. Um dennoch eine gute Interaktion der beiden Phasen zu erreichen ist es möglich die Schichtsilikatplättchen mit hydrophoberen Molekülen zu modifizieren und damit die Oberflächenenergie herabzusetzen. Durch diesen Schritt kann eine bessere Kompatibilität mit hydrophoben Matrixpolymeren geschaffen werden, wodurch eine verbesserte Kompatibilität der beiden Materialien dazu führt, dass Polymerketten leichter in die Zwischenschicht interkalieren können (*164*).

Schichtsilikatplättchen können durch den Austausch von Kationen modifiziert werden. Dabei werden Natrium- oder Calciumkationen aus der Zwischenschicht der Schichtsilikate durch Alkylammoniumionen oder Alkylphosphoniumionen (allgemein Oniumionen) ersetzt (*170*). Diese Eigenschaft ist mit der Kationenaustauschkapazität (CEC, engl. *cation exchange capacity*) als Schichtsilikat-spezifische Größe quantifiziert und liegt bei dem in dieser Arbeit verwendeten Na-hec bei 127 meq/100 g. Zusätzlich zu einer angepassten Oberflächenpolarität und erhöhter Hydrophobizität wird durch das Einbringen von Oniumionen der Zwischenschichtabstand erweitert. Diese Erweiterung erleichtert zudem im nächsten Schritt die Interkalation von Polymerketten und somit die Herstellung von Nanokompositen (*171*). Außerdem können die eingelagerten Oniumionen weitere funktionelle Gruppen tragen, die dann mit den Matrixpolymeren interagieren oder sogar reagieren können und somit die Interaktionen zwischen den Phasen zusätzlich stärken. Modifikationen von Schichtsilikaten sind einfach durchzuführen. Monovalente Na^+-Ionen können hydratisiert werden, wodurch die Interaktion mit der Oberfläche der Schichtsilikate in wässrigem Milieu geschwächt und der Ionenaustausch gefördert wird (*155*).

Für eine zielgerichtete Anwendung als Barrierebeschichtung wurde in dieser Arbeit das Schichtsilikat Natrium-Fluorohektorite (Na-hec) ausgewählt, das aufgrund eines sehr hohen Aspekt-Verhältnisses (>20000) und seiner Fähigkeit spontan in deionisertem Wasser zu delaminieren einen optimalen Ausgangsstoff für dieses Vorhaben darstellt.

1.5 Spinnenseide

1.5.1 Natürliche Spinnenseide von Radnetzspinnen

Ungefähr die Hälfte der aktuell bekannten 44750 Spinnenarten (*172*) nutzen Spinnenseidennetze zum Beutefang. Dabei werden etwa 130 verschiedene Arten von Netzen verwendet (*173*). Eine der bekanntesten Netzformen ist das Radnetz, das zum Beispiel von Spinnenarten wie der europäischen Gartenkreuzspinne (*Araneus diadematus*) konstruiert wird. Spinnen nutzen ihre Seide allerdings nicht nur zum Beutefang, sondern auch um ihre Beute einzuwickeln und Kokons zum Schutz ihrer Nachkommen zu bauen. Hierfür können weibliche Radnetzspinnen bis zu sieben verschiedene Seidenarten erzeugen, die für ihre entsprechenden Aufgaben angepasste Eigenschaften aufweisen (Abbildung 8) (*128, 174, 175*).

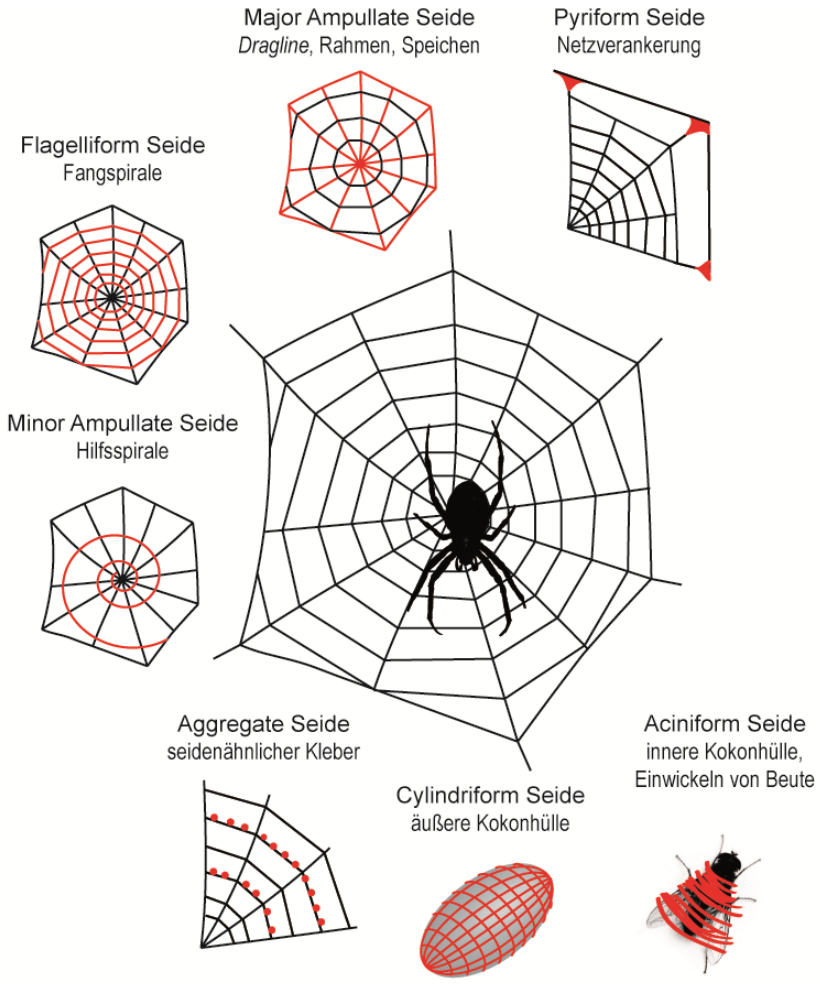

Abbildung 8: Darstellung der verschiedenen Seidenarten, die von einer weiblichen Radnetzspinne produziert werden. Modifiziert nach (*176*) mit freundlicher Genehmigung von Springer aus E. Doblhofer, A. Heidebrecht, T. Scheibel, To spin or not to spin: spider silk fibers and more. *Appl Microbiol Biotechnol* **99**, 9361 (2015). Copyright (2015) Springer.

Die mit Abstand am häufigsten untersuchte Seidenart ist die *Dragline* Seide (engl. *dragline* = Schleppseil oder Major Ampullate Seide). Sie wird neben Rahmen und Speichen im Netz auch als Abseilfaden verwendet und ist daher leicht zugänglich (*177*). Die *Dragline*-Seiden verschiedener Spinnenarten zeigen einen sehr ähnlichen hierarchischen Aufbau dem eine Kern-Mantel-Struktur zugrunde liegt (*178-182*). Dabei bestimmt vor allem der Kern die mechanischen Eigenschaften der Faser (*183*). Dieser wird aus Mikro- und Nanofibrillen gebildet, die entlang der Faserachse ausgerichtet sind, einen Durchmesser von 100-150 nm aufweisen und aus mindestens zwei verschiedenen Proteinarten, den so genannten Spidroinen, bestehen (*183-185*). Im Falle der Europäischen Gartenkreuzspinne (*Araneus diadematus*) sind zwei entsprechende Proteine, *Araneus diadematus* Fibroin 3 und 4 (ADF3 und ADF4) genannt, bekannt (*175*).

Generell weisen nahezu alle Spidroine der verschiedenen Spinnenseidenarten eine ähnliche Grundstruktur mit einem Molekulargewicht zwischen 250 und 350 kDa auf (*186*). Sie beinhalten eine repetitive Kerndomäne, die aus bis zu 100 Wiederholungen von hochkonservierten Sequenzmotiven (40 bis 100 Aminosäuren) besteht, die bis zu 50 % aus den Aminosäuren Alanin und Glycin gebildet werden und in kleineren Einheiten definierte Sekundärstrukturen bilden (Abbildung 9) (*187-191*). Diese Sekundärstrukturmotive sind in ihrer Zusammensetzung charakteristisch für Spinnenseidenproteine und bilden die Grundlage für den strukturell geordneten Aufbau des Kerns und die mechanischen Eigenschaften der Spinnenseidenfaser (Abbildung 9) (*188, 189, 192-195*).

Der repetitive Kern der Proteinstruktur wird von kurzen, etwa 100 bis 150 Aminosäuren langen, nicht repetitiven (NR) terminalen Domänen flankiert, die eine wichtige Rolle bei der kontrollierten Faserassemblierung spielen. Sie zeigen überwiegend α-helicale Strukturen, die in 5-Helix-Bündeln angeordnet sind. Die NR-Regionen kontrollieren die natürliche Lagerung der Spidroine in hoher Konzentration im Drüsensack der Spinne (*196*) und initiieren im Spinnkanal durch Ausrichtung des repetitiven Parts ihre Assemblierung zum Faden (*127, 197-204*).

1.5.2 Rekombinante Spinnenseidenproteine eADF4

Im Hinblick auf industrielle Verarbeitung von Spinnenseidenproteinen zeigte sich schnell, dass für eine großtechnische Nutzung die natürliche Quelle nicht ausreicht. Dies liegt zum einen daran, dass von einer Spinne durch so genanntes Melken nur geringe Mengen des Rohmaterials gewonnen werden können und die Qualität der Seide von

Spinnen in Gefangenschaft im Vergleich zu der in freier Wildbahn produzierten Seide abnimmt. Erschwerend kommt hinzu, dass Spinnen ein stark territoriales und kannibalisches Verhalten an den Tag legen, wodurch eine Massenhaltung dieser Tiere auf engstem Raum nicht möglich ist (*205-208*). Aufgrund dessen wurde angestrebt, das Material auf anderem Weg biotechnologisch herzustellen.

1.5.2.1 Rekombinante Herstellung

Für die rekombinante Herstellung von Spinnenseidenproteinen wurden Gene/Proteine konstruiert, welche die Hauptmerkmale der natürlichen Seidenproteine aufweisen, gleichzeitig aber bestmöglich für die Produktion in einem Wirtsorganismus angepasst sind (*Codon Usage*, Molekulargewicht, etc.). Als Wirtsorganismus zur Expression der rekombinanten Spinnenseidenproteine wurde das gram-negative Enterobakterium *Escherichia coli* (*E. coli*) gewählt, da dieser Organismus mit wenig Aufwand manipuliert und kostengünstig und schnell in hoher Zelldichte kultiviert werden kann. (*209, 210*).

Für die Herstellung der künstlichen Spinnenseidenproteine, die in dieser Arbeit verwendet wurden, dienten das Spinnenseidenprotein ADF4 als Vorbild, wobei die terminalen NR-Domänen bei der Konstruktion des artifiziellen Spinnenseidenproteins nicht berücksichtigt wurden (Abbildung 9) (*175, 204*). So wurde die Zusammensetzung der Primärstrukturmotive aus den repetitiven Teilen des Proteins ähnlich der Originalsequenz kombiniert und zum so genannten C-Modul zusammengefasst, in eine Codon-optimierte DNA-Sequenz rückübersetzt und mittels Festphasensynthese hergestellt. Um den repetitiven Charakter des ADF4 zu imitieren, wurde für die Produktion des rekombinanten Spidroins eADF4(C16) in einem nahtlosen Klonierungsverfahren die Gensequenz für das C-Modul in einem geeigneten Vektor 16-fach wiederholt und ein geeigneter *E. coli* Expressionsstamm mit dem Expressionsvektor transformiert (Abbildung 9) (*204*). Durch Fermentation der transformierten *E. coli* und einem anschließenden Chromatographiesäulen-freien zweistufigen Reinigungsprozess (durch Hitze- und selektive Salzfällung) konnten Ausbeuten zwischen 140-360 mg gereinigten Proteins pro Liter Zellsuspension erzielt werden (*211, 212*). Die rekombinante Herstellung von Spinnenseiden-ähnlichen Proteinen bietet die Möglichkeit weitere, nicht-natürliche Modifikationen in die Sequenz einzubauen.

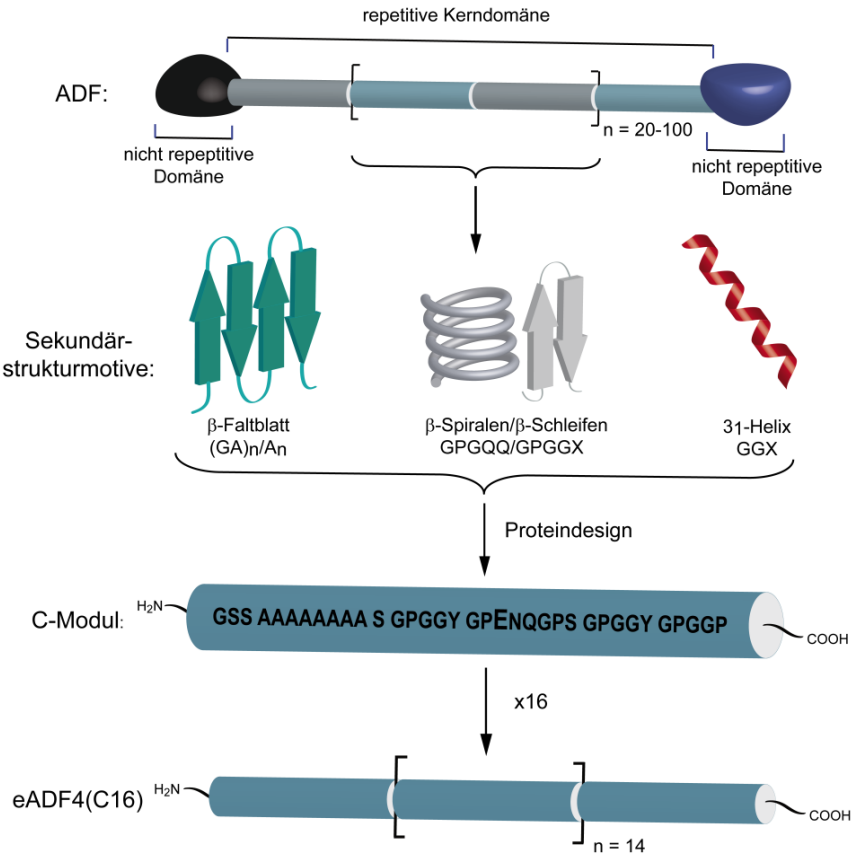

Abbildung 9: Schematischer Aufbau des nativen Spinnenseidenproteins ADF4, der darin enthaltenen Sekundärstrukturmotiven, sowie die Grundlage und der Aufbau des davon abgeleiteten rekombinanten Spinnenseidenproteins eADF4(C16).

1.5.2.2 Assemblierungsmorphologien rekombinanter Spinnenseidenproteine

Rekombinant hergestelltes eADF4 bietet nicht nur den Vorteil, in relativ großen Mengen und in für die jeweilige Anwendung maßgeschneiderten Variationen produziert, sondern auch durch geeignete Verarbeitungswege in unterschiedliche Morphologien assembliert werden zu können (Abbildung 10) (*213, 214*). Die Herstellung von Partikeln, Fasern und Hydrogelen kann in wässrigen Lösungen abhängig von Änderungen des pH-Werts, Menge und Art von Additiven (z.B. Kaliumphosphat, Alkohole oder Polymere), mechanischen Scherkräften oder Änderung der Temperatur induziert werden. Des Weiteren können durch Lösen und Verarbeiten der Proteine in organischen Lösungsmitteln, wie Ameisensäure oder 1,1,1,3,3,3-Hexafluoroisopropanol (HFIP), Filme oder Vliese hergestellt werden. Die Struktur der Proteine in den einzelnen Morphologien ist stark von den verwendeten Agenzien während der Verarbeitung der Proteine abhängig. So können wasserlösliche α-helikale Spinnenseidenproteinstrukturen durch Nachbehandlung mit kosmotropen Salzlösungen (Kaliumphosphatpuffer) oder einwertigen Alkoholen (z.B. Methanol, Ethanol, Isopropanol) überwiegend β-Faltblatt-Strukturen

erzielt werden. Diese β-Faltblatt-reichen kristallinen Strukturen machen die Spinnenseidenproteinformkörper wasserunlöslich (*127, 203, 215-221*).

In dieser Arbeit wurden überwiegend Filme und Partikel aus rekombinanten Spinnenseidenproteinen eADF4 untersucht, weshalb im Folgenden näher auf diese Morphologien eingegangen werden soll.

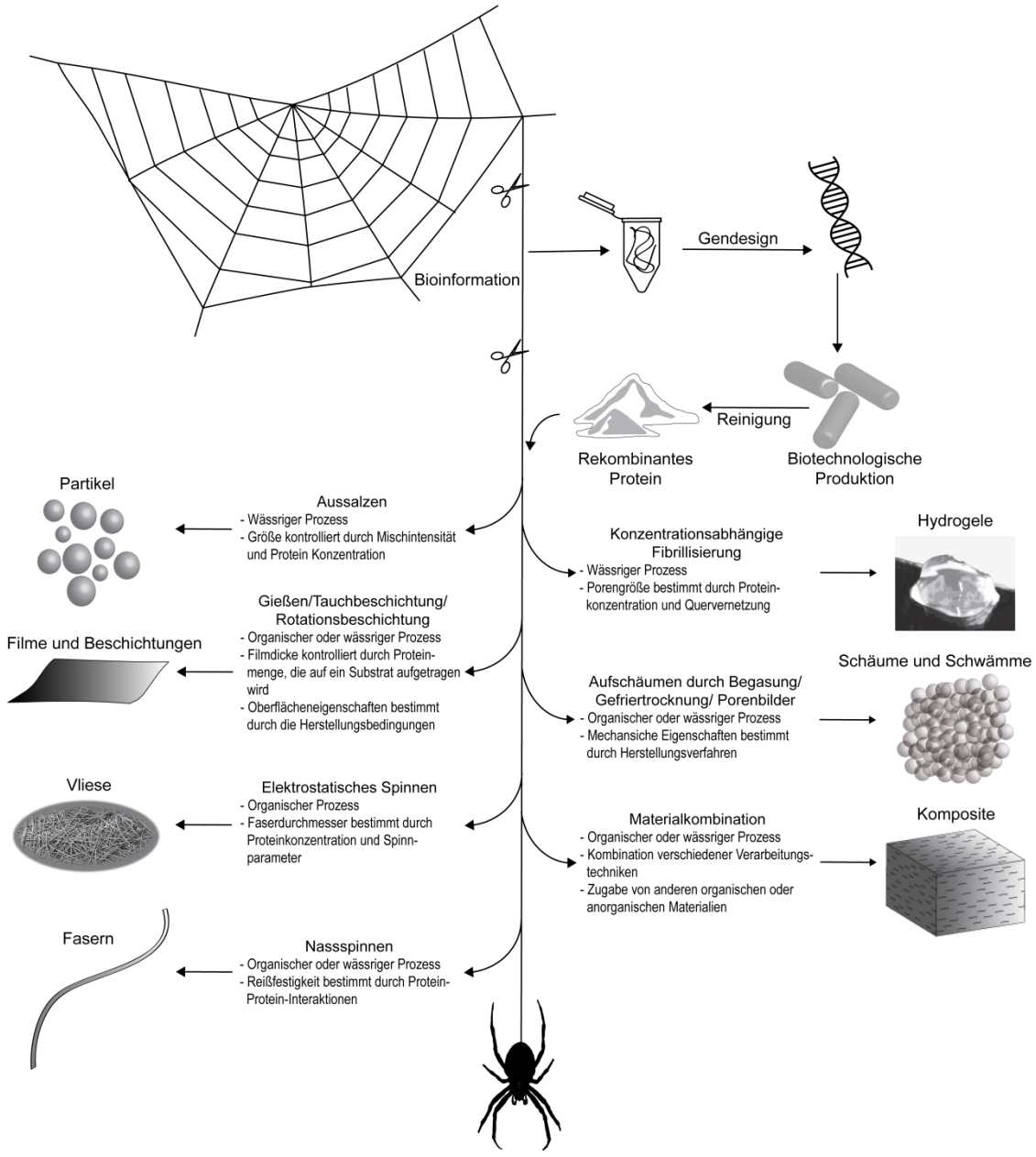

Abbildung 10: Schema des Designs, der Produktion und der Verarbeitung von rekombinanten Spinnenseidenproteinen: Der Weg von der Identifikation der Bioinformation des natürlichen Materials, über das gentechnische Design bis hin zu möglichen Modifikationen. Modifiziert nach (*176*) mit freundlicher Genehmigung von Springer aus E. Doblhofer, A. Heidebrecht, T. Scheibel, To spin or not to spin: spider silk fibers and more. *Appl Microbiol Biotechnol* **99**, 9361 (2015). Copyright (2015) Springer.

1.5.2.3 Partikel aus eADF4

Partikel gehören zu den am besten charakterisierten Morphologien von eADF4. Sie können durch eine gute mechanische Stabilität als Füllstoff von Kompositmaterialien, oder aufgrund der guten Biokompatibilität und geringen Immunogenität der zugrunde liegenden Proteine als Wirkstofftransporter im menschlichen Körper fungieren (*176*). Bei der Herstellung (Abbildung 11A) wird durch Zugabe eines Fällreagenz in Form von hohen Konzentrationen kosmotroper Ionen (wie zum Beispiel >400 mM Kaliumphosphat) ein Ausfällen der Proteine aus einer wässrigen Lösung in partikulärer Form induziert.

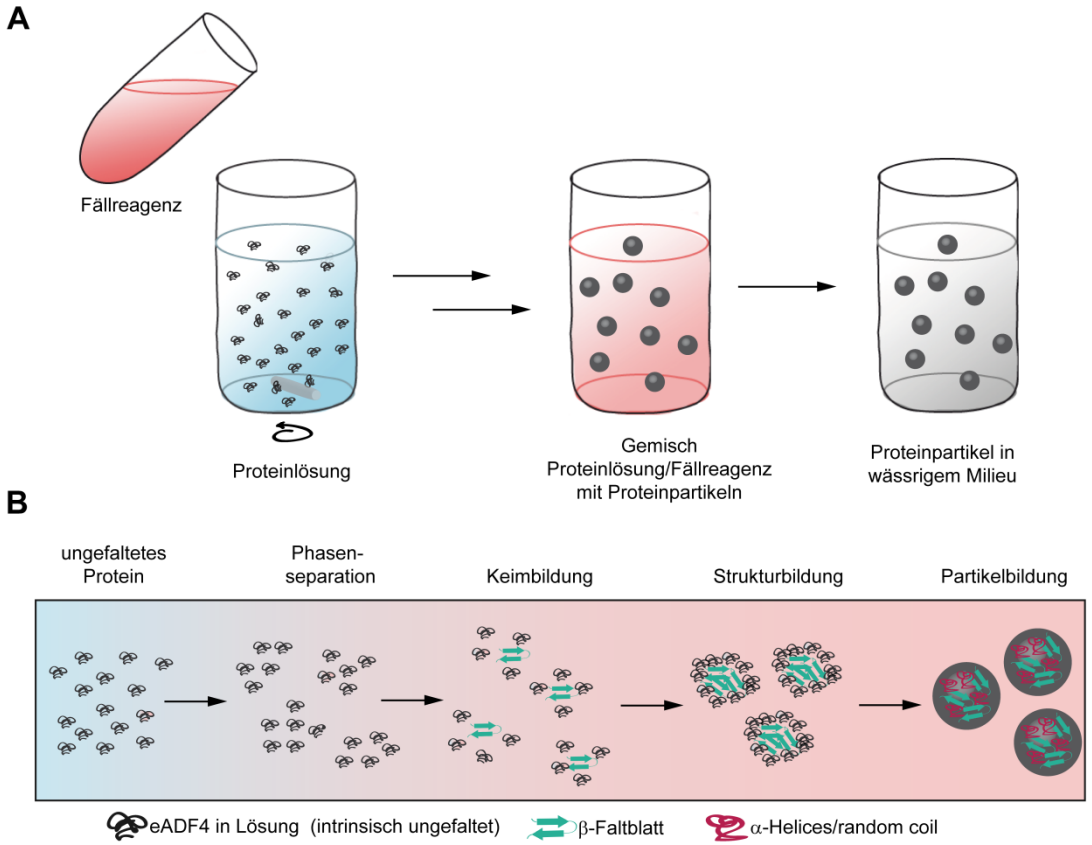

Abbildung 11: Partikelherstellung: (A) auf makroskopischer Ebene durch Fällung von eADF4 Proteinen mittels kosmotropen Salzlösungen (Fällreagenz) und Überführen in wässriges Milieu; (B) Modell der Partikelbildung auf molekularer Ebene.

Im Detail (Abbildung 11B) wird durch Zugabe von Kaliumphosphat den zunächst intrinsisch ungefaltet vorliegenden Proteinen in wässrigen Lösungen die Hydrathülle entzogen. Dies führt zu einer Verstärkung hydrophober Wechselwirkungen und folglich zur Phasenseparation in der Proteinlösung, wobei eine proteinreiche und eine lösungsmittelreiche Phase entsteht. Sobald eine kritische Konzentration in der proteinreichen Phase erreicht ist, bilden sich durch intermolekulare Wechselwirkungen und Strukturumlagerungen Nukleationskeime (Keimbildung, Abbildung 11B), die durch

weitere Anlagerung von Spinnenseidenproteinmolekülen (Strukturbildung) zu kugelförmigen Partikeln heranwachsen (Partikelbildung). Dieser Vorgang dauert so lange an, bis ein Löslichkeitsgleichgewicht erreicht wird und führt zu stabilen, wasserunlöslichen, β-Faltblatt-reichen Partikeln. Ihre Größe liegt zwischen 250 nm und 3 µm und ist abhängig von Mischgeschwindigkeit und Konzentrationen der einzelnen, im Herstellungsprozess verwendeten Komponenten (*216, 222, 223*).

Proteinpartikel, die auf diese Weise hergestellt werden, weisen jedoch meist eine starke Polydispersität auf (*214, 216, 222, 224*). Die Verwendung von ionischen Flüssigkeiten als Alternative zu wässrigen Lösungsmitteln führt hingegen zu einer erhöhten Kontrolle der Partikelgröße und somit einer Verringerung der Polydisperistät (*225*). Spinnenseidenpartikel aus eADF4(C16) sind in getrocknetem Zustand mechanisch mit einem E-Modul von ca. 1 GPa außerordentlich stabil und plastisch verformbar. Durch Hydratisierung der Partikel quellen diese auf das 2,3 fache Volumen. Dabei reduziert sich das E-Modul der Partikel um drei Größenordnungen auf ca. 3 MPa, wobei die hydratisierten Partikel nun eine elastische Verformbarkeit aufweisen. Die Verformbarkeit der Partikel kann durch Quervernetzung gesteuert werden (*226*). Weitere Analysen zeigten, dass wässrige Suspensionen von eADF4(C16) Partikeln eine hohe kolloidale Stabilität aufweisen (*227*). Dies ist auf den Aufbau der Partikel zurückzuführen. Sie bestehen aus einem festen Kern, von dem aus einzelne Proteinmoleküle in die Umgebung vorstehen. Diese vorstehenden Proteinmoleküle ähneln einer sterischen Schicht, wie sie für Polymerpartikel häufig künstlich aufgebaut wird, um durch Interaktion mit dem Lösungsmittel und anderen Partikeln eine Agglomeration verhindern (*228*)

Es konnte bereits in vergangenen Studien gezeigt werden, dass Partikel aus rekombinantem Spinnenseidenprotein sowohl kleine Modelwirkstoffe, als auch größere Moleküle, wie zum Beispiel BSA (Bovine Serum Albumin) oder Lysozym, aufnehmen können (*223, 227*). Hierfür ist es möglich die Partikel sowohl durch Diffusion, als auch durch Copräzipitation mit den gewünschten hydrophilen Substanzen zu beladen. Während die Variante der Copräzipitation zu einer höheren Ladungseffizienz führt, beeinflusst der Weg der Partikelbeladung den Zeitraum der Substanzfreisetzung nicht (*224*). Allerdings konnten in den durchgeführten Studien mit eADF4(C16) Partikeln, die bei neutralem pH eine negative Nettoladung aufweisen, aufgrund von Ladungsabstoßung nur mit Substanzen beladen werden, die eine positive Nettoladung aufwiesen. Somit war die Auswahl der Substanzen die in eADF4(C16) Partikeln aufgenommen und transportiert werden können

stark eingeschränkt (*223*). Versuche mit neutralen, hydrophilen Substanzen zeigten zwar, dass hier ebenfalls eine Beladung der Partikel möglich ist, die Freisetzung aber ungehindert und unabhängig vom Freisetzungsmedium in sehr kurzem Zeitraum stattfindet (*224*). Durch eine Beladung mittels Copräzipitation konnten neben hydrophilen auch hydrophobe Substanzen, wie zum Beispiel β-Carotin in die Partikel eingebracht werden. Dabei ergab sich der Vorteil, dass solche Substanzen in wässriger Umgebung nicht durch Diffusion freigesetzt werden, sondern eine Freisetzung erst durch hydrolytischen oder enzymatischen Abbau des Spinnenseidenproteins möglich ist (*229*). Die dabei entstandenen Abbauprodukte, proteinogene Aminosäuren, können vom menschlichen Körper weiter verwertet oder ausgeschieden werden. Trotz vieler Studien, in denen gezeigt werden konnte, dass eADF4(C16) gut für die Anwendung als Träger zum Wirkstofftransport geeignet ist, wird durch die negative Ladung dieses Proteins der Anwendungsbereich stark eingeschränkt.

1.5.2.4 Filme hergestellt aus eADF4

Eine weitere sehr gut untersuchte Morphologie aus rekombinanten Spinnenseidenproteinen stellen Filme dar. Sie sind transparent und unter milden Bedingungen chemisch stabil (*230*)

Neben der am häufigsten verwendeten Methode, dem so genannten Gießen oder *Drop Casting* können Filme auch durch Sprühbeschichtung (*Spray Coating*), Rotationsbeschichtung (*Spin Coating*), Tauchbeschichtung (*Dip Coating*) oder Rakeln hergestellt werden (*230-233*). Beim Gießen (Abbildung 12) wird eine Proteinlösung in eine Form gegeben, aus der das Lösungsmittel verdampft.

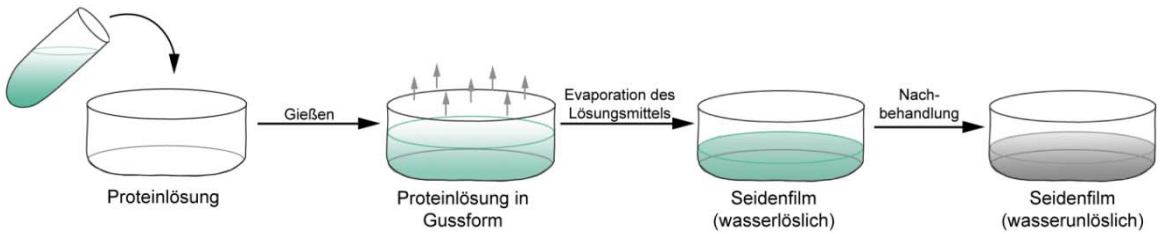

Abbildung 12: Herstellung von Filmen und Beschichtungen aus rekombinantem Spinnenseidenprotein eADF4 durch Gießen mit anschließender Nachbehandlung zur Generierung wasserunlöslicher Filme.

Während dieses Abdampfens entsteht vermutlich eine partielle Separation der kristallisierbaren, poly-Alanin-reichen, hydrophoben Bereiche von den Glycin-reichen Primärstrukturblöcken (*234, 235*). In dieser Mesophase werden abhängig vom verwendeten Lösungsmittel und den damit korrelierenden Trocknungszeiten bereits

teilweise β-Faltblatt-Strukturen gebildet. So entsteht zum Beispiel bei Verwendung von HFIP zur Herstellung der Proteinlösung eine überwiegende α-helikale Struktur, während der Anteil an β-Faltblatt in Filmen, gegossen aus Ameisensäure-Lösungen, erhöht ist (*236-238*). Die Filme aus rekombinantem Spinnenseidenprotein sind jedoch in den meisten Fällen nach dem Trocknen wasserlöslich. Dies ist von Nachteil, da für viele medizinische und technische Anwendungen eine Stabilität der Filme in feuchter Umgebung vorausgesetzt wird. Eine Nachbehandlung der Filme mit kosmotropen Salzen, einwertigen Alkoholen, Temperaturerhöhung oder Wasserdampf führt durch Herauslösen der verbliebenen Lösungsmittelmoleküle zu einem Bruch der intramolekularen Wasserstoffbrückenbindung und somit zu einer spontanen Umlagerung der Proteinstruktur. Dabei entstehen überwiegend intermolekulare Wasserstoffbrückenbindungen und aus den verbleibenden poly-Alanin-reichen Aminosäuresequenzen werden β-Faltblatt-Strukturen gebildet. Dieses Verfahren führt dazu, dass Filme aus rekombinanten Spinnenseidenproteinen chemisch stabiler und wasserunlöslich werden (*218, 230-232, 236*).

Der β-Faltblatt-Anteil bestimmt aber nicht nur die chemische Stabilität der Filme, sondern auch deren mechanische Stabilität. So haben die Filme mit hohem β-Faltblatt-Anteil ein hohes E-Modul und eine hohe Festigkeit, wobei ihre Elastizität allerdings abnimmt. Die Filme werden mit höher werdendem β-Faltblatt-Anteil immer brüchiger. Um die optimalen Eigenschaften der Filme zu erreichen, kann der Anteil dieses Sekundärstrukturelements durch die Art der Nachbehandlung beeinflusst werden, wobei Wassermoleküle als Weichmacher fungieren (*236, 239*).

2 Zielsetzung

Der Ersatz von Kunststoffen aus synthetischen Polymeren in medizinischen, und technischen Anwendungen durch besser verträgliche, bioabbaubare Materialien aus nachhaltigen Produktionsquellen stellt eine große Herausforderung dar. Spinnenseide kann aufgrund ihrer Biokompatibilität, Bioabbaubarkeit und den außergewöhnlichen mechanischen Eigenschaften als solches Ersatzmaterial für viele verschiedene Anwendungen dienen. Die biotechnologische Entwicklung in den letzten Jahren ermöglichte dabei zusätzlich, designte spinnenseidenähnliche Proteine in großen Mengen und gleichbleibender Qualität herzustellen (*204*). Dennoch gibt es bei der Verwendung dieser Proteine Einschränkungen; so trägt das etablierte, rekombinante Spinnenseidenprotein eADF4(C16) ausschließlich negative Ladungen, die aufgrund elektrostatischer Abstoßung und dem Fehlen von Zellinteraktionsmotiven für eine Aufnahme in eukaryotischen Zellen ungeeignet sind. Außerdem wird die Anwendung des anionischen Proteins dadurch eingeschränkt, dass keine Wechselwirkungen mit anionischen Wirkstoffen möglich sind, wodurch die Verwendung als Wirkstofftransporter, sowie die Interaktion mit negativ geladenen Füllstoffen bei der Herstellung von Kompositmaterialien stark eingeschränkt ist.

Um die Anwendbarkeit von rekombinanten Spinnenseidenproteinen zu erweitern und die beschriebenen Herausforderungen zu überwinden, sollte in dieser Arbeit ein kationisches Spinnenseidenprotein eADF4(κ16) durch Austausch der negativ geladenen Aminosäure L-Glutaminsäure (E) gegen die positiv geladene Aminosäure L-Lysin (K) designt und durch biotechnologische Herstellung verfügbar gemacht werden. Durch die Entwicklung von Partikeln aus der kationischen Spinnenseidenproteinvariante eADF4(κ16) ergibt sich die Möglichkeit, auch negativ geladene Wirkstoffe transportieren zu können und die initiale elektrostatische Interaktion der Partikel mit Säugerzellen zu verbessern. In diesem Zusammenhang sollte in dieser Arbeit analysiert werden, in wie weit sich Aufnahme und Freisetzung von kleinen Wirkstoffmolekülen aus Partikeln der rekombinanten Spinnenseidenproteine eADF4(κ16) und eADF4(C16) unterscheiden, und ob diese durch *Layer-by-Layer*-Beschichtung (LbL; engl. Schicht-für-Schicht (*240*)) beeinflusst werden kann. Aufgrund ihrer positiven Ladung bieten Partikel aus eADF4(κ16) zudem die Möglichkeit, als Transporter für siRNA zu fungieren und somit zukünftig potenziell Einsatz in der Gentherapie zu finden. Daher sollten hier eADF4(κ16) Partikel

mit kurzen DNA-Strängen, als Modell für siRNA, beladen und deren Freisetzung getestet werden. Außerdem stellte sich die Frage, wie sich eine Beladung von eADF4(κ16) Partikeln mit den genannten DNA-Molekülen auf deren kolloidale Eigenschaften auswirkt und die zelluläre Aufnahme beeinflusst. Als Vergleich wurden PEI-beladene Partikel verschiedener eADF4(C16)-Varianten mit und ohne Zellinteraktionsmotive (eADF4(C16), eADF4(C16)RGD und eADF4(C16)R_8G) herangezogen.

Für ein besseres Verständnis dieser Spinnenseidenproteinmorphologie sollten in dieser Arbeit abschließend auch die kolloidalen Eigenschaften (Partikelmorphologie, elektrophoretische Mobilität, kolloidale Stabilität, etc.) von Spinnenseidenpartikeln aus eADF4(κ16), eADF4(C16) und *Layer-by-Layer* beschichteten eADF4 Partikeln untersucht werden. Zusätzlich sollte hierbei auch festgestellt werden, ob durch Charakterisierung der kolloidalen Partikeleigenschaften ein Verfahren entwickelt werden kann, das sich zur Qualitätskontrolle von Proteinpartikeln eignet.

Neben medizinischen Anwendungen eignen sich rekombinante Spinnenseidenproteine auch für technische Anwendungen. Auch hier wurde bisher nur das polyanionische eADF4(C16) untersucht, um Vliese für Filtermedien herzustellen (*241*). Es sollte in der vorliegenden Arbeit ein Verfahren zur Herstellung eines Nanokomposit-Materials aus eADF4(κ16) und dem Schichtsilikat Natrium-Fluorohektorit entwickelt werden. Nanokomposite, die Schichtsilikate mit hohen Aspektverhältnissen enthalten eignen sich besonders gut als Diffusionsbarrieren zum Ausschluss von Gasen. Aus diesem Grund sollte das hier erstellte Nanokomposit-Material hinsichtlich seiner Anwendung als Barrierebeschichtung für Lebensmittelverpackungen getestet werden. Abbildung 13 zeigt zusammengefasst die Ziele dieser Arbeit.

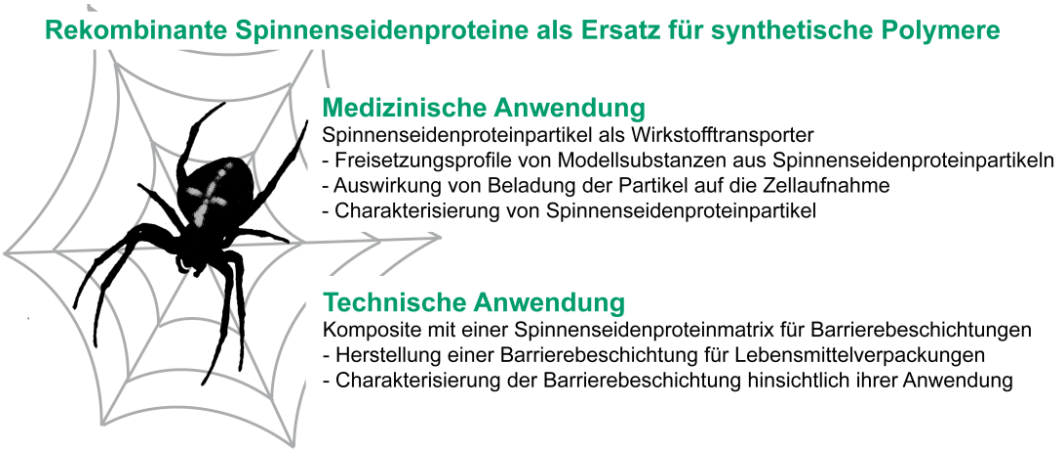

Abbildung 13: Zusammenfassung der Zielsetzung der vorliegenden Arbeit.

3 Synopsis

Die vorliegende Arbeit beinhaltet fünf Publikationen, die in Kapitel 5 dargestellt sind, und behandelt die Verwendung von Spinnenseidenproteinen als Ausgangsmaterial für den Ersatz von synthetischen Polymeren. Sie lässt sich thematisch in zwei Teile gliedern: Der erste Teil enthält die Charakterisierung von Partikeln aus einer neuen, bei pH 7 kationischen Variante des rekombinanten Spinnenseidenproteins eADF4(C16) im Hinblick auf potentielle medizinische Anwendungsmöglichkeiten als Wirkstofftransporter. Im zweiten Teil wird die Herstellung einer Nanokomposit-Barrierebeschichtung mit Spinnenseidenprotein als Matrix beschrieben, wobei diese Anwendung in Lebensmittelverpackungen finden kann. Dieser Teil zielt darauf ab, ein Beispiel einer technisch orientierten Anwendung des Materials Spinnenseidenprotein zu zeigen.

Zur Herstellung der neuen Spinnenseidenproteinvariante wurde die (bei pH 7) negativ geladene Aminosäure Glutaminsäure in der Primärsequenz des C-Moduls von eADF4(C16) gegen die (bei pH 7) positiv geladene Aminosäure Lysin ausgetauscht. Das so entstandene κ-Modul wurde dann analog zur Herstellung von eADF4(C16) in eine Codon-optimierte DNA-Sequenz rückübersetzt, 16-fach wiederholt und das so genannte eADF4(κ16) (Abbildung 14) durch Fermentation in *E. coli* exprimiert. Die Reinigung dieses Proteins konnte ebenfalls durch einen zuvor beschriebenen zweistufigen Reinigungsprozess (Hitzebehandlung und Salzfällung) durchgeführt werden (*204*).

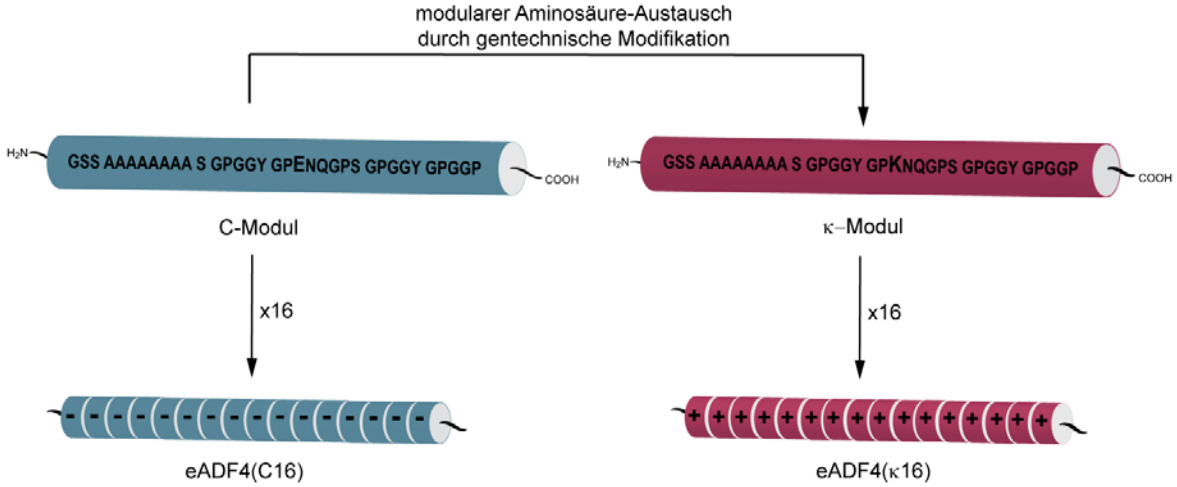

Abbildung 14: Schema zum Design des kationischen rekombinanten Spinnenseidenproteins eADF4(κ16)

Das gereinigte eADF4(κ16) zeigte, analog zu eADF4(C16), durch Verarbeitung in wässrigem und organischem Milieu verschiedene Assemblierungsmorphologien, wodurch es potentiell Anwendungen in verschiedensten medizinischen und technischen Bereichen finden kann. In dieser Arbeit wurden vor allem Partikel und Filme aus eADF4(κ16) auf ihre Anwendbarkeit untersucht und die wichtigsten Ergebnisse der durchgeführten Studien in diesem Kapitel zusammengefasst.

3.1 Spinnenseidenproteinpartikel als Wirkstofftransporter

Aufgrund ihrer biokompatiblen Eigenschaften eignen sich Partikel aus rekombinantem Spinnenseidenprotein sehr gut als Träger von Wirkstoffen zur Verabreichung von Medikamenten. In vergangenen Studien wurde hierzu vor allem die Optimierung der Herstellung, Beladung mit Wirkstoffen und deren Freisetzung, sowie mechanische und kolloidale Stabilität von eADF4(C16) Partikeln analysiert (*204, 216, 223, 224, 226-228*). Da eADF4(C16) eine negative Nettoladung und keine Zellinteraktionsmotive aufweist, eignen sich daraus hergestellte Partikel nur bedingt für diese Anwendung. Die negative Ladung verhindert dabei aufgrund elektrostatischer Abstoßung zum einen die Beladung der Partikel mit negativ geladenen Wirkstoffen, wie zum Beispiel siRNA zur Verwendung in der Gentherapie, und eignet sich somit zum anderen auch nicht für eine schnelle Aufnahme in Zellen zur intrazellulären Freisetzung von Wirkstoffen (*225*). Für eine verbesserte Interaktion im ersten Kontakt zwischen Zellmembran und Spinnenseidenproteinpartikeln, sowie um ein breiteres Anwendungsspektrum von Spinnenseidenproteinpartikeln zu erreichen, wurde in dieser Arbeit die (bei pH 7) positiv geladene Variante eADF4(κ16) zu Mikro- und Nanopartikeln verarbeitet. Anschließend wurden diese Partikel vor allem im Hinblick auf Beladung mit Modellwirkstoffen, deren Freisetzung und die Aufnahme von beladenen Partikeln in eukaryotische Zellen, sowie ihre kolloidalen Eigenschaften analysiert. In den folgenden Abschnitten sollen hierzu die wichtigsten Ergebnisse und Schlussfolgerungen aus den einzelnen Publikationen dieses Teilbereichs zusammengefasst dargestellt werden.

3.1.1 Beladung und Freisetzung von Modellwirkstoffen mit unterschiedlichen Molekulargewichten und Ladung

Um das Anwendungsspektrum der rekombinanten Spinnenseidenproteinpartikel zu erweitern, wurden in Teilarbeit I (Kapitel 5) Partikel aus eADF4(κ16) erfolgreich hergestellt und deren Interaktion mit negativ geladenen Modellwirkstoffen getestet. Die Aufnahme und Freisetzung der Substanzen wurde unter verschiedenen Bedingungen untersucht und mit den entsprechenden Eigenschaften von eADF4(C16) Partikeln verglichen.

Zu diesem Zweck wurde zunächst fluoreszenzmarkierte, einzelsträngige DNA (Rho-ODN) als Modell für siRNA genutzt, um eine mögliche Verwendung von eADF4(κ16) Partikel im Bereich der Gentherapie zu bestätigen. Dabei konnte gezeigt

werden, dass die Partikel Rho-ODN aufnahmen und langsam, ohne initialen *Burst* (engl. *Burst* = Explosion; beschreibt hier eine sehr schnelle Freisetzung eines großen Teils der geladenen Modellwirkstoffe) wieder freizusetzten (Abbildung 15), wodurch starke elektrostatische Wechselwirkungen der kurzen Nukleinsäuremoleküle mit dem Trägermaterial unter physiologischen Bedingungen angenommen werden konnten (Abbildung 15C). Diese starken Wechselwirkungen, und somit die geringe Freisetzungsrate von Rho-ODN in den ersten Stunden, machen Partikel aus eADF4(κ16) zu einem geeigneten Träger für siRNA-Moleküle, da durch die Ausnutzung des EPR-Effekts der Großteil des Wirkstoffs erst am Wirkort freigesetzt wird.

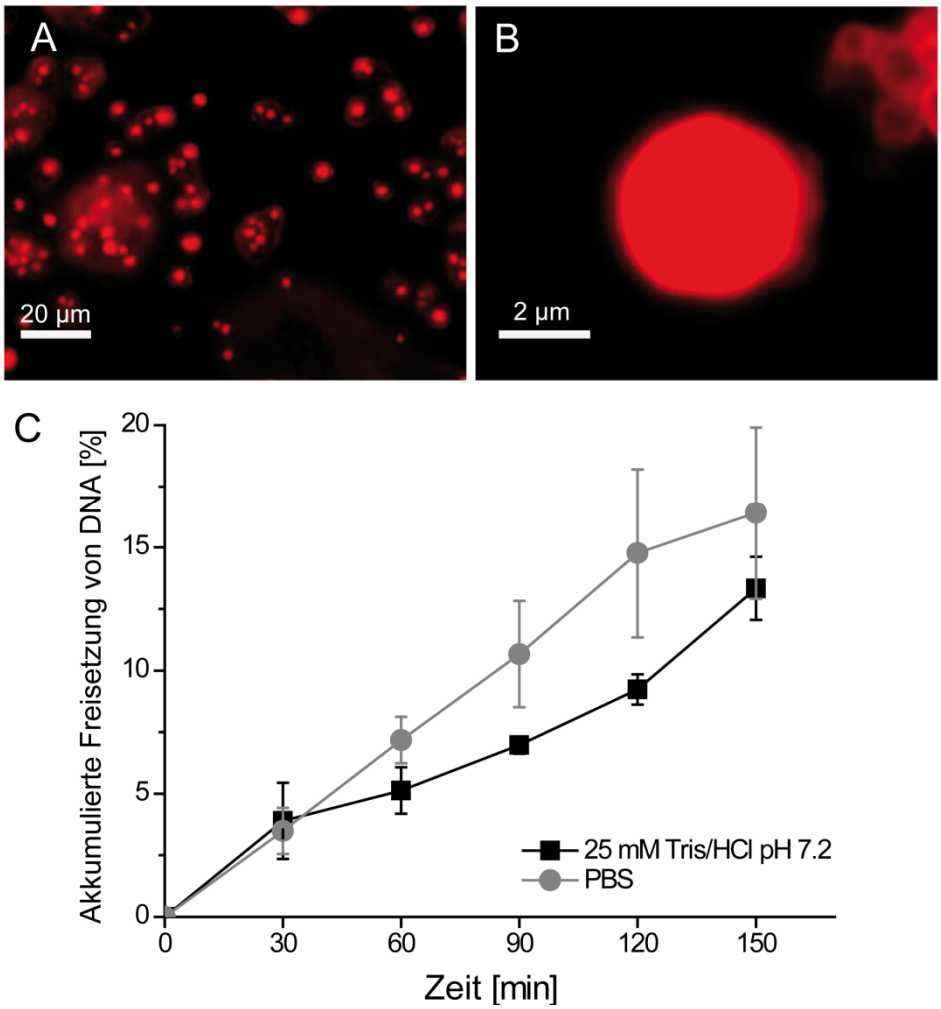

Abbildung 15: (A) und (B) Konfokalmikroskopische Aufnahme von eADF4(κ16) Partikeln mit fluoreszenzmarkierter DNA in zwei verschiedenen Auflösungen; (C) Auftragung der akkumulierten Freisetzung der fluoreszenzmarkierten DNA aus eADF4(κ16) Partikel im Zeitraum von 150 min unter zwei verschiedenen Pufferbedingungen. PBS = Phosphatgepufferte Salzlösung, Tris = Tris(hydroxymethyl)-aminomethan. Modifiziert nach *(254)* mit freundlicher Genehmigung von Elsevier aus E. Doblhofer, T. Scheibel, Engineering of Recombinant Spider Silk Proteins Allows Defined Uptake and Release of Substances. *Journal of pharmaceutical sciences* **104**, 988 (2015). Copyright (2015) Elsevier.

Zur Untersuchung der Interaktion kleiner Modellwirkstoffe mit der Spinnenseidenproteinmatrix in Partikeln wurden drei Farbstoffe gewählt: Das negativ geladene Carboxyfluorescein (CFl) und die beiden positiv geladenen Farbstoffe Acridinorange (AO) und Kristallviolett (CV). Die Modellsubstanzen wurden so ausgewählt, dass sie sich nur gering in Molekulargewicht und Hydrophobizität unterscheiden (Figure 3a, b, c, Teilarbeit I, Kapitel 5). Wie erwartet konnten die positiv geladenen Farbstoffe nur in anionischen eADF4(C16) Partikeln aufgenommen werden, während das negativ geladene CFl ausschließlich in Partikel aus eADF4(κ16) geladen werden konnten. Es ergaben sich jedoch trotz gleicher Ladungsverhältnisse der Farbstoffe zu den Proteinpartikeln unterschiedliche Beladungseffizienzen. Dies konnte zum einen auf eine unterschiedliche Molekülstruktur zurückgeführt werden, da das planare AO-Molekül im Gegensatz zu CFl und CV in die β-Faltblattstruktur der Proteinpartikel interkalieren konnte. Die Struktur von CFl und CV deutete im Gegensatz dazu darauf hin, dass eine weitere Aufnahme in die Partikel sterisch verhindert wird. Zum anderen konnte die unterschiedliche Beladungseffizienz auf eine abweichende Eindringtiefe der Proteinpartikel für das verwendete Lösungsmittel bezogen werden, was auch in Teilarbeit III (vgl. Abschnitt 3.1.3 und 5.2) gezeigt werden konnte.

Die Freisetzung der Farbstoffe wurde unter verschiedenen Salzbedingungen getestet. Dabei war festzustellen, dass die Freisetzung von CFl aus eADF4(κ16) Partikel sehr viel schneller von statten geht als die Freisetzung von AO oder CV aus eADF4(C16) Partikeln. Zusätzlich konnte gezeigt werden, dass die Freisetzung nicht nur von der Art des Partikels abhing, sondern auch von der Art des geladenen Farbstoffs. Besonders erwähnenswert ist dabei, dass zwar durch erhöhte Salzkonzentration eine beschleunigte Freisetzung der Modellsubstanzen stattfand, eine Konzentration von ≥ 400 mM Kaliumphosphatpuffer pH 7,5 aber zu einer deutlichen Reduktion der Freisetzung der Modellsubstanzen führte. Eine Behandlung der geladenen Partikel mit hohen Konzentrationen Kaliumphosphatpuffer führte jedoch nicht zu der erwarteten permanenten Verlangsamung der Modellwirkstoff-Freisetzung (Figure 4, Teilarbeit I, Kapitel 5).

Um eine gezielte Retardierung zu erreichen, wurden daraufhin CFl beladene eADF4(κ16) durch eine *Layer-by-Layer*-Beschichtung mit einer negativ geladenen eADF4(C16)-Hülle umgeben. Diese Beschichtung sollte in der Theorie durch elektrostatische Abstoßung ein Zurückhalten der Modellsubstanz im Partikel bewirken (*240*). Zwar wurde daraufhin gezeigt, dass beladene eADF4(κ16) Partikel erfolgreich mit

eADF4(C16) beschichtet werden konnten (Figure 7, Teilarbeit I, Kapitel 5), der gewünschte Effekt allerdings auch hierdurch nicht erreicht wurde. Die Freisetzung von CFl wurde entgegen der Erwartungen sogar noch weiter beschleunigt (Figure 8, Teilarbeit I, Kapitel 5).

Aus den in dieser Studie erhaltenen Ergebnissen lässt sich ablesen, dass keine pauschalen Aussagen über die Eignung von rekombinanten Spinnenseidenproteinpartikeln zum Transport von Wirkstoffen aus kleinen Molekülen auf Basis von elektrostatischen Wechselwirkungen getroffen werden kann, sondern diese für jeden Wirkstoff einzeln getestet werden muss. Jedoch können elektrostatische Wechselwirkungen sehr gut genutzt werden, um hochmolekulare Wirkstoffe, wie kurze DNA-Moleküle als Modell für siRNA, mit Hilfe von eADF4(κ16) Partikeln zu transportieren.

3.1.2 Auswirkungen von Beladung mit Modellwirkstoffen auf Partikeleigenschaften und Zellaufnahme

Die Aufnahme von Partikeln hergestellt aus eADF4(κ16), sowie aus eADF4(C16) und den N- bzw. C-terminal modifizierten Varianten eADF4(C16)RGD und eADF4(C16)R_8G, in HeLa-Zellen wurde bereits von Elsner *et al*. im Jahr 2015 getestet (*225*). Dabei konnte nachgewiesen werden, dass N- bzw. C-terminale Modifikationen von eADF4(C16) mit CPPs zu einer effizienteren Aufnahme der Partikel in HeLa-Zellen führte. Bemerkenswert war jedoch, dass vor allem bei der Verwendung von eADF4(κ16) als Partikelmatrix die Aufnahme verstärkt stattfand. Dies äußerte sich durch eine erhöhte Anzahl an Partikeln pro Zelle und durch einen höheren prozentualen Anteil an Zellen, die Spinnenseidenpartikel enthielten (*225*). In Teilarbeit II (Kapitel 5) wurde als Weiterführung der Veröffentlichung von Elsner *et al.* (2015) die Auswirkung einer Beladung der Partikel auf die zelluläre Aufnahme untersucht. Hierfür wurden Partikel aus dem Spinnenseidenprotein eADF4(κ16) mit der bereits in Teilarbeit I (Abschnitt 3.1.1 und 5.1) verwendeten Modell-DNA, in dieser Arbeit jedoch mit Fluoreszein markiert (Fl-ODN), beladen. Als Kontrollen wurden hier eADF4(C16), eADF4(C16)RGD und eADF4(C16)R_8G verwendet, die mit dem Fluoreszein-markiertem Polymer PEI (PEI-Fl) versehen wurden (vgl. Abschnitt 3.1.1).

Analysen der Partikelaufnahme in HeLa-Zellen zeigten bereits bei der geringsten Partikelbeladung leichte und bei höherer Beladung der Partikel signifikante Unterschiede (Abbildung 16). Davon ausgehend, dass positive Ladungen auf der Oberfläche die

Interaktionen der Partikel mit den Zellen fördern und somit zu einer erhöhten Aufnahme führen können, war zunächst wie erwartet zu beobachten, dass eine Beladung von eADF4(C16) und eADF4(C16)RGD mit dem polykationischen PEI-Fl zu einer erhöhten Aufnahmerate führte. In diesem Zusammenhang war es folglich ebenso wenig überraschend, dass eADF4(κ16) Partikel nach einer Beladung mit dem polyanionischen Fl-ODN weniger effizient in HeLa-Zellen aufgenommen wurden. Durch eine Beschichtung der beladenen eADF4(κ16) Partikel mit einer weiteren eADF4(κ16)-Schicht mittels LbL-Methode konnte dieser Effekt auf die zelluläre Partikelaufnahme jedoch nahezu gänzlich aufgehoben werden. Erstaunlich war jedoch, dass die zelluläre Aufnahme von PEI-Fl beladenen eADF4(C16)R_8G Partikeln drastisch reduziert war. Dabei ist anzumerken, dass durch die C-terminale Modifikation von eADF4(C16) mit dem CPP R_8 im unbeladenen Zustand eine Erhöhung der Aufnahmeeffizienz von Spinnenseidenpartikeln von ca. 17 % auf ca. 70 % stattfand (Table 2, Teilarbeit II, Kapitel 5). Da durch Zellviabilitätstests ausgeschlossen werden konnte, dass eine toxische Wirkung von beladenen Spinnenseidenproteinpartikeln vorlag (Fig. 3, Teilarbeit II, Kapitel 5), deutete das hier beschriebene Ergebnis darauf hin, dass eine Interaktion zwischen PEI-Fl und der R_8G-Sequenz für diese Entwicklung verantwortlich ist (Fig. 1, Teilarbeit II, Kapitel 5).

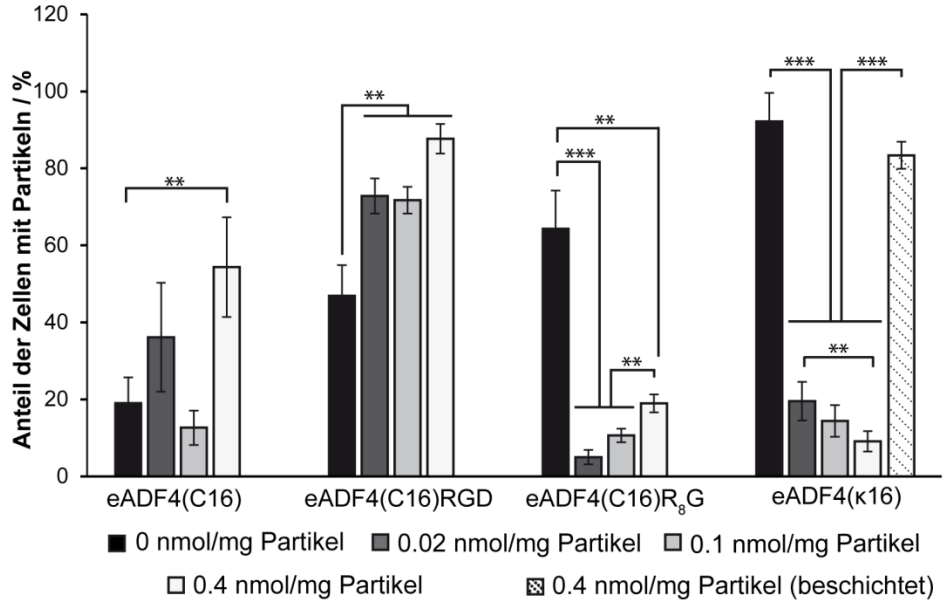

Abbildung 16: Analyse mittels Durchflusszytometrie von HeLa-Zellen, die in Anwesenheit von beladenen Spinnenseidenpartikeln inkubiert wurden. Die verwendeten Partikel aus eADF4(C16), eADF4(C16)RGD und eADF4(C16) wurden jeweils mit 0, 0.02, 0.1 und 0.4 nmol PEI-Fl und eADF4(κ16) mit 0, 0.02, 0.1 und 0.4 nmol Fl-ODN pro mg Partikel versehen. eADF4(κ16) Partikel, die mit 0.4 nmol Fl-ODN pro mg Partikel beladen waren wurden mit einer weiteren Schicht eADF4(κ16) umgeben (***hoch signifikant; ** signifikant). Modifiziert nach *(255)* mit freundlicher Genehmigung von *The Royal Chemical Society (RCS)* aus M. B. Schierling, E. Doblhofer, T. Scheibel, Cellular uptake of drug loaded spider silk particles. *Biomaterials Science* **4**, 1515 (2016). Copyright (2016) RCS.

Für eine Charakterisierung der Partikel und ein besseres Verständnis der veränderten zellulären Partikelaufnahmeeffizienz wurden ihre elektrophoretische Mobilität, sowie ihre kolloidale Stabilität getestet. Dabei stellte sich heraus, dass unabhängig von der Partikelart diese beiden Partikeleigenschaften durch eine Beladung nicht signifikant beeinflusst wurden (Table 1 und Fig. S2, Teilarbeit II, Kapitel 5). Analysen der endozytotischen Aufnahmewege der Partikel in die Zellen durch Verwendung von Dansylcadaverin (DC) zur Inhibition der Clathrin-vermittelten Endozytose und di-Methylamilorid (DMA) zur Inhibition des Macropinozytose konnte ebenfalls keine eindeutigen Veränderungen der Aufnahmeroute von beladenen Partikeln im Vergleich zu unbeladenen Partikeln vorweisen. Daher konnte zwar geschlussfolgert werden, dass durch Beladung von Spinnenseidenpartikeln die Aufnahmeeffizienz verändert wird, jedoch aus den vorliegenden Ergebnissen keine Ursache für diese Veränderungen gefunden werden.

LbL-beschichtete eADF4(κ16) Partikel wurden in Teilarbeit II (Kapitel 5) auch zum intrazellulären Transport von Doxorubicin (Dox) verwendet. Dox ist ein in der Krebstherapie häufig verabreichter Wirkstoff mit starken Nebenwirkungen und wurde in dieser Arbeit als therapeutisch relevante Modellsubstanz eingesetzt (*242*). Um einen Transport in der positiv geladenen Proteinmatrix von eADF4(κ16) zu ermöglichen, wurde Plasmid-DNA als Interaktionsvermittler zwischen Dox und eADF4(κ16) verwendet. Zur Überprüfung der Zytotoxizität von DNA/Dox-beladenen (und beschichteten) eADF4(κ16) Partikeln wurden HeLa-Zellen mit den entsprechenden Partikeln inkubiert. Als Kontrolle wurde jeweils freies Dox in gleicher Konzentration zu den Zellen gegeben. Dabei ergab sich, dass freies Dox nach 6 h keine Wirkung auf die Zellen ausübte, während nach 24 h die Zellviabilität in Anwesenheit von freiem Dox um nahezu 80 % reduziert war. Diese Wirkung konnte durch die Inkubation der Zellen mit DNA/Dox beladenen (und beschichteten) eADF4(κ16) Partikeln stark verzögert werden (Reduktion der Zellviabilität um 50 % nach 48 h). Dabei konnte durch vorhergehende Analyse gezeigt werden, dass Dox erst nach Behandlung der Partikel mit Proteasen aus dem DNA/Dox-eADF4(κ16) freigesetzt wurden, wodurch eine Aufnahme der Partikel für die Wirkung essenziell zu sein schien. Als Kontrolle wurden weitere Zelllinien (Neuroblastom-Zelllinie Kelly und Mausfibroblasten BALB/3T3) ebenso wie HeLa-Zellen mit DNA/Dox beladenen eADF4(κ16) Partikeln behandelt. Dabei zeigte sich, dass BALB/3T3 Zellen ähnlich wie HeLa-Zellen auf die Behandlung mit freiem Dox und dem DNA/Dox-eADF4(κ16)-

Komplex reagierten. Im Gegensatz dazu war die Reduktion der Kelly-Zellen erst nach 48 h im gleichen Maß ausgeprägt. Eine Erhöhung der Partikelkonzentration intensivierte auch in den beiden Kontrollzelllinien den zuvor beobachteten Effekt (Fig. 5, Teilarbeit II, Kapitel 5).

3.1.3 Charakterisierung der Partikel bezüglich elektrophoretischer Mobilität

Wie bereits beschrieben, können Partikel aus rekombinant hergestellten Spinnenseidenproteinen als mobile Transportsysteme für Wirkstoffe zur medikamentösen Behandlung von Patienten eingesetzt werden (*216, 227, 243*). Um jedoch auch kommerziell Anwendung zu finden, muss bei der Herstellung der Partikel eine gleichbleibende Qualität gewährleistet und diese zudem mit geeigneten Analysemethoden sichergestellt werden. Hierfür wurde in Teilarbeit III (Kapitel 5) die Bestimmung der Oberflächenchemie von rekombinanten Spinnenseidenproteinpartikeln gewählt. Dazu dienten zum einen die Bestimmung der elektrophoretischen Mobilitäten und zum anderen die Analyse der diffusen Schicht und sterischer Kräfte an der Oberfläche der Partikel durch *direct force* (engl. direkte Kraft) Messungen. Diese Methoden wurden gewählt, da der angewandte Herstellungsprozess und somit auch die oberflächenchemischen Eigenschaften der Partikel stark von einer großen Vielfalt an Parametern abhängt, die nur schwierig zu kontrollieren sind. Dazu gehören unter anderem Rührgeschwindigkeit und lokale Protein- bzw. Salzkonzentrationen.

Im Fokus dieser Arbeit lagen Partikel aus dem kationischen Spinnenseidenprotein eADF4(κ16), die durch Salzfällung mittels Dialyse hergestellt wurden (*223*). Als Kontrolle dienten Partikel aus eAF4(C16), die bereits in vorangehenden Studien analysiert wurden (*228*).

Durch die Messung der elektrophoretischen Mobilität μ beider Partikelarten in Abhängigkeit von pH und in drei verschiedenen ionischen Stärken des Lösungsmittels (I = 0,1 mM, I = 1,0 mM und I = 10 mM) konnten jeweils die PZM (engl. *point of zero mobility*, Nullpunkt der Mobilität) durch einen Vorzeichenwechsel der Messwerte empirisch festgelegt werden. Diese stimmten in beiden Fällen gut mit dem berechneten pI (isoelektrischer Punkt) der Proteinmoleküle überein (eADF4(κ16): pI = 9,7, PZM = 9,3-9,7; eADF4(C16): pI = 3,5, PZM = 3,5-4,0), wodurch eine gleichmäßige Verteilung der funktionellen Gruppen auf der Partikeloberfläche ähnlich zu deren Verteilung in den einzelnen Molekülen angenommen werden konnte.

Quantitative Analysen der elektrophoretischen Mobilität μ der Partikel aus rekombinanter Spinnenseide ergaben außerdem, dass eADF4(κ16) Partikel nur eine geringe Abhängigkeit von der Elektrolytkonzentration in Lösung zeigten. So ergaben sich für μ Werte zwischen 1,2 $m^2V^{-1}s^{-1}$ (I = 10 mM) und 1,5 $m^2V^{-1}s^{-1}$ (I = 0,1-1 mM) ($4 \leq pH \leq 8$). Eine so schwache Abhängigkeit der elektrophoretischen Mobilität von der ionischen Stärke der Umgebung wurde in klassischen Kolloiden bisher nur für weiche Partikel bei deutlich höheren Salzkonzentration ($I \geq 100$ mM) beobachtet. Dies deutete darauf hin, dass eADF4(κ16) Partikel nur wenig geladen sind und ihre elektrophoretische Mobilität von einer starken Penetration des elektroosmotischen Flusses in die Partikel bestimmt wurde (hohe Werte für $1/\lambda_0$; Theorie nach Ohshima und Duval (*244-246*); genauere Erläuterung siehe Teilarbeit I, Kapitel 5). Durch weitere quantitative Interpretation von μ konnte außerdem gezeigt werden, dass bei kleineren Ionenstärken eine Verringerung der Penetrationslänge $1/\lambda_0$ des elektroosmotischen Flusses von 11 nm auf 3 nm stattfand, wodurch ein Quellen des Materials bei geringen Ionenstärken angenommen werden musste. Die elektrophoretische Mobilität der anionischen eADF4(C16) Partikeln war im Gegensatz dazu von der ionischen Stärke ihrer Umgebung abhängig. So ergab sich Werte zwischen $\mu \approx$ -2,2 $m^2V^{-1}s^{-1}$ für I = 10 mM und $\mu \approx$ -2,9 $m^2V^{-1}s^{-1}$ für I = 0,1-1 mM ($pH \geq 6$). Die Penetrationslänge des elektroosmotischen Flusses blieb im Gegensatz zu eADF4(κ16) gleich ($1/\lambda_0 = 17$).

Die Tatsache, dass nur die äußeren Bereiche der Spinnenseidenpartikel für ihr Verhalten im elektrischen Feld verantwortlich gemacht werden konnte, wurde auch durch die elektrokinetische Untersuchung *Layer by Layer* beschichteten Partikel verifiziert. Dabei wurden die kationischen Spinnenseidenpartikel mittels elektrostatischer Wechselwirkungen mit einer eADF4(C16)-Schicht versehen bzw. anionische Spinnenseidenpartikel mit einer eADF4(κ16)-Schicht (*240*). Dabei konnte gezeigt werden, dass die elektrophoretische Mobilität von eADF4(C16) beschichteten eADF4(κ16) Partikeln über den gemessenen pH-Bereich sehr gut mit den μ-Werten von unbeschichteten eADF4(κ16) übereinstimmten. Dies traf ebenfalls auf eADF4(κ16) beschichtete eADF4(C16) Partikel zu, die ähnliche Werte wie unbeschichtete eADF4(C16) Partikel zeigten. Einzig am PZM der äußeren Partikelschicht ergaben sich in beiden Fällen größere Abweichungen, was gut nachvollziehbar ist, da an diesem Punkt, dem pI des jeweiligen Proteins an der Oberfläche, durch die Neutralisierung der äußeren Schicht die

elektrophoretischen Eigenschaften der zugrundeliegenden Partikel zum Tragen kamen (Abbildung 17).

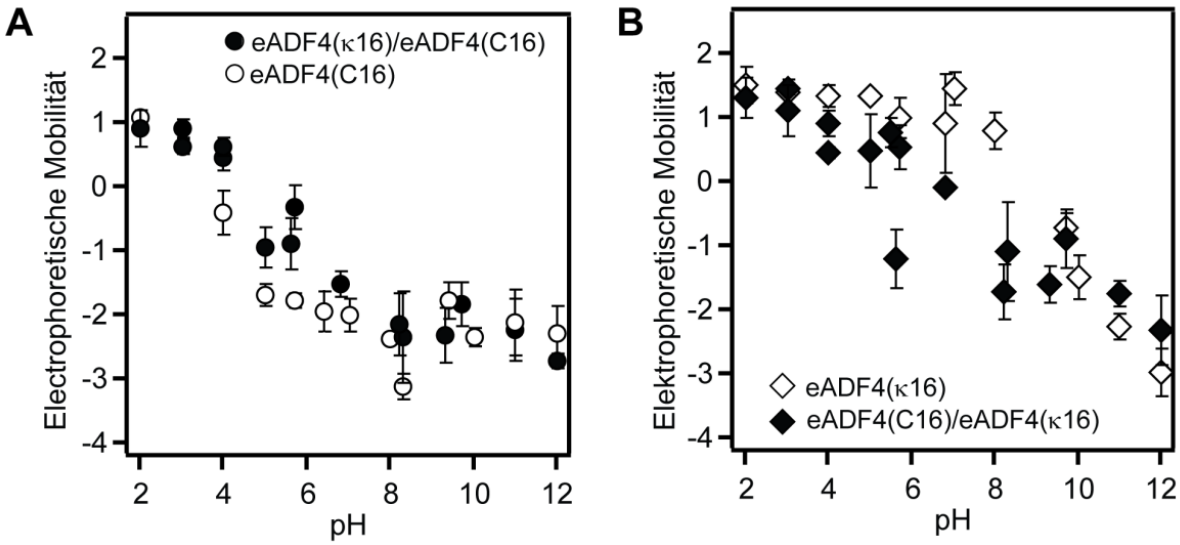

Abbildung 17: Elektrophoretischen Mobilität der *Layer-by-Layer* beschichteten Spinnenseidenproteinpartikel im Vergleich zu entsprechenden unbeschichteten Spinnenseidenproteinpartikeln. (A) eADF4(κ16) Partikel mit eADF4(C16)-Beschichtung (gefüllte Symbole) im Vergleich mit eADF4(C16) Partikel (offene Symbole) (B) eADF4(C16) Partikel mit eADF4(κ16)-Beschichtung (gefüllte Symbole) im Vergleich mit eADF4(κ16) Partikel (offene Symbole). Modifiziert nach *(256)* mit freundlicher Genehmigung von *American Chemical Society (ACS)* aus N. Helfricht, E. Doblhofer, J. F. L. Duval, T. Scheibel, G. Papastavrou, Colloidal Properties of Recombinant Spider Silk Protein Particles. *The Journal of Physical Chemistry C* **120**, 18015 (2016). Copyright (2016) ACS.

Zusätzlich zu den Ergebnissen der elektrokinetischen Analysen bestätigten *direct force*-Messungen die geringe Ladung der Proteinpartikel und deren flaumartige, peripher poröse Struktur, die von starken sterischen Kräften verursacht wird (bürstenähnliche Struktur). Durch die Anwendung der CP (engl. *colloidal probe* = kolloidale Sonde) - Methode und der FluidFM-Technik konnte in Teilarbeit III gezeigt werden, dass die Partikel aus rekombinanter Spinnenseide relativ weich waren. Dadurch konnte keine eindeutige Aussage über eine definierte Debye-Länge (κ^{-1}) gemacht werden (Figure 7, Teilarbeit III, Kapitel 5). Durch Anwendung der Alexander-deGennes-Theorie (AdG) auf die erhaltenen Kraft-Abstands-Kurven, die zwar für bürstenartige Strukturen ungeladener Polymere entwickelt wurde, konnte auch für die beiden hier getesteten Partikelarten die durchschnittlichen Abstände der Ankerpunkte (*s*) der einzelnen vorstehenden Peptide bestimmt werden. Diese waren für beide Partikelarten mit *s* (eADF4(κ16)) = 4,8 ± 1 nm und *s* (eADF4(C16)) = 6,7 ± 3,7 nm sehr ähnlich. Wesentlich größere Unterschiede der beiden Partikelarten ergaben sich bei der Bestimmung der Bürstenlängen (*L*) in den einzelnen Partikelarten. Mit *L* = 321 ± 87 nm zeigten Partikel aus eADF4(C16) eine

wesentlich größere Bürstenlänge als Partikel aus eADF4(κ16) mit $L = 192 \pm 47$ nm. Dies ist in gutem Einklang mit den Ergebnissen für $1/\lambda_0$, da die mittlere Penetrationslänge des elektroosmotischen Flusses ebenfalls für eADF4(C16) Partikel größer war als für eADF4(κ16) Partikel, was auf eine erhöhte Lösungsmittelaufnahme in den anionischen Proteinpartikeln hinweist. Die Bürstenlängen von eADF4(C16) in dieser Arbeit weichen allerdings sehr stark von den zuvor gemessenen *L*-Werten ab. Dies ist vor allem auf ein nicht automatisiertes Herstellungsverfahren zurückzuführen und zeigt, dass durch die hier durchgeführten Methoden sehr gut die Unterschiede verschiedener Herstellungschargen analysiert werden kann.

3.2 Spinnenseide als Matrix in Barriere-Beschichtungen

Die Entwicklung von einfach zu verarbeitenden Barriere-Beschichtungen, die Sauerstoff und Wasserdampf an der Diffusion in die Verpackung hindern, bieten einen großen Nutzen für Industrie und Verbraucher. Im Bereich der Lebensmittelverpackungen spielt es jedoch auch eine große Rolle, dass möglichst gut verträgliche, sowie Halogen- und Schwermetall-freie Materialien für diesen Zweck verwendet werden (*247, 248*).

Rekombinante Spinnenseidenproteine bieten unter diesem Gesichtspunkt die idealen Voraussetzungen als Matrix für eben solche Barriere-Beschichtungen eingesetzt zu werden. Daher wurde in dieser Arbeit (Teilarbeit IV, Kapitel 5) ein einfaches, wasserbasiertes Verfahren entwickelt, ein Nanokomposit-Material aus dem kationischen Spinnenseidenprotein eADF4(κ16) als Matrix und dem Schichtsilikat Natrium-Fluorohektorit (Na-hec), als Füllstoff, herzustellen. Dies folgt einem bereits bekannten Prinzip, in dem durch flache, undurchlässige Füllstoff-Plättchen, wie z.B. Schichtsilikate, in einem Nanokomposit die Durchlässigkeit verschiedener Substanzen unspezifisch durch die Verlängerung des Diffusionsweges reduziert wird (vgl. Abbildung 3, Seite 12) (*26*).

Die Herstellung des Nanokomposits verlief in dieser Arbeit wie folgt (Abbildung 18): In einem ersten Schritt wurde Na-hec in MQ-H_2O dispergiert und dabei durch die Hydratisierung der Zwischenschichtionen die einzelnen Plättchen vollständig delaminiert. Im Anschluss daran folgte eine Anpassung der Oberflächenenergie der Schichtsilikatplättchen durch Ionenaustausch der Zwischenschichtkationen Na^+ gegen die Aminosäure L-Lysin (Lys-hec) (*249, 250*). Diese Modifikation wurde benötigt, um im nächsten Schritt, der Compounding von eADF4(κ16) und Lys-hec (Gewichtsverhältnis: 62 % Hektorit, 38 % eADF4(κ16)), eine moderate Interaktion zwischen dem positiv geladenen Spinnenseidenprotein und den negativ geladenen Füllstoffplättchen hervorzurufen, wodurch zwar eine großflächige Interaktion, jedoch keine vorzeitige Präzipitation der einzelnen Komponenten stattfand. Durch das Gießen des wässrigen Materialgemischs auf ein Substrat und langsames Trocknen konnte abschließend das gewünschte Bio-Nanokomposit erhalten werden.

Die entstandenen lamellaren Strukturen waren dabei den parallelen Anordnungen der Hektorit-Plättchen geschuldet, die sich während des Selbstassemblierungsprozesses der Spinnenseide (Konversion von überwiegend Random-Coil zu β-Sheet Sekundärstrukturelementen, Fig. 2A, Teilarbeit IV, Kapitel 5) aufgrund ihres großen

Aspekt-Verhältnisses (ca. 20000) und dem hohen Massenanteil (62 %) parallel zur Substratoberfläche anordneten (Abbildung 18) (*163*). In dieser Arbeit wurde aufgrund der Vergleichbarkeit mit anderen kommerziell erhältlichen, Barriere-beschichteten Verpackungsmaterialien PET als Substrat verwendet.

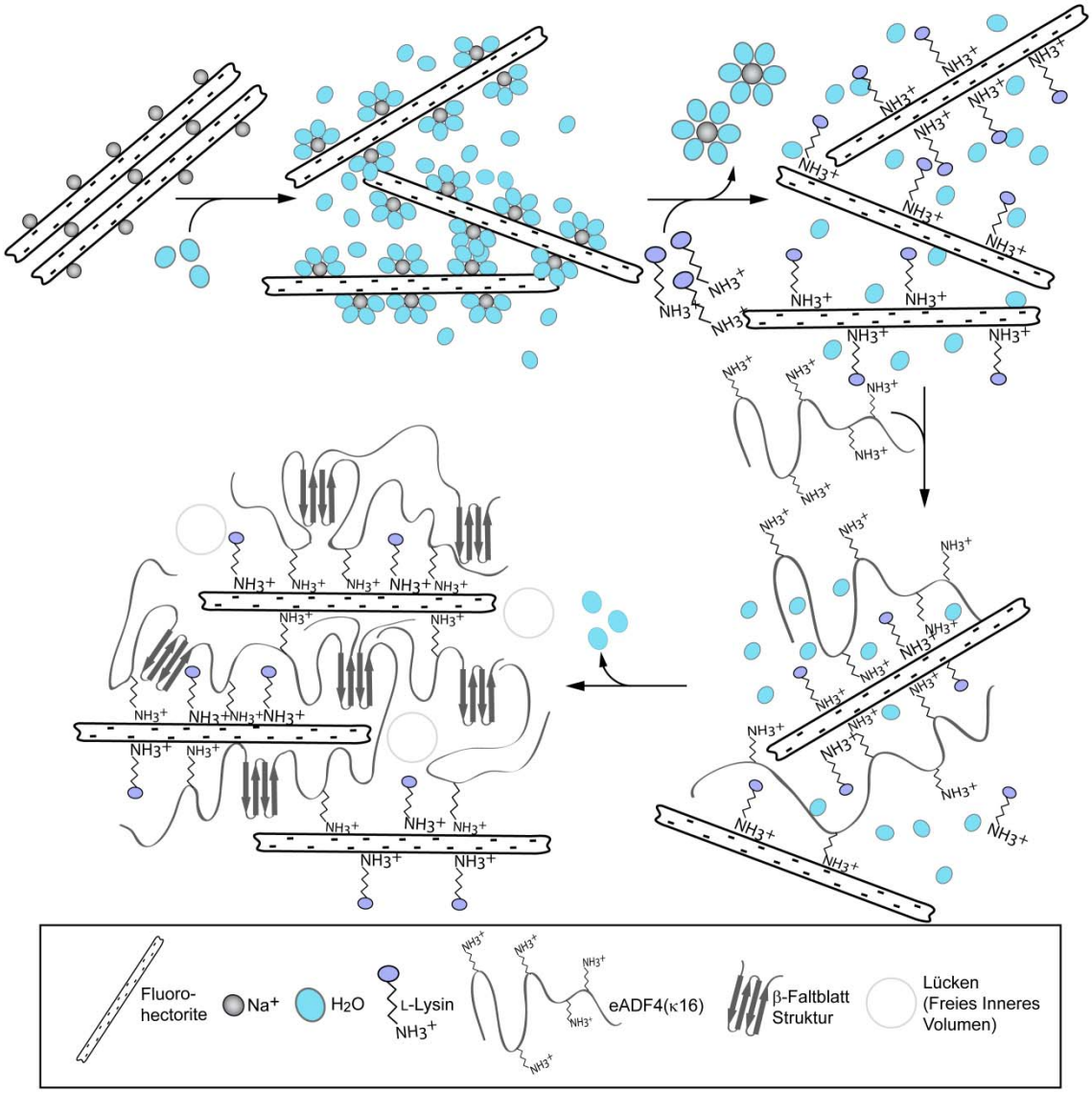

Abbildung 18: Herstellungsschritte der Nanokomposit-Barriere-Beschichtung aus wässriger Verarbeitung. Modifiziert nach *(257)* mit freundlicher Genehmigung von *American Chemical Society (ACS)* aus E. Doblhofer *et al.*, Structural Insights into Water-Based Spider Silk Protein–Nanoclay Composites with Excellent Gas and Water Vapor Barrier Properties. *ACS Appl Mater Interfaces* **8**, 25535 (2016). Copyright (2016) ACS.

Zur Charakterisierung des Bio-Nanokomposits wurde zunächst die Güte der Kristallstruktur des Materials durch PXRD (engl. *Powder X-ray diffraction* = Pulver-Röntgen-Diffraktometrie) untersucht. Dabei konnte auch der Zuwachs des Zwischenschichtabstands in den einzelnen Stufen des Herstellungsprozesses verfolgt

werden (Fig. 1B, Teilarbeit IV, Kapitel 5). Abzüglich der van-der-Waals Schicht des Hectorits von 0,96 nm und der Schichtdicke der Lysin-Modifikation konnte aus den PXRD-Messungen eine eADF4(κ16)-Schicht von 1,10 nm berechnet werden. Durch Messungen bei erhöhter relativer Luftfeuchte (Fig. 1B, Teilarbeit IV) konnte außerdem durch die PXRD-Messungen festgestellt werden, dass eine geringe Menge Wasser aus der Umgebung im Material aufgenommen wurde. Dies zeigt sich durch eine Quellung der Zwischenschicht von einer Dicke von 2,5 nm auf 2,7 nm.

Die Proteinsekundärstrukturanalyse mittels FTIR (Fourier transformierte Infrarot) Spektroskopie in Kombination mit FSD (engl. *Fourier self-deconvolution* = Fourier Selbstentfaltung), bei der anhand der Amid I Bande (1600-1700 cm^{-1}, C=O-Streckschwingung des Amidrückrads) die Anteile einzelner Sekundärstrukturen in einem Protein bestimmt werden, konnte des Weiteren gezeigt werden, dass die Proteinmatrix im hier hergestellten Bio-Nanokomposit zu ca. 28 % β-Faltblatt-Strukturen einnimmt, während dieser Anteil in unbehandelten eADF4(κ16)-Filmen (gegossen aus Ameisensäurelösung) nur bei ca. 17 % lag (Fig. 2A, Teilarbeit IV, Kapitel 5) (*236, 251*). Ein erhöhter β-Faltblattanteil ist hierbei von großer Bedeutung, um eine erhöhte chemische und thermische Stabilität durch gute inter- und intramolekulare Wechselwirkungen zu gewährleisten (*236*). Diese Stabilität konnte daraufhin in Thermogravimetrischer Analyse, Dynamischer Differenzkalorimetrie und Abbauanalysen des Bio-Nanokomposits in Wasser, 70 % Ethanol und 1 % Ameisensäure bestätigt werden (Fig. 3A, B und C, Teilarbeit VI, Kapitel 5). Neben Proteinstrukturaufklärung konnte in dieser Arbeit FTIR–Spektroskopie auch zur Detektion der Interaktion zwischen eADF4(κ16) und den Schichtsilikaten genutzt werden. Durch IR-Absorption der Hektorit *in-plane* Si-O Bindungen bei 1003 cm^{-1} (Maximum) und der Hektorit *out-of-plane* Si-O Bindungen bei 1080 cm^{-1} (Schulter) konnten zunächst eindeutig die verwendeten Schichtsilikatplättchen als Na-hec identifiziert werden. Bei der Analyse des hier entwickelten Bio-Nanokomposits konnte daraufhin durch eine Verschiebung des Absorptions-Maximums von 1003 cm^{-1} und der Schulter bei 1080 cm^{-1} hin zu kleineren Wellenzahlen eine gute Interaktion der Matrix mit dem Füllstoff nachgewiesen werden (Fig. 2B, Teilarbeit IV, Kapitel 5) (*252, 253*).

Durch die Messung von OTR (engl. *Oxygen Transmission Rate* = Sauerstofftransmissionsrate) und WVTR (engl. *Water Vapor Transmission Rate* = Wasserdampftransmissionsrate) kann die Diffusion von Sauerstoff und Wasserdampf durch verschiedene Materialien getestet werden. Durch diese Methode

konnte hier gezeigt werden, dass die Beschichtung von PET-Folien mit dem Spinnenseiden-Hektorit-Nanokomposit zu einer Reduktion der OTR um ca. 90 % ($2{,}32 \pm 0{,}38$ $cm^3 \cdot m^{-2} \cdot d^{-1}$) und der WVTR um 96 % ($0{,}18 \pm 0{,}05$ $g \cdot m^{-2} \cdot d^{-1}$) gegenüber dem unbeschichteten Substrat (PET OTR: $22{,}3 \pm 0{,}33$ $cm^3 \cdot m^{-2} \cdot d^{-1}$, PET WVTR: $4{,}20 \pm 0{,}64$ $g \cdot m^{-2} \cdot d^{-1}$) führte (Fig. 6, Teilarbeit IV, Kapitel 5). Bemerkenswert ist hier vor allem, dass die Barriere-Beschichtung zu einer starken Reduktion der WVTR führte, obwohl die Herstellung aus einem wässrigen System und ohne Additive stattfand.

4 Literaturverzeichnis

1. A. L. Andrady, M. A. Neal, Applications and societal benefits of plastics. *Philosophical Transactions of the Royal Society of London B: Biological Sciences* **364**, 1977 (2009).

2. R. C. Thompson, C. J. Moore, F. S. vom Saal, S. H. Swan, Plastics, the environment and human health: current consensus and future trends. *Philos T R Soc B* **364**, 2153 (2009).

3. E. J. North, R. U. Halden, Plastics and environmental health: the road ahead. *Reviews on environmental health* **28**, 1 (2013).

4. R. C. Thompson, S. H. Swan, C. J. Moore, F. S. vom Saal, Our plastic age. *Philos T R Soc B* **364**, 1973 (2009).

5. P. Europe, "Plastic - The Facts 2010 An analysis of European plastics production, demand and recovery for 2009" (Plastics Europe, 2010).

6. PlasticsEurope, "Plastics – the Facts 2015 An analysis of European plastics production, demand and waste data" (Association of Plastic Manufacturers Europe, Brüssel, 2016).

7. P. N. Europe. (2015).

8. Jürgen Dispan, M. Vassiliadis, "Kunstoffverarbeitung in Deutschland - Branchenanalyse" (Industriegewerkschaft Bergbau, Chemie, Energie VB 1 – Gesamtleitung/Globalisierung/Industrie, Hannover, 2014).

9. D. K. A. Barnes, F. Galgani, R. C. Thompson, M. Barlaz, Accumulation and fragmentation of plastic debris in global environments. *Philosophical Transactions of the Royal Society of London B: Biological Sciences* **364**, 1985 (2009).

10. M. R. Gregory, Environmental implications of plastic debris in marine settings—entanglement, ingestion, smothering, hangers-on, hitch-hiking and alien invasions. *Philosophical Transactions of the Royal Society of London B: Biological Sciences* **364**, 2013 (2009).

11. L. Robinson, R. Miller, The Impact of Bisphenol A and Phthalates on Allergy, Asthma, and Immune Function: a Review of Latest Findings. *Curr Environ Health Rep* **2**, 379 (2015).

12. T. Mekonnen, P. Mussone, H. Khalil, D. Bressler, Progress in bio-based plastics and plasticizing modifications. *J Mater Chem A* **1**, 13379 (2013).

13. J. A. Ivar do Sul, M. F. Costa, The present and future of microplastic pollution in the marine environment. *Environmental Pollution* **185**, 352 (2014).

14. J. H. Song, R. J. Murphy, R. Narayan, G. B. H. Davies, Biodegradable and compostable alternatives to conventional plastics. *Philos T R Soc B* **364**, 2127 (2009).

15. P. M. Lemieux, C. C. Lutes, J. A. Abbott, K. M. Aldous, Emissions of Polychlorinated Dibenzo-p-dioxins and Polychlorinated Dibenzofurans from the Open Burning of Household Waste in Barrels. *Environ Sci Technol* **34**, 377 (2000).

16. S. Salmaso, P. Caliceti, Stealth Properties to Improve Therapeutic Efficacy of Drug Nanocarriers. *Journal of Drug Delivery* **2013**, 374252 (2013).

17. R. Langer, 1994 whitaker lecture: Polymers for drug delivery and tissue engineering. *Ann Biomed Eng* **23**, 101 (1995).

18. P. V. Devarajan, S. Jain, *Targeted Drug Delivery: Concepts and Design*. (Springer, 2015).

19. Q. Yang *et al.*, Accelerated drug release and clearance of PEGylated epirubicin liposomes following repeated injections: a new challenge for sequential low-dose chemotherapy. *International Journal of Nanomedicine* **8**, 1257 (2013).

20. D. A. Herold, K. Keil, D. E. Bruns, Oxidation of polyethylene glycols by alcohol dehydrogenase. *Biochemical Pharmacology* **38**, 73 (1989).

21. F. M. Veronese, G. Pasut, PEGylation, successful approach to drug delivery. *Drug Discovery Today* **10**, 1451 (2005).

22. J. Gustavsson, C. Cederberg, U. Sonesson, R. v. Otterdijk, A. Meybeck, "Global food losses and food waste" (Food and Agriculture Organization of the United Nations, Rome, 2011).

23. V. Nordrhein-Westfalen, "Lebensmittelverschwendung und Mindesthaltbarkeitsdatum Position und Forderungen der Verbraucherzentrale NRW" (Düsseldorf, 2012).

24. A. I. Alateyah, H. N. Dhakal, Z. Y. Zhang, Processing, Properties, and Applications of Polymer Nanocomposites Based on Layer Silicates: A Review. *Advances in Polymer Technology* **32**, (2013).

25. D. Gunasekera, Food production: Cut food waste to help feed world. *Nature* **524**, 415 (2015).

26. A. Arora, G. W. Padua, Review: Nanocomposites in Food Packaging. *J Food Sci* **75**, R43 (2010).

27. C. Bach, X. Dauchy, M.-C. Chagnon, S. Etienne, Chemical compounds and toxicological assessments of drinking water stored in polyethylene terephthalate (PET) bottles: A source of controversy reviewed. *Water Research* **46**, 571 (2012).

28. R. W. G. van Willige, J. P. H. Linssen, M. B. J. Meinders, H. J. van der Stege, A. G. J. Voragen, Influence of flavour absorption on oxygen permeation through

LDPE, PP, PC and PET plastics food packaging. *Food Additives and Contaminants Part a-Chemistry Analysis Control Exposure & Risk Assessment* **19**, 303 (2002).

29. T. Iwata, Biodegradable and Bio-Based Polymers: Future Prospects of Eco-Friendly Plastics. *Angewandte Chemie International Edition* **54**, 3210 (2015).

30. H.-J. Endres, A. Siebert-Raths, Technische Biopolymere. *Rahmenbedingungen, Marktsituation, Herstellung, Aufbau und Eigenschaften. 1st ed. München: Hanser*, (2009).

31. X. Kornmann, H. Lindberg, L. A. Berglund, Synthesis of epoxy-clay nanocomposites. Influence of the nature of the curing agent on structure. *Polymer* **42**, 4493 (2001).

32. K. Yano, A. Usuki, A. Okada, T. Kurauchi, O. Kamigaito, Synthesis and Properties of Polyimide Clay Hybrid. *Journal of Polymer Science Part a-Polymer Chemistry* **31**, 2493 (1993).

33. M. Jamshidian, E. A. Tehrany, M. Imran, M. Jacquot, S. Desobry, Poly-Lactic Acid: Production, Applications, Nanocomposites, and Release Studies. *Comprehensive Reviews in Food Science and Food Safety* **9**, 552 (2010).

34. A. K. Mohanty, M. Misra, G. Hinrichsen, Biofibres, biodegradable polymers and biocomposites: An overview. *Macromol Mater Eng* **276**, 1 (2000).

35. V. P. Cyras, C. M. Soledad, V. Analia, Biocomposites based on renewable resource: Acetylated and non acetylated cellulose cardboard coated with polyhydroxybutyrate. *Polymer* **50**, 6274 (2009).

36. C. Bastioli, *Handbook of biodegradable polymers*. (iSmithers Rapra Publishing, 2005).

37. S. Nitta, K. Numata, Biopolymer-Based Nanoparticles for Drug/Gene Delivery and Tissue Engineering. *International Journal of Molecular Sciences* **14**, 1629 (2013).

38. M. M. Reddy, S. Vivekanandhan, M. Misra, S. K. Bhatia, A. K. Mohanty, Biobased plastics and bionanocomposites: Current status and future opportunities. *Progress in Polymer Science* **38**, 1653 (2013).

39. A. Gennadios, *Protein-based films and coatings*. (CRC Press, 2002).

40. A. Jerez, P. Partal, I. Martinez, C. Gallegos, A. Guerrero, Protein-based bioplastics: effect of thermo-mechanical processing. *Rheol Acta* **46**, 711 (2007).

41. S. Domenek, P. Feuilloley, J. Gratraud, M.-H. Morel, S. Guilbert, Biodegradability of wheat gluten based bioplastics. *Chemosphere* **54**, 551 (2004).

42. J. Heller, Polymers for controlled parenteral delivery of peptides and proteins. *Advanced Drug Delivery Reviews* **10**, 163 (1993).

43. A. O. Elzoghby, W. M. Samy, N. A. Elgindy, Protein-based nanocarriers as promising drug and gene delivery systems. *Journal of Controlled Release* **161**, 38 (2012).

44. J. W. Lawton, Zein: A history of processing and use. *Cereal Chemistry* **79**, 1 (2002).

45. P. B. Malafaya, G. A. Silva, R. L. Reis, Natural–origin polymers as carriers and scaffolds for biomolecules and cell delivery in tissue engineering applications. *Advanced Drug Delivery Reviews* **59**, 207 (2007).

46. R. Nakamura, A. N. Netravali, A. B. Morgan, M. R. Nyden, J. W. Gilman, Effect of halloysite nanotubes on mechanical properties and flammability of soy protein based green composites. *Fire and Materials* **37**, 75 (2013).

47. S. Chabba, A. N. Netravali, 'Green' composites Part 1: Characterization of flax fabric and glutaraldehyde modified soy protein concentrate composites. *Journal of Materials Science* **40**, 6263 (2005).

48. A. N. Netravali, S. Chabba, Composites get greener. *Materials Today* **6**, 22 (2003).

49. S. Chabba, A. N. Netravali, 'Green' composites Part 2: Characterization of flax yarn and glutaraldehyde/poly(vinyl alcohol) modified soy protein concentrate composites. *Journal of Materials Science* **40**, 6275 (2005).

50. P. Lodha, A. N. Netravali, Characterization of Phytagel® modified soy protein isolate resin and unidirectional flax yarn reinforced "green" composites. *Polymer Composites* **26**, 647 (2005).

51. X. Huang, A. N. Netravali, Environmentally Friendly Green Materials from Plant-Based Resources: Modification of Soy Protein using Gellan and Micro/Nano-Fibrillated Cellulose. *Journal of Macromolecular Science, Part A* **45**, 899 (2008).

52. P. Lodha, A. N. Netravali, Characterization of interfacial and mechanical properties of "green" composites with soy protein isolate and ramie fiber. *Journal of Materials Science* **37**, 3657 (2002).

53. P. Lodha, A. N. Netravali, Characterization of stearic acid modified soy protein isolate resin and ramie fiber reinforced 'green' composites. *Composites Science and Technology* **65**, 1211 (2005).

54. X. Huang, A. Netravali, Characterization of flax yarn and flax fabric reinforced nanoclay modified soy protein resin green composites. *Compos. Sci. Technol* **67**, 2005 (2007).

55. S. Khosravi, F. Khabbaz, P. Nordqvist, M. Johansson, Protein-based adhesives for particleboards. *Industrial Crops and Products* **32**, 275 (2010).

56. Z. Peles, M. Zilberman, Novel soy protein wound dressings with controlled antibiotic release: Mechanical and physical properties. *Acta Biomater* **8**, 209 (2012).

57. H. Tian, Processing and properties of soy protein/silica nanocomposites fabricated in situ synthesis. *Journal of Composite Materials*, (2011).

58. M. Santin, L. Ambrosio, Soybean-based biomaterials: preparation, properties and tissue regeneration potential. *Expert Review of Medical Devices* **5**, 349 (2008).

59. B. Liu, L. Jiang, H. Liu, J. Zhang, Synergetic Effect of Dual Compatibilizers on in Situ Formed Poly(Lactic Acid)/Soy Protein Composites. *Industrial & Engineering Chemistry Research* **49**, 6399 (2010).

60. Y. Otani, Y. Tabata, Y. Ikada, Hemostatic capability of rapidly curable glues from gelatin, poly(L-glutamic acid), and carbodiimide. *Biomaterials* **19**, 2091 (1998).

61. L. Chen, M. Subirade, Elaboration and Characterization of Soy/Zein Protein Microspheres for Controlled Nutraceutical Delivery. *Biomacromolecules* **10**, 3327 (2009).

62. B. Lagrain, B. Goderis, K. Brijs, J. A. Delcour, Molecular Basis of Processing Wheat Gluten toward Biobased Materials. *Biomacromolecules* **11**, 533 (2010).

63. N. Gontard, S. Guilbert, J. L. CUQ, Water and glycerol as plasticizers affect mechanical and water vapor barrier properties of an edible wheat gluten film. *J Food Sci* **58**, 206 (1993).

64. R. M. Dicharry *et al.*, Wheat Gluten−Thiolated Poly(vinyl alcohol) Blends with Improved Mechanical Properties. *Biomacromolecules* **7**, 2837 (2006).

65. T. Kunanopparat, P. Menut, M. H. Morel, S. Guilbert, Reinforcement of plasticized wheat gluten with natural fibers: From mechanical improvement to deplasticizing effect. *Composites Part A: Applied Science and Manufacturing* **39**, 777 (2008).

66. X. Zhang, M. D. Do, K. Dean, P. Hoobin, I. M. Burgar, Wheat-Gluten-Based Natural Polymer Nanoparticle Composites. *Biomacromolecules* **8**, 345 (2007).

67. A. Papadopoulou, R. A. Frazier, Characterization of protein–polyphenol interactions. *Trends in Food Science & Technology* **15**, 186 (2004).

68. J. Taylor, J. O. Anyango, J. R. Taylor, Developments in the science of zein, kafirin, and gluten protein bioplastic materials. *Cereal Chemistry* **90**, 344 (2013).

69. P. Pontieri *et al.*, Sorghum, a Healthy and Gluten-free Food for Celiac Patients As Demonstrated by Genome, Biochemical, and Immunochemical Analyses. *J Agric Food Chem* **61**, 2565 (2013).

70. K. Bruyninckx, K. J. A. Jansens, B. Goderis, J. A. Delcour, M. Smet, Removal of disulfide cross-links from wheat gluten and the effect thereof on the mechanical properties of rigid gluten bioplastic. *European Polymer Journal* **68**, 573 (2015).

71. C. Diao, H. Xia, R. S. Parnas, Wheat Gluten Blends with Maleic Anhydride-Functionalized Polyacrylate Cross-Linkers for Improved Properties. *ACS Appl Mater Interfaces* **7**, 22601 (2015).

72. A. Gennadios, H. Park, C. L. Weller, Relative humidity and temperature effects on tensile strength of edible protein and cellulose ether films. *Biological Systems Engineering: Papers and Publications*, 91 (1993).

73. J. Jane, S. Lim, I. Paetau, K. Spence, S. Wang, Biodegradable plastics made from agricultural biopolymers. (1994).

74. N. Parris, D. R. Coffin, Composition Factors Affecting the Water Vapor Permeability and Tensile Properties of Hydrophilic Zein Films. *J Agric Food Chem* **45**, 1596 (1997).

75. M. Zhang, C. A. Reitmeier, E. G. Hammond, D. J. Myers, Production of Textile Fibers from Zein and a Soy Protein-Zein Blend 1. *Cereal Chemistry* **74**, 594 (1997).

76. J. Dong, Q. Sun, J.-Y. Wang, Basic study of corn protein, zein, as a biomaterial in tissue engineering, surface morphology and biocompatibility. *Biomaterials* **25**, 4691 (2004).

77. S. Gong, H. Wang, Q. Sun, S.-T. Xue, J.-Y. Wang, Mechanical properties and in vitro biocompatibility of porous zein scaffolds. *Biomaterials* **27**, 3793 (2006).

78. L. Lai, H. Guo, Preparation of new 5-fluorouracil-loaded zein nanoparticles for liver targeting. *International Journal of Pharmaceutics* **404**, 317 (2011).

79. L. Liu, M. L. Fishman, K. B. Hicks, M. Kende, G. Ruthel, Pectin/zein beads for potential colon-specific drug delivery: synthesis and in vitro evaluation. *Drug delivery* **13**, 417 (2006).

80. G. W. Padua, Q. Wang, Y. Wang, in *NSTI-Nanotech*. (2010), vol. 3, pp. 202-205.

81. H.-J. Wang, Z.-X. Lin, X.-M. Liu, S.-Y. Sheng, J.-Y. Wang, Heparin-loaded zein microsphere film and hemocompatibility. *Journal of Controlled Release* **105**, 120 (2005).

82. Y. Wang, L. Chen, Electrospinning of prolamin proteins in acetic acid: the effects of protein conformation and aggregation in solution. *Macromol Mater Eng* **297**, 902 (2012).

83. Z.-H. Qu *et al.*, Evaluation of the zein/inorganics composite on biocompatibility and osteoblastic differentiation. *Acta Biomater* **4**, 1360 (2008).

84. R. Smith, *Biodegradable polymers for industrial applications*. (CRC Press, 2005).

85. R. L. Reis *et al.*, *Natural-based polymers for biomedical applications*. (Elsevier, 2008).

86. G. A. Digenis, T. B. Gold, V. P. Shah, Cross-linking of gelatin capsules and its relevance to their in vitro-in vivo performance. *Journal of Pharmaceutical Sciences* **83**, 915 (1994).

87. E. Esposito, R. Cortesi, C. Nastruzzi, Gelatin microspheres: influence of preparation parameters and thermal treatment on chemico-physical and biopharmaceutical properties. *Biomaterials* **17**, 2009 (1996).

88. A. Bigi, G. Cojazzi, S. Panzavolta, N. Roveri, K. Rubini, Stabilization of gelatin films by crosslinking with genipin. *Biomaterials* **23**, 4827 (2002).

89. M. Pereda, A. G. Ponce, N. E. Marcovich, R. A. Ruseckaite, J. F. Martucci, Chitosan-gelatin composites and bi-layer films with potential antimicrobial activity. *Food Hydrocolloids* **25**, 1372 (2011).

90. R. N. Tharanathan, Biodegradable films and composite coatings: past, present and future. *Trends in Food Science & Technology* **14**, 71 (2003).

91. K. S. TenHuisen, P. W. Brown, The formation of hydroxyapatite-gelatin composites at 38°C. *Journal of Biomedical Materials Research* **28**, 27 (1994).

92. T. N. Gerhart, A. A. Renshaw, R. L. Miller, R. J. Noecker, W. C. Hayes, In vivo histologic and biomechanical characterization of a biodegradable particulate composite bone cement. *Journal of Biomedical Materials Research* **23**, 1 (1989).

93. K. TenHuisen, P. Brown, Microstructural Development and Formation Kinetics in a Mineralizing System: Gelatin-Gypsum. *Biomimetics* **1**, 131 (1992).

94. N. Zhang *et al.*, Phase composition and interface of starch–gelatin blends studied by synchrotron FTIR micro-spectroscopy. *Carbohydr Polym* **95**, 649 (2013).

95. Q. T. H. Shubhra, A. K. M. M. Alam, M. D. H. Beg, Mechanical and degradation characteristics of natural silk fiber reinforced gelatin composites. *Materials Letters* **65**, 333 (2011).

96. S.-T. Chang, L.-C. Chen, S.-B. Lin, H.-H. Chen, Nano-biomaterials application: Morphology and physical properties of bacterial cellulose/gelatin composites via crosslinking. *Food Hydrocolloids* **27**, 137 (2012).

97. Y. Zhang, H. Ouyang, C. T. Lim, S. Ramakrishna, Z. M. Huang, Electrospinning of gelatin fibers and gelatin/PCL composite fibrous scaffolds. *Journal of Biomedical Materials Research Part B: Applied Biomaterials* **72**, 156 (2005).

98. J. Su *et al.*, Enhanced compatibilization and orientation of polyvinyl alcohol/gelatin composite fibers using carbon nanotubes. *Journal of Applied Polymer Science* **107**, 4070 (2008).

99. A. Ullah, T. Vasanthan, D. Bressler, A. L. Elias, J. Wu, Bioplastics from Feather Quill. *Biomacromolecules* **12**, 3826 (2011).

100. J. R. Barone, W. F. Schmidt, N. T. Gregoire, Extrusion of feather keratin. *Journal of Applied Polymer Science* **100**, 1432 (2006).

101. K. Yamauchi, A. Yamauchi, T. Kusunoki, A. Kohda, Y. Konishi, Preparation of stable aqueous solution of keratins, and physiochemical and biodegradational properties of films. *Journal of Biomedical Materials Research* **31**, 439 (1996).

102. P. M. M. Schrooyen, P. J. Dijkstra, R. C. Oberthür, A. Bantjes, J. Feijen, Partially Carboxymethylated Feather Keratins. 1. Properties in Aqueous Systems. *J Agric Food Chem* **48**, 4326 (2000).

103. P. M. M. Schrooyen, P. J. Dijkstra, R. C. Oberthür, A. Bantjes, J. Feijen, Partially Carboxymethylated Feather Keratins. 2. Thermal and Mechanical Properties of Films. *J Agric Food Chem* **49**, 221 (2001).

104. J. R. Barone, W. F. Schmidt, C. F. Liebner, Compounding and molding of polyethylene composites reinforced with keratin feather fiber. *Composites Science and Technology* **65**, 683 (2005).

105. J. G. Rouse, M. E. Van Dyke, A Review of Keratin-Based Biomaterials for Biomedical Applications. *Materials* **3**, 999 (2010).

106. T. Tanabe, N. Okitsu, A. Tachibana, K. Yamauchi, Preparation and characterization of keratin–chitosan composite film. *Biomaterials* **23**, 817 (2002).

107. K. Lee, S. Kong, W. Park, W. Ha, I. Kwon, Effect of surface properties on the antithrombogenicity of silk fibroin/S-carboxymethyl kerateine blend films. *Journal of Biomaterials Science, Polymer Edition* **9**, 905 (1998).

108. A. Tachibana, Y. Furuta, H. Takeshima, T. Tanabe, K. Yamauchi, Fabrication of wool keratin sponge scaffolds for long-term cell cultivation. *Journal of Biotechnology* **93**, 165 (2002).

109. C. Tonin *et al.*, Thermal and structural characterization of poly (ethylene-oxide)/keratin blend films. *Journal of thermal analysis and calorimetry* **89**, 601 (2006).

110. M. Zoccola *et al.*, Electrospinning of polyamide 6/modified-keratin blends. *e-Polymers* **7**, 1204 (2007).

111. T. Fujii, Y. Ide, Preparation of Translucent and Flexible Human Hair Protein Films and Their Properties. *Biological and Pharmaceutical Bulletin* **27**, 1433 (2004).

112. A. Tachibana, S. Kaneko, T. Tanabe, K. Yamauchi, Rapid fabrication of keratin–hydroxyapatite hybrid sponges toward osteoblast cultivation and differentiation. *Biomaterials* **26**, 297 (2005).

113. K. Katoh, T. Tanabe, K. Yamauchi, Novel approach to fabricate keratin sponge scaffolds with controlled pore size and porosity. *Biomaterials* **25**, 4255 (2004).

114. A. Aluigi *et al.*, Electrospinning of keratin/poly (ethylene oxide) blend nanofibers. *Journal of Applied Polymer Science* **104**, 863 (2007).

115. A. Aluigi *et al.*, Structure and properties of keratin/PEO blend nanofibres. *European Polymer Journal* **44**, 2465 (2008).

116. K. Katoh, M. Shibayama, T. Tanabe, K. Yamauchi, Preparation and properties of keratin–poly (vinyl alcohol) blend fiber. *Journal of Applied Polymer Science* **91**, 756 (2004).

117. P. Sierpinski *et al.*, The use of keratin biomaterials derived from human hair for the promotion of rapid regeneration of peripheral nerves. *Biomaterials* **29**, 118 (2008).

118. A. Gennadios, C. L. Weller, M. A. Hanna, G. W. Froning, Mechanical and Barrier Properties of Egg Albumen Films. *J Food Sci* **61**, 585 (1996).

119. A. K. Zimmer, P. Chetoni, M. F. Saettone, H. Zerbe, J. r. Kreuter, Evaluation of pilocarpine-loaded albumin particles as controlled drug delivery systems for the eye. II. Co-administration with bioadhesive and viscous polymers. *Journal of Controlled Release* **33**, 31 (1995).

120. O. Krätz, Aufstieg und Niedergang des Galaliths. *Chemie in unserer Zeit* **38**, 133 (2004).

121. J. M. Gosline, P. A. Guerette, C. S. Ortlepp, K. N. Savage, The mechanical design of spider silks: From fibroin sequence to mechanical function. *Journal of Experimental Biology* **202**, 3295 (1999).

122. L. Roemer, T. Scheibel, Basis for new material - Spider silk protein. *Chemie in Unserer Zeit* **41**, 306 (2007).

123. M. K. Shin *et al.*, Synergistic toughening of composite fibres by self-alignment of reduced graphene oxide and carbon nanotubes. *Nature Communications* **3**, (2012).

124. G. H. Altman *et al.*, Silk-based biomaterials. *Biomaterials* **24**, 401 (2003).

125. V. B. Gerritsen, The tiptoe of an airbus. *Protein Spotlight, Swiss Prot* **24**, 1 (2002).

126. F. Vollrath, P. Barth, A. Basedow, W. Engstrom, H. List, Local tolerance to spider silks and protein polymers in vivo. *In vivo* **16**, 229 (2002).

127. A. Rising, Controlled assembly: A prerequisite for the use of recombinant spider silk in regenerative medicine? *Acta Biomater* **10**, 1627 (2014).

128. F. Vollrath, D. P. Knight, Liquid crystalline spinning of spider silk. *Nature* **410**, 541 (2001).

129. AMSilkGmbH. (2013), vol. 2016, pp. Technology Insights.

130. K. E. Uhrich, S. M. Cannizzaro, R. S. Langer, K. M. Shakesheff, Polymeric systems for controlled drug release. *Chemical Reviews* **99**, 3181 (1999).

131. R. Langer, Polymeric Delivery Systems for Controlled Drug Release. *Chemical Engineering Communications* **6**, 1 (1980).

132. Volker Wagner, A. Zweck, "Nanomedizin - Innovationspotentiale in Hessen für Medizintechnik und Pharmazeutische Industrie" (Hessisches Ministerium für Wirtschaft, Verkehr und Landesentwicklung, Wiesbaden, 2008).

133. J. R. B. J. Brouwers, Advanced and controlled drug delivery systems in clinical disease management. *Pharmacy World & Science* **18**, 153 (1996).

134. A. G. Deboer, D. D. Breimer, The Blood-Brain-Barrier - Clinical Implications for Drug-Delivery to the Brain. *Journal of the Royal College of Physicians of London* **28**, 502 (1994).

135. K. A. Walter, R. J. Tamargo, A. Olivi, P. C. Burger, H. Brem, Intratumoral Chemotherapy. *Neurosurgery* **37**, 1129 (1995).

136. G. S. Kwon, K. Kataoka, Block copolymer micelles as long-circulating drug vehicles. *Advanced Drug Delivery Reviews* **16**, 295 (1995).

137. V. Torchilin, Targeted pharmaceutical nanocarriers for cancer therapy and imaging. *The AAPS Journal* **9**, E128 (2007).

138. M. Dellian, F. Yuan, V. S. Trubetskoy, V. P. Torchilin, R. K. Jain, Vascular permeability in a human tumour xenograft: molecular charge dependence. *British Journal of Cancer* **82**, 1513 (2000).

139. C. He, Y. Hu, L. Yin, C. Tang, C. Yin, Effects of particle size and surface charge on cellular uptake and biodistribution of polymeric nanoparticles. *Biomaterials* **31**, 3657 (2010).

140. X. Zhang, Y. Lin, R. J. Gillies, Tumor pH and Its Measurement. *Journal of Nuclear Medicine* **51**, 1167 (2010).

141. M. P. Gamcsik, M. S. Kasibhatla, S. D. Teeter, O. M. Colvin, Glutathione levels in human tumors. *Biomarkers : biochemical indicators of exposure, response, and susceptibility to chemicals* **17**, 671 (2012).

142. J. Liu *et al.*, Redox-Responsive Polyphosphate Nanosized Assemblies: A Smart Drug Delivery Platform for Cancer Therapy. *Biomacromolecules* **12**, 2407 (2011).

143. L. Patel, J. Zaro, W.-C. Shen, Cell Penetrating Peptides: Intracellular Pathways and Pharmaceutical Perspectives. *Pharmaceutical Research* **24**, 1977 (2007).

144. L. H. Krumpe, T. Mori, The Use of Phage-Displayed Peptide Libraries to Develop Tumor-Targeting Drugs. *International Journal of Peptide Research and Therapeutics* **12**, 79 (2006).

145. E. Gros *et al.*, A non-covalent peptide-based strategy for protein and peptide nucleic acid transduction. *Biochimica et Biophysica Acta (BBA) - Biomembranes* **1758**, 384 (2006).

146. C. Foerg, H. P. Merkle, On the biomedical promise of cell penetrating peptides: Limits versus prospects. *Journal of pharmaceutical sciences* **97**, 144 (2008).

147. D. J. Mitchell, L. Steinman, D. T. Kim, C. G. Fathman, J. B. Rothbard, Polyarginine enters cells more efficiently than other polycationic homopolymers. *The Journal of Peptide Research* **56**, 318 (2000).

148. S. Futaki *et al.*, Arginine-rich Peptides: An Abundant Source of Membrane-Permeable Peptides Having Potential as Carrier for Intracellular Protein Delivery. *Journal of Biological Chemistry* **276**, 5836 (2001).

149. S. Yigit, O. Tokareva, A. Varone, I. Georgakoudi, D. L. Kaplan, Bioengineered Silk Gene Delivery System for Nuclear Targeting. *Macromolecular Bioscience* **14**, 1291 (2014).

150. F. Zhao *et al.*, Cellular Uptake, Intracellular Trafficking, and Cytotoxicity of Nanomaterials. *Small* **7**, 1322 (2011).

151. J. Dausend *et al.*, Uptake Mechanism of Oppositely Charged Fluorescent Nanoparticles in HeLa Cells. *Macromolecular Bioscience* **8**, 1135 (2008).

152. J. Li *et al.*, Fusion protein from RGD peptide and Fc fragment of mouse immunoglobulin G inhibits angiogenesis in tumor. *Cancer Gene Ther* **11**, 363 (2004).

153. G. Bendas, L. Borsig, Cancer Cell Adhesion and Metastasis: Selectins, Integrins, and the Inhibitory Potential of Heparins. *International Journal of Cell Biology* **2012**, 10 (2012).

154. F. L. Matthews, R. D. Rawlings, in *Composite Materials,* F. L. Matthews, R. D. Rawlings, Eds. (Woodhead Publishing, 1999), pp. 29-77.

155. S. Sinha Ray, M. Okamoto, Polymer/layered silicate nanocomposites: a review from preparation to processing. *Progress in Polymer Science* **28**, 1539 (2003).

156. I. Armentano, M. Dottori, E. Fortunati, S. Mattioli, J. M. Kenny, Biodegradable polymer matrix nanocomposites for tissue engineering: A review. *Polymer Degradation and Stability* **95**, 2126 (2010).

157. R. Qiao, L. Catherine Brinson, Simulation of interphase percolation and gradients in polymer nanocomposites. *Composites Science and Technology* **69**, 491 (2009).

158. S. C. Tjong, Structural and mechanical properties of polymer nanocomposites. *Materials Science and Engineering: R: Reports* **53**, 73 (2006).

159. M. Alexandre, P. Dubois, Polymer-layered silicate nanocomposites: preparation, properties and uses of a new class of materials. *Materials Science and Engineering: R: Reports* **28**, 1 (2000).

160. J. Breu, W. Seidl, A. J. Stoll, K. G. Lange, T. U. Probst, Charge homogeneity in synthetic fluorohectorite. *Chem Mater* **13**, 4213 (2001).

161. L. W. Carter, J. G. Hendricks, D. S. Bolley. (Google Patents, 1950).

162. J. Breu, W. Seidl, J. Senker, Synthese von dreidimensional geordneten Einlagerungsverbindungen des Hectorits. *Zeitschrift für anorganische und allgemeine Chemie* **630**, 80 (2004).

163. D. A. Kunz *et al.*, Clay-Based Nanocomposite Coating for Flexible Optoelectronics Applying Commercial Polymers. *ACS Nano* **7**, 4275 (2013).

164. A. Olad, in *Advances in Diverse Industrial Applications of Nanocomposites,* D. B. Reddy, Ed. (2011).

165. B. Reddy, Ed., *Advances in Diverse Industrial Applications of Nanocomposites*, (InTech, Rijeka, 2011).

166. E. Ferrage *et al.*, Investigation of dioctahedral smectite hydration properties by modeling of X-ray diffraction profiles: Influence of layer charge and charge location. *American Mineralogist* **92**, 1731 (2007).

167. H. Kalo, W. Milius, J. Breu, Single crystal structure refinement of one- and two-layer hydrates of sodium fluorohectorite. *Rsc Advances* **2**, 8452 (2012).

168. D. A. Kunz, Universität Bayreuth (2013).

169. J. E. F. C. Gardolinski, G. Lagaly, M. Czank, On the destruction of kaolinite and gibbsite by phenylphosphonic, phenylphosphinic and phenylarsonic acids: evidence for the formation of new Al compounds. *Clay Minerals* **39**, 391 (2004).

170. M. B. Ahmad, W. H. Hoidy, N. A. B. Ibrahim, E. A. J. AI-Mulla, Modification of MontmorUlonite by New Surfactants. *Journal of Engineering and Applied Sciences* **4**, 184 (2009).

171. G. Chigwada, C. A. Wilkie, Synergy between conventional phosphorus fire retardants and organically-modified clays can lead to fire retardancy of styrenics. *Polymer Degradation and Stability* **81**, 551 (2003).

172. N. I. Platnick. (2015), vol. 2015.

173. L. Römer, T. Scheibel, Basis for new material - Spider silk protein. *Chemie in Unserer Zeit* **41**, 306 (2007).

174. S. L. Stauffer, S. L. Coguill, R. V. Lewis, Comparison of Physical Properties of Three Silks from Nephila clavipes and Araneus gemmoides. *Journal of Arachnology* **22**, 5 (1994).

175. P. A. Guerette, D. G. Ginzinger, B. H. F. Weber, J. M. Gosline, Silk properties determined by gland-specific expression of a spider fibroin gene family. *Science* **272**, 112 (1996).

176. E. Doblhofer, A. Heidebrecht, T. Scheibel, To spin or not to spin: spider silk fibers and more. *Appl Microbiol Biotechnol* **99**, 9361 (2015).

177. T. A. Blackledge, A. P. Summers, C. Y. Hayashi, Gumfooted lines in black widow cobwebs and the mechanical properties of spider capture silk. *Zoology* **108**, 41 (2005).

178. C. P. Brown *et al.*, Rough Fibrils Provide a Toughening Mechanism in Biological Fibers. *ACS Nano* **6**, 1961 (2012).

179. S. Keten, M. J. Buehler, Geometric Confinement Governs the Rupture Strength of H-bond Assemblies at a Critical Length Scale. *Nano Lett* **8**, 743 (2008).

180. E. Munch *et al.*, Tough, Bio-Inspired Hybrid Materials. *Science* **322**, 1516 (2008).

181. A. Smith, T. Scheibel, in *Materials Design Inspired by Nature: Function Through inner Architecture,* P. Fratzl, J. Dunlop, R. Weinkamer, Eds. (RSC Publishing, Cambridge, 2013), pp. 256-281.

182. A. Sponner *et al.*, Composition and Hierarchical Organisation of a Spider Silk. *PLoS One* **2**, e998 (2007).

183. K. Augsten, P. Muhlig, C. Herrmann, Glycoproteins and skin-core structure in Nephila clavipes spider silk observed by light and electron microscopy. *Scanning* **22**, 12 (2000).

184. Frische, Maunsbach, Vollrath, Elongate cavities and skin–core structure in Nephila spider silk observed by electron microscopy. *Journal of Microscopy* **189**, 64 (1998).

185. R. V. Lewis, Spider silk: the unraveling of a mystery. *Accounts of Chemical Research* **25**, 392 (1992).

186. J. Gatesy, C. Hayashi, D. Motriuk, J. Woods, R. Lewis, Extreme Diversity, Conservation, and Convergence of Spider Silk Fibroin Sequences. *Science* **291**, 2603 (2001).

187. M. Xu, R. V. Lewis, Structure of a protein superfiber: spider dragline silk. *Proceedings of the National Academy of Sciences* **87**, 7120 (1990).

188. M. B. Hinman, R. V. Lewis, Isolation of a clone encoding a second dragline silk fibroin. *Nephila clavipes* dragline silk is a two-protein fiber. *The Journal of biological chemistry* **267**, 19320 (1992).

189. N. A. Ayoub, J. E. Garb, R. M. Tinghitella, M. A. Collin, C. Y. Hayashi, Blueprint for a High-Performance Biomaterial: Full-Length Spider Dragline Silk Genes. *PLoS One* **2**, e514 (2007).

190. M. Heim, D. Keerl, T. Scheibel, Spider silk: from soluble protein to extraordinary fiber. *Angewandte Chemie International Edition* **48**, 3584 (2009).

191. A. Rising *et al.*, Spider silk proteins - Mechanical property and gene sequence. *Zoological Science* **22**, 273 (2005).

192. D. T. Grubb, L. W. Jelinski, Fiber morphology of spider silk: The effects of tensile deformation. *Macromolecules* **30**, 2860 (1997).

193. J. D. van Beek, S. Hess, F. Vollrath, B. H. Meier, The molecular structure of spider dragline silk: Folding and orientation of the protein backbone. *Proc Natl Acad Sci U S A* **99**, 10266 (2002).

194. C. Y. Hayashi, N. H. Shipley, R. V. Lewis, Hypotheses that correlate the sequence, structure, and mechanical properties of spider silk proteins. *Int J Biol Macromol* **24**, 271 (1999).

195. M. B. Hinman, J. A. Jones, R. V. Lewis, Synthetic spider silk: a modular fiber. *Trends in Biotechnology* **18**, 374 (2000).

196. D. Motriuk-Smith, A. Smith, C. Y. Hayashi, R. V. Lewis, Analysis of the Conserved N-Terminal Domains in Major Ampullate Spider Silk Proteins. *Biomacromolecules* **6**, 3152 (2005).

197. R. J. Challis, S. L. Goodacre, G. M. Hewitt, Evolution of spider silks: conservation and diversification of the C-terminus. *Insect Molecular Biology* **15**, 45 (2006).

198. L. Eisoldt, A. Smith, T. Scheibel, Decoding the secrets of spider silk. *Materials Today* **14**, 80 (2011).

199. L. Eisoldt, J. G. Hardy, M. Heim, T. R. Scheibel, The role of salt and shear on the storage and assembly of spider silk proteins. *Journal of Structural Biology* **170**, 413 (2010).

200. F. Hagn, C. Thamm, T. Scheibel, H. Kessler, pH-dependent dimerization and salt-dependent stabilization of the N-terminal domain of spider dragline silk – implications for fiber formation. *Angewandte Chemie International Edition* **50**, 310 (2011).

201. F. Hagn *et al.*, A conserved spider silk domain acts as a molecular switch that controls fibre assembly. *Nature* **465**, 239 (2010).

202. M. Hedhammar *et al.*, Structural Properties of Recombinant Nonrepetitive and Repetitive Parts of Major Ampullate Spidroin 1 from *Euprosthenops australis*: Implications for Fiber Formation†. *Biochemistry* **47**, 3407 (2008).

203. A. Heidebrecht *et al.*, Biomimetic Fibers Made of Recombinant Spidroins with the Same Toughness as Natural Spider Silk. *Adv Mater* **27**, 2189 (2015).

204. D. Huemmerich *et al.*, Primary structure elements of spider dragline silks and their contribution to protein solubility. *Biochemistry* **43**, 13604 (2004).

205. F. Vollrath, D. P. Knight, Structure and function of the silk production pathway in the spider *Nephila edulis*. *Int J Biol Macromol* **24**, 243 (1999).

206. C. L. Craig *et al.*, Evidence for diet effects on the composition of silk proteins produced by spiders. *Molecular biology and evolution* **17**, 1904 (2000).

207. B. Madsen, Z. Z. Shao, F. Vollrath, Variability in the mechanical properties of spider silks on three levels: interspecific, intraspecific and intraindividual. *Int J Biol Macromol* **24**, 301 (1999).

208. L. R. Fox, Cannibalism in natural populations. *Annual Review of Ecology and Systematics* **6**, 87 (1975).

209. H. P. Sørensen, K. K. Mortensen, Advanced genetic strategies for recombinant protein expression in *Escherichia coli*. *Journal of Biotechnology* **115**, 113 (2005).

210. A. Heidebrecht, T. Scheibel, Recombinant production of spider silk proteins. *Adv. Appl. Microbiol* **82**, 115 (2013).

211. C. Vendrely, T. Scheibel, Biotechnological production of spider-silk proteins enables new applications. *Macromolecular Bioscience* **7**, 401 (2007).

212. E. Doblhofer, Masterarbeit, Universität Bayreuth (2011).

213. J. G. Hardy, L. M. Romer, T. R. Scheibel, Polymeric materials based on silk proteins. *Polymer* **49**, 4309 (2008).

214. K. Spiess, A. Lammel, T. Scheibel, Recombinant spider silk proteins for applications in biomaterials. *Macromolecular Biosciences* **10**, 998 (2010).

215. K. Schacht, T. Scheibel, Controlled hydrogel formation of a recombinant spider silk protein. *Biomacromolecules* **12**, 2488 (2011).

216. A. Lammel, M. Schwab, U. Slotta, G. Winter, T. Scheibel, Processing conditions for the formation of spider silk microspheres. *ChemSusChem* **1**, 413 (2008).

217. S. Rammensee, D. Huemmerich, K. D. Hermanson, T. Scheibel, A. R. Bausch, Rheological characterization of hydrogels formed by recombinantly produced spider silk. *Applied Physics A: Materials Science & Processing* **82**, 261 (2006).

218. D. Huemmerich, U. Slotta, T. Scheibel, Processing and modification of films made from recombinant spider silk proteins. *Applied Physics A: Materials Science & Processing* **82**, 219 (2006).

219. K. Numata, J. Hamasaki, B. Subramanian, D. L. Kaplan, Gene delivery mediated by recombinant silk proteins containing cationic and cell binding motifs. *Journal of Controlled Release* **146**, 136 (2010).

220. U. Slotta *et al.*, Spider silk and amyloid fibrils: A structural comparison. *Macromolecular Bioscience* **7**, 183 (2007).

221. K. Schacht, J. Vogt, T. Scheibel, Foams made of Engineered Recombinant Spider Silk Proteins as Optimized 3D Scaffolds for Cell Growth. *Biomaterials Science and Engineering*, eingereicht (2015).

222. U. K. Slotta, S. Rammensee, S. Gorb, T. Scheibel, An engineered spider silk protein forms microspheres. *Angewandte Chemie International Edition* **47**, 4592 (2008).

223. A. Lammel, M. Schwab, M. Hofer, G. Winter, T. Scheibel, Recombinant spider silk particles as drug delivery vehicles. *Biomaterials* **32**, 2233 (2011).

224. C. Blüm, T. Scheibel, Control of drug loading and release properties of spider silk sub-microparticles. *BioNanoScience* **2**, 67 (2012).

225. M. B. Elsner, H. M. Herold, S. Muller-Herrmann, H. Bargel, T. Scheibel, Enhanced cellular uptake of engineered spider silk particles. *Biomaterials Science* **3**, 543 (2015).

226. M. P. Neubauer *et al.*, Micromechanical characterization of spider silk particles. *Biomaterials Science* **1**, 1160 (2013).

227. M. Hofer, G. Winter, J. Myschik, Recombinant spider silk particles for controlled delivery of protein drugs. *Biomaterials* **33**, 1554 (2012).

228. N. Helfricht *et al.*, Surface properties of spider silk particles in solution. *Biomaterials Science* **1**, 1166 (2013).

229. B. Liebmann, D. Huemmerich, T. Scheibel, M. Fehr, Formulation of poorly water-soluble substances using self-assembling spider silk protein. *Colloids and Surfaces a-Physicochemical and Engineering Aspects* **331**, 126 (2008).

230. U. Slotta, M. Tammer, F. Kremer, P. Koelsch, T. Scheibel, Structural analysis of spider silk films. *Supramolecular Chemistry* **18**, 465 (2006).

231. K. Spiess, S. Wohlrab, T. Scheibel, Structural characterization and functionalization of engineered spider silk films. *Soft Matter* **6**, 4168 (2010).

232. E. Metwalli *et al.*, Structural changes of thin films from recombinant spider silk proteins upon post-treatment. *Applied Physics a-Materials Science & Processing* **89**, 655 (2007).

233. P. H. Zeplin *et al.*, Spider Silk Coatings as a Bioshield to Reduce Periprosthetic Fibrous Capsule Formation. *Advanced Functional Materials* **24**, 2658 (2014).

234. X. Hu, Q. Lu, D. L. Kaplan, P. Cebe, Microphase Separation Controlled β-Sheet Crystallization Kinetics in Fibrous Proteins. *Macromolecules* **42**, 2079 (2009).

235. S. Wohlrab, K. Spieß, T. Scheibel, Varying surface hydrophobicities of coatings made of recombinant spider silk proteins. *Journal of Materials Chemistry* **22**, 22050 (2012).

236. K. Spiess *et al.*, Impact of initial solvent on thermal stability and mechanical properties of recombinant spider silk films. *Journal of Materials Chemistry* **21**, 13594 (2011).

237. K. Gast, A. Siemer, D. Zirwer, G. Damaschun, Fluoroalcohol-induced structural changes of proteins: some aspects of cosolvent-protein interactions. *European biophysics journal : EBJ* **30**, 273 (2001).

238. F. D. Sonnichsen, J. E. Van Eyk, R. S. Hodges, B. D. Sykes, Effect of trifluoroethanol on protein secondary structure: an NMR and CD study using a synthetic actin peptide. *Biochemistry* **31**, 8790 (1992).

239. Y. Termonia, Molecular Modeling of Spider Silk Elasticity. *Macromolecules* **27**, 7378 (1994).

240. G. Decher, J. D. Hong, J. Schmitt, Buildup of ultrathin multilayer films by a self-assembly process: III. Consecutively alternating adsorption of anionic and cationic polyelectrolytes on charged surfaces. *Thin Solid Films* **210–211, Part 2**, 831 (1992).

241. G. Lang, S. Jokisch, T. Scheibel, Air Filter Devices Including Nonwoven Meshes of Electrospun Recombinant Spider Silk Proteins. *Jove-Journal of Visualized Experiments*, (2013).

242. D. D. Von Hoff *et al.*, Risk Factors for Doxorubicin-lnduced Congestive Heart Failure. *Annals of Internal Medicine* **91**, 710 (1979).

243. A. Florczak, A. Mackiewicz, H. Dams-Kozlowska, Functionalized Spider Silk Spheres As Drug Carriers for Targeted Cancer Therapy. *Biomacromolecules* **15**, 2971 (2014).

244. J. F. L. Duval, H. Ohshima, Electrophoresis of Diffuse Soft Particles. *Langmuir* **22**, 3533 (2006).

245. J. F. L. Duval, F. Gaboriaud, Progress in electrohydrodynamics of soft microbial particle interphases. *Current Opinion in Colloid & Interface Science* **15**, 184 (2010).

246. H. Ohshima, Electrophoresis of soft particles. *Advances in Colloid and Interface Science* **62**, 189 (1995).

247. A. Sorrentino, G. Gorrasi, V. Vittoria, Potential perspectives of bio-nanocomposites for food packaging applications. *Trends in Food Science & Technology* **18**, 84 (2007).

248. H. J. Bae, H. J. Park, D. O. Darby, R. M. Kimmel, W. S. Whiteside, Development and characterization of PET/Fish Gelatin–nanoclay composite/LDPE laminate. *Packaging Technology and Science* **22**, 371 (2009).

249. M. W. Moller *et al.*, Barrier Properties of Synthetic Clay with a Kilo-Aspect Ratio. *Adv Mater* **22**, 5245 (2010).

250. M. Stöter *et al.*, Nanoplatelets of Sodium Hectorite Showing Aspect Ratios of ≈20 000 and Superior Purity. *Langmuir* **29**, 1280 (2013).

251. X. Hu, D. Kaplan, P. Cebe, Determining beta-sheet crystallinity in fibrous proteins by thermal analysis and infrared spectroscopy. *Macromolecules* **39**, 6161 (2006).

252. L. Lerot, P. F. Low, Effect of Swelling on Infrared-Absorption Spectrum of Montmorillonite. *Clays and Clay Minerals* **24**, 191 (1976).

253. W. L. Ijdo, S. Kemnetz, D. Benderly, An infrared method to assess organoclay delamnination and orientation in organoclay polymer nanocomposites. *Polym Eng Sci* **46**, 1031 (2006).

254. E. Doblhofer, T. Scheibel, Engineering of Recombinant Spider Silk Proteins Allows Defined Uptake and Release of Substances. *Journal of pharmaceutical sciences* **104**, 988 (2015).

255. M. B. Schierling, E. Doblhofer, T. Scheibel, Cellular uptake of drug loaded spider silk particles. *Biomaterials Science* **4**, 1515 (2016).

256. N. Helfricht, E. Doblhofer, J. F. L. Duval, T. Scheibel, G. Papastavrou, Colloidal Properties of Recombinant Spider Silk Protein Particles. *The Journal of Physical Chemistry C* **120**, 18015 (2016).

257. E. Doblhofer *et al.*, Structural Insights into Water-Based Spider Silk Protein–Nanoclay Composites with Excellent Gas and Water Vapor Barrier Properties. *ACS Appl Mater Interfaces* **8**, 25535 (2016).

5 Teilarbeiten und Darstellung des Eigenanteils

Die in dieser Dissertation beschriebenen Ergebnisse wurden in Zusammenarbeit mit diversen Kooperationspartnern erzielt und in den unten aufgeführten Journalen veröffentlicht, oder zur Veröffentlichung vorbereitet. Nachfolgend werden die Teilarbeiten aufgeführt und die jeweiligen Beiträge der einzelnen Autoren angegeben.

5.1 Teilarbeit I

Engineering of Recombinant Spider Silk Proteins Allows Defined Uptake and Release of Substances

Autoren: Elena Doblhofer und Prof. Dr. Thomas Scheibel

Alle Experimente dieser Teilarbeit, sowie die Konzipierung dieser Veröffentlichung wurden von mir vorgenommen. Das Manuskript wurde von mir verfasst und zusammen mit Thomas Scheibel fertig gestellt. Thomas Scheibel betreute das Projekt und war an den wissenschaftlichen Diskussionen beteiligt.

Der Artikel wurde am 27.12.2014 im *Journal of Pharmaceutical Sciences* veröffentlicht.

Engineering of Recombinant Spider Silk Proteins Allows Defined Uptake and Release of Substances

ELENA DOBLHOFER,[1] THOMAS SCHEIBEL[1,2,3,4,5]

[1]Thomas Scheibel, Lehrstuhl Biomaterialien, Fakultät für Ingenieurwissenschaften, Universität Bayreuth, Bayreuth 95440, Germany
[2]Bayreuther Zentrum für Kolloide und Grenzflächen (BZKG), Universität Bayreuth, Bayreuth 95440, Germany
[3]Institut für Bio-Makromoleküle (bio-mac), Universität Bayreuth, Bayreuth 95440, Germany
[4]Bayreuther Zentrum für Molekulare Biowissenschaften (BZMB), Universität Bayreuth, Bayreuth 95440, Germany
[5]Bayreuther Materialzentrum (BayMAT), Universität Bayreuth, Bayreuth 95440, Germany

Received 20 August 2014; revised 13 November 2014; accepted 14 November 2014

Published online 27 December 2014 in Wiley Online Library (wileyonlinelibrary.com). DOI 10.1002/jps.24300

ABSTRACT: Drug delivery carriers stabilize drugs and control their release, expanding the therapeutic window, and avoiding side effects of otherwise freely diffusing drugs in the human body. Materials used as carrier vehicles have to be biocompatible, biodegradable, nontoxic, and nonimmunogenic. Previously, particles made of the recombinant spider silk protein eADF4(C16) could be effectively loaded with positively and neutrally charged model substances. Here, a new positively charged variant thereof, named eADF4(κ16), has been engineered. Its particle formation is indistinguishable to that of polyanionic eADF4(C16), but in contrast polycationic eADF4(κ16) allows incorporation of negatively charged substances. Both high-molecular-weight substances, such as nucleic acids, and low-molecular-weight substances could be efficiently loaded onto eADF4(κ16) particles, and release of nucleic acids was shown to be well controlled. © 2014 Wiley Periodicals, Inc. and the American Pharmacists Association J Pharm Sci 104:988–994, 2015
Keywords: biodegradable polymers; biomaterials; biotechnology; DNA/oligonucleotide delivery; drug delivery system

INTRODUCTION

Drug delivery systems can overcome many disadvantages of drugs such as poor solubility, rapid breakdown *in vivo*, unfavorable pharmacokinetics, poor biodispersity, and lack of selectivity,[1] all of which result in lower drug efficacy and unwanted side effects.[2] Colloidal micro- and nanoparticulate carriers have been used extensively as drug reservoirs because they have programmable degradability ranging from a few days to several months.[3] When mobile particulate drug vehicles are decorated with specific recognition motifs on their surface, they can also be used for targeted delivery, for example, to malignant tumor cells.[2]

In addition to being biocompatible, biodegradable, nontoxic, and nonimmunogenic,[3] drug delivery vehicles must fulfill numerous requirements, for example, controlled particle size and mechanical stability.[7] Furthermore, solubility, stability, molecular weight, and charge of the drug substances must be considered for choosing suitable carrier materials.[1] Synthetic polymers are often used for designing of drug carriers, but natural polymers, such as polysaccharides and polypeptides, have also been employed. The advantage of such biopolymers in comparison to synthetic ones is their ability to undergo enzymatic or hydrolytic degradation in natural environments accompanied by release of nonhazardous byproducts that can be biologically eliminated.[5]

Spider silk protein particles have recently been established as drug delivery carriers.[6] As the availability of natural spider silk proteins is limited and farming of spiders is not practical because of their cannibalistic behavior,[7] engineered recombinant spider silk proteins have been developed as a reliable source.[8] It has been shown that engineered spider silk proteins, such as eADF4(C16), can be processed into a variety of assembly morphologies, such as fibrils, hydrogels, capsules, and particles.[9–14] Materials based on spider silk proteins are biocompatible, biodegradable, nontoxic, and do not induce immune reactions,[7,15–19] fulfilling important prerequisites for their use as a drug delivery carrier. Spider silk protein particles have high mechanical stability and can be stored in a dried state because of their fully reversible swelling behavior.[20,21] Furthermore, it has been shown that model drugs, small-molecular-weight molecules as well as proteins, can be loaded onto eADF4(C16) particles in various amounts depending on the physicochemical properties of the loaded substance.[6,22,23] Because of the negative net charge of eADF4(C16) at neutral pH, drugs have to be positively or neutrally charged in order to be taken up.

Currently investigated drug delivery systems that are able to transport negatively charged molecules are cationic liposomes or cationic polymers. Liposomes have the major disadvantage of often inducing rapid immune response and accumulation in the liver without carrying liver-specific target sequences.[24–26] Linear and branched polyethylenimines (PEIs), one of the most extensively studied polymeric drug delivery system, are also commonly used in gene delivery.[27] Although complexes of DNA and PEI are currently the most effective nonviral gene delivery systems, they still exhibit problems, such as toxicity, nonspecificity, and nonbiodegradability. Large amounts of nondegradable PEI remain in free form inside the transfected cells causing cell dysfunction.[28] Recently, silk proteins containing RGD sequences were used to enhance transfection efficiency of PEI/DNA complexes.[29] However, this approach did not

Correspondence to: Thomas Scheibel (Telephone: +49-921-55-7361; Fax: +49-921-55-7346; E-mail: thomas.scheibel@bm.uni-bayreuth.de)

Journal of Pharmaceutical Sciences, Vol. 104, 988–994 (2015)

overcome the stated problems associated with PEI. Therefore, spider silk protein-based hybrids were developed in a separate approach for gene delivery.[12] These hybrid proteins contain 30 lysine residues that are responsible for electrostatic interactions between the hybrid silk proteins and DNA, providing a functional, biodegradable construct. Additionally, again RGD sequences were utilized to enhance transfection efficiency. However, it has been shown that polylysine sequences have an inherent cytotoxicity because of their high-charge density.[30,31]

Here, we engineered a new variant of eADF4(C16), called eADF4(κ16), with a positive net-charge and low-charge density at neutral pH. This approach was accomplished without using additional tags as all charged residues were part of the spider silk core sequence, avoiding side effects as seen in previous attempts. Importantly, most properties of eADF4(C16) were retained in eADF4(κ16), allowing its use as drug carrier material.

MATERIALS AND METHODS

Protein Design and Production

eADF4(C16) containing the sequence T7-$(GSSAAAAAAAAASGPGGYGPENQGPSGPGGYGPGGPG)_{16}$ was produced and purified as described previously.[8] To design eADF4(κ16), glutamic acid residues of eADF4(C16) were replaced by lysine residues within the encoding DNA sequence. A κ2 DNA sequence with *Bam*HI and *Hind*III restriction sites was purchased from GeneArt® Gene Synthesis, and the DNA construct encoding eADF4(κ16) was generated using a previously established cloning strategy.[8] eADF4(κ16) was expressed in *E. coli* BL21 gold (DE3), and the protein was purified using a heat step and ammonium sulfate precipitation as described previously.[8]

Particle Preparation

Lyophilized eADF4(κ16) or eADF4(C16) was dissolved in 6 M guanidinium thiocyanate (GdmSCN) and dialyzed against 25 mM Tris/HCl pH 7.5 (Tris buffer). Samples were dialyzed for 16 h with three buffer changes at 25°C, using a dialysis membrane with a molecular weight cut-off of 6000–8000 Da (Spectrum® Laboratories, Irving, Texas). The resulting spider silk protein solutions were diluted to a concentration of 50 μM using Tris buffer. Aliquots of 200 μL (10 nmol) were mixed at a 1:1 ratio with 2 M potassium phosphate, pH 7.5. The mixtures were incubated for 30 min at 25°C and then centrifuged at 17000*g* for 2 min to obtain a pellet that consisted of the precipitated protein particles.[9,10] The particles were washed three times with MQ-H_2O, and, if needed, stored in MQ-H_2O at 25°C. The eADF4(κ16) particles used in this experiment had diameters of 1533 ± 238, and eADF4(C16) particles diameters of 1286 ± 206 nm.

Particle Size Determination

Particle sizes were determined via dynamic light scattering measurements. These measurements were performed using a ZetaSizer Nano ZS (Malvern Industries Ltd., Malvern, UK). Refractive indices of 1.33 for water and 1.60 for protein were used for computation of particle sizes. Aliquots of freshly prepared and washed particles were resuspended in 2 mL Tris buffer and 500 μL of these suspensions were used to measure particle sizes.

Particle Loading

Protein particles were loaded via diffusion with the model substances carboxy fluorescein (CFl), crystal violet (CV), and acridine orange (AO). CFI, CV, and AO were dissolved in ethanol at a concentration of 25 mM each. Dye solutions were then diluted 500-fold (1 eq), 100-fold (5 eq), 50-fold (10 eq), or 25-fold (20 eq) using Tris buffer. For particle loading, 200 μL of dye solution were added to freshly washed particle pellets and incubated for 30 min at 25°C, followed by centrifugation at 17,000*g* for 2 min. The supernatant was then analyzed using UV/Vis spectroscopy at wavelengths matching the absorbance maxima of the dyes used (CFl: λ_{max} = 492 nm; CV: λ_{max} = 552 nm; AO: λ_{max} = 467 nm) to determine both the loading and the loading efficiency of the particles (Eqs. (1) and (2).

For loading of eADF4(κ16) particles with Rho-ODN [rhodamine-labeled dsDNA: Rho-C6-5′-ggt cac ttc gtg gct aac g-3′ (7387.43 Da)], the labeled DNA was dissolved in MQ-H_2O at a concentration of 125 μM and 200 μL (25 nmol) were added to eADF4(κ16) particles, incubated for 30 min and then centrifuged at 17,000*g* for 2 min at 25°C. The supernatant was analyzed using UV/Vis spectroscopy at the absorption maximum of λ_{max} = 560 nm to determine the loading and the loading efficiency of the protein particles (Eqs. (1) and (2).

$$\text{Loading}\,(\%) = \frac{\text{Amount of substance in particles}}{\text{Amount of silk protein in particles}} \times 100 \quad (1)$$

$$\text{Loading efficiency}\,(\%) = \frac{\text{Amount of substance in particles}}{\text{Amount of dye added}} \times 100 \quad (2)$$

Model Substance Release

To analyze the release kinetics of loaded substances, particles were thoroughly resuspended in release buffer and incubated in a shaker (Thermomixer compact; Eppendorf, Germany) for 30 min at 37°C, followed by centrifugation at 17,000*g* for 2 min at 25°C. Supernatants were carefully removed, and pellets were resuspended in 200 μL of fresh Tris buffer and the corresponding salt concentrations (NaCl or sodium acetate), phosphate buffer or PBS. The removed supernatants were then centrifuged again and analyzed using UV/Vis spectroscopy at the absorption maximum of the loaded substances (see also section *Particle Loading*).

Layer-by-Layer Particle Coating

Freshly washed or freshly loaded eADF4(C16/κ16) particles were resuspended in 200 μL of the corresponding charge counterpart at a protein concentration of 0.5 mg/mL. After 1 h of incubation, particles were centrifuged at 17,000*g* for 2 min and washed once with MQ-H_2O at 25°C.

Microscopy

Scanning electron microscopy (SEM) images were taken using a 1450Es Beam (Zeiss, Oberkochen, Germany) at an accelerating voltage of 3 kV. Particles were pipetted onto Thermanox™ plastic cover slips and washed three times with distilled water. Before imaging, the particles were air dried and sputtered with platinum.

Confocal scanning laser microscopy (CLSM) was performed using a LSM710 (Zeiss, Oberkochen, Germany). Particles were pipetted on a glass slide and analyzed in a wet state.

Zeta Potential Measurements

Zeta potential (ZP) measurements of particles were performed using a Zetaview PMX 100 (ParticleMetrix, Meerbusch, Germany). The ZP was calculated from the electrophoretic mobility of particles after the theory of Smoluchowski.[32] Freshly washed particles were resuspended in 200 μL of 5 mM citrate buffer pH 7.5. 50 μl of the particle suspension were diluted in 10 mL of 5 mM citrate buffer. Each measurement was repeated three times.

RESULTS AND DISCUSSION

It has been previously shown that high-molecular-weight molecules such as proteins, as well as small-molecular-weight substances, can be loaded onto and released from eADF4(C16) particles.[6,22,23] Here, a new variant of this recombinant spider silk protein, called eADF4(κ16), was engineered containing 16 positively charged amino acids (lysine residues) replacing the 16 negatively charged amino acids (glutamic acid residues) of eADF4(C16). eADF4(κ16) was assembled into spherical particles with diameters between 1 and 2 μm in the presence of molar concentrations of potassium phosphate, which were indistinguishable from eADF4(C16)particles.[10]

eADF4(κ16) Particles Can Be Used as a Nucleic Acid Carrier

As polyanionic eADF4(C16) particles cannot be loaded with anionic substances,[6] we tested the ability of polycationic eADF4(κ16) to be loaded with nucleic acids, which can, in the case of siRNA, be used for RNAi therapy.

Labeled dsDNA (Rho-ODN) was tested as a model substance because of its easier handling in comparison to siRNA. After incubation, the uptake efficiency of Rho-ODN in eADF4(κ16) particles was 16.9 ± 5.5 % corresponding to 4.3 nmol Rho-ODN per 10 nmol protein. CLSM measurements revealed that all particles were loaded with labeled DNA, even after washing (Fig. 1).

For release measurements, Rho-ODN-loaded particles were resuspended in PBS and, as a control, in Tris buffer (25 mM Tris/HCl, pH 7.5) (Fig. 2). Importantly, in both cases, no burst release was observable; release was slow and linear similar to the release rates of biologicals (e.g., lysozyme) from eADF4(C16) particles.[23] This linear release may be because of a strong interaction between the highly negatively charged Rho-ODN and the positively charged particle matrix. The ionic strength of PBS was not able to significantly suppress Rho-ODN binding and to accelerate its release.

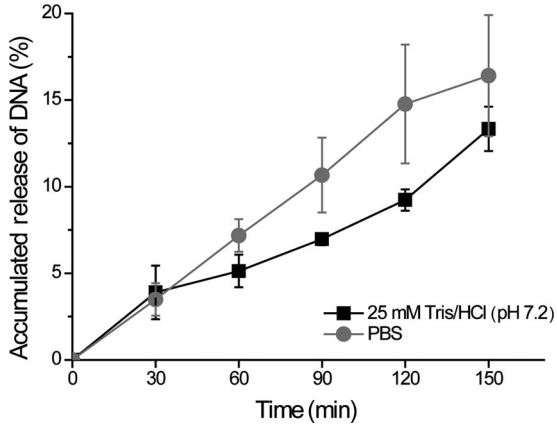

Figure 2. Release of Rho-ODN from eADF4(κ16) particles in the presence of PBS (gray) and 25 mM Tris/HCl, pH 7.2, (black) at 37°C.

Release Control of Low-Molecular-Weight Substances from Spider Silk Particles

Loading of Low-Molecular-Weight Model Substances

Carboxy fluorescein (Fig. 3a) was tested as a model for negatively charged substances and loaded onto eADF4(κ16) particles. CV (Fig. 3b) and AO (Fig. 3c) were used as models for positively charged substances and loaded onto eADF4(C16) particles for comparison. As their loading onto eADF4(κ16) was not possible because of charge–charge repulsion, as well as loading of negatively charged substances onto eADF4(C16) (data not shown), a general comparison of substance uptake and release between the well-established eADF4(C16) and the newly developed eADF4(κ16) system was the only possibility.

Loading efficiencies of the individual dyes were tested at different dye/protein ratios (1, 5, 10, and 20 eq). Particles were made of 10 nmol eADF4(C16) or 10 nmol eADF4(κ16) (concentration of each protein solution: 50 μM), and the dye concentration was adjusted according to the individual ratio. The maximum loading efficiency of CFl was 98% when using

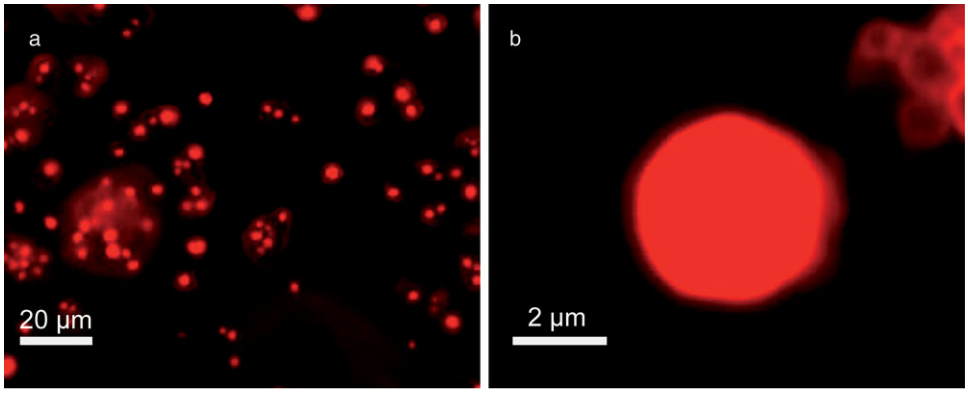

Figure 1. Confocal scanning laser microscopy pictures of eADF4(κ16) loaded with Rho-ODN; (a) overview and (b) single particle.

 DOI 10.1002/jps.24300

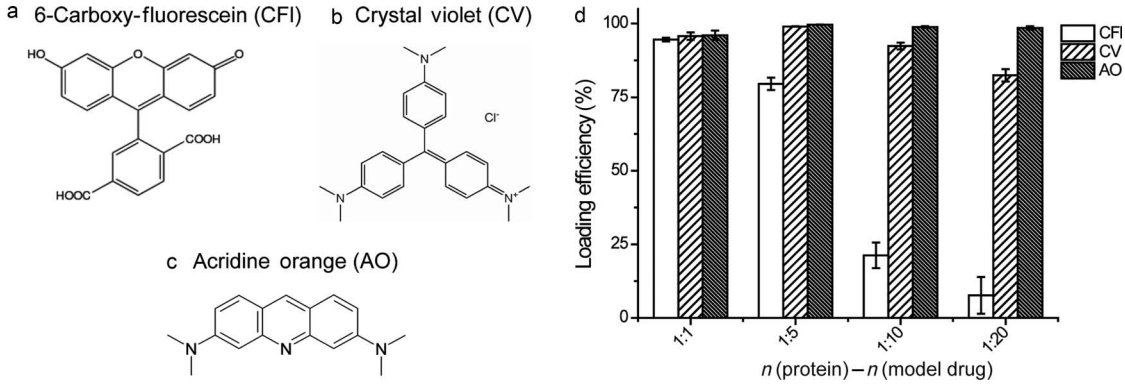

Figure 3. Model substances: (a) CFl, (b) CV, and (c) AO. (d) Loading efficiencies of CFl on eADF4(κ16) and CV/AO on eADF4(C16) particles at 25°C.

a 1:1 molar ratio [CFl/eADF4(κ16)] (Fig. 3d). The loading efficiencies decreased with increasing dye concentration. For CV, the maximum loading to eADF4(C16) particles was reached at 5 eq. The maximum loading efficiency of AO could not be determined within the tested molar ratios, as the loading efficiency was still 98.5% at the highest ratio, in agreement with the maximum loading described previously.[33]

The maximum amount of CFl incorporated into eADF4(κ16) particles was 39.77 ± 1.06 nmol at a protein to dye ratio of 1:5. For eADF4(C16), the maximum amount of loaded CV was 79.54 ± 2.13 nmol at a ratio of 1:20 and that of AO 197.10 ±1.10 nmol. Difference in loading was probably not because of different electrostatic interactions or the structure of the protein, but more likely because of the shape of the dye molecules. AO is a flat molecule with three aromatic rings, possibly intercalating with beta-sheets of the spider silk protein. In contrast, CV and CFl are larger molecules and occupy a greater volume. Another argument for steric considerations in addition to electrostatic interactions is based on the assumption that protein monomers provide 16 charged amino acids (plus amino- and carboxy-termini), while each dye contains only one single charge at neutral pH values. Based thereon in eADF4(κ16) only 25 % of the charges are covered, whereas in eADF4(C16) loaded with CV 50% are covered, and upon loading with AO the coverage is 123%. The latter indicates that AO is not only bound by charge–charge but also by hydrophobic interactions as described previously.[33]

Release of Low-Molecular-Weight Model Substances

Previous experiments have shown that low-molecular-weight substances such as Rhodamine B are captured in the outer regime of eADF4(C16) particles with no or little interaction within the particle matrix.[20,22] Release is completed within 2 h, and the presence of salt has only a slight impact on release kinetics.[22] Under the experimental conditions, only partial release of CV and AO could be detected from eADF4(C16) particles within 2 h. Interestingly, the addition of salt exhibited different effects on CV and AO release, dependent on ion composition and strength. Although NaCl showed little effect on the release of CV, it had the strongest effect on AO release, independent of ionic strength. KCl had a stronger concentration-dependent impact on CV release than NaCl, but less effect on AO release. Sodium acetate had the strongest effect on CV release and also some influence on AO release but only at a concentration ≥200 mM (Fig. 4a).

The release kinetics of CFl from eADF4(κ16) particles, in contrast, was in general faster than any release from eADF4(C16) particles, independent of the presence of salt. In case of CFl release from eADF4(κ16) particles, all used salts induced a complete release after 2 h of incubation (exemption: 100 mM sodium acetate).

As the radii of chloride anions are smaller than those of CFl, the local ionic strength is slightly higher allowing a tighter interaction between chloride and the amino groups of

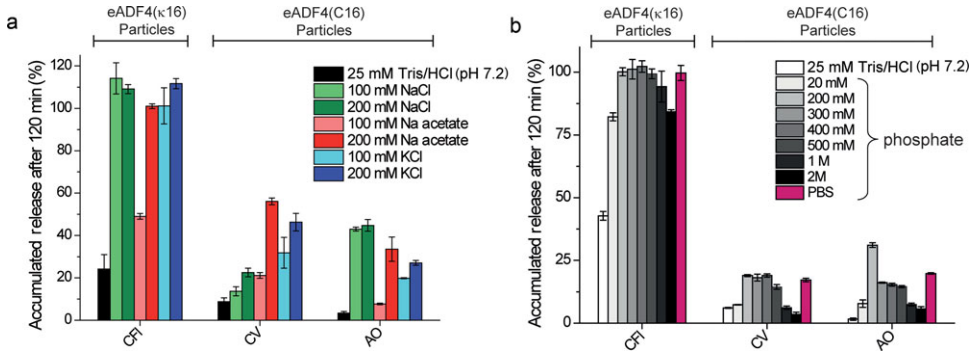

Figure 4. (a) Salt-dependent release of CFl from eADF4(κ16) particles and CV and AO from eADF4(C16) particles. (b) Release of CFl from eADF4(κ16) particles and CV and AO from eADF4(C16) particles in the presence of potassium phosphate. Release experiments were performed at 37°C.

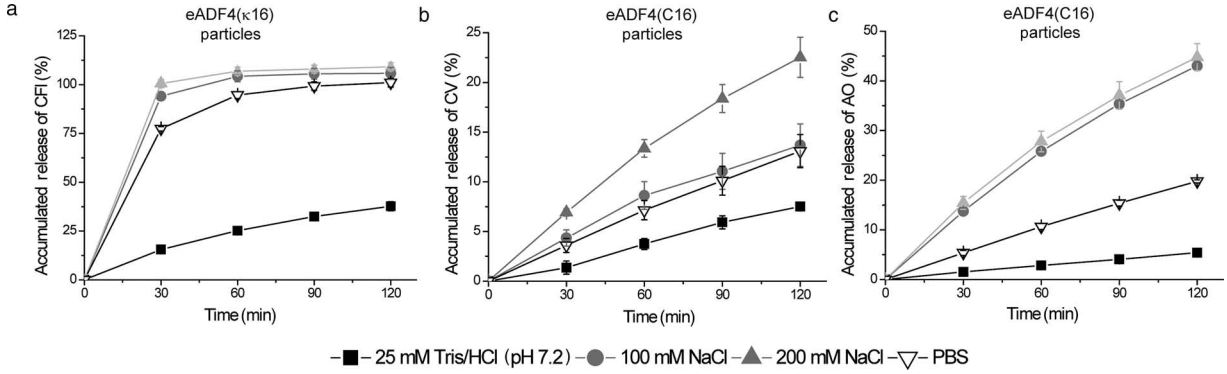

Figure 5. Time course of dye release depending on ionic strength. (a) CFl release from eADF4(κ16) particles, (b) CV, and (c) AO release from eADF4(C16) particles. Release experiments were performed at 37°C.

lysine residues in eADF4(κ16). Acetate ions are slightly larger than chloride ions, and, therefore, the interaction with lysine residues in eADF4(κ16) is not as pronounced (Fig. 4a). In contrast, in case of polyanionic eADF4(C16) particles, the influence of cations should be high. However, not only cations but also their counter anions significantly affected the release of model substances from eADF4(C16) particles. In the presence of KCl, release of CV from eADF4(C16) particles was increased, whereas NaCl had only a negligible influence. Sodium acetate showed the highest impact on CV release at 200 mM. Release of AO was strongly accelerated in the presence of NaCl after 2 h, whereas in the presence of KCl or sodium acetate release of AO was lower (Fig. 4b).

Influence of ions on release depends not only on charge and hydrodynamic radii but also on kosmotropic properties. According to the Hofmeister series, acetate anions are more kosmotropic than chloride ions.[34] Although sodium acetate had the greatest impact on CV release from eADF4(C16) particles, the release of AO from eADF4(C16) particles was only moderately accelerated in the presence of sodium acetate, probably because of the fact that acetate can increase hydrophobic interactions.[34] As AO is not solely bound to the particles via electrostatic interactions but also via hydrophobic interactions, this behavior is not surprising. The presence of kosmotropic salts strengthens the interactions between AO and eADF4(C16) particles.

To confirm this finding, the influence of physiologically relevant kosmotropic potassium phosphate was tested. Although release of CFl from eADF4(κ16) particles was complete in the presence of PBS or potassium phosphate after 2 h, less release was detected at phosphate concentrations above 400 mM (Fig. 4b). The salting-out effect of phosphate might induce a collapse of the brush-like outer shell of silk particles,[21] lowering the particle pore sizes and, therefore, decelerating release rates of bound substances. Furthermore, phosphate is more kosmotropic in comparison to acetate and is, therefore, increasing the hydrophobic effect. In case of AO, the interaction between the hydrophobic dye and the hydrophobic amino acids of spider silk proteins is strengthened, and thus release rates are decreased (Fig. 4b).

Alternatively, differences between the uptake and release behavior of eADF4(C16) and eADF4(κ16) particles could rely on their different "local" hydrophobicities. Lysine residues are slightly more hydrophilic with hydropathy indices of −3.9 in comparison to −3.5 of glutamic acid residues.[35] Furthermore, their solvation energies differ slightly (glutamate: −112.74 kcal/mol; lysine: −132.27 kcal/mol).[36] Therefore, lysine residues are more hydrated and hence more accessible to salt ions and less affected by kosmotropic salts that strengthen hydrophobic interactions.

Release Kinetics

Release rates of CFl from eADF4(κ16) particles were rapid in the presence of NaCl and only slightly slower in the presence of PBS. In contrast, release rates of CV and AO from eADF4(C16) particles were generally slower than the release rate of CFl from eADF4(κ16) and exhibited linear behavior, indicating stronger interactions between the dyes and eADF4(C16) in comparison to binding of CFl to eADF4(κ16).

As lysine residues are more hydrophilic and thus more easily accessible to both solvent and salts,[35] salt impact is more pronounced in case of eADF4(κ16) particles. As expected, a linear release could be determined in the control (Tris buffer; Fig. 5a). The release rates of dyes from eADF4(C16) particles were almost linear, also in the presence of salts. However, NaCl accelerated the release rates, especially in case of AO, because the salting-in properties of NaCl weakened the hydrophobic interactions between dye and silk proteins.

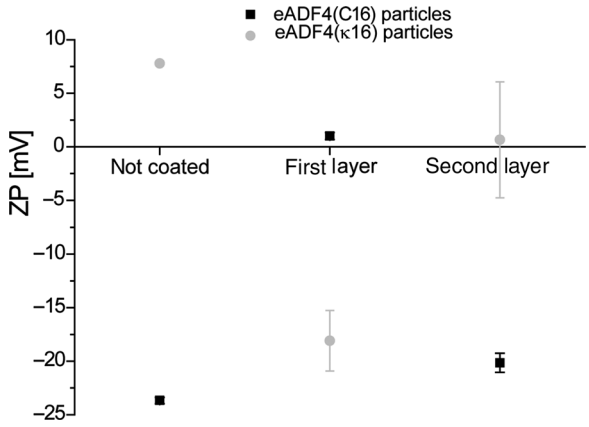

Figure 6. Zeta potential measurements of coated spider silk protein particles. Particles were measured without loading (not coated) and after coating with the oppositely charged protein [e.g., first layer: eADF4(C16) particles plus eADF4(κ16) layer] or upon a successive second coating [e.g., second layer: eADF4(C16) particles + eADF4(κ16) layer + eADF4(C16) layer].

 DOI 10.1002/jps.24300

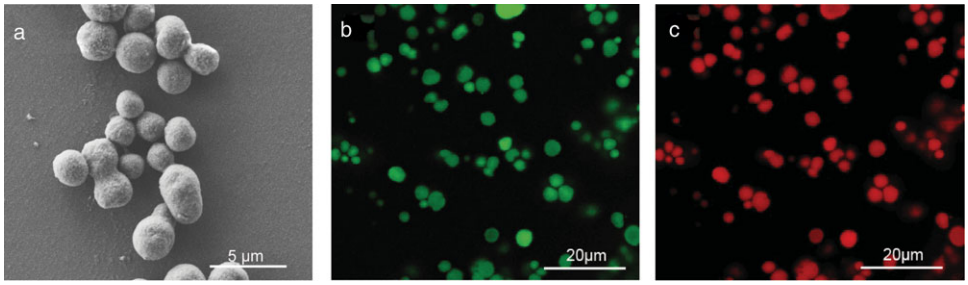

Figure 7. Microscopic analysis of samples of dye-loaded and eADF4(C16)-coated eADF4(κ16) particles. (a) SEM image of CFl-loaded and eADF4(C16)-Rho-coated eADF4(κ16) particles. CLSM images of eADF4(κ16) particles showing (b) CFl fluorescence and (c) eADF4(C16)-Rho fluorescence.

Control of Drug Release Using Layer-by-Layer Silk Particles

eADF4(κ16) particles are suitable carriers for negatively charged substances. However, the release of small-molecular-weight substances is too fast for most applications. To overcome this deficit, layer-by-layer (LbL) coating of eADF4(κ16) particles was tested using soluble eADF4(C16). As both spider silk proteins reflect polyelectrolytes with opposite charges, it was possible to deposit ultrathin films of the second protein on the particles of the first one based on electrostatic interactions between the two spider silk proteins.[37–40] Efficiency of the coating procedure was shown using ZP measurements (Fig. 6).

Successful eADF4(C16) coating of substance-loaded eADF4(κ16) particles was confirmed by SEM showing that LbL particles maintained the shape of the original ones (Fig. 7a). This was further confirmed using CLSM revealing that there were eADF4(κ16) particles with both CFl and eADF4(C16)-Rho fluorescence (Figs. 7b and 7c).

Next, release of CFl was tested from LbL particles [eADF4(κ16) particles with eADF4(C16) coatings, Fig. 8]. Contrary to our expectations, the release from coated particles was slightly increased in comparison to that from uncoated particles. Although the eADF4(C16) layer surrounding eADF4(κ16) particles is negatively charged, it accelerated release rather than slowed it down. A reasonable explanation is that the pores in the top eADF4(C16) layer may be too large to prohibit release, and, therefore, release was driven by electrostatic repulsion instead of physical barriers.

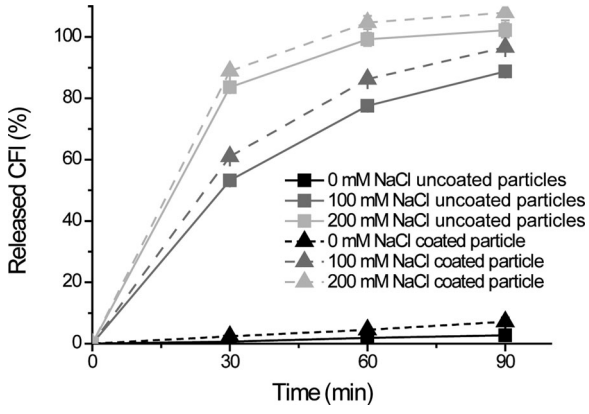

Figure 8. Comparison of CFl release from uncoated and eADF4(C16)-coated eADF4(κ16) particles in dependence of NaCl concentration at 37°C.

CONCLUSIONS

It was shown that particles of the newly designed polycationic spider silk protein eADF4(κ16) can be used to encapsulate negatively charged substances. Nucleic acids are bound to eADF4(κ16) particles by strong electrostatic interactions because of the high-charge density of DNA. In the presence of salt, nucleic acids are slowly released, in contrast to small molecular weight substances, such as CFl, which show a burst release within the first 30 min of incubation under all tested conditions. The weak electrostatic interactions of CFl with eADF4(κ16) are based on its low-charge density and the high hydrophilicity of lysine residues in the recombinant spider silk protein. In comparison, release kinetics of positively charged substances from polyanionic eADF4(C16) is slow and linear, but is salt dependent. Importantly, it is possible to slow down release in the presence of kosmotropic salts inducing a collapse of the brush-like outer particle shell and strengthening inter- and intramolecular hydrophobic interactions. Interestingly, LbL coating of eADF4(κ16) particles with eADF4(C16) did not slow down the release of small molecular substances. In summary, release kinetics of substances from spider silk protein particles is mainly influenced by the compound's properties with dependence on charge, hydrophobicity, molecular weight, and steric aspects.

ACKNOWLEDGMENTS

This work was supported by the SFB840 TP A8. The authors would like to thank Johann Erath for technical support at the CLSM and Martin Humenik, Joschka Bauer, and Kristin Schacht for scientific discussions.

REFERENCES

1. Allen TM, Cullis PR. 2004. Drug delivery systems: Entering the mainstream. Science 303:1818–1822.
2. Langer R. 1990. New methods of drug delivery. Science 249:1527–1533.
3. Arshady R. 1990. Review: Biodegradable microcapsular drug delivery systems: Manufacturing methodology, release control and targeting prospects. J Bioact Compat Polym 5:315–342.
4. Altman GH, Diaz F, Jakuba C, Calabro T, Horan RL, Chen J, Lu H, Richmond J, Kaplan DL. 2003. Silk-based biomaterials. Biomaterials 24:401–416.
5. Shelke NB, James R, Laurencin CT, Kumbar SG. 2014. Polysaccharide biomaterials for drug delivery and regenerative engineering. Polym Advan Technol 25:448–460.

6. Lammel A, Schwab M, Hofer M, Winter G, Scheibel T. 2011. Recombinant spider silk particles as drug delivery vehicles. Biomaterials 32:2233–2240.
7. Roemer L, Scheibel T. 2007. Grundlage für neue Materialien—Spinnenseidenproteine. Chem Unserer Zeit 41:306–314.
8. Huemmerich D, Helsen CW, Quedzuweit S, Oschmann J, Rudolph R, Scheibel T. 2004. Primary structure elements of spider dragline silks and their contribution to protein solubility. Biochemistry 43:13604–13612.
9. Lammel A, Schwab M, Slotta U, Winter G, Scheibel T. 2008. Processing conditions for the formation of spider silk microspheres. ChemSusChem 1:413–416.
10. Slotta UK, Rammensee S, Gorb S, Scheibel T. 2008. An engineered spider silk protein forms microspheres. Angew Chem Int Ed 47:4592–4594.
11. Schacht K, Scheibel T. 2011. Controlled hydrogel formation of a recombinant spider silk protein. Biomacromolecules 12:2488–2495.
12. Numata K, Hamasaki J, Subramanian B, Kaplan DL. 2010. Gene delivery mediated by recombinant silk proteins containing cationic and cell binding motifs. J Control Release 146:136–143.
13. Blüm C, Nichtl A, Scheibel T. 2014. Spider silk capsules as protective reaction containers for enzymes. Adv Funct Mater 24:763–768.
14. Humenik M, Magdeburg M, Scheibel T. 2014. Influence of repeat numbers on self-assembly rates of repetitive recombinant spider silk proteins. J Struct Biol 186:431–437.
15. Vollrath F, Barth P, Basedow A, Engstrom W, List H. 2002. Local tolerance to spider silks and protein polymers in vivo. In Vivo 16:229–234.
16. Leal-Egaña A, Scheibel T. 2010. Silk-based materials for biomedical applications. Biotechnol Appl Biochem 55:155–167.
17. Allmeling C, Jokuszies A, Reimers K, Kall S, Choi CY, Brandes G, Kasper C, Scheper T, Guggenheim M, Vogt PM. 2008. Spider silk fibres in artificial nerve constructs promote peripheral nerve regeneration. Cell Prolif 41:408–420.
18. Lammel A, Keerl D, Römer L, Scheibel T. 2008. Proteins: Polymers of natural origin. In Recent advances in biomaterials research; Jie Hu, Ed. Transworld Research Network, Kerala, India pp 1–22.
19. Spiess K, Lammel A, Scheibel T. 2010. Recombinant spider silk proteins for applications in biomaterials. Macromol Biosci 10:998–1007.
20. Neubauer MP, Blüm C, Agostini E, Engert J, Scheibel T, Fery A. 2013. Micromechanical characterization of spider silk particles. Biomater Sci 1:1160–1165.
21. Helfricht N, Klug M, Mark A, Kuznetsov V, Blum C, Scheibel T, Papastavrou G. 2013. Surface properties of spider silk particles in solution. Biomater Sci 1:1166–1171.
22. Blüm C, Scheibel T. 2012. Control of drug loading and release properties of spider silk sub-microparticles. Bio Nano Sci 2:67–74.
23. Hofer M, Winter G, Myschik J. 2012. Recombinant spider silk particles for controlled delivery of protein drugs. Biomaterials 33:1554–1562.
24. Sakurai H, Kawabata K, Sakurai F, Nakagawa S, Mizuguchi H. 2008. Innate immune response induced by gene delivery vectors. Int J Pharm 354:9–15.
25. Yu B, Hsu SH, Zhou C, Wang X, Terp MC, Wu Y, Teng L, Mao Y, Wang F, Xue W, Jacob ST, Ghoshal K, Lee RJ, Lee LJ. 2012. Lipid nanoparticles for hepatic delivery of small interfering RNA. Biomaterials 33:5924–5934.
26. Williford JM, Wu J, Ren Y, Archang MM, Leong KW, Mao HQ. 2014. Recent advances in nanoparticle-mediated siRNA delivery. Annu Rev Biomed Eng 16:347–370.
27. Kichler A. 2004. Gene transfer with modified polyethylenimines. J Gene Med: 6 3–10.
28. Clamme JP, Azoulay J, Mely Y. 2003. Monitoring of the formation and dissociation of polyethylenimine/DNA complexes by two photon fluorescence correlation spectroscopy. Biophys J 84:1960–1968.
29. Liu Y, You R, Liu G, Li X, Sheng W, Yang J, Li M. 2014. Antheraea pernyi silk fibroin-coated PEI/DNA complexes for targeted gene delivery in HEK 293 and HCT 116 cells. Int J Mol Sci 15:7049–7063.
30. Fischer D, Li Y, Ahlemeyer B, Krieglstein J, Kissel T. 2003. In vitro cytotoxicity testing of polycations: Influence of polymer structure on cell viability and hemolysis. Biomaterials 24:1121–1131.
31. Frohlich E. 2012. The role of surface charge in cellular uptake and cytotoxicity of medical nanoparticles. Int J Nanomed 7:5577–5591.
32. Hunter RJ. 1981. Zeta potential in colloid science. New York: Academic Press.
33. Holmberg EG, Verkman AS, Dix JA. 1989. Mechanism of acridine orange interaction with phospholipids and proteins in renal microvillus vesicles. Biophys Chem 33:245–256.
34. Hofmeister F. 1888. Zur Lehre von der Wirkung der Salze. Archiv f. experiment. Pathol. u. Pharmakol 24:247–260.
35. Kyte J, Doolittle RF. 1982. A simple method for displaying the hydropathic character of a protein. J Mol Biol 157:105–132.
36. Dixit SB, Bhasin R, Rajasekaran E, Jayaram B. 1997. Solvation thermodynamics of amino acids assessment of the electrostatic contribution and force-field dependence. J Chem Soc Faraday Trans 93:1105–1113.
37. Decher G, Hong JD, Schmitt J. 1992. Buildup of ultrathin multilayer films by a self-assembly process: III. Consecutively alternating adsorption of anionic and cationic polyelectrolytes on charged surfaces. Thin Solid Films 210–211, Part 2:831–835.
38. Wang X, Kim HJ, Xu P, Matsumoto A, Kaplan DL. 2005. Biomaterial coatings by stepwise deposition of silk fibroin. Langmuir 21:11335–11341.
39. Donath E, Sukhorukov GB, Caruso F, Davis SA, Möhwald H. 1998. Novel hollow polymer shells by colloid-templated assembly of polyelectrolytes. Angew Chem Int Ed 37:2201–2205.
40. Antipov AA, Sukhorukov GB, Leporatti S, Radtchenko IL, Donath E, Möhwald H. 2002. Polyelectrolyte multilayer capsule permeability control. Colloids Surf A 198–200:535–541.

5.2 Teilarbeit II

Cellular uptake of drug loaded spider silk particles

Autoren: Martina B. Schierling*, **Elena Doblhofer*** und Thomas Scheibel

Die Analysen zur Elektrokinetik und kolloidalen Stabilität der eADF4 Partikel und die chemische Modifikation, sowie Analysen der Modellsubstanzen wurde von mir vorgenommen. Die Zellkulturexperimente und die Studien zur Freisetzung von Doxorubizin aus eADF4 Partikeln wurde von Martina B. Schierling durchgeführt. Dieses Projekt wurde von Martina B. Schierling und mir zusammen mit Thomas Scheibel konzipiert. Das Manuskript wurde ebenfalls von Martina B. Schierling und mir verfasst und zusammen mit Thomas Scheibel fertig gestellt.

Der Artikel wurde am 23.08.2017 im Journal *Biomaterials Science* veröffentlicht

* Gleichberechtigte Co-Autorenschaft

Biomaterials Science

PAPER

Cite this: *Biomater. Sci.*, 2016, **4**, 1515

Cellular uptake of drug loaded spider silk particles†

Martina B. Schierling,‡[a] Elena Doblhofer‡[a] and Thomas Scheibel*[a,b,c,d,e]

Received 29th June 2016,
Accepted 23rd August 2016

DOI: 10.1039/c6bm00435k

www.rsc.org/biomaterialsscience

Medical therapies are often accompanied by un-wanted side-effects or, even worse, targeted cells can develop drug resistance leading to an ineffective treatment. Therefore, drug delivery systems are under investigation to lower the risk thereof. Drug carriers should be biocompatible, biodegradable, nontoxic, non-immunogenic, and should show controllable drug loading and release properties. Previous studies qualified spider silk particles as drug delivery carriers, however, cellular uptake was only tested with unloaded spider silk particles. Here, the effect of drug loading on cellular uptake of previously established spider silk-based particles made of eADF4(C16), eADF4(C16)RGD, eADF4(C16)R_8G and eADF4(κ16) was investigated. Fluorescently labelled polyethylenimine was used as a model substance for loading eADF4(C16), eADF4(C16)RGD or eADF4(C16)R_8G particles, and fluorescently labelled ssDNA was used for loading eADF4(κ16) particles. Upon loading polyanionic eADF4(C16) and eADF4(C16)RGD particles with polycationic polyethylenimine the cellular uptake efficiency was increased, while the uptake of eADF4(C16)R_8G and polycationic eADF4(κ16) particles was decreased upon substance loading. The latter could be circumvented by coating substance-loaded eADF4(κ16) particles with an additional layer of eADF4(κ16) (layer-by-layer coating). Further, it could be shown that eADF4(C16)RGD and eADF4(κ16) uptake was based on clathrin-mediated endocytosis, whereas macropinocytosis was more important in case of eADF4(C16) and eADF4(C16)R_8G particle uptake. Finally, it was confirmed that drugs, such as doxorubicin, can be efficiently delivered into and released within cells when spider silk particles were used as a carrier.

Introduction

The severe side-effects of some conventional medical therapies strongly influence quality of life or cause even mortality. To minimize these effects, drug delivery systems are envisioned to direct drugs to specific tissues or even inside targeted cells. These systems have to fulfil several requirements like controllable physicochemical properties, colloidal stability, the shielding of drug degradation by hydrolysis or enzymatic reactions as well as the controllable release of the drug at the target tissue or within the target cell.[1] Polymers are the preferred material for carrier systems, because they can be modified according to the desired application. Additionally, polymers can be tuned for controllable interactions with drugs allowing a defined drug release over days or even months.[2,3] Unfortunately, several synthetic polymers are not biocompatible or need organic solvents and harsh formulation conditions during processing or generate toxic degradation products. Natural polymers, in contrast, are biocompatible, can often be processed under mild conditions, and can be degraded by enzymatic reactions without yielding toxic side products.[4,5] Drug carriers made of natural polymers can further be functionalized to enhance their cellular uptake specificity by modifications with cell interacting motifs like the RGD sequence or cell penetrating peptides (CPP).[6–8]

Among biopolymers, spider silk proteins and materials made thereof are promising candidates for biomedical applications due to their biocompatibility, biodegradability and mechanical properties.[9] Since natural spider silk proteins are not available in high amounts due to the cannibalistic behavior of spiders, recombinant production techniques of the proteins have been developed.[10,11] The well-established recombinant spider silk protein eADF4(C16) is based on one major ampullate spidroin (MaSp) of the dragline silk of the European

[a]*Lehrstuhl Biomaterialien, Universitätsstraße 30, Universität Bayreuth, Bayreuth D-95447, Germany. E-mail: thomas.scheibel@bm.uni-bayreuth.de; Fax: +49 (0)921 55 7346; Tel: +49 (0)921 55 7361*
[b]*Bayreuther Zentrum für Kolloide und Grenzflächen (BZKG), Universitätsstraße 30, Universität Bayreuth, Bayreuth D-95447, Germany*
[c]*Bayreuther Zentrum für Bio-Makromoleküle (bio-mac), Universitätsstraße 30, Universität Bayreuth, Bayreuth D-95447, Germany*
[d]*Bayreuther Zentrum für Molekulare Biowissenschaften (BZMB), Universitätsstraße 30, Universität Bayreuth, Bayreuth D-95447, Germany*
[e]*Bayreuther Materialzentrum (BayMAT), Universitätsstraße 30, Universität Bayreuth, Bayreuth D-95447, Germany*

†Electronic supplementary information (ESI) available: Loading efficiency, SEM images of the particles, sedimentation curves. See DOI: 10.1039/c6bm00435k

‡Contributed equally.

garden spider (*Araneus diadematus*).[12] eADF4(C16) can be processed into different morphologies like films,[13,14] non-woven mats,[15] hydrogels,[16] capsules,[17,18] and particles.[19,20] The particles can be loaded with different low molecular weight substances or small proteins.[21–23] Due to the negative net charge of eADF4(C16) at neutral pH (based on 16 glutamic acid residues) only positively charged or neutral substances can be loaded onto particles made therefrom. Replacement of all glutamic acid residues by lysines yielded the engineered positively charged spider silk protein, eADF4(κ16).[23] eADF4(κ16) particles can be loaded with negatively charged substances with low and high molecular weights.[23] The loading and release efficiencies for both types of particles have been thoroughly analyzed previously.[21–23] It could be shown that HeLa cells take up eADF4(κ16) particles quite well. Also particles made of fusions between eADF4(C16) and the cell penetrating peptide R_8G or the integrin-binding peptide RGD are taken up but to a lower extent, and the lowest cellular uptake was detected for eADF4(C16) particles.[24]

Since drug loading influences the surface properties of spider silk particles, this particular feature has been investigated here concerning its impact on the cellular uptake of eADF4(κ16), eADF4(C16), eADF4(C16)RGD and eADF4(C16)R_8G particles. Single stranded DNA was loaded onto eADF4(κ16) particles, and polyethylenimine was loaded onto eADF4(C16), eADF4(C16)RGD and eADF4(C16)R_8G particles as model substances. Loading of such highly charged model substances significantly and differently influenced the cellular uptake of spider silk particles dependent on the silk protein employed. Further, upon using doxorubicin as a model drug it could be shown that drugs can efficiently be delivered into and released within the target cells by using spider silk particles as carrier.

Experimental section

Protein production and purification

The recombinant spider silk proteins eADF4(C16), eADF4(C16)RGD, eADF4(C16)R_8G and eADF4(κ16) were produced and purified as described previously.[12,23,24]

Coupling of rhodamine to spider silk proteins

Lyophilized spider silk proteins were dissolved in 6 M guanidinium thiocyanate and dialyzed against 10 mM HEPES, pH 7.0. Dialyzed spider silk proteins were incubated with a 15-fold molar excess of 5/6-carboxy-tetramethyl-rhodamine succinimidyl ester (ThermoFisher, Darmstadt, Germany) in the absence of light for 2 h at 25 °C. Afterwards, the labeled proteins were precipitated by adding 2 M potassium phosphate, pH 8.0 in a 1 : 1 volume ratio, and the mixture was incubated for 1 h at 25 °C. The precipitated, labelled protein was washed three times with ultra-pure water and then lyophilized.

Spider silk particle formation

The particles were produced according to Elsner *et al.*[24] Briefly, lyophilized proteins were dissolved in 1-ethyl-3-methyl-imidazolium acetate (EMiM[acetate]). Particle formation was initiated by mixing of 0.1 mg ml^{-1} protein in EMiM[acetate] with 5 equivalents (eq.) (v/v) of 2 M potassium phosphate, pH 8.0.[19,24] After incubation for 1 h at 25 °C, the particles were centrifuged (15 min, 17 000*g*, 4 °C), and then the pellets washed three times with ultra-pure water.

Fluorescence labelling of DNA and polyethylenimine

1 eq. NH_2-ODN (NH_2-C_6-5-ggt cac ttc gtg gct aac g-3 (6971 Da), biomers.net, Ulm, Germany) was dissolved in 100 mM sodium phosphate buffer, pH 7.9 containing 25 eq. NHS-Fl (*N*-hydroxy succinimidyl fluorescein dissolved in DMSO). After 3 h of incubation the sample was mixed with 4 M sodium acetate, pH 5.0 and ethanol p.a. to final concentrations of 100 mM and 70%, respectively. For precipitation of the resulting Fl-ODN (Fluorescein-C_6-5-ggt cac ttc gtg gct aac g-3 (7302 Da)) the mixture was incubated for 30 min at −20 °C, centrifuged at 8500 rpm and 4 °C and washed with ethanol p.a. The Fl-ODN pellet was resuspended, and the precipitation repeated with ethanol p.a. twice. Finally, Fl-ODN was resuspended in ultra-pure water at the appropriate concentrations for particle loading.

Polyethylenimine (PEI; M_n = 8000 Da, PDI 1.1, Sigma-Aldrich, Seelze, Germany) was dissolved in sodium carbonate buffer, pH 7.9 at a concentration of 2 mg ml^{-1}. Afterwards, NHS-Fl (1 mg ml^{-1} in DMSO) was added slowly to the PEI solution while stirring followed by 8 h of incubation at 4 °C. The reaction was stopped by addition of 50 mM ammonium chloride and further 2 h of incubation at 4 °C. To separate remaining NHS-Fl, NH_4Cl or sodium phosphate from the resulting PEI-Fl (fluorescein labelled PEI), the reaction mixture was dialyzed against ultra-pure water for 46 h at 25 °C, using dialysis membranes with a molecular weight cut-off of 500–1000 Da (SPECTRUM® LABORATORIES, Irving, Texas).

Loading of spider silk particles

All particles were loaded by diffusion. Fl-ODN was dissolved in ultra-pure water and added to 0.5 mg eADF4(κ16) particles at various concentrations (0.02, 0.1 and 0.4 nmol mg^{-1} particles) in a volume of 100 µl. The particles were incubated in the respective Fl-ODN solution for 1 h, then centrifuged (17 000*g*, 15 min, 25 °C) and washed twice with ultra-pure water.

eADF4(C16), eADF4(C16)RGD and eADF4(C16)R_8G particles were loaded with 0.02, 0.1 and 0.4 nmol PEI-Fl per mg protein as described for eADF4(κ16) particles loaded with Fl-ODN. After 1 h of incubation, the particles were centrifuged (17 000*g*, 15 min, 25 °C) and washed twice with ultra-pure water.

2 mM of doxorubicin (Dox) were incubated with 14.77 µg of plasmid DNA (pEGFP-N1) for 12 h at 25 °C. The DNA/Dox mixture or Dox alone were then added to the eADF4(κ16) particles and incubated for 2 h at 25 °C, centrifuged (17 000*g*, 15 min, 25 °C) and washed twice with ultra-pure water. The supernatant was analyzed using UV/Vis spectroscopy ($\lambda_{max,Dox}$ = 501 nm) to determine the loading and loading efficiency (eqn (1) and (2)). Afterwards, particles were treated

using the layer-by-layer (LbL) coating procedure described in the section above.

$$\text{Loading}\,(\%) = \frac{\text{Amount of substance in particles}}{\text{Amount of silk protein}} \times 100 \quad (1)$$

$$\text{Loading efficiency}\,(\%) = \frac{\text{Amount of substance in particles}}{\text{Amount of dye added}} \times 100 \quad (2)$$

Release of Dox from DNA/Dox loaded eADF4(κ16) particles

Release of Dox from eADF4(κ16) particles was analyzed by UV/Vis spectroscopy at $\lambda_{max,Dox}$ = 501 nm every 30 min in PBS for 180 min at 37 °C. At each time point particles were centrifuged (17 000*g*, 2 min, 25 °C), the supernatant was analyzed, and the pellet resuspended in fresh PBS. The accumulated release was plotted against time, with the start of the experiment being set to zero minutes. After 180 min of incubation, particles were treated with DNaseI (2000 U ml^{-1}), Trypsin (1 μl ml^{-1}) or both for 24 h at 37 °C (10 mM Tris/HCl, 10 mM $MgCl_2$, 10 mM $CaCl_2$, pH 7.5), centrifuged (17 000*g*, 2 min, 25 °C), and the supernatant was analyzed using again UV/Vis spectroscopy to detect released Dox.

Layer-by-layer coating of spider silk particles

LbL-Coating of spider silk particles was performed as described previously.[23] Loaded (Fl-ODN, DNA/Dox or Dox) eADF4(κ16) particles were resuspended in 1 ml of freshly prepared eADF4(κ16) protein solution at a protein concentration of 0.8 mg ml^{-1}. After 1 h of incubation, particles were centrifuged (17 000*g*, 2 min, 25 °C) and washed with ultra-pure water.

Electrophoretic mobility determination

Spider silk particles were analyzed concerning their electrophoretic mobility in 1/11 PBS pH 7.4 (0.4 mM KH_2PO_4, 1.6 mM Na_2HPO_4, 11.5 mM NaCl) at 25 °C (ZetaSizer, NanoZS, Malvern Instruments, Worcestershire, UK). The zeta potential was calculated according to the theory of Smoluchowski.[25]

Particle size determination

The size of dehydrated particles was analyzed by scanning electron microscopy (SEM) imaging and subsequent diameter determination using the analytical software *ImageJ*. The number of analyzed particles was at least n = 30.

SEM images were taken using a 1450Es Beam (Zeiss, Germany) at an accelerating voltage of 3 kV. Particles were pipetted onto Thermanox™ plastic cover slips and washed three times with distilled water. Before imaging, the particles were air dried and sputtered with platinum.

Colloidal stability analysis

Colloidal stability of spider silk particles was analyzed in ultrapure water using a LUMiFuge®114 (L.U.M. GmbH, Berlin, Germany) with a rotation frequency of 300, 600 and 900 rpm and different time intervals of 200, 300, and 1000 s. Particle suspensions were placed in tubes in horizontal positions on the disc of the LUMiFuge®114. Transparencies of the particle suspensions were measured in the area between the menisci and bottom of the vial three times for each particle type. Transmission was measured every 10 s over 1800 s, and the integral of transmission between meniscus and bottom of the vial was plotted against time.

Cell culture

HeLa cells (German Collection of Microorganism and Cell Cultures DSMZ) and BALB/3T3 mouse fibroblast (European Collection of Cell Culture) were cultured in DMEM (Dulbecco's Modified Eagle Medium, Biochrom, Berlin, Germany) supplemented with 10% v/v fetal bovine serum (Biochrom, Berlin, Germany), 1% v/v GlutaMAX (Gibco, Grand Island, USA) and 0.1% v/v gentamicin sulfate (Sigma-Aldrich, Seelze, Germany). Kelly neuroblastoma cells (German Collection of Microorganism and Cell Cultures DSMZ) were cultured in RPMI 1640 (Roswell Park Memorial Institute 1640 Medium, Lonza, Verviers, Belgium) supplemented with 10% v/v fetal bovine serum (Biochrom, Berlin, Germany), 1% v/v GlutaMAX (Gibco, Grand Island, USA) and 0.1% v/v gentamicin sulfate (Sigma-Aldrich, Seelze, Germany). The cell viability was confirmed by trypan blue staining (Sigma-Aldrich, Seelze, Germany) before seeding the cells. Cells were cultured in a CO_2-incubator (Heraeus, Hanau, Germany) at 5% CO_2, 95% humidity and at 37 °C.

Analysis of cytotoxicity

Cells were seeded on treated 96-well cell culture plates (Nunc, Langenselbold, Germany) at a density of 20 000 cells per cm^2 (HeLa, BALB/3T3) or 50 000 cells per cm^2 (Kelly). The seeded cells were pre-incubated with spider silk particles (9.6, 48, or 96 ng μl^{-1}) for 6 or 24 h at 37 °C. Medium was changed after 6 h, 24 h or 48 h followed by analysis of cell viability using the CellTiter Blue assay. Cells were washed twice with phosphate buffered saline (PBS). Fresh medium was added containing 10% v/v CellTiter Blue reagent® (Promega, Madison, USA), and cells were incubated for 2.5 h at 37 °C. The transformation of the blue fluorescent dye resazurin into red fluorescent resorufin (λ_{ex} = 530 nm; λ_{em} = 590 nm) was measured using a plate reader (Mithras LB 940, Bertold, Bad Wildbach, Germany) with 530 nm excitation and 600 nm emission filters and a counting time of 0.5 s. Cell culture experiments were repeated 3 times with 3 replicates for each particle type and drug.

Uptake analysis and identification of the uptake mechanism

For uptake studies and identification of the uptake mechanism, HeLa cells were cultured on treated 6-well cell culture plates (Nunc, Langenselbold, Germany) at a density of 30 000 cells per cm^2 in the presence of loaded spider silk particles for 24 h. Cells were washed with PBS twice, treated with trypan blue, washed again with PBS, detached using 0.05% Trypsin/EDTA and pelleted by centrifugation (300*g*, 5 min, 25 °C). Cells were resuspended in fresh media, and uptake was measured using flow cytometry (Cytomics FC500, Beckman-Coulter,

Krefeld, Germany). Cells only appeared fluorescent upon internalization of Rhodamine-labeled particles.

Endocytotic inhibitors were used for identification of the uptake mechanism. Cells were seeded at a density of 30 000 cells per cm^2. 100 μM dansylcadaverine (DC) for inhibition of clathrin-mediated endocytosis and 100 μM di-methyl-amiloride (DMA) for inhibition of macropinocytosis were added to the cells 30 min prior to particle addition (9.6 ng μl^{-1}), and all samples were further incubated for 24 h at 37 °C.

For fluorescence microscopy, HeLa cells were cultured on μ-slides (8-well, ibidi GmbH, Martinsried, Germany) at a cell density of 20 000 cells per cm^2 and incubated with loaded (Fl-ODN or Fl-PEI) rhodamine-labeled particles for 24 h at 37 °C. The cells were fixed with 4% w/v paraformaldehyde for 15 min at 25 °C, washed with PBS and permeabilized with 0.1% v/v Triton-X-100 for 3 min. After two additional washing steps with PBS, cells were incubated with HCS CellMask™ Blue stain (Invitrogen, Darmstadt, Germany) for 30 min and washed again with PBS. All samples were kept in PBS and analyzed using a fluorescence microscope (DMi8, Leica, Wetzlar, Germany).

Statistical analysis

An unpaired two-side *t*-test was performed with $n = 5$ for eADF4(κ16), $n = 4$ for eADF4(C16) and $n = 3$ for eADF4(C16)RGD and eADF4(C16)R_8G particles for statistical analysis. The significance was confirmed by a statistical certainty higher than 99.9% (significance level of <0.1%; ***).[24]

Results and discussion

Particle production and characterization

All recombinant spider silk proteins were dissolved in EMiM [acetate] and then precipitated as described previously yielding particles with low diameters and small size distribution.[24] Particles were loaded by diffusion with different amounts of model substances. In the case of eADF4(κ16) Fl-ODN was chosen as a negatively charged high molecular weight substance and as model for siRNA, and PEI-Fl, a highly positively charged synthetic polymer, as a model substance in the cases of eADF4(C16), eADF4(C16)RGD, and eADF4(C16)R_8G (0.02, 0.1 or 0.4 nmol model substance per mg particles). Due to the detection limit, loading efficiencies were only determined for the highest loading amounts. All particles (eADF4(C16) variants) loaded with PEI-Fl showed a similar loading efficiency of around 25%, and no significant difference in the particle's interaction with the model substance was detectable regardless of the underlying protein. The loading efficiency of Fl-ODN onto eADF4(κ16) particles was higher in comparison to all eADF4(C16) variants (41%). This effect could be in part attributed to a lower molecular weight and a lower charge density of the model substance Fl-ODN in comparison to PEI-Fl (Table S1†).

SEM imaging showed that the diameter of dehydrated particles was roughly between 200 and 400 nm, and no significant deviation was detectable amongst the different spider silk proteins (Table 1, Fig. S1†). However, due to the previously determined hierarchical set-up of the particles with a polymer-brush-like outer layer (thickness 30–50 nm) and a mechanically robust inner core,[26] diameters below 100 nm can hardly be achieved without losing the general properties of the particles. In addition, electrophoretic mobility and colloidal stability were indistinguishable in most cases before and after loading of the particles with either PEI-Fl or Fl-ODN (Table 1 and Fig. S2†). Analysis of loaded and unloaded eADF4(C16) and eADF4(C16)RGD particles in suspension showed only little sedimentation of the particles in the absence as well as in the presence of PEI-Fl upon exposure to a centrifugal field (LUMIFuge®) (Fig. S2A and B†). In the case of eADF4(C16)R_8G,

Table 1 Particle size, and electrophoretic mobility of unloaded and PEI-Fl or Fl-ODN loaded spider silk particles measured at an ionic strength of 12 mM (1/11 PBS) and pH 7.4 ($n = 6$); C: layer-by-layer coated particle

Spider silk particles	Model drug	Loading nmol mg^{-1} particles	Electrophoretic mobility/ 10^{-8} m^2 s^{-1} V^{-1}	Zeta potential[a]/mV	Particle diameter (dehydrated)/nm
eADF4(C16)	—	—	−2.10 ± 0.10	−26.78 ± 1.25	397 ± 115
	PEI-Fl	0.02	−1.97 ± 0.12	−25.15 ± 1.60	
	PEI-Fl	0.1	−1.88 ± 0.20	−23.93 ± 2.58	
	PEI-Fl	0.4	−1.99 ± 0.08	−25.43 ± 1.05	
eADF4(C16)RGD	—	—	−1.87 ± 0.25	−23.90 ± 3.25	232 ± 56
	PEI-Fl	0.02	−1.56 ± 0.07	−19.85 ± 0.85	
	PEI-Fl	0.1	−1.54 ± 0.05	−19.67 ± 0.59	
	PEI-Fl	0.4	−1.47 ± 0.06	−18.73 ± 0.83	
eADF4(C16)R_8G	—	—	−1.66 ± 0.06	−21.20 ± 0.82	315 ± 69
	PEI-Fl	0.02	−1.56 ± 0.06	−19.90 ± 0.79	
	PEI-Fl	0.1	−1.65 ± 0.04	−20.95 ± 0.53	
	PEI-Fl	0.4	−1.70 ± 0.06	−21.73 ± 0.75	
eADF4(κ16)	—	—	1.15 ± 0.09	14.68 ± 1.20	269 ± 60
	Fl-ODN	0.02	1.11 ± 0.08	14.12 ± 0.95	
	Fl-ODN	0.1	1.13 ± 0.08	14.43 ± 1.02	
	Fl-ODN	0.4	1.16 ± 0.06	14.85 ± 0.73	
eADF4(κ16)-C	Fl-ODN	0.4	0.73 ± 0.25	9.36 ± 3.17	—

[a] Calculated according to the theory of Smoluchowski.[25]

all samples showed increased sedimentation at a centrifugal speed of 900 rpm independent of the loading of the particles (Fig. S2C†). eADF4(κ16) particles were colloidally unstable with fast sedimentation at 300 rpm, 600 rpm and 900 rpm (Fig. S2D†). The incubation of the particles with Fl-ODN had only little influence on their colloidal stability. Surprisingly, coating of loaded eADF4(κ16) particles with another layer of this protein seemed to stabilize the particles in suspension (Fig. S2D†).

The lack of influence of substance loading on the electrophoretic mobility of the particles (Table 1) is possibly due to very low molar model-substance/protein ratios of 1 : 52 (0.4 nmol substance per mg protein), 1 : 208 (0.1 nmol substance per mg protein) and 1 : 1040 (0.02 nmol substance per mg protein). Further, it can be assumed that the largest proportion of the uptaken substance is not surface exposed.

Uptake analysis of loaded spider silk particles

Previously, eADF4(C16), eADF4(C16)RGD, and eADF4(C16)R_8G particles showed lower uptake efficiency in comparison to positively charged spider silk protein particles made of eADF4 (κ16) in HeLa cells.[23] While HeLa Cells revealed in general a very high uptake efficiency, other cell lines, like the neuroblastoma cell line Kelly and the mouse fibroblasts BALB 3T3 showed only limited uptake of the spider silk protein particles. Interestingly, protein modification with *e.g.* RGD had a negligible impact on this behavior (Data not shown). Furthermore, it was shown that the release of single stranded DNA (ssDNA) from eADF4(κ16) particles into buffer was rather slow in comparison to that of low molecular weight substances.[23] Here, eADF4(κ16), eADF4(C16), eADF4(C16)RGD and eADF4(C16)R_8G particles were loaded with Fl-ODN and PEI-Fl, respectively, as described above.

HeLa cells were incubated with 9.6 ng μl^{-1} of loaded eADF4 (κ16) particles for 24 h and analyzed using flow cytometry (Fig. 1) or fluorescence microscopy (Fig. 2). Interestingly, the uptake of loaded eADF4(κ16) particles was significantly reduced and depended on the amount of loading (Fig. 1). The higher the loading, the lower the number of cells which contained particles, and also the number of particles per cell was reduced (Fig. 2). Coating of loaded particles with an additional layer of eADF4(κ16) (eADF4(κ16)-0.4-C) increased the number of cells with incorporated particles as well as the average number of particles within each cell. HeLa cells were also incubated in the presence of eADF4(C16), eADF4(C16)RGD and eADF4(C16)R_8G particles loaded with 0.02, 0.1, and 0.4 nmol PEI-Fl per mg particles (eADF4(C16)-0.02, eADF4(C16)-0.1, eADF4(C16)-0.4, *etc.*). eADF4(C16) particles were internalized in 19.0% of HeLa cells after 24 h of incubation. Although the uptake efficiency was only slightly affected by loading the particles with 0.02 or 0.1 nmol PEI-Fl per mg particles, cells incubated with eADF4(C16)-0.4 particles showed a significantly higher uptake (54.4%). Unloaded eADF4(C16)RGD and eADF4 (C16)R_8G particles revealed a cellular uptake in the range between that of eADF4(C16) and eADF4(κ16) particles. While treatment of HeLa cells with loaded eADF4(C16)RGD particles

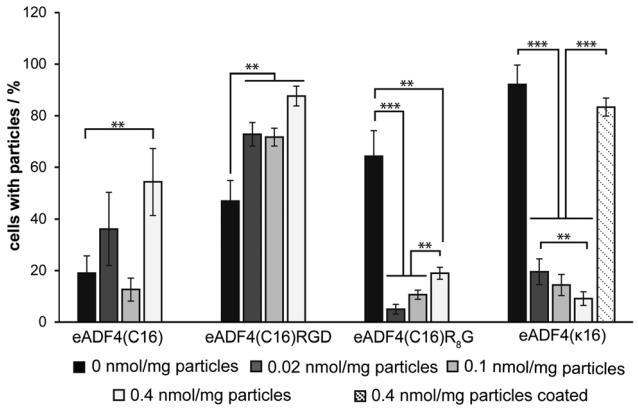

Fig. 1 Flow cytometry analysis of HeLa cells incubated in the presence of loaded spider silk particles. The HeLa cells were incubated together with 9.6 ng μl^{-1} of spider silk particles. eADF4(C16), eADF4(C16)RGD and eADF4(C16)R_8G particles were loaded with 0, 0.02, 0.1 and 0.4 nmol of PEI-Fl and eADF4(κ16) with 0, 0.02, 0.1 and 0.4 nmol of Fl-ODN per mg of particles and incubated for 24 h. eADF4(κ16) particles loaded with 0.4 nmol mg^{-1} particles of Fl-ODN were additionally coated with eADF4(κ16) using a layer-by-layer technique. Before measurements, cells were washed and treated with trypan blue quenching the fluorescence of Rhodamine labeled particles outside the cells (***highly significant; ** significant).

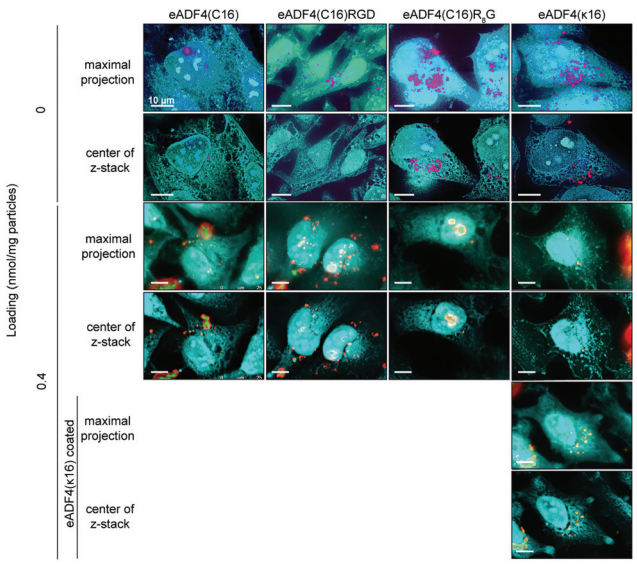

Fig. 2 Fluorescence microscopy images (maximal projections and middle of *z*-stack) of HeLa cells incubated in the presence of 9.6 ng μl^{-1} of spider silk particles for 24 h. eADF4(C16), eADF4(C16)RGD and eADF4 (C16)R_8G particles were loaded with 0 or 0.4 nmol PEI-Fl per mg particles and eADF4(κ16) particles with 0 or 0.4 nmol Fl-ODN per mg particles. As indicated, eADF4(κ16) particles were also coated with an additional layer of eADF4(κ16) after Fl-ODN loading using the layer-by-layer technique. Cells were fixed, permeabilized and stained with HCS CellMask™ blue stain. Cells: blue; particles: red; loaded drug (PEI-Fl or Fl-ODN): green. Scale bar: 10 μm.

increased the uptake efficiency to nearly 90%, the number of cells containing PEI-Fl loaded eADF4(C16)R_8G particles was significantly decreased to less than 20%. Conspicuous here is

the fact that, except for eADF4(C16) particles, even the smallest amount of loaded substance induced a divergent interaction between cells and particles. Loading with PEI-Fl increased cellular uptake with increasing loading in the case of eADF4(C16) and eADF4(C16)RGD particles. Most strikingly, in the case of eADF4(C16)R8G loading with PEI-Fl led to a tremendous reduction of internalized particles, which was again reversed to some extent when the PEI-Fl concentration within the particles was increased. However, this could not be attributed to changes in surface properties, since loading did apparently not affect the electrophoretic mobility of the particles, as described above. Since it was shown previously that cellular uptake was increased for particles containing the CPP R8G compared to plain eADF4(C16) particles, it can only be presumed that an interference of PEI-Fl with the R8G sequence is accountable for the rapid decrease in cellular uptake of loaded eADF4(C16)R8G particles. In fact, the PEI transfection mechanism has not yet been clarified on a cellular level.[27] Consequently, the conclusions from the obtained results remain open.

Identification of the uptake mechanism

To investigate the influence of drug loading on the internalization pathway of silk particles, HeLa cells were incubated in the presence of different endocytic inhibitors (dansylcadaverine (DC): inhibitor of clathrin-mediated endocytosis; dimethyl-amiloride (DMA): inhibitor of macropinocytosis)[28–31] prior to particle incubation for 24 h, and the uptake was analyzed using flow cytometry (Table 2).

In case of unloaded eADF4(κ16) particles, the percentage of cells with internalized particles was considerably reduced in the presence of the clathrin-mediated endocytosis inhibitor DC compared to the macropinocytosis inhibitor DMA. By loading eADF4(κ16) particles with different amounts of Fl-ODN, the percentage of eADF4(κ16) containing cells decreased further in the presence of DC indicating that clathrin-mediated endocytosis plays an important role. Coating of loaded eADF4(κ16) particles resulted in an uptake efficiency comparable to that of unloaded ones. The role of clathrin-mediated endocytosis and macropinocytosis of coated eADF4(κ16) particles was also similar to that of unloaded eADF4(κ16) particles.

As shown previously, the role of both clathrin-mediated endocytosis and macropinocytosis were similar for unloaded eADF4(C16) particles,[24] and no significant influence of PEI-Fl loading on the uptake mechanism of eADF4(C16) particles could be detected.

eADF4(C16)RGD-0.02, eADF4(C16)RGD-0.1 and eADF4(C16)RGD-0.4 were always taken up by slightly less cells in the presence of DC than in the presence of DMA. However, the decrease in numbers of cells containing loaded particles in the presence of DC was not as high as reported for unloaded ones. The uptake of unloaded eADF4(C16)R_8G particles occurred mostly by clathrin-mediated endocytosis and only partly by macropinocytosis.[24] The reduction of cells containing loaded eADF4(C16)R_8G particles was similar in the presence of DC and DMA. The results of the identification of the uptake mechanism of loaded eADF4(C16)RGD and eADF4(C16)R_8G particles lead to the conclusion that both uptake mechanisms are likewise important, whereas clathrin-mediated endocytosis plays a more important role in unloaded particle uptake.

Analysis of cell viability was conducted 24 h after addition of loaded and unloaded spider silk particles (using the CellTiter Blue® assay) ensuring that the change in uptake efficiencies cannot be ascribed to cytotoxic effects of the particles (Fig. 3). HeLa cells cultured in the presence of loaded or unloaded particles showed normal growth behavior. Thereby, neither the type of the particle, loaded or not, nor the loading concentration seemed to have a cytotoxic effect on HeLa cells.

Table 2 Cells at a starting density of 50 000 cells per cm^2 were incubated together with particles for 24 h in the absence or presence of endocytosis inhibitors (100 μM of Dansylcadaverine (DC) or di-methyl-amiloride (DMA)) at 37 °C. Inhibitors were added 30 min before particle addition; C: layer-by-layer coated particle

Spider silk particles	Model drug	Loading nmol mg^{-1} particles	Cells with particles/%		
			—	DC	DMA
eADF4(C16)	—	—	17.1 ± 5.0	9.0 ± 4.0	8.7 ± 5.2
	PEI-Fl	0.02	36.1 ± 14.2	7.1 ± 3.6	15.0 ± 0.2
	PEI-Fl	0.1	12.6 ± 4.5	12.0 ± 3.7	4.7 ± 2.0
	PEI-Fl	0.4	54.4 ± 12.9	36.3 ± 4.0	26.5 ± 6.8
eADF4(C16)RGD	—	—	51.4 ± 11.8	20.4 ± 10.9	34.3 ± 8.6
	PEI-Fl	0.02	72.8 ± 4.6	58.8 ± 4.8	69.4 ± 7.5
	PEI-Fl	0.1	71.7 ± 3.5	53.1 ± 6.3	57.1 ± 11.2
	PEI-Fl	0.4	87.7 ± 3.9	69.6 ± 2.6	78.6 ± 2.5
eADF4(C16)R_8G	—	—	69.0 ± 11.7	23.9 ± 6.3	63.9 ± 15.1
	PEI-Fl	0.02	5.0 ± 1.9	2.3 ± 1.1	3.3 ± 0.9
	PEI-Fl	0.1	10.6 ± 1.8	5.0 ± 3.9	5.3 ± 1.0
	PEI-Fl	0.4	18.9 ± 2.3	15.2 ± 1.3	9.0 ± 2.1
eADF4(κ16)	—	—	94.5 ± 3.2	47.8 ± 13.0	73.9 ± 7.5
	Fl-ODN	0.02	19.5 ± 5.0	1.2 ± 0.3	8.5 ± 3.8
	Fl-ODN	0.1	14.4 ± 4.1	0.9 ± 0.1	6.7 ± 2.7
	Fl-ODN	0.4	9.1 ± 2.6	0.8 ± 0.2	3.6 ± 1.1
eADF4(κ16)-C	Fl-ODN	0.4	83.4 ± 3.5	45.1 ± 13.7	58.4 ± 1.7

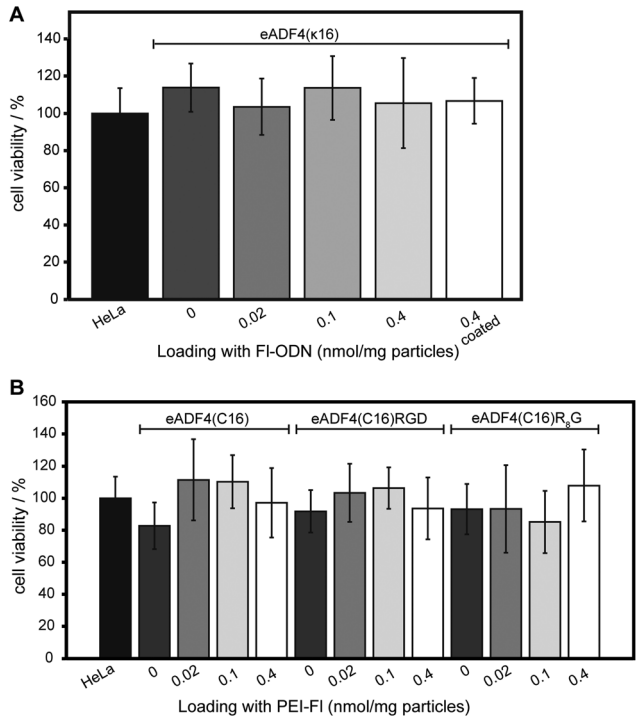

Fig. 3 Viability of HeLa cells incubated in the presence of 9.6 ng μl^{-1} of eADF4(κ16) (A) and eADF4(C16), eADF4(C16)RGD or eADF4(C16)R_8G (B) particles after 24 h of incubation. Starting cell densities were 20 000 cells per cm^2. Spider silk particles were loaded with 0, 0.02, 0.1, and 0.4 nmol of PEI-FI (eADF4(C16), eADF4(C16)RGD, and eADF4(C16)R_8G).

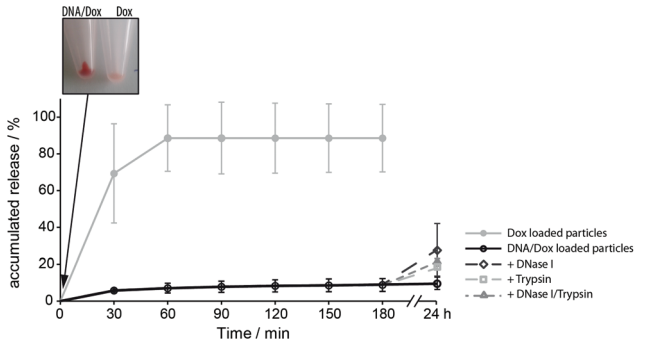

Fig. 4 Release of Dox from DNA/Dox loaded (black circles) or Dox loaded (grey circles) eADF4(κ16) particles in PBS (pH 7.2) at 37 °C. After 180 min DNase I, Trypsin or both enzymes were added, and the samples were incubated for additional 24 h at 37 °C.

Release of DNA/Dox upon eADF4(κ16) particle degradation

The drug doxorubicin (Dox) is often used in cancer therapy and was thus chosen here as a therapeutically relevant model drug to show the properties of spider silk particles as drug carrier systems. eADF4(κ16) was selected as a suitable silk carrier since it showed the best cellular uptake. Due to its positive charge Dox was first intercalated into plasmid DNA, and the DNA/Dox complex was then loaded onto positively charged eADF4(κ16) particles (loading efficiency of DNA/Dox was 73.5 ± 30.4%, while the loading efficiency of Dox was 3.5 ± 0.3%). Next, release of Dox from DNA/Dox loaded particles was investigated *in vitro*. While in the absence of DNA, Dox was completely washed out of the particles due to charge–charge repulsion of the drug and the positively charged particles (Fig. 4), the release of Dox from DNA/Dox loaded particles was very slow with a maximal release of about 10% of the initial loading after 24 h of incubation. Since it is possible that the release of Dox might be triggered by DNA and/or protein degradation *in vivo*, DNaseI, Trypsin or both enzymes were used to analyze the impact of protein and DNA degradation on Dox release.

Interestingly, both DNaseI as well as Trypsin slightly triggered the release of Dox, but no additive effect could be detected. Within 24 h of incubation up to 27.3% of the initially loaded Dox could be released in the presence of DNaseI and 18.0% in the presence of Trypsin, which reflects about double the amount of released Dox as detected in the absence of enzymes.

Cytotoxicity of DNA/Dox loaded eADF4(κ16) particles

The DNA/Dox loaded eADF4(κ16) particles were added to HeLa cells after additional coating with eADF4(κ16), as described above, and incubated for 6, 24 and 48 h at different spider silk particle concentrations (9.6 ng μl^{-1}; 48 ng μl^{-1}; 96 ng μl^{-1}). As a control, eADF4(κ16) particles were incubated with doxorubicin in the absence of DNA prior to incubation with HeLa cells. In a further experiment, Dox was added to the media to test for its direct impact on HeLa cells. Upon washing, Dox was released from the spider silk particles in the absence of DNA, but the DNA/Dox complex was retained within the particles. Again, the cytotoxicity was analyzed using the CellTiter Blue® assay (Fig. 5). After 6 h of incubation no effect was detected on the viability of HeLa cells either in the presence of DNA/Dox loaded eADF4(κ16) particles or in the presence of Dox in the media. After 24 h, cell viability decreased to 22% in the presence of free Dox. Only a slight effect could be detected in the case of DNA/Dox loaded particles at concentrations of 9.6 ng μl^{-1}, but the effect was identical to that of free Dox at DNA/Dox particle concentrations of 48 ng μl^{-1}. Interestingly, cell viability was significantly reduced to only 8% in the presence of 96 ng μl^{-1} of DNA/Dox loaded particles. After 48 h of incubation, the effect of free Dox and DNA/Dox loaded eADF4(κ16) particles was indistinguishable, and nearly no living cell could be detected. There was no detectable effect of Dox-loaded eADF4(κ16) particles (without DNA), since Dox was washed out of the particles before internalization of the particles by the cells as stated above. Importantly, eADF4(κ16) or DNA loaded eADF4(κ16) particles showed no effect on the viability of HeLa cells. As further control the uptake of the Dox-loaded particles was tested in the neuroblastoma cell line Kelly and the non-tumorigenic cell line BALB-3T3 mouse fibroblasts. It turned out that a higher particle concentration and incubation time was needed to induce similar effects like in HeLa cells.

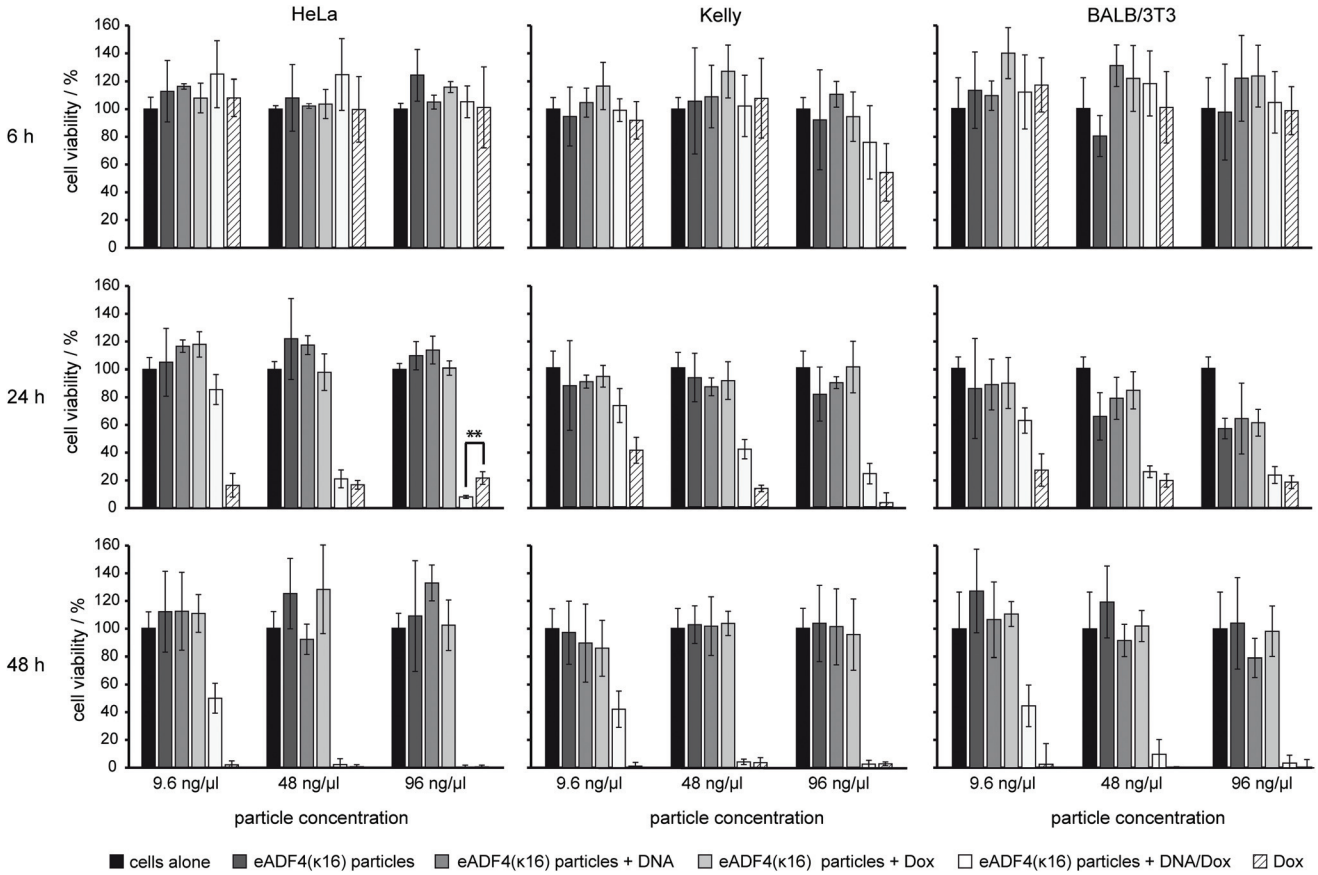

Fig. 5 Cell viability of HeLa, Kelly and BALB/3T3 cells in the presence of eADF4(κ16) particles loaded with DNA or Dox or loaded with a complex of DNA/Dox. 9.6, 48 or 96 ng µl^{-1} of particles were added to the cells which were incubated for 6, 24 or 48 h at 37 °C. The Dox concentration in DNA/Dox loaded particles was 2 µM (9.6 ng µl^{-1} of particles). In the control experiments with free Dox 2 µM, 10 µM and 20 µM were used, corresponding to the calculated amount of Dox in Dox loaded particles which were added to the cells in concentrations of 9.6 ng µl^{-1}, 48 ng µl^{-1} and 96 ng µl^{-1}. Cell viability was determined using the CellTiter Blue Assay (** significant difference).

Conclusions

Spider silk particles have been established as carrier of low molecular weight substances, small proteins or DNA. Further, it has been shown that unloaded spider silk particles can be taken up by cells dependent on the molecular composition of the underlying spider silk protein.[21–23,32] In this study, it could be demonstrated that the loading of a charged substance influences the cellular uptake of these particles. Loading of polycationic substances on polyanionic eADF4(C16) or eADF4(C16)RGD particles increased the uptake by nearly a factor of two. Surprisingly, the uptake of eADF4(C16)R_8G particles loaded with polycationic substances and that of DNA-loaded eADF4(κ16) particles was significantly decreased, indicating that the loaded substance has a severe influence on the uptake mechanism in dependence of the spider silk variant used.

It could be further shown that eADF4(κ16) particles loaded with a DNA/Dox complex can be easily uptaken by HeLa cells and also to a lesser extent by Kelly cells and BALB/3T3 fibroblasts, followed by Dox-related cell death, especially in the case of HeLa cells and BALB/3T3 fibroblasts. In the case of Kelly cells, an effect of Dox could only be detected at high particle concentrations, and the effect was lower compared to that of free Dox. Hence, HeLa cells were more sensitive to intracellular Dox as shown in the case of 24 h of incubation with DNA/Dox loaded eADF4(κ16) particles.

Since HeLa cells are known to uptake particles easily, whereas Kelly cells avoid uptake of foreign substances, future experiments have to deal with the improvement of spider silk particles concerning targeted transport of substances to, for example, specific cancerous cell lines. Further investigations are also necessary in terms of intracellular release of DNA from eADF4(κ16) particles in order to make them viable as transport systems for *e.g.* gene therapy.

Acknowledgements

We gratefully thank Andreas Schmidt and Johannes Diehl for fermentation of eADF4(C16)RGD, eADF4(C16)R8G and eADF4(κ16), Heike Herold for help with the Kelly and BALB 3T3 cell lines, Nicolas Helfricht for critical discussions on zeta poten-

tial measurements, Eileen Lintz for proof reading, as well as Dr Martin Humenik for discussions and comments on the manuscript. Further we acknowledge funding by the Deutsche Forschungsgemeinschaft (SFB840 TP A8).

References

1 T. M. Allen and P. R. Cullis, *Science*, 2004, **303**, 1818–1822.
2 S. Grund, M. Bauer and D. Fischer, *Adv. Eng. Mater.*, 2011, **13**, B61–B87.
3 A. H. Faraji and P. Wipf, *Bioorg. Med. Chem.*, 2009, **17**, 2950–2962.
4 S. K. Nitta and K. Numata, *Int. J. Mol. Sci.*, 2013, **14**, 1629–1654.
5 N. B. Shelke, R. James, C. T. Laurencin and S. G. Kumbar, *Polym. Adv. Technol.*, 2014, **25**, 448–460.
6 F. Milletti, *Drug Discovery Today*, 2012, **17**, 850–860.
7 S. Wohlrab, S. Muller, A. Schmidt, S. Neubauer, H. Kessler, A. Leal-Egana and T. Scheibel, *Biomaterials*, 2012, **33**, 6650–6659.
8 F. H. Wang, Y. Wang, X. Zhang, W. J. Zhang, S. R. Guo and F. Jin, *J. Controlled Release*, 2014, **174**, 126–136.
9 M. Humenik, A. M. Smith and T. Scheibel, *Polymers*, 2011, **3**, 640–661.
10 A. Heidebrecht and T. Scheibel, *Adv. Appl. Microbiol.*, 2013, **82**, 115–153.
11 C. Vendrely and T. Scheibel, *Macromol. Biosci.*, 2007, **7**, 401–409.
12 D. Huemmerich, C. W. Helsen, S. Quedzuweit, J. Oschmann, R. Rudolph and T. Scheibel, *Biochemistry*, 2004, **43**, 13604–13612.
13 U. Slotta, M. Tammer, F. Kremer, P. Koelsch and T. Scheibel, *Supramol. Chem.*, 2006, **18**, 465–471.
14 K. Spiess, S. Wohlrab and T. Scheibel, *Soft Matter*, 2010, **6**, 4168–4174.
15 A. Leal-Egana, G. Lang, C. Mauerer, J. Wickinghoff, M. Weber, S. Geimer and T. Scheibel, *Adv. Eng. Mater.*, 2012, **14**, B67–B75.
16 K. Schacht and T. Scheibel, *Biomacromolecules*, 2011, **12**, 2488–2495.
17 K. D. Hermanson, D. Huemmerich, T. Scheibel and A. R. Bausch, *Adv. Mater.*, 2007, **19**, 1810–1815.
18 C. Blüm, A. Nichtl and T. Scheibel, *Adv. Funct. Mater.*, 2014, **24**, 763–768.
19 U. K. Slotta, S. Rammensee, S. Gorb and T. Scheibel, *Angew. Chem., Int. Ed.*, 2008, **47**, 4592–4594.
20 A. Lammel, M. Schwab, U. Slotta, G. Winter and T. Scheibel, *ChemSusChem*, 2008, **1**, 413–416.
21 A. Lammel, M. Schwab, M. Hofer, G. Winter and T. Scheibel, *Biomaterials*, 2011, **32**, 2233–2240.
22 M. Hofer, G. Winter and J. Myschik, *Biomaterials*, 2012, **33**, 1554–1562.
23 E. Doblhofer and T. Scheibel, *J. Pharm. Sci.*, 2015, **104**, 988–994.
24 M. B. Elsner, H. M. Herold, S. Muller-Herrmann, H. Bargel and T. Scheibel, *Biomater. Sci.*, 2015, **3**, 543–551.
25 R. J. Hunter, *Zeta Potential in Colloid Science: Principles and Applications*, Academic Press Inc., San Diego, 1981.
26 N. Helfricht, M. Klug, A. Mark, V. Kuznetsov, C. Blum, T. Scheibel and G. Papastavrou, *Biomater. Sci.*, 2013, **1**, 1166–1171.
27 Y. K. Oh, D. Suh, J. M. Kim, H. G. Choi, K. Shin and J. J. Ko, *Gene Ther.*, 2002, **9**, 1627–1632.
28 A. I. Ivanov, in *Exocytosis and Endocytosis*, ed. A. I. Ivanov, Humana Press, Totowa, Editon edn, 2008, vol. 440, pp. 15–33.
29 S. Schutze, T. Machleidt, D. Adam, R. Schwandner, K. Wiegmann, M. L. Kruse, M. Heinrich, M. Wickel and M. Kronke, *J. Biol. Chem.*, 1999, **274**, 10203–10212.
30 R. J. Davis and M. P. Czech, *J. Biol. Chem.*, 1985, **260**, 2543–2551.
31 M. Koivusalo, C. Welch, H. Hayashi, C. C. Scott, M. Kim, T. Alexander, N. Touret, K. M. Hahn and S. Grinstein, *J. Cell Biol.*, 2010, **188**, 547–563.
32 C. Blüm and T. Scheibel, *BioNanoScience*, 2012, **2**, 67–74.

Electronic Supplementary Material (ESI) for Biomaterials Science.

Cellular uptake of drug loaded spider silk particles

Martina B. Schierling[a*], Elena Doblhofer[a*], Thomas Scheibel[a-]

Supplementary Information

Table S 1: Loading efficiency of different protein particles upon incubation with 0.4 nmol of the corresponding model substance Fl-ODN or PEI-Fl per mg particle

Protein particle	Uptake efficiency Fl-ODN / %	Uptake efficiency PEI-Fl / %
eADF4(C16)	-	26.6 ± 0.4
eADF4(C16)RGD	-	26.9 ± 0.4
eADF4(C16)R_8G	-	23.6 ± 0.3
eADF4(κ16)	40.6 ± 0.3	-

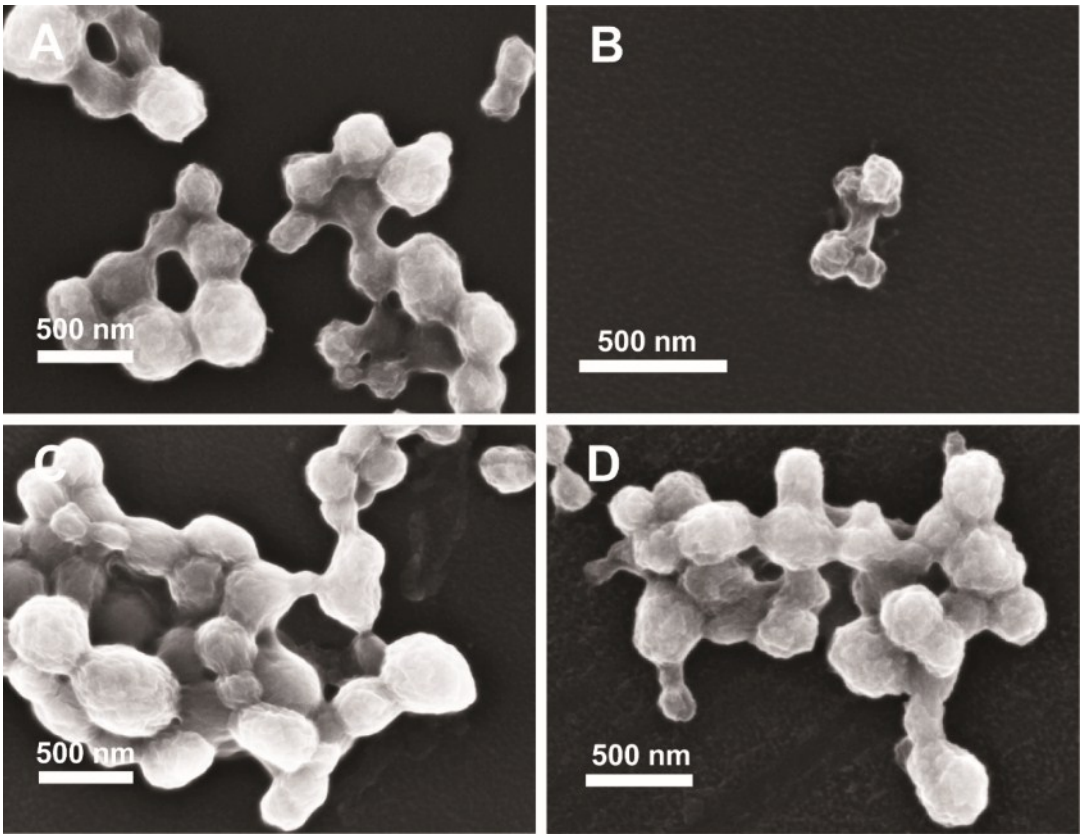

Fig. S 1 SEM Images of spider silk protein particles in dry state, A) eADF4(C16), B) eADF4(C16)R_8G, C) eADF4(C16)RGD, and D) eADF4(κ16). Particles were produced after resuspending the respective protein in EMiM[acetate] followed by potassium phosphate precipitation. SEM images were taken at an accelerating voltage of 3 kV. Before imaging, the particles were air dried and sputtered with platinum.

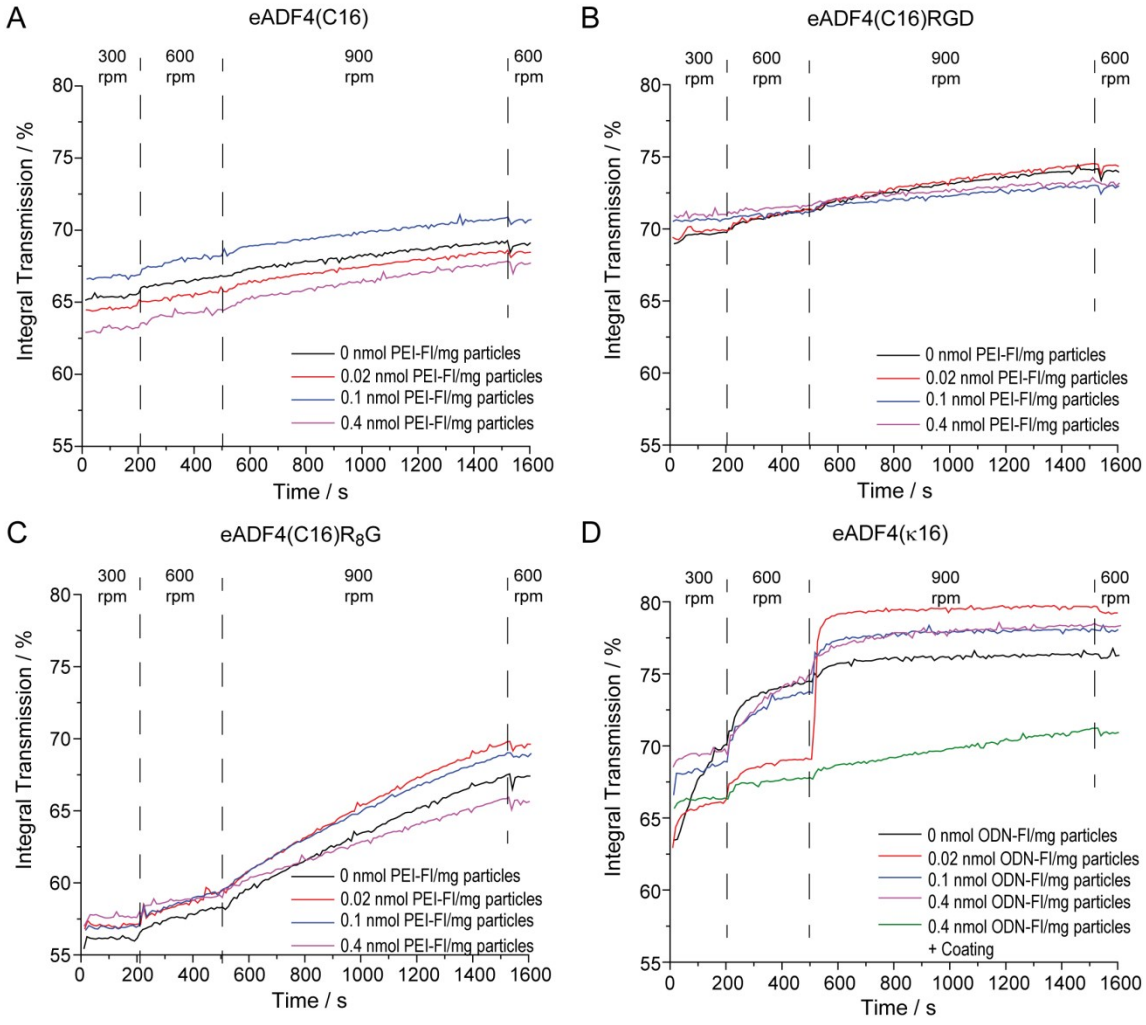

Fig. S 2 Representative sedimentation curves of spider silk and PEI-Fl or Fl-ODN loaded spider silk particles prepared from a 2 mg ml^{-1} solution in EMiM[acetate] and analyzed at a concentration of 1.25 mg ml^{-1}, measured at an ionic strength of 12 mM (1/11 PBS) and pH 7.4. The single graphs show (A) eADF4(C16) particles, (B) eADF4(C16)RGD particles, (C) eADF4(C16)R_8G and (D) eADF4(κ16) particles, each in the absence and presence model drug as indicated.

5.3 Teilarbeit III

Colloidal Properties of Recombinant Spider Silk Protein Particles

Autoren: Nicolas Helfricht, **Elena Doblhofer**, Jérôme. F.L. Duval, Thomas Scheibel und Georg Papastavrou

Diese Veröffentlichung entstand aus der Zusammenarbeit mit dem Lehrstuhl für Physikalische Chemie II der Universität Bayreuth und dem Laboratoire Interdisciplinaire des Environnements Continentaux der Université de Lorraine. Der experimentelle Teil wurde hierbei von Nicolas Helfricht und mir durchgeführt. Während ich für die Herstellung von eADF4 Partikeln und deren Beschichtung zuständig war, wurde die Analyse der elektrokinetischen Eigenschaften der Partikel, sowie die *direct force* Messungen von Nicolas Helfricht durchgeführt. Die Auswertung der Messergebnisse wurde hauptsächlich durch Nicolas Helfricht und Jérôme F.L. Duval in Zusammenarbeit mit Prof. Dr. Georg Papastavrou vorgenommen. Die Erstellung des Manuskripts erfolgte durch Zusammenarbeit aller beteiligten Autoren.

Das Manuskript wurde am 12.06.2016 im *Journal of Physical Chemistry C* veröffentlicht.

THE JOURNAL OF PHYSICAL CHEMISTRY C

Article

pubs.acs.org/JPCC

Colloidal Properties of Recombinant Spider Silk Protein Particles

Nicolas Helfricht,[†] Elena Doblhofer,[‡] Jérôme F. L. Duval,[*,§,∥] Thomas Scheibel,[‡] and Georg Papastavrou[*,†]

[†]Physikalische Chemie / Physik der Polymere, Universität Bayreuth, Universitätsstrasse 30, 95440 Bayreuth, Germany

[‡]Biomaterialien, Fakultät für Ingenieurswissenschaften, Universität Bayreuth, Universitätsstrasse 30, 95440 Bayreuth, Germany

[§]Laboratoire Interdisciplinaire des Environnements Continentaux, UMR 7360, Université de Lorraine, Vandœuvre-lès-Nancy, F-54501, France

[∥]CNRS, Laboratoire Interdisciplinaire des Environnements Continentaux, UMR 7360, Vandœuvre-lès-Nancy, F-54501, France

Supporting Information

ABSTRACT: Colloidal particles have been prepared from polyanionic and polycationic recombinant spider silk protein. The amino acid sequences of these spider silk proteins are identical except for 16 residues bearing either a cationic or an anionic ionizable group. Electrophoretic titration showed that protonation of the acidic and basic amino acids had significant impact on the electrophoretic mobility of the protein particles and, in particular, on their point of zero mobility (PZM). The experimentally determined PZMs are in good agreement with the theoretical values evaluated on the basis of the relevant amino acid sequences. A comprehensive description of the electrokinetic properties of the recombinant spider silk protein particles as a function of pH and solution ionic strength was provided from adequate application of electrokinetic theory for soft particles. Within the framework of this formalism, spider silk protein particles are viewed as porous colloids penetrable for ions and characterized by a finite penetration length for the electroosmotic flow. The differentiated electrokinetic properties of the particles were shown to be solely governed by the electrohydrodynamic features of their poorly charged outer peripheral layer with a thickness of about 10−20 nm. This finding was further corroborated experimentally by demonstrating that electrokinetics of particles bearing an additional outer layer consisting of oppositely charged spider silk proteins is entirely dominated thereby. The presence of a fuzzy, ion-permeable particle interface with an extension of several tenths of a nanometer was confirmed by direct measurement of the resulting steric forces using the colloidal probe atomic force microscopy (AFM) technique.

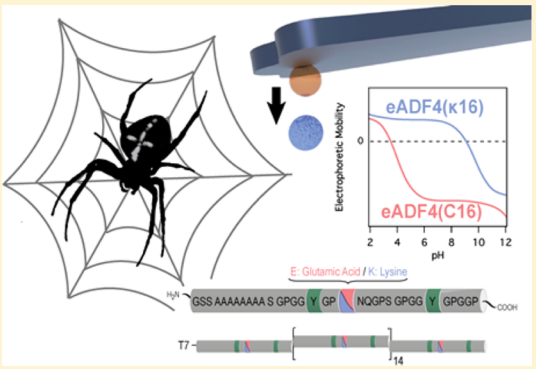

INTRODUCTION

Structural proteins play an increasing role in the development of biomaterials for drug delivery systems or drug depots.[1] The recombinant production of such structural proteins in combination with genetic engineering allows establishing tailor-made materials.[1−3] Such engineered proteinaceous materials offer both predictable biofunctionality and precise tenability, a combination lacking in most synthetic polymer materials.[4] Like synthetic polymers, structural proteins can be assembled into morphologies with no counterpart in nature, such as films, membranes, coatings, or particles.[5,6]

Spider silk proteins, called spidroins, represent a prominent and well-known example[7] of such structural proteins and consist of highly repetitive core sequences. One well-established recombinant spidroin is based on the sequence of one of the proteins of the dragline silk of the European garden spider *Araneus diadematus*, which is referred to as eADF4(C16). It can be processed into a variety of morphologies such as foams,[8] fibers,[9] nonwoven meshes,[10] hydrogels,[11] films, and colloidal particles.[12−14] By varying the amino acid sequences and substituting all glutamic acid (E) residues of eADF4(C16) with lysine (K) ones, the negative net-charge at neutral pH is converted into a positive one. For the modified protein, which is denoted hereafter as eADF4(κ16), the processing properties are indistinguishable to that of eADF4(C16).[14]

Particles made of recombinant spidroins are of special interest for the encapsulation of pharmaceutically active substances as they combine a unique set of properties, including biocompatibility and stability.[14−17] Surface chemistry of such colloids is in some aspects fundamentally different to that of "classical" solid colloids. For protein-based colloids the chemical composition should expectedly remain constant throughout the whole particle. Moreover, the density of ionizable groups is determined by the amino acid composition of the constituting structural proteins. Electrophoretic methods

Received: April 19, 2016
Revised: July 3, 2016
Published: July 12, 2016

DOI: 10.1021/acs.jpcc.6b03957
J. Phys. Chem. C 2016, 120, 18015−18027

are, in this respect, valuable techniques commonly used for the analytical characterization of spidroin particles.[7,13,14]

A basic theory for electrophoresis of so-called hard particles, i.e., particles impermeable to ions and solvent, has been developed about a century ago and refined over the years to, e.g., account for surface ion-conduction processes and electric double layer polarization.[18] The numerical treatment of the standard electrokinetic model by O'Brien and White[19] is pivotal for analyzing situations where simplified analytical equations derived within the framework of the Debye−Hückel approximation are not applicable. In comparison, only recently precise modeling has been established for describing the electrokinetics of soft particles.[20,21] Following the definition by Ohshima,[22] soft particles consist partly or entirely of ion- and solvent-permeable materials with electrophoretic properties significantly different to those of their hard counterparts. Examples of such particles include bacteria, viruses, and dendrimers.[20,23] The presence of a charged permeable layer is manifested prominently by the existence of a nonzero mobility plateau value reached at large electrolyte concentrations at which particle charges are completely screened by ions from a background electrolyte.[20,22] This feature originates from intralayer electroosmotic flow and has been confirmed experimentally for various systems.[20,23]

Since the pioneering work by Hermans and Fujita,[24] Levine et al.,[25] and Ohshima,[22] on electrophoresis of soft particles there has been a rich body of theoretical and experimental studies on electrohydrodynamics of core−shell or porous (nano)particles. For these systems the concept of ζ-potential, only strictly applicable to hard particles, is not playing any role.[20] In particular, Hill et al.[26] and Duval and Ohshima[40] established a formalism to account for heterogeneous (or diffuse) distribution of charged polymer segments across a particle's shell. While in the literature a large number of models exist to describe the electrokinetic properties of soft colloidal particles,[20,27−29] these models have never been applied for protein particles prepared by salting-out procedures.

Here, the properties of colloidal spidroin particles were determined by electrophoretic mobility and direct force measurements. Two different types of spidroin particles were evaluated, which have been prepared from spidroins with nearly identical amino acid sequences, namely, eADF4(C16) and eADF4(κ16). A number of electrokinetic measurements have been reported for spidroin particles so far, and determination of their ζ-potential is an important, generally used analytical tool.[14,30,31] However, a recent study combining electrophoretic mobility with direct force measurements demonstrated that for such recombinant spidroin particles a pronounced diffuse interface with protruding protein segments exists, limiting the application of the classical O'Brien−White theory[19] (valid only for hard colloidal particles) to provide a comprehensive interpretation of the electrophoretic mobility as a function of pH and solution ionic strength.[13] Since the features of the spidroin particle surface depend critically on the production processing by salting-out,[32] a large number of parameters has to be taken into account.[12] Here, we address how far electrokinetic methods can be employed to characterize protein particles and to predict their overall colloidal stability.

METHODS AND MATERIALS

Protein Production and Particle Preparation. The spider silk proteins eADF4(C16) with the amino acid sequence **T7**-(GSSAAAAAAAASGPGGYGP**E**NQGPSGPGGYGPGG-PG)$_{16}$ and eADF4(κ16) with the sequence **T7**-(GSSAAAA-AAAASGPGGYGP**K**NQGPSGPGGYGPGGPG)$_{16}$, have been produced and purified as described elsewhere.[14,33] The T7-tag has the following sequence: MASMTGGQQM. For particle preparation, lyophilized eADF4(κ16) and eADF4(C16) were dissolved in 6 M guanidinium thiocyanate (GdmSCN, Carl Roth GmbH & Co. KG, Karlsruhe, Germany) and dialyzed against 25 mM Tris/HCl (Carl Roth GmbH & Co. KG, Karlsruhe, Germany), pH 7.5 (Tris buffer). The dialysis continued for 16 h with three buffer changes at 25 °C using a dialysis membrane with a molecular weight cutoff of 6000−8000 Da (SpectrumR Laboratories, Irving, Texas). The resulting spider silk protein solutions were diluted to a concentration of 3 mg/mL using Tris buffer. Aliquots of 2 mL of the diluted solutions were dialyzed against 1 M potassium phosphate (Carl Roth GmbH & Co. KG, Karlsruhe, Germany), pH 7.0, over a period of 1 h at room temperature. Then, the occurring particle suspension was centrifuged at 17 000*g* for 2 min to obtain a pellet consisting of the precipitated protein particles. The particles were washed three times with Millipore water (MQ-H_2O).

Layer-by-layer coatings of the particles were produced by diluting the particle suspension to a concentration of 1 mg/mL, centrifugation of the particle suspension at 17 000*g* for 2 min, and resuspending the particle pellet in a protein solution containing 0.5 mg/mL of the oppositely charged protein in the same volume of Tris buffer (i.e., eADF4(C16) for eADF4(κ16) particles and eADF4(κ16) for eADF4(C16) particles). This mixture was incubated under continuous mixing conditions (1000 rpm) for 1 h at room temperature. The particles were finally washed with MQ-H_2O.

Particle suspensions were systematically sonicated for 5 min at room temperature prior to use.

Particle Immobilization. The recombinant spider silk protein particles were immobilized on a substrate for the direct force measurements by atomic force microscopy (AFM). For that purpose, WillCo dishes (series GWSB-5040 with a glass bottom and a diameter of 47.0 mm, WillCo Wells, Amsterdam, Netherlands) were cleaned with Millipore water and pure ethanol (VWR). Afterward, the dishes were exposed to air plasma for 10 min (Zepto, Diener electronic GmbH & Co. KG, Ebhausen, Germany). Half of the glass dish was modified with polyethylenimine (branched PEI, 1 g/L, av $M_w \approx 25\,000$ g/mol, Aldrich) serving as adhesion promoter for negatively charged particles. After 15 min, the PEI solution was removed, and the Petri dish was cleaned thoroughly with Millipore water.

Optical Microscopy. Modified glass dishes (see above) were filled with potassium chloride solution (1 mM, pH 5.5; BioUltra, ≥ 99.5%, Sigma). A diluted suspension of both types of protein particles was added to separate dishes that were transferred to an inverted optical microscope (Axio Observer.Z1, Carl Zeiss Microscopy GmbH, Jena, Germany). The particles were allowed to sediment, and afterward the particle diameter was determined based on optical micrographs using ImageJ software.

Scanning Electron Microscopy (SEM). Silicon wafers were cut into pieces of 10 mm × 10 mm and cleaned with a CO_2 Snow Jet (tectra, Frankfurt, Germany). Afterward, the substrates were rinsed with 100% ethanol (VWR) and dried in a nitrogen stream. Diluted particle suspensions were placed on the cleaned substrates, allowing the liquid to evaporate. After complete drying, the samples were rinsed twice with Millipore water. The prepared samples were sputtered with a 1.3 nm

DOI: 10.1021/acs.jpcc.6b03957
J. Phys. Chem. C 2016, 120, 18015−18027

layer of platinum and then examined with a scanning electron microscope (Leo 1530 VP Gemini, Zeiss).

Electrokinetic Measurements. The electrophoretic mobility of recombinant spidroin particles was measured using a Zetasizer Nano-ZS (Malvern Instruments Ltd., Worcestershire, U.K.). This instrument is based on laser-Doppler-microelectrophoresis and uses M3-PALS (phase analysis light scattering). Disposable capillary cells (DTS1060, Malvern Instruments Ltd., Worcestershire, U.K.) were used for the measurements, and their performance/quality was evaluated using a Malvern transfer standard particle suspension. The electrophoretic mobility was investigated as a function of pH at different ionic strengths (0.1, 1, and 10 mM, respectively). The pH value of the electrolyte solutions was adjusted with HCl and KOH (1 M, Titrisol, Merck). The total ionic strength of each solution (0.1, 1, and 10 mM, respectively) was obtained by addition of KCl (BioUltra, ≥ 99.5%, Sigma). The pH value was controlled after each measurement.

Direct Force Measurements. Interaction forces between individual pairs of particles were measured with a FluidFM setup mounted on an inverse optical microscope (Axio Observer.Z1, Carl Zeiss Microscopy GmbH, Jena, Germany). The FluidFM is a combination of an atomic force microscope (FlexAFM V5 head equipped with a C3000 controller, Nanosurf AG, Liestal, Switzerland) and a pressure control unit (Cytosurge AG, Glattbrugg, Switzerland). This microfluidic controller is connected to special hollow cantilevers, so-called FluidFM micropipettes (Cytosurge AG, Glattbrugg, Switzerland), premounted on a Cytoclip with a spherical aperture at the free end of the lever arm with an opening diameter of 2 μm. The used FluidFM cantilevers had a nominal spring constant of 0.2 N/m. The actual spring constant was determined by the added mass method after the measurements to avoid any contaminations of the lever arm.[34] To that end, small tungsten spheres were picked up from a glass surface, and the corresponding shifts in resonant frequency were monitored and evaluated.

Prior to direct force measurements, the FluidFM cantilevers were treated with air plasma for 10 min (Zepto, Diener electronic GmbH & Co. KG, Ebhausen, Germany). All solutions were degassed and filtered through PES syringe filters (pore size = 0.2 μm; Carl Roth GmbH & Co. KG, Karlsruhe, Germany). A liquid reservoir at the end of the Cytoclip was filled with 50 μL of the measurement solution (ionic strength 1 mM, pH 3). Beside both types of spidroin particles, silica particles (average diameter 6.8 μm, Bangs Laboratories Inc., Fishers, IN, U.S.A.) were immobilized on the functionalized dishes as "hard" internal standard.[13]

The FluidFM setup enables the use of exchangeable colloidal probes.[35] First, the cantilever was approached near a silica particle, and an aspiration pressure of −800 mbar was applied. After aspirating a single particle to the aperture, the pressure was reduced to −300 mbar to retain the captured bead during the measurements. The silica particles were used as probe particles to determine the inverse optical lever sensitivity (*InvOLS*) in a symmetric system involving two silica particles being aligned using an optical microscope. Interaction forces were hence measured in the sphere−sphere geometry. Force versus distance curves were recorded with a piezo travel velocity of 500 nm s^{-1}. For each pair of particle combinations, around 30 force profiles were acquired. After completing the experiment, the aspirated particle was finally released with an overpressure pulse (+1000 mbar).

The recorded raw data were converted into force versus distance curves and evaluated using a custom-written procedure programmed in FORTRAN and IgorPro (Wavemetrics).[13,36] The *InvOLS*, as determined in a symmetric system between two silica particles, was used as a constant to convert the raw data due to the soft and deformable behavior of the spider silk particles.[37]

For the interaction of a hard colloidal particle with a polymer brush, measured interaction forces were fitted by the asymmetric Alexander−de Gennes (AdG) model according to[38,39]

$$\frac{F(D)}{R_{\mathrm{eff}}} = 2\pi\frac{2kTL}{35s^3}\left(7\left(\frac{L}{D}\right)^{5/4} + 5\left(\frac{D}{L}\right)^{7/4} - 12\right) \quad (1)$$

where $F(D)/R_{\mathrm{eff}}$ is the normalized interaction force at separation D, L is the brush thickness, and s is the anchor distance between the polymer brushes.

THEORY SECTION

Electrokinetic Theory of Soft Porous Particles. The fundamental equations governing the mobility of soft particles in an externally applied (static) electrical field have been previously described in detail.[22,26,40] Briefly, the mobility of soft particles is evaluated from the numerical solution of highly coupled electrostatic and hydrodynamic flow equations including (i) the nonlinear Poisson−Boltzmann equation taking into account the three-dimensional distribution of the structural charges in the particle shell, (ii) the Navier−Brinkman equation that comprises the friction force exerted by the particle on the electroosmotic flow, taking into account that this friction term depends on the distribution of polymer segments,[41] and (iii) the continuity equations for all mobile ions present in the system and for the steady incompressible flow. For situations where the density of charges and polymer segments within the soft component of the particle do not depend on position, evaluation of particle electrophoretic mobility only requires the adjustment of two basic parameters (in case particle core size and shell thickness are known): the net density ρ_0 of charges throughout the homogeneous peripheral surface structure of the soft particle and the characteristic penetration length $1/\lambda_0$ of the electroosmotic flow within this structure (cf. Figure 1a).[22] In cases where the density of charges carried by the polymer segments constituting the soft particle is not homogeneous, the density distributions of charges and polymer segments need to be further specified.[40] The strategy to do so is recalled below for the specific example of spidroin particles.

Electrohydrodynamics of Spidroin Particles. The spidroin particles are *stricto sensu* devoid of an ion-impermeable core and carry both negative as well as positive charges (cf. Figure 1a). The negative charges are originating from the deprotonation of acid (e.g., carboxylic) groups, and the positive charges originate from the protonation of basic (e.g., amine) groups:

$$\equiv R_a H \rightleftharpoons \equiv R_a^- + H^+ \quad (2)$$

$$\equiv R_c H^+ \rightleftharpoons \equiv R_c + H^+ \quad (3)$$

where $\equiv R_a H$ and $\equiv R_c$ refer to the functional acid or basic groups in the particles whose total (effective) volume densities are hereafter denoted as ρ_a/F and ρ_c/F, respectively, with F being the Faraday constant. Following the strategy by Duval

DOI: 10.1021/acs.jpcc.6b03957
J. Phys. Chem. C 2016, 120, 18015−18027

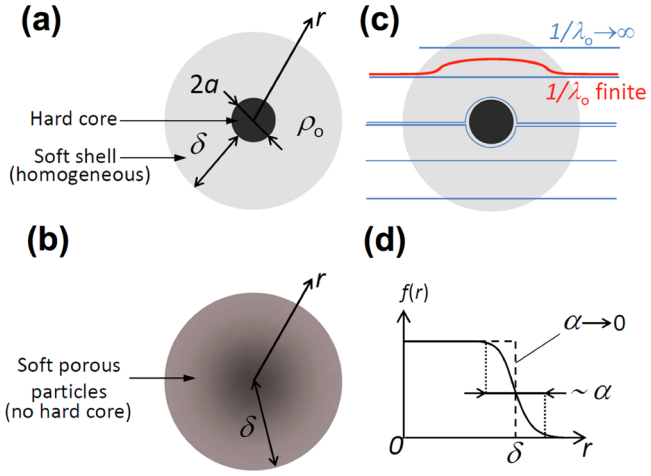

Figure 1. Illustration of various parameters introduced in the text for core−shell particles (a) and soft porous particles (b) devoid of a core component. (c) Schematic representation of the flow streamlines under electrophoretic conditions in the extreme of a free-draining particle shell ($1/\lambda_0 \to \infty$) and for a finite value of $1/\lambda_0$. (d) The radial function $f(r)$ from eqs 4 and 6 and its dependence on the parameter α.

and Ohshima,[40] the local charge density within the particles depends on pH according to

$$\rho(r) = f(r)\left\{\frac{\rho_c}{1 + 10^{pH-pK_c}\exp[y(r)]} - \frac{\rho_a}{1 + 10^{pK_a-pH}\exp[-y(r)]}\right\} \quad (4)$$

where $y(r) = zF\psi(r)/RT$ is the local dimensionless electrostatic potential at the radial position r (origin set at the particle center, cf. Figure 1) with R being the gas constant, T the temperature, z the valence of the z/z electrolyte, and $\psi(r)$ the local electrostatic potential derived from the nonlinear Poisson−Boltzmann equation. pK_a and pK_c depict the negative logarithms of the dissociation constants pertaining to reactions 2 and 3, respectively. Obviously, in view of the intrinsic heterogeneous chemical composition of the spidroin particles, pK_a and pK_c have to be seen as mean dissociation constants. Equation 4 includes the radial function f that pertains to the radial density distribution of proteins bearing the ionizable residues $\equiv R_aH$ and $\equiv R_c$ in the particle (cf. Figure 1b). Sufficiently far from the particles interface, f necessarily satisfies the condition $f(r \gg \delta) = 0$, where δ is the particle radius. This condition expresses the required vanishing of the polymer interphase at sufficiently large r. As previously reported,[20,40] the following form for $f(r)$ may be adopted

$$f(r) = \chi\{1 - \tanh[(r - \delta)/\alpha]\}/2 \quad (5)$$

where α is the length scale defining the gradual transition of segment density distribution from the bulk particle to the outer electrolyte solution (Figure 1b). The limit $\alpha \to 0$ corresponds to the situation of a homogeneous distribution of polymer segments in the porous particles, and the scalar χ in eq 5 further ensures that the total amount of polymer segments across the interphase is conserved upon modification of the spatial profiles $f(r)$ via changes in α as a result of, e.g., swelling processes.

On the basis of eqs 4 and 5, the friction coefficient $k(r)$ describing the resistance at position r of the polymer chains to flow is[20,40]

$$k(r) = \chi\eta\lambda_0^2 f(r) \quad (6)$$

where η is the dynamic viscosity of water and $1/\lambda_0$ is the flow penetration length scale introduced in the preceding section. In the limit $1/\lambda_0 \to 0$, there is no flow penetration within the particle and the hard particle case is retrieved, while the limit of free-draining particle is reached at $1/\lambda_0 \to \infty$ (cf. Figure 1). For a given set of $\rho_{a,c}$, $pK_{a,c}$, and $1/\lambda_0$ parameters, the dependence of the particle electrophoretic mobility μ on solution pH and solution ionic strength can be evaluated from numerically solving the governing electrostatic and electrohydrodynamic equations using the COLSYS package,[42] as described in previous studies.[20,23,40]

RESULTS AND DISCUSSION

In this study, we determined the electrophoretic mobility and interfacial properties of spidroin particles. Their properties depend on the underlying amino acid sequences, depicted as κ- and C-module (Figure 2a), which are repeated 16 times in the individual proteins. The glutamic acid (E) residues present in eADF4(C16) are replaced by lysine (K) ones in the κ-module of eADF4(κ16). Glutamic acid is an acidic amino acid, while lysine is a basic amino acid. Both repetitive modules contain additionally two tyrosine (Y) residues also bearing ionizable groups. However, these groups contribute only to the charging behavior under very basic pH conditions due to their high pK_a value. In addition, both proteins comprise an aminoterminal T7-tag, which shows a pH-dependent ionization behavior. However, the termini constitute only about 4% of the total number of ionizable groups (cf. Table S1 in the Supporting Information). Therefore, the termini have only a minor influence on the overall particle charging state.

Particle Morphology. Colloidal particles were prepared by a salting-out process schematically depicted in Figure 2b. The preparation of protein-based particles by salting-out in potassium phosphate buffer represents a standard preparation method and has been reported previously for eADF4(C16)[13,14] and for eADF4(κ16).[14] The particle radius was selected in the micrometer range, e.g., to allow for direct force measurements by AFM. The size of the particles was adjusted by controlling the mixing conditions, in particular the mixing speed.[17]

Parts c and d of Figure 2 show SEM images of eADF4(κ16) and eADF4(C16) particles in dried state, respectively. The spidroin particles' diameters were determined by *in situ* optical microscopy (electrolyte solution with KCl 1 mM, pH 5.5). Parts e and f of Figure 2 show the corresponding size distributions in the hydrated state for both types of protein particles. The hydrated eADF4(κ16) particles are in average about 20% larger in diameter compared to eADF4(C16) particles. The size distributions are highly polydisperse, which is typical for colloids prepared by a salting-out process.[12]

Electrophoretic Mobility of Spidroin Particles. Figure 3 shows the electrophoretic mobility μ of eADF4(κ16) and eADF4(C16) particles, respectively, at three solution ionic strengths I = 10 mM (Figure 3, parts a and d), 1 mM (Figure 3, parts b and e), and 0.1 mM (Figure 3, parts c and f) as a function of pH. Qualitatively, μ of eADF4(κ16) particles was positive and approximately constant for $4 \le pH \le 8$, regardless of the ionic strength. At pH ≈ 9.3−9.7, the mobility switched sign, indicating the point of zero mobility (PZM). The PZM nearly coincided with the theoretical pI = 9.7 estimated for eADF4(κ16) by ExPASy ProtParam.[43] With increasing pH above the PZM, μ increased by approximately 1 order of magnitude. Only for I = 1 mM an increase of μ with decreasing pH (pH 4 → pH 3) could be observed. However, this increase

DOI: 10.1021/acs.jpcc.6b03957
J. Phys. Chem. C 2016, 120, 18015−18027

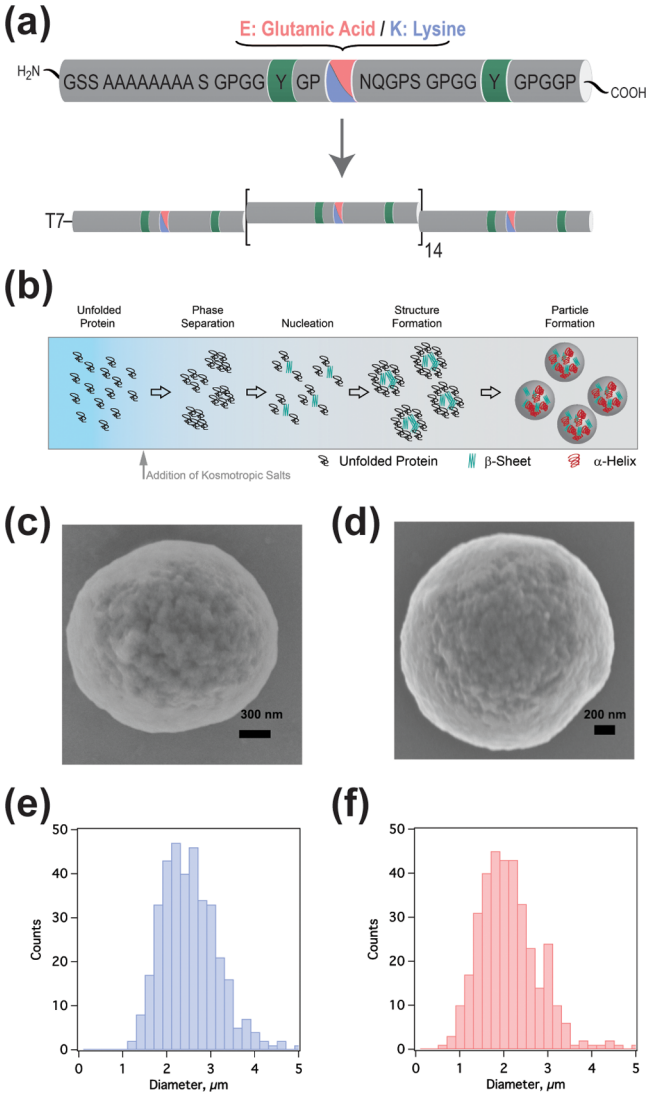

Figure 2. (a) Schematic representation of the modular structure of the two recombinant spider silk proteins eADF4(κ16) and eADF4(C16), which differ only by one amino acid per module, which is repeated 16 times. (b) Outline of the particle preparation by salting-out of the protein using a kosmotropic salt. (c and d) Representative SEM images of dried spider silk particles prepared from (c) eADF4(κ16) and (d) eADF4(C16), respectively. (e and f) Particle size distributions in the hydrated state as determined at an ionic strength of 1 mM and pH 5.5 by optical microscopy for (e) eADF4(κ16) and (f) eADF4(C16), respectively.

was not detected under the two other ionic strength conditions. Basically, the obtained data are consistent with previous electrokinetic data reported for particles prepared from eADF4(κ16) but measured at a single pH and ionic strength.[14]

Due to the relatively small fraction of residual groups in the proteins that can be ionized in the investigated pH range, the amino acid replacement from lysine to glutamic acid leads to pronounced differences concerning the dependence of eADF4(C16) electrophoretic mobility on pH (Figure 3d–f) as compared to that of eADF4(κ16) (cf. Figure 3a–c). In particular, the PZM was reached at lower pH values (ca. pH 3.5–4) for eADF4(C16) particles. Again, the PZM correlated well with the theoretical value pI = 3.5 calculated using ExPASy ProtParam.[43] The electrophoretic mobility of eADF4(C16) particles depended more significantly on the solution ionic strength compared to that of eADF4(κ16) particles. These differences between electrokinetic response of eADF4(κ16) and eADF4(C16) particles may originate from a different particle structure, and therewith from changes in flow permeability (parameter $1/\lambda_0$) as further discussed below upon quantitative modeling of the electrokinetic data (solid and dashed lines in Figure 3).

Electrophoretic Mobility of eADF4(κ16) Particles. For eADF4(κ16) particles, the mobility plateau values reached in the pH range of 4–8 at I = 10 mM and I = 1–0.1 mM depended only weakly on electrolyte concentration, with mean values of $\mu \sim 1.2 \times 10^{-8}$ m^2 V^{-1} s^{-1} and $\mu \sim 1.4$–1.5×10^{-8} m^2 V^{-1} s^{-1}, respectively. Such a weak dependence of μ on I is classically observed for soft particles even at much higher electrolyte concentrations ($I \geq 100$ mM) when particle charges are completely screened by ions.[20,22,40] For this limit of an infinitely thin electrical double layer ($\kappa\delta \gg 1$), μ is defined by $\mu \sim \rho_0/(\eta\lambda_0^2)$,[22] with $\lambda_0\delta \gg 1$. Here, κ^{-1} is the Debye length, and ρ_0 and $1/\lambda_0$ have been defined in the theoretical section. The finding that μ is practically independent of the ionic strength at a low range of 0.1–10 mM strongly suggests that eADF4(κ16) particles are poorly charged (i.e., their dimensionless radial potential satisfies $y(r) \ll 1$) and that their electrophoretic mobility is essentially determined by a strong penetration of the electroosmotic flow within the particle, which corresponds to large values of $1/\lambda_0$. These anticipations are confirmed below by the quantitative interpretation of the data upon application of the electrokinetic theory for soft particles.

The key electrohydrodynamic parameters $\rho_{a,c}$, p$K_{a,c}$, and $1/\lambda_0$ of eADF4(κ16) particles were determined as follows: In the pH range of 4–8, μ does not depend on solution pH, indicating that the inequalities pH $\gg$ pK_a and pH $\ll$ pK_c are essentially satisfied in this pH range, i.e., the dissociation of acid groups and the protonation of basic groups in the protein particles are complete. Consequently, in this pH range the following relationship is valid

$$\rho(r) = f(r)\rho_0 \tag{7}$$

with $\rho_0 = \rho_c - \rho_a$. This expression is derived from eq 4 in the limits of pH $\gg$ pK_a and pH $\ll$ pK_c. In addition, a homogeneous distribution of charged polymer segments within the particle (i.e., $\alpha \to 0$) can be legitimately assumed in a first approach. This assumption is valid either at sufficiently high salt concentrations and/or for poorly charged porous particles for which repulsive interactions between ionizable groups are least significant.[20,40] Under these conditions $\rho_0 \sim \rho(0 \leq r \leq \delta)$ can be approximated, which is the case for pH 4–8. As a result, only two unknown parameters have to be determined, ρ_0 and $1/\lambda_0$, in order to rationalize the particle mobility values μ as measured in the pH range from pH 4 to 8 at I = 10, 1, and 0.1 mM.

The parameters ρ_0 and $1/\lambda_0$ cannot be fitted independently but have to be determined simultaneously. Figure 4 summarizes the ensemble of (ρ_0; $1/\lambda_0$) pairs obtained by numerically solving the set of governing electrohydrodynamic equations in order to reproduce the measured μ value for pH 4–8 at the three different ionic strengths. Within the range of particle sizes (cf. Figure 2e) it is emphasized that particle mobility does not depend on δ (cf. Supporting Information, Figure S2). Basically, this independence of μ on δ results from the fact that the particle size largely exceeds the key length scales pertaining to the distribution of the electrostatic (κ^{-1} = 3–30 nm under the investigated electrolyte conditions) and hydrodynamic flow

DOI: 10.1021/acs.jpcc.6b03957
J. Phys. Chem. C 2016, 120, 18015–18027

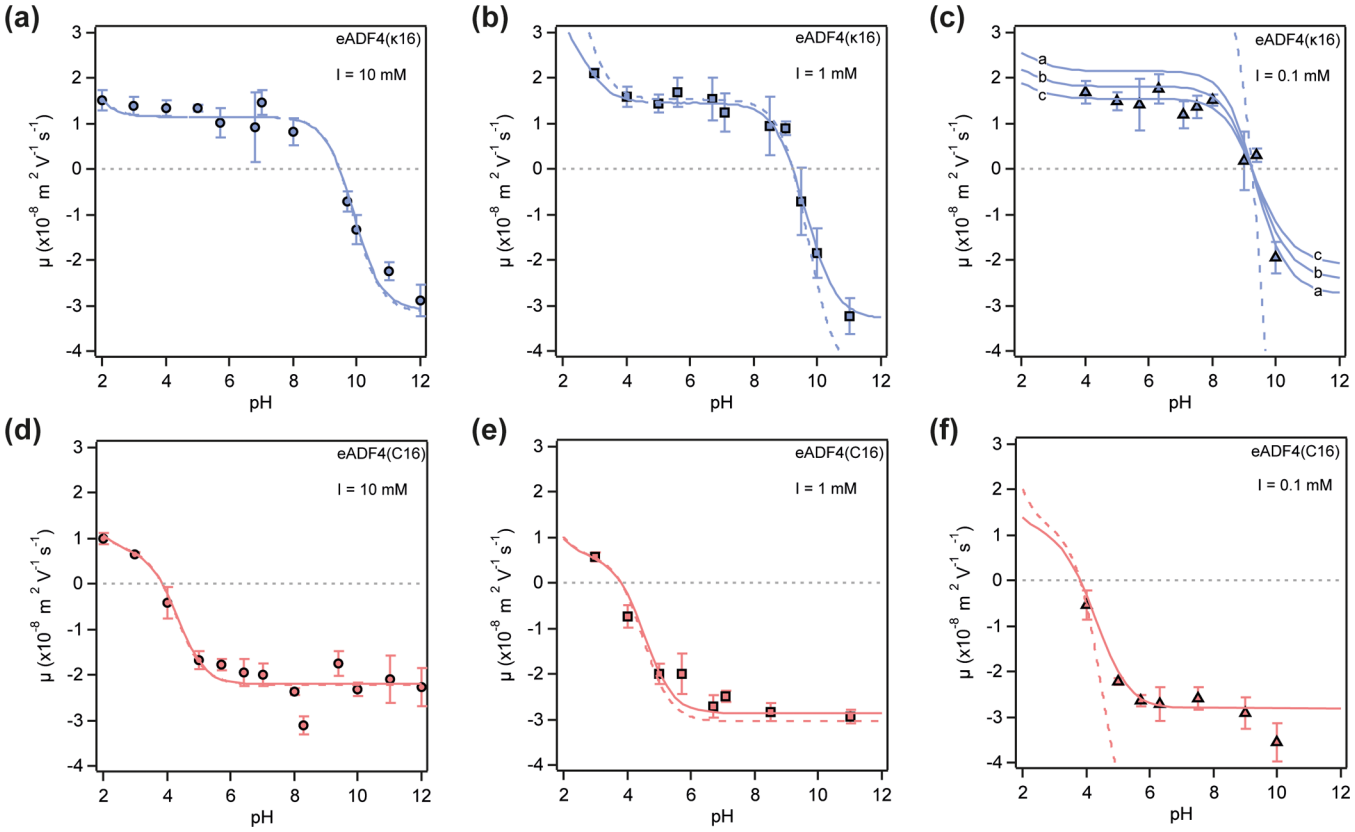

Figure 3. Electrophoretic mobility of eADF4(κ16) and eADF4(C16) particles at an ionic strength of 10 mM (a and d), 1 mM (b and e), and 0.1 mM (c and f) as a function of pH. Symbols correspond to the experimental data. The dashed lines correspond to eq 9, and the solid lines are computations performed on the basis of Duval−Ohshima's theory (ref 45) in the limit of homogeneous polymer segment density distribution in the porous eADF4(κ16) and eADF4(C16) particles (i.e., $\alpha \rightarrow 0$). Model parameter values for ρ_c/F, ρ_a/F, pK_c, pK_a, and $1/\lambda_0$ are summarized in Table 1. Calculations were performed with $\delta = 1.5$ μm (eADF4(κ16) particles) and $\delta = 1.0$ μm (eADF4(C16) particles). Lines a, b, and c in panel c refer to $1/\lambda_0 = 11$, 7, and 3 nm, respectively. See text for further details.

fields ($1/\lambda_0$ ~tens of nanometers at most). Ohshima demonstrated an analogous independence of μ on δ by deriving analytically his well-known soft particle mobility expression in ref 22 valid in the limit of "large" core sizes and "large" shell thickness.

Figure 4 highlights that the value of ρ_0 is required to decrease with increasing $1/\lambda_0$ in order to match the measured mobility μ at a fixed ionic strength I. This trend is the direct consequence of the relationship $\mu \sim \rho_0/(\eta\lambda_0^2)$ as stated before. Interestingly, the analysis showed that there is a unique pair of (ρ_0; $1/\lambda_0$) values leading to a consistent recovery of the measured mobility values at $I = 10$ mM and $I = 1$ mM at low pH. This pair corresponded to the coordinates of the intersection point of the curves depicted in Figure 4 for $I = 10$ mM and $I = 1$ mM. The obtained values $\rho_0/F = 0.84 \pm 0.05$ mM, expressed as equivalent concentration of elementary charges, and $1/\lambda_0 = 11 \pm 0.5$ nm (Figure 4a) allowed us to reconstruct the dependence of μ on pH over the entire range of tested pH values (cf. Figure 3, parts a and b). For that purpose, additional adjustments of $pK_{a,c}$ and either ρ_a or ρ_c are necessary, with the constraint that the difference $\rho_c - \rho_a$ must correspond to the value of ρ_0 evaluated from Figure 4. It has to be emphasized that pK_a, pK_c, and ρ_c primarily control (i) the range of pH where μ is constant, (ii) the pH value where mobility changes sign, and (iii) the mobility level at high pH. The analysis lead to $\rho_c/F = 3.24 \pm 0.1$ mM, $\rho_a/F = 2.4 \pm 0.1$ mM, $pK_c = 9.8 \pm 0.1$, and $pK_a = 1.2$−2.5. The uncertainty on pK_a is rather large as this parameter essentially determines the rate of variation of μ at low pH where the experimental value of μ is practically constant. Taken in the limit $\alpha \rightarrow 0$ and $y(r) \rightarrow 0$, from eq 4 followed the definition of the point of zero mobility defined by the pH value where $\mu = 0$, by

$$\mathrm{PZM} = \log\left\{\left[\frac{\rho_c/\rho_a - 1}{K_c} + \left[\left(\frac{\rho_c/\rho_a - 1}{K_c}\right)^2 + 4\frac{\rho_c/\rho_a}{K_aK_c}\right]^{1/2}\right]/2\right\} \quad (8)$$

Based thereon, eq 8 reduces to the well-known result PZM = $(pK_a + pK_c)/2$ in the specific case of $\rho_c/\rho_a = 1$. For eADF4(κ16) particles eq 8 leads to PZM = 9.4 ± 0.1, which is in excellent agreement with the theoretical isoelectric point of 9.7 estimated by ExPASy ProtParam.[43] It was verified that the PZM for eADF4(κ16) is independent of pK_a and is solely defined by the quantities pK_c and $\rho_{a,c}$.

Electrophoretic Mobility of eADF4(κ16) Particles at Low Ionic Strength. At the lowest ionic strength of $I = 0.1$ mM, the mobility of eADF4(κ16) particles could not be modeled within the framework outlined in the previous paragraph. Figure 3c shows the comparison between pH-dependent mobility measured at $I = 0.1$ mM and predictions from theory using the electrohydrodynamic parameters $pK_{a,c}$, $\rho_{a,c}$, and $1/\lambda_0$ determined according to the aforementioned procedure. While mobility for pH ≥ 8 was correctly reproduced, the experimental data at pH ≤ 8 (cf. curve a in

DOI: 10.1021/acs.jpcc.6b03957
J. Phys. Chem. C 2016, 120, 18015−18027

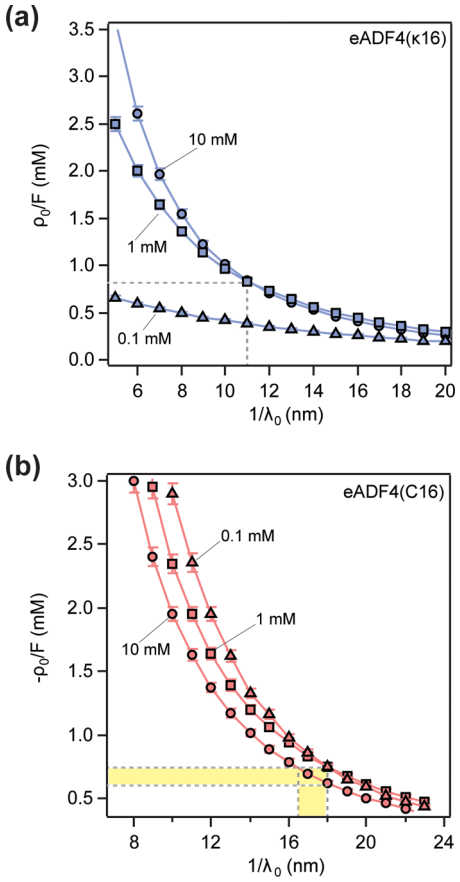

Figure 4. Sets of $(\rho_0/F;\ 1/\lambda_0)$ pairs adopted for retrieving the experimentally determined mobility plateau values reached at low pH (eADF4(κ16), panel a) or high pH (eADF4(C16), panel b) (see Figure 3) employing the Duval−Ohshima theory (ref 45). The parameter $1/\lambda_0$ pertains to the characteristic electroosmotic flow penetration length scale in the particle, and ρ_0/F is the net (volume) particle charge density (expressed in equivalent molar concentration of elementary charges). Computations were carried out assuming a homogeneous distribution of polymer segment density ($\alpha \rightarrow 0$). Standard deviations were evaluated from the uncertainty of the experimental mobility values. In panel a, the dotted lines illustrate the way the $(\rho_0/F;\ 1/\lambda_0)$ couple was determined leading to a fit of mobility data at large ionic strengths (10, 1 mM) in the pH range of 4−8. In panel b, the dotted lines and shadow areas illustrate the way the $(-\rho_0/F;\ 1/\lambda_0)$ couple was determined leading to a fit of mobility data at 10, 1, and 0.1 mM ionic strengths for pH ≥ 6.

Figure 3c) were overestimated. This deviation suggested that the $(\rho_0;\ 1/\lambda_0)$ pair determined by analyzing the electrokinetic data collected at I = 10 mM and I = 1 mM was not appropriate for interpreting electrokinetic behavior of eADF4(κ16) particles at 0.1 mM in the pH range where μ was constant. The absence of a common intersection point between the curves pertaining to I = 0.1 mM and I = 10 mM or I = 1 mM (cf. Figure 4a) confirmed this result. Figure 4a shows that a successful description of the experimental mobility values measured at pH ≤ 8 and I = 0.1 mM required a lower ρ_0 and/or a lower $1/\lambda_0$ compared to that used for I = 10 mM or I = 1 mM. Decreasing $1/\lambda_0$ from 11 nm (cf. curve a in Figure 3c) to ca. 3 nm (cf. curve c, Figure 3c) indeed provided a satisfactory fit of the electrokinetic data measured at I = 0.1 mM, while leaving the other parameters unaffected. A decrease in $1/\lambda_0$ with decreasing ionic strength is in line with a particle swelling process. The peripheral charged chains that mostly determine the electrokinetic flow structure[20,21] extend due to enhanced repulsion between their charged groups, increasing the overall resistance to flow (or particle drag), which contributes *in fine* to a lowered particle mobility.[40,44] As revealed by X-ray/neutron diffusion and reflectivity studies of numerous soft polyelectrolyte interfaces,[20,40,45] interfacial swelling is generally heterogeneous and leads to enhanced decay lengths of the segment density distribution from the bulk particle to the outer electrolyte solution, as illustrated in Figure 1b (eq 5).[44] In line with this representation, the mobility values measured at I = 0.1 mM could also be correctly reproduced upon adjustment of α from 0 (no significant swelling) at pH = 12 to about 35 nm (maximum swelling) at pH ≤ 8 (Figure 5)

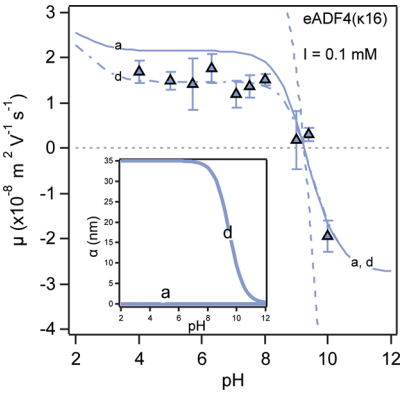

Figure 5. Influence of diffuse segment density distribution on the electrophoretic mobility and comparison to experimental values. The solid line (a) corresponds to $\alpha \rightarrow 0$, and the dotted line (d) corresponds to Duval−Ohshima's theory (ref 40) evaluations with diffuse segment density distribution at the eADF4(κ16)/solution interface as described by the pH-dependent parameter α (see inset). Other model parameter values: δ = 1.5 μm, $1/\lambda_0$ = 11 ± 0.5 nm, ρ_c/F = 3.24 ± 0.1 mM, ρ_a/F = 2.4 ± 0.1 mM, pK_c = 9.8 ± 0.1, pK_a = 1.2−2.5.

using values of p$K_{a,c}$, $\rho_{a,c}$, and $1/\lambda_0$ as estimated at higher ionic strengths. Additional spatially resolved data would obviously be required to determine whether the particle swelling process at 0.1 mM significantly affects the interfacial homogeneous segment density distribution at larger ionic strengths, or not. This would help determining whether the reconstruction of the electrokinetic data upon variation of $1/\lambda_0$ at constant $\alpha \sim 0$ (Figure 3c) or variation of α at constant $1/\lambda_0$ (Figure 5) is eligible. Regardless of this uncertainty, interpretation reveals in all cases an increase of the overall hydrodynamic particle drag with decreasing salt concentration as a result of a particle surface structure that further protrudes toward the outer electrolyte solution due to osmotic swelling.

Validity of the Debye−Hückel Limit for Porous Particles. To compare our results with results obtained from rigorous numerical treatment of the governing electrokinetic equations, we consider below the (approximate) theoretical mobility μ_{HF} to be based on the Hermans−Fujita's expression and derived in the Debye−Hückel limit for homogeneous porous particles satisfying $\kappa\delta \gg 1$ and $\lambda_0\delta \gg 1$:[22,24]

$$\mu_{HF} = \frac{1}{\eta\lambda_0^{\,2}}\left[\frac{\rho_c}{1+10^{pH-pK_c}} - \frac{\rho_a}{1+10^{pK_a-pH}}\right]\left[1+\left(\frac{\lambda_0}{\kappa}\right)^2\frac{1+\lambda_0/2\kappa}{1+\lambda_0/\kappa}\right] \quad (9)$$

DOI: 10.1021/acs.jpcc.6b03957
J. Phys. Chem. C 2016, 120, 18015−18027

Table 1. Summary of the Electrohydrodynamic Parameters Estimated for eADF4(κ16) and eADF4(C16) Particles

	ρ_a/F (mM)	ρ_c/F (mM)	pK_a	pK_c	$1/\lambda_0$ (nm)
eADF4(κ16)	2.4 ± 0.1	3.24 ± 0.1	1.2−2.5	9.8 ± 0.1	11 ± 0.5
eADF4(C16)	0.69 ± 0.07	0.87 ± 0.03	1.2 ± 0.1	4.4 ± 0.1	17.3 ± 0.7

Using the electrohydrodynamic parameters reported in Table 1, results indicated that eq 9 was satisfactorily applicable at I = 10 mM (cf. Figure 3a), since only insignificant deviations were observed upon comparison with rigorous numerical treatment of the electrokinetics of porous particles. However, with decreasing I (cf. Figure 3, parts b and c), eq 9 became increasingly inadequate as (i) potentials in the bulk particle and at the interface with the outer electrolyte solution significantly exceeded justification by the Debye−Hückel approximation and the corresponding linearization of Poisson−Boltzmann equation and (ii) electrical double layer polarization, ignored in eq 9, became significant. Under the conditions $\kappa\delta \gg 1$, the potential reached in the bulk particle corresponded to the Donnan potential ψ_D, which is defined by $\psi_D = \frac{RT}{F}\sinh^{-1}\left[\frac{\rho_c - \rho_a}{2FI}\right]$ at 4 ≤ pH ≤ 8.[22] Using the data summarized in Table 1, $\psi_D \sim 1$, 11, and 55 mV for I = 10, 1, and 0.1 mM were obtained at 4 ≤ pH ≤ 8, respectively.

Electrophoretic Mobility of eADF4(C16) Particles. The mobility μ of eADF4(C16) particles depended weakly on the ionic strength with $\mu \sim -2.2 \times 10^{-8}$ m^2 V^{-1} s^{-1} for I = 10 mM and $\mu \sim -2.9 \pm 0.1 \times 10^{-8}$ m^2 V^{-1} s^{-1} for I = 1−0.1 mM at pH ≥ 6 (cf. Figure 3d−f). In order to evaluate the parameters p$K_{a,c}$, $\rho_{a,c}$, and $1/\lambda_0$ for eADF4(C16) particles, the approach was used as described previously for eADF4(κ16) particles. However, the mobility values measured at pH ≥ 6 for I = 10, 1, and 0.1 mM were now considered to identify the set of ($\rho_0 = \rho_a$; $1/\lambda_0$) pairs describing the electrokinetic behavior of eADF4(C16) at high pH. The corresponding results are shown in Figure 4b. Unlike eADF4(κ16) particles, eADF4(C16) particles showed a common intersection point for the curves at I = 10, 1, and 0.1 mM within the experimental errors, with $-\rho_0/F = \rho_a/F$ = 0.69 ± 0.07 mM and $1/\lambda_0$ = 17.3 ± 0.7 nm. Adopting these parameters, full dependence of μ on pH was reproduced by further setting ρ_c/F = 0.87 ± 0.03 mM, pK_c = 4.4 ± 0.1, and pK_a = 1.2 ± 0.1, as indicated by the solid lines in Figure 3d−f.

The PZM of eADF4(C16) particles was about 3.8 ± 0.1 as evaluated from eq 8 using the determined p$K_{a,c}$ and $\rho_{a,c}$, which is again in good agreement with the theoretical isoelectric point of 3.5 calculated by ExPASy ProtParam.[43] Analogously to eADF4(κ16) particles, eq 9 was of limited use to accurately reproduce the pH-dependent electrokinetic features of eADF4(C16) particles at low ionic strength (cf. dashed lines in Figure 3). The Donnan potential for bulk eADF4(C16) particles was $\psi_D \sim -0.9$, −9, and −50 mV for I = 10, 1, and 0.1 mM, respectively, at pH ≥ 6. Table 1 summarizes the set of electrohydrodynamic parameters determined for eADF4(κ16) and eADF4(C16) particles.

Multilayered Spidroin Particles. Preparation of multilayer systems is well established for oppositely charged macromolecules in interface and colloid science.[46−49] The corresponding process is also often referred to as layer-by-layer (LbL) preparation. While this concept has been mostly exploited for combinations of polyelectrolytes, LbL films and capsules can also be prepared from polyelectrolyte/protein or protein/protein combinations.[6] Due to the opposite charge of eADF4(C16) and eADF4(κ16) (cf. Figure 3), LbL systems with alternating layers of these spidroins were obtained as reported previously.[14]

LbL particles with one additional layer of oppositely charged protein type (i.e., eADF4(C16) particles with a layer of eADF4(κ16) and eADF4(κ16) particles with a layer of eADF4(C16), respectively) were examined in terms of their respective electrophoretic mobility. The outer layer allowed deciphering its role in the overall electrokinetic properties of the spidroin particles. In Figure 6 the electrophoretic mobility

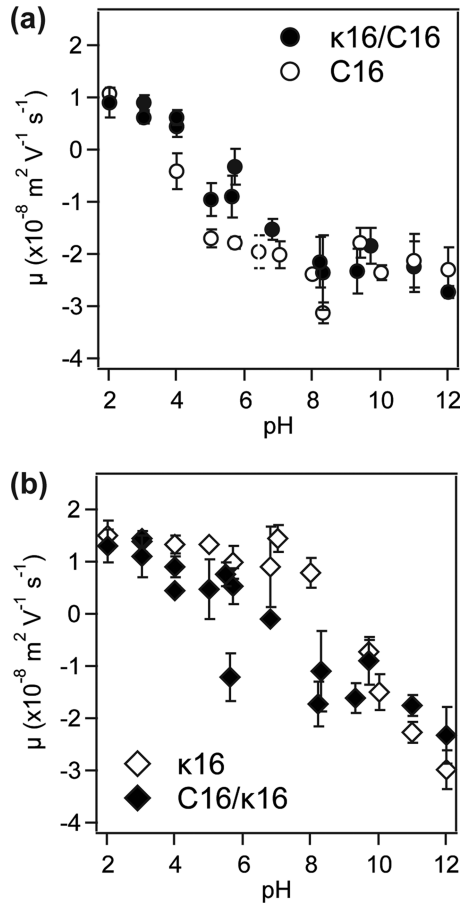

Figure 6. Electrophoretic mobility of layer-by-layer spider silk protein particles compared to that of homogeneous particles (i.e., without additional protein layer). (a) eADF4(C16) particles (open symbols) and eADF4(κ16) particles coated with a layer of eADF4(C16) (filled symbols). (b) eADF4(κ16) particles (open symbols) and eADF4(C16) particles coated with a layer of eADF4(κ16) (closed symbols).

of the particles prepared from a single protein type is compared with the mobility of particles having an additional outer layer. Each graph displays the electrophoretic mobility as a function of pH for particles terminated with the same type of protein. All measurements have been performed at a constant ionic strength of 10 mM.

Figure 6a shows that within the accuracy of the measurements the mobility of eADF4(κ16) particles and eADF4(C16) particles coated with a layer of eADF4(κ16) was practically

DOI: 10.1021/acs.jpcc.6b03957
J. Phys. Chem. C 2016, 120, 18015−18027

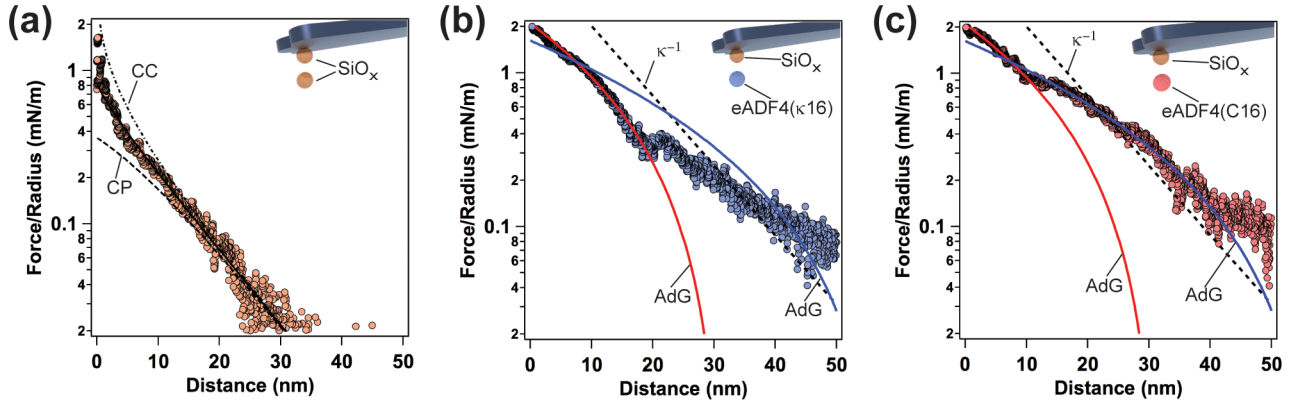

Figure 7. (a) Interaction forces between two silica particles. The lines indicate fits based on the full solutions of the Poisson−Boltzmann equation under constant potential (CP) or constant charge (CC) boundary conditions (see labels) as well as including charge regulation (solid line). The interaction between the silica particles is dominated by diffuse layer overlap, and the decay length corresponds to the theoretical Debye length. (b and c) Interaction forces between a silica particle and eADF4(κ16) and eADF4(C16) particles (indicated). Steric interactions dominate the force profiles, which were measured at an ionic strength of 1 mM at pH 3. In panels b and c, red and blue solid lines are fits of force versus distance profiles collected for eADF4(κ16) and eADF4(C16) particles, according to the Alexander−de Gennes (AdG) model. For the sake of comparison, these curves are reported both in panels b and c.

identical over the entire pH range examined in this work, and likewise the mobility of eADF4(C16) particles and eADF4(κ16) particles coated by a layer of eADF4(C16) (cf. Figure 6b). In both cases, the largest differences between "bare" and coated particles were observed near the PZM. At the respective PZM values of the coatings, the outermost particle region is uncharged with the charge of the underlying particle component, consisting of a different protein (with distinct electrostatic features) impacting the particle mobility. However, as reported for polyelectrolyte multilayers,[49] despite intercalation of the layers the overall charge was primarily dominated by the outermost layer.

Direct Force Measurements of Spidroin Particles. Direct force measurements were performed using the colloidal probe AFM technique in sphere−sphere geometry,[50,51] as recently reported.[13] The spidroin particles, either eADF4(C16) or eADF4(κ16), were coadsorbed on a solid substrate together with silica particles. The interaction force profiles were determined with a silica colloidal probe. The FluidFM technique allows for attaching silica particles in a temporary manner and exchanging them in case of contamination.[35] The silica particles immobilized on the substrate served as "internal standards" as they are incompressible and have well-known diffuse layer properties.[52,53] The direct force measurements were performed at pH 3 in a 1 mM solution ionic strength, the condition at which the mobility of both types of spidroins was similar in terms of magnitude and sign (cf. Figure 3, parts b and e).

Figure 7a shows the force profile obtained between a silica colloidal probe and an immobilized silica particle. The measured forces were systematically normalized to the effective radius R_{eff} given by $1/R_{eff} = 1/\delta + 1/\delta_{SiOx}$ with δ_{SiOx} being the radius of the probe particle and δ that of the immobilized particle (i.e., either silica or spidroin particle). The lines represent fits of the measured force versus distance profiles using theoretical predictions based on the full solutions of the Poisson−Boltzmann equation under standard boundary conditions of constant charge (CC), constant potential (CP), or charge regulation. The latter corresponds to the solid line and provides a superior description of experimental data collected at small separation distances, i.e., below approximately one Debye length.[54] The Debye length of $\kappa^{-1} = 9.3$ nm has been calculated on the basis of the nominal ionic strength of 1 mM adopted in these experiments. The decay of the interaction forces coincided with this theoretical Debye length value at larger separation distances, indicating that the interaction forces resulted from diffuse layer overlap, thus being of pure electrostatic origin. The obtained diffuse layer potential $\psi = -25$ mV is in good agreement with that expected for the well-documented ionization behavior of silica.[54−56]

Parts b and c of Figure 7 show representative examples of the interaction force profiles measured between colloidal silica probes and eADF4(κ16) or eADF4(C16) particles, respectively. The spidroin particles were relatively soft and could be easily compressed.[13,37] Due to the softness of these particles, the relative distance between the AFM colloidal probe and the spider silk protein particle could not be determined in an unambiguous manner. Since eADF4(C16) and eADF4(κ16) particles showed comparable elastic moduli, the separation distance between the colloidal probe and the protein particles was set to zero for an applied force of $F_m = 2$ mN/m, below which the force acting on the cantilever resulted only from the mechanical compression of the particle.

The dashed lines in Figure 7, parts b and c, indicate the interaction decay length expected for a scenario where diffuse layers overlap (i.e., the same κ^{-1} as that obtained for the interaction between two silica particles, see Figure 7a). Obviously, the interaction force profiles for both types of spidroin particles were not compatible with such a diffuse layer overlap scenario, since the slope of the force profiles was not constant (plotted in a semilogarithmic representation) with distance even at large separations. More than 75% of the force profiles showed also secondary minima measured for both types of spidroin particles. In addition, the silica probes were only slightly negatively charged at pH 3,[54] while both protein particles were positively charged (Figure 3). The absence of long-ranged attractive forces, as expected for interacting oppositely charged particles, provided evidence that other forces than electrostatics, e.g., steric forces, govern the interparticular interactions. Steric repulsive forces can be described by means of the AdG model due to the compression of the flexible protein structures by the silica particle (cf. eq

DOI: 10.1021/acs.jpcc.6b03957
J. Phys. Chem. C 2016, 120, 18015−18027

1).[57−62] While this model was established for the interaction of uncharged polymer brushes, it can be also applied for describing interaction forces between physisorbed polyelectrolyte layers.[38,39] Over a significant range of separation distances D ($0.1L < D < 0.9L$), the interaction profile could be described with sufficient accuracy in terms of a purely exponential decay (albeit with a characteristic decay length that differed from the theoretical κ^{-1}).[59] If additional electrostatic contributions are taken into account the resulting electrosteric interaction profiles follow as well an approximately exponential force law.[63]

The solid lines in Figure 7, parts b and c, resulted from fits of force versus distance profiles according to the AdG model at separation distances in the range of 10−20 nm for eADF4(κ16) (blue curve) and of 20−40 nm for eADF4(C16) (red curve), respectively. For both particles, comparable average anchor densities were obtained with $s = 4.8 \pm 1$ nm for eADF4(κ16) and 6.7 ± 3.7 nm for eADF4(C16), respectively. However, the obtained brush lengths were significantly different with $L = 192 \pm 47$ nm and $L = 321 \pm 87$ nm for eADF4(κ16) and eADF4(C16) particles, respectively. It is premature and speculative at this stage to quantitatively relate protein segment density distributions, interaction force profiles (Figure 7), and electrokinetics, in particular friction forces under lateral flow conditions (Figure 3), due to the lack of a sufficiently detailed description of the actual protein distribution within the particles prepared by salting-out.[45] Despite this difficulty, AFM and electrokinetics showed some key colloidal features of eADF4(κ16) and eADF4(C16) particles that are further discussed below.

SUMMARY AND DISCUSSION

The electrophoretic mobility of spidroin particles is determined by the electrohydrodynamic properties of their outer surface layer, a feature that has been reported for other soft micrometer-sized particles and films.[20] The relevant protolytic, electrostatic, and flow penetration length parameters are summarized in Table 1. The electrophoretic mobility was basically independent of particle size and was governed by the volume charge density and the friction characteristics of the electrokinetically active particle region located at the outer particle periphery. The thickness of this region is controlled by the hydrodynamic penetration depth $1/\lambda_0$ and the Debye length κ^{-1}(i.e., few tens of nanometers).[20,21,23] The existence of this electrokinetically active layer of limited thickness at the particle's outer region was further confirmed by the electrokinetic response of multilayered particles. The measured electrophoretic mobility was shown to be primarily governed by the electrohydrodynamic features only of the outer protein layer (cf. Figure 6). In addition, direct force measurements confirmed that the protein particles are poorly charged and they exhibit a fuzzy, peripheral porous structure leading to significant steric forces at large separation distances when interacting with hard silica spheres. The existence of such a peripheral porous structure was supported by the significant electroosmotic flow penetration lengths as derived from analysis of electrokinetics. Compilation and analysis of electrohydrodynamic data collected for various Gram-positive and Gram-negative bacteria, also displaying soft proteinaceous and/or polysaccharidic surface structures, revealed charge densities and flow penetration lengths in the range of 1−200 mM and 0.5−7 nm, respectively.[20] In the framework of the AdG model, assuming a brushlike structure, the steric forces were comparable for both types of protein particles and the brushlike structure extended to several tenths of nanometers. In order to model the interaction force with more realistic interaction potentials including electrosteric and mechanical particle deformation contributions,[28] a more refined density profile of the protein segments at the particle/solution interface would be required. The larger brush length of eADF4(C16) particles in comparison to that of eADF4(κ16) ones could be indicative for a larger solvent uptake, and thus for a larger flow penetration length scale under electrokinetic conditions, agreeing with the larger $1/\lambda_0$ value obtained for eADF4(C16) particles (Table 1).

AFM force profiles and measured electrophoretic mobilities for spidroin particles can significantly differ depending on the particle batches investigated. These variations are probably connected to differences in the segment density profiles resulting from preparation conditions and to slight changes thereof, a result that is well-known for particles produced by salting-out.[12] In line with this, previous work demonstrated that the electrophoretic mobility of silkworm silk fibroin particles strongly depends on tiny changes in particle preparation conditions.[12,64]

The derived electrohydrodynamic parameters are in agreement with the chemical composition of the constitutive amino acid sequence of the spidroins. The obtained effective dissociation constants $pK_{a,c}$ and charge densities $\rho_{a,c}/F$ lead to points of zero mobility being in very good agreement with the theoretical isoelectric points calculated by ExPASy ProtParam. Using this algorithm, the complete amino acid sequence (including every single pK_a value of each amino acid involved) is taken into account to calculate a theoretical pI. The consistency of the results provided by the ExPASy tool was addressed in several other studies and compared within a good accuracy to experimental data obtained from isoelectric focusing.[65,66] Due to the simple structure of the spider silk proteins studied here, one can assume a good prediction of the pI by ExPASy ProtParam, which has been confirmed here by isoelectric focusing, thus making a separate analysis of the single proteins (electrokinetic/potentiometric titration) not mandatory. The ionization behavior of the amino acids in the side chains of the two spider silk proteins (i.e., lysine and glutamic acid, respectively) coincide largely with the pK_a found experimentally (cf. Table 1 and Table S1 in the Supporting Information). The experimentally determined ionization constants pK_a most likely include contributions from ion adsorption to the hydrophobic parts of the proteins, as reported for poly(ethylene glycol) (PEG) or hydrophobic self-assembled monolayers.[53] The influence of such counterion binding could be addressed by measuring the electrophoretic mobility of single proteins as demonstrated for lysozyme.[67] However, the recombinant spider silk proteins are intrinsically unfolded as shown by circular dichroism spectroscopy.[33] Hence, electrophoretic measurements will be not as conclusive as for the compact lysozymes. The volume charge densities $\rho_{a,c}/F$ obtained from the fits of electrokinetic measurements fall in the range of 3.2−0.7 mM for both particle types (cf. Table 1). In order to verify if these values for $\rho_{a,c}/F$ are reasonable, we estimated in the following the number of ionizable groups per volume in the eADF4(C16) spidroin particles: For the particles a density of 1.35 g/cm^3 can be assumed in the hydrated state.[68] The spidroin eADF4(C16) has a molecular mass of $M_w = 47\,698.3$ g/mol, and we obtained $(1.35\ \text{g/cm}^3 - 1\ \text{g/cm}^3)/M_w$ for the concentration of one protein molecule per unit volume

DOI: 10.1021/acs.jpcc.6b03957
J. Phys. Chem. C 2016, 120, 18015−18027

neglecting the volume occupied by the protein. Assuming that the charge primarily originates from lysine or glutamic acid residues (i.e., one ionized group per protein module) an upper limit of 0.46 mM is found for $\rho_{a,c}/F$. Despite the inherent heterogeneities in particle structure/size and the difficulties to relate electrokinetic and titrable charge densities,[22] the above estimate compares remarkable well with values for $\rho_{a,c}/F$ reported in Table 1 and derived here from electrokinetic analysis. It should be pointed out that, for practical applications, the eq 9 is a good approximation for the relationship between electrophoretic mobility and volume charge density at sufficiently high ionic strengths.

CONCLUSIONS

Changing the amino acid composition of spidroins induces profound changes in electrokinetics of colloidal particles made thereof. However, the influence of the preparation method is experimentally more difficult to control than the amino acid composition. Salting-out processes influence the interfacial/bulk particle structure (e.g., in terms of arrangement of constitutive proteins) that may change even after small variations of the preparation conditions (stirring speed, local electrolyte concentrations, local pH gradient, etc.). The resulting charge density profile of the outer layer of the protein particle predominantly affects the particle's electrophoretic mobility. Direct force measurements by AFM support conclusions drawn from the electrokinetic analysis, i.e., eADF4(κ16) and eADF4(C16) particles are poorly charged colloidal systems, displaying a fuzzy (soft) polymer-like structure, and their stability versus aggregation is primarily ensured via repulsive steric forces. The measurement of the electrophoretic mobility of the particles as a function of pH and salt concentration provided a direct analytical approach to efficiently probe their interface and, thus, characterize their electrohydrodynamic features.

ASSOCIATED CONTENT

Supporting Information

The Supporting Information is available free of charge on the ACS Publications website at DOI: 10.1021/acs.jpcc.6b03957.

Table compiling all amino acids including their physical properties, SEM images of several spidroin particles, and demonstration of the independency of theoretical electrophoretic mobility with respect to particle size under the electrolyte conditions relevant for this work (PDF)

AUTHOR INFORMATION

Corresponding Authors

*E-mail: jerome.duval@univ-lorraine.fr. Phone: 00 33 3 83 59 62 63.

*E-mail: georg.papastavrou@uni-bayreuth.de. Phone: +49 0 921/55-2335.

Notes

The authors declare no competing financial interest.

ACKNOWLEDGMENTS

The authors thank C. Kunert for her help with scanning electron microscopy measurements. We further thank Christian Bippes, Patrick Frederix (Nanosurf AG), and Pablo Dörig (Cytosurge AG) for technical support. This work has been supported by the Deutsche Forschungsgesellschaft (German research council) in the framework of the SFB 840 (TP C4 and TP A8).

REFERENCES

(1) Desai, M. S.; Lee, S.-W. Protein-Based Functional Nanomaterial Design for Bioengineering Applications. *Wires Nanomed Nanobi* **2015**, *7*, 69−97.

(2) DiMarco, R. L.; Heilshorn, S. C. Multifunctional Materials Through Modular Protein Engineering. *Adv. Mater.* **2012**, *24*, 3923−3940.

(3) Nettles, D. L.; Chilkoti, A.; Setton, L. A. Applications of Elastin-Like Polypeptides in Tissue Engineering. *Adv. Drug Delivery Rev.* **2010**, *62*, 1479−1485.

(4) Romano, N. H.; Sengupta, D.; Chung, C.; Heilshorn, S. C. Protein-Engineered Biomaterials: Nanoscale Mimics of the Extracellular Matrix. *Biochim. Biophys. Acta, Gen. Subj.* **2011**, *1810*, 339−349.

(5) Schacht, K.; Scheibel, T. Processing of Recombinant Spider Silk Proteins into Tailor-Made Materials for Biomaterials Applications. *Curr. Opin. Biotechnol.* **2014**, *29*, 62−69.

(6) Wang, X.; Kim, H. J.; Xu, P.; Matsumoto, A.; Kaplan, D. L. Biomaterial Coatings by Stepwise Deposition of Silk Fibroin. *Langmuir* **2005**, *21*, 11335−11341.

(7) Doblhofer, E.; Heidebrecht, A.; Scheibel, T. To Spin or Not to Spin: Spider Silk Fibers and More. *Appl. Microbiol. Biotechnol.* **2015**, *99*, 9361−9380.

(8) Schacht, K.; Vogt, J.; Scheibel, T. Foams Made of Engineered Recombinant Spider Silk Proteins as 3D Scaffolds for Cell Growth. *ACS Biomater. Sci. Eng.* **2016**, *2*, 517−525.

(9) Heidebrecht, A.; Eisoldt, L.; Diehl, J.; Schmidt, A.; Geffers, M.; Lang, G.; Scheibel, T. Biomimetic Fibers Made of Recombinant Spidroins with the Same Toughness as Natural Spider Silk. *Adv. Mater.* **2015**, *27*, 2189−2194.

(10) Lang, G.; Jokisch, S.; Scheibel, T. Air Filter Devices Including Nonwoven Meshes of Electrospun Recombinant Spider Silk Proteins. *J. Visualized Exp.* **2013**, *75*, e50492.

(11) Schacht, K.; Scheibel, T. Controlled Hydrogel Formation of a Recombinant Spider Silk Protein. *Biomacromolecules* **2011**, *12*, 2488−2495.

(12) Lammel, A.; Schwab, M.; Slotta, U.; Winter, G.; Scheibel, T. Processing Conditions for the Formation of Spider Silk Microspheres. *ChemSusChem* **2008**, *1*, 413−416.

(13) Helfricht, N.; Klug, M.; Mark, A.; Kuznetsov, V.; Blüm, C.; Scheibel, T.; Papastavrou, G. Surface Properties of Spider Silk Particles in Solution. *Biomater. Sci.* **2013**, *1*, 1166−1171.

(14) Doblhofer, E.; Scheibel, T. Engineering of Recombinant Spider Silk Proteins Allows Defined Uptake and Release of Substances. *J. Pharm. Sci.* **2015**, *104*, 988−994.

(15) Florczak, A.; Mackiewicz, A.; Dams-Kozlowska, H. Functionalized Spider Silk Spheres as Drug Carriers for Targeted Cancer Therapy. *Biomacromolecules* **2014**, *15*, 2971−2981.

(16) Hofer, M.; Winter, G.; Myschik, J. Recombinant Spider Silk Particles for Controlled Delivery of Protein Drugs. *Biomaterials* **2012**, *33*, 1554−1562.

(17) Lammel, A.; Schwab, M.; Hofer, M.; Winter, G.; Scheibel, T. Recombinant Spider Silk Particles as Drug Delivery Vehicles. *Biomaterials* **2011**, *32*, 2233−2240.

(18) Lyklema, J. *Fundamentals of Colloid and Interface Science*; Academic Press: New York, 1995; Vol. *1*, pp 4.1−4.135.

(19) O'Brien, R.; White, L. Electrophoretic Mobility of a Spherical Colloidal Particle. *J. Chem. Soc., Faraday Trans. 2* **1978**, *74*, 1607−1626.

(20) Duval, J. F. L.; Gaboriaud, F. Progress in Electrohydrodynamics of Soft Microbial Particle Interphases. *Curr. Opin. Colloid Interface Sci.* **2010**, *15*, 184−195.

(21) Zimmermann, R.; Dukhin, S. S.; Werner, C.; Duval, J. F. L. On the Use of Electrokinetics for Unraveling Charging and Structure of Soft Planar Polymer Films. *Curr. Opin. Colloid Interface Sci.* **2013**, *18*, 83−92.

(22) Ohshima, H. Electrophoresis of Soft Particles. *Adv. Colloid Interface Sci.* **1995**, *62*, 189−235.
(23) Moussa, M.; Caillet, C.; Town, R. M.; Duval, J. F. L. Remarkable Electrokinetic Features of Charge-Stratified Soft Nanoparticles: Mobility Reversal in Monovalent Aqueous Electrolyte. *Langmuir* **2015**, *31*, 5656−5666.
(24) Hermans, J. J.; Fujita, H. Electrophoresis of Charged Polymer Molecules with Partial Free Drainage. *Proc. Koninkl. Ned. Akad.* **1955**, *B58*, 182−187.
(25) Levine, S.; Levine, M.; Sharp, K. A.; Brooks, D. E. Theory of the Electrokinetic Behavior of Human Erythrocytes. *Biophys. J.* **1983**, *42*, 127−135.
(26) Hill, R.; Saville, D.; Russel, W. Electrophoresis of Spherical Polymer-Coated Colloidal Particles. *J. Colloid Interface Sci.* **2003**, *258*, 56−74.
(27) Ohshima, H. Electrophoretic Mobility of Soft Particles. *J. Colloid Interface Sci.* **1994**, *163*, 474−483.
(28) Duval, J. F. L.; Merlin, J.; Narayana, P. A. L. Electrostatic Interactions between Diffuse Soft Multi-Layered (Bio)Particles: Beyond Debye−Hückel Approximation and Deryagin Formulation. *Phys. Chem. Chem. Phys.* **2011**, *13*, 1037−1053.
(29) Ohshima, H. Electrokinetic Phenomena of Soft Particles. *Curr. Opin. Colloid Interface Sci.* **2013**, *18*, 73−82.
(30) Hofer, M.; Winter, G.; Myschik, J. Recombinant Spider Silk Particles for Controlled Delivery of Protein Drugs. *Biomaterials* **2012**, *33*, 1554−1562.
(31) Blüm, C.; Scheibel, T. Control of Drug Loading and Release Properties of Spider Silk Sub-Microparticles. J. *Bionanosci.* **2012**, *2*, 67−74.
(32) Pritchard, E. M.; Dennis, P. B.; Omenetto, F.; Naik, R. R.; Kaplan, D. L. Review Physical and Chemical Aspects of Stabilization of Compounds in Silk. *Biopolymers* **2012**, *97*, 479−498.
(33) Huemmerich, D.; Helsen, C. W.; Quedzuweit, S.; Oschmann, J.; Rudolph, R.; Scheibel, T. Primary Structure Elements of Spider Dragline Silks and Their Contribution to Protein Solubility. *Biochemistry* **2004**, *43*, 13604−13612.
(34) Cleveland, J. P.; Manne, S.; Bocek, D.; Hansma, P. K. A Nondestructive Method for Determining the Spring Constant of Cantilvers for Scanning Force Microscopy. *Rev. Sci. Instrum.* **1993**, *64*, 403−405.
(35) Dörig, P.; Ossola, D.; Truong, A. M.; Graf, M.; Stauffer, F.; Vörös, J.; Zambelli, T. Exchangeable Colloidal AFM Probes for the Quantification of Irreversible and Long-Term Interactions. *Biophys. J.* **2013**, *105*, 463−472.
(36) Kuznetsov, V.; Papastavrou, G. Adhesion of Colloidal Particles on Modified Electrodes. *Langmuir* **2012**, *28*, 16567−16579.
(37) Neubauer, M. P.; Blüm, C.; Agostini, E.; Engert, J.; Scheibel, T.; Fery, A. Micromechanical Characterization of Spider Silk Particles. *Biomater. Sci.* **2013**, *1*, 1160.
(38) Block, S.; Helm, C. A. Measurement of Long-Ranged Steric Forces between Polyelectrolyte Layers Physisorbed From 1 M NaCl. *Phys. Rev. E* **2007**, *76*, 030801.
(39) Block, S.; Helm, C. A. Conformation of Poly(Styrene Sulfonate) Layers Physisorbed From High Salt Solution Studied by Force Measurements on Two Different Length Scales. *J. Phys. Chem. B* **2008**, *112*, 9318−9327.
(40) Duval, J. F. L.; Ohshima, H. Electrophoresis of Diffuse Soft Particles. *Langmuir* **2006**, *22*, 3533−3546.
(41) Dukhin, S. S.; Zimmermann, R.; Duval, J. F. L.; Werner, C. On the Applicability of the Brinkman Equation in Soft Surface Electrokinetics. *J. Colloid Interface Sci.* **2010**, *350*, 1−4.
(42) Ascher, U.; Christiansen, J.; Russell, R. D. Collocation Software for Boundary-Value ODEs. *ACM Trans. Math. Softw.* **1981**, *7*, 209−222.
(43) Gasteiger, E.; Hoogland, C.; Gattiker, A.; Duvaud, S.; Appel, R. D.; Bairoch, A.; Wilkins, M. R. Protein Identification and Analysis Tools on the ExPASy Server. In *The Proteomics Protocols Handbook*; Walker, J. M., Ed.; Humana Press: Totowa, NJ, 2005; pp 571−607.
(44) Martin, J. R. S.; Bihannic, I.; Santos, C.; Farinha, J. P. S.; Demé, B.; Leermakers, F. A. M.; Pinheiro, J. P.; Rotureau, E.; Duval, J. F. L. Structure of Multiresponsive Brush-Decorated Nanoparticles: A Combined Electrokinetic, DLS, and SANS Study. *Langmuir* **2015**, *31*, 4779−4790.
(45) Zimmermann, R.; Romeis, D.; Bihannic, I.; Cohen Stuart, M.; Sommer, J.-U.; Werner, C.; Duval, J. F. L. Electrokinetics as an Alternative to Neutron Reflectivity for Evaluation of Segment Density Distribution in PEO Brushes. *Soft Matter* **2014**, *10*, 7804−7809.
(46) Decher, G. Fuzzy Nanoassemblies: Toward Layered Polymeric Multicomposites. *Science* **1997**, *277*, 1232−1237.
(47) Sukhorukov, G.; Mohwald, H.; Decher, G.; Lvov, Y. Assembly of Polyelectrolyte Multilayer Films by Consecutively Alternating Adsorption of Polynucleotides and Polycations. *Thin Solid Films* **1996**, *284-285*, 220−223.
(48) Schonhoff, M. Layered Polyelectrolyte Complexes: Physics of Formation and Molecular Properties. *J. Phys.: Condens. Matter* **2003**, *15*, R1781−R1808.
(49) von Klitzing, R. Internal Structure of Polyelectrolyte Multilayer Assemblies. *Phys. Chem. Chem. Phys.* **2006**, *8*, 5012−5033.
(50) Rentsch, S.; Pericet-Camara, R.; Papastavrou, G.; Borkovec, M. Probing the Validity of the Derjaguin Approximation for Heterogeneous Colloidal Particles. *Phys. Chem. Chem. Phys.* **2006**, *8*, 2531−2538.
(51) Borkovec, M.; Szilagyi, I.; Popa, I.; Finessi, M.; Sinha, P.; Maroni, P.; Papastavrou, G. Investigating Forces Between Charged Particles in the Presence of Oppositely Charged Polyelectrolytes with the Multi-Particle Colloidal Probe Technique. *Adv. Colloid Interface Sci.* **2012**, *179−182*, 85−98.
(52) Hartley, P.; Larson, I.; Scales, P. Electrokinetic and Direct Force Measurements between Silica and Mica Surfaces in Dilute Electrolyte, Solutions. *Langmuir* **1997**, *13*, 2207−2214.
(53) Kuznetsov, V.; Papastavrou, G. Ion Adsorption on Modified Electrodes as Determined by Direct Force Measurements Under Potentiostatic Control. *J. Phys. Chem. C* **2014**, *118*, 2673−2685.
(54) Pericet-Camara, R.; Papastavrou, G.; Behrens, S.; Borkovec, M. Interaction Between Charged Surfaces on the Poisson-Boltzmann Level: the Constant Regulation Approximation. *J. Phys. Chem. B* **2004**, *108*, 19467−19475.
(55) Kobayashi, M.; Juillerat, F.; Galletto, P.; Bowen, P.; Borkovec, M. Aggregation and Charging of Colloidal Silica Particles: Effect of Particle Size. *Langmuir* **2005**, *21*, 5761−5769.
(56) Porus, M.; Maroni, P.; Borkovec, M. Highly-Sensitive Reflectometry Setup Capable of Probing the Electrical Double Layer on Silica. *Sens. Actuators, B* **2010**, *151*, 250−255.
(57) Klein, J. Forces Between Mica Surfaces Bearing Layers of Adsorbed Polystyrene in Cyclohexane. *Nature* **1980**, *288*, 248−250.
(58) DeGennes, P. Polymers at an Interface - a Simplified View. *Adv. Colloid Interface Sci.* **1987**, *27*, 189−209.
(59) Israelachvili, J. N. *Intermolecular and Surface Forces*, 2nd ed.; Academic Press: London, 1992.
(60) Butt, H.; Kappl, M.; Mueller, H.; Raiteri, R.; Meyer, W.; Ruhe, J. Steric Forces Measured with the Atomic Force Microscope at Various Temperatures. *Langmuir* **1999**, *15*, 2559−2565.
(61) Kleshchanok, D.; Tuinier, R.; Lang, P. R. Direct Measurements of Polymer-Induced Forces. *J. Phys.: Condens. Matter* **2008**, *20* (7), 073101.
(62) Kaufmann, S.; Papastavrou, G.; Kumar, K.; Textor, M.; Reimhult, E. A Detailed Investigation of the Formation Kinetics and Layer Structure of Poly(Ethylene Glycol) Tether Supported Lipid Bilayers. *Soft Matter* **2009**, *5*, 2804−2814.
(63) Abraham, T.; Christendat, D.; Xu, Z.; Masliyah, J.; Gohy, J.; Jerome, R. Role of Polyelectrolyte Charge Density in Tuning Colloidal Forces. *AIChE J.* **2004**, *50*, 2613−2626.
(64) Lammel, A. S.; Hu, X.; Park, S.-H.; Kaplan, D. L.; Scheibel, T. R. Controlling Silk Fibroin Particle Features for Drug Delivery. *Biomaterials* **2010**, *31*, 4583−4591.
(65) Bjellqvist, B.; Hughes, G. J.; Pasquali, C.; Paquet, N.; Ravier, F.; Sanchez, J.-C.; Frutiger, S.; Hochstrasser, D. The Focusing Positions of

DOI: 10.1021/acs.jpcc.6b03957
J. Phys. Chem. C 2016, 120, 18015−18027

Polypeptides in Immobilized pH Gradients Can Be Predicted From Their Amino Acid Sequences. *Electrophoresis* **1993**, *14*, 1023−1031.
(66) Bjellqvist, B.; Basse, B.; Olsen, E.; Celis, J. E. Reference Points for Comparisons of Two-Dimensional Maps of Proteins From Different Human Cell Types Defined in a pH Scale Where Isoelectric Points Correlate with Polypeptide Compositions. *Electrophoresis* **1994**, *15*, 529−539.
(67) Yamaguchi, A.; Kobayashi, M. Quantitative Evaluation of Shift of Slipping Plane and Counterion Binding to Lysozyme by Electrophoresis Method. *Colloid Polym. Sci.* **2016**, *294*, 1019−1026.
(68) Termonia, Y. Molecular Modeling of Spider Silk Elasticity. *Macromolecules* **1994**, *27*, 7378−7381.

DOI: 10.1021/acs.jpcc.6b03957
J. Phys. Chem. C 2016, 120, 18015−18027

Supporting Information

Colloidal Properties of Recombinant Spider Silk Protein Particles

Nicolas Helfricht,[1] Elena Doblhofer,[2] Jérôme F. L. Duval,[3,4*] Thomas Scheibel,[2] Georg Papastavrou[1*]

[1]Physikalische Chemie / Physik der Polymere, University of Bayreuth, Universitätsstrasse 30, Bayreuth 95440, Germany; E-mail: georg.papastavrou@uni-bayreuth.de

[2]Biomaterialien, Fakultät für Ingenierswissenschaften, Universität Bayreuth, Universitätsstrasse 30, Bayreuth 95440, Germany

[3]Laboratoire Interdisciplinaire des Environnements Continentaux, UMR 7360, Université de Lorraine, Vandœuvre-lès-Nancy, F-54501, France ; E-mail : jerome.duval@univ-lorraine.fr

[4] CNRS, Laboratoire Interdisciplinaire des Environnements Continentaux, UMR 7360, Vandœuvre-lès-Nancy, F-54501, France

S1. Summary of ionizable groups of the recombinant spider silk proteins eADF4(C16) and eADF4(κ16)

Table S1: Ionizable groups of recombinant spider silk proteins eADF4(κ16) and eADF4(C16)

	κ-module	**C-module**	**Both modules**	**C-terminus**	**N-terminus**	**T7-Tag**
Amino acid	Lysine	Glutamic acid	Tyrosine	Glycine	Methionine	Arginine
	L	E	Y	G	M	R
$pK_{side\ chain}$	10.53[1]	4.25[1]	10.07[1]	-	-	12.28[1]
$pK_{carboxy\text{-}term.}$	-	-	-	2.34[1]	-	-
$pK_{amino\text{-}terminal}$	-	-	-	-	9.21[1]	-
Groups/ molecule	16	16	32	1	1	1
Hydropathy index	-3.9[1]	-3.5[1]	-1.3[1]	-0.4[1]	1.9[1]	-4.5[1]

S2. SEM images of spidroin particles

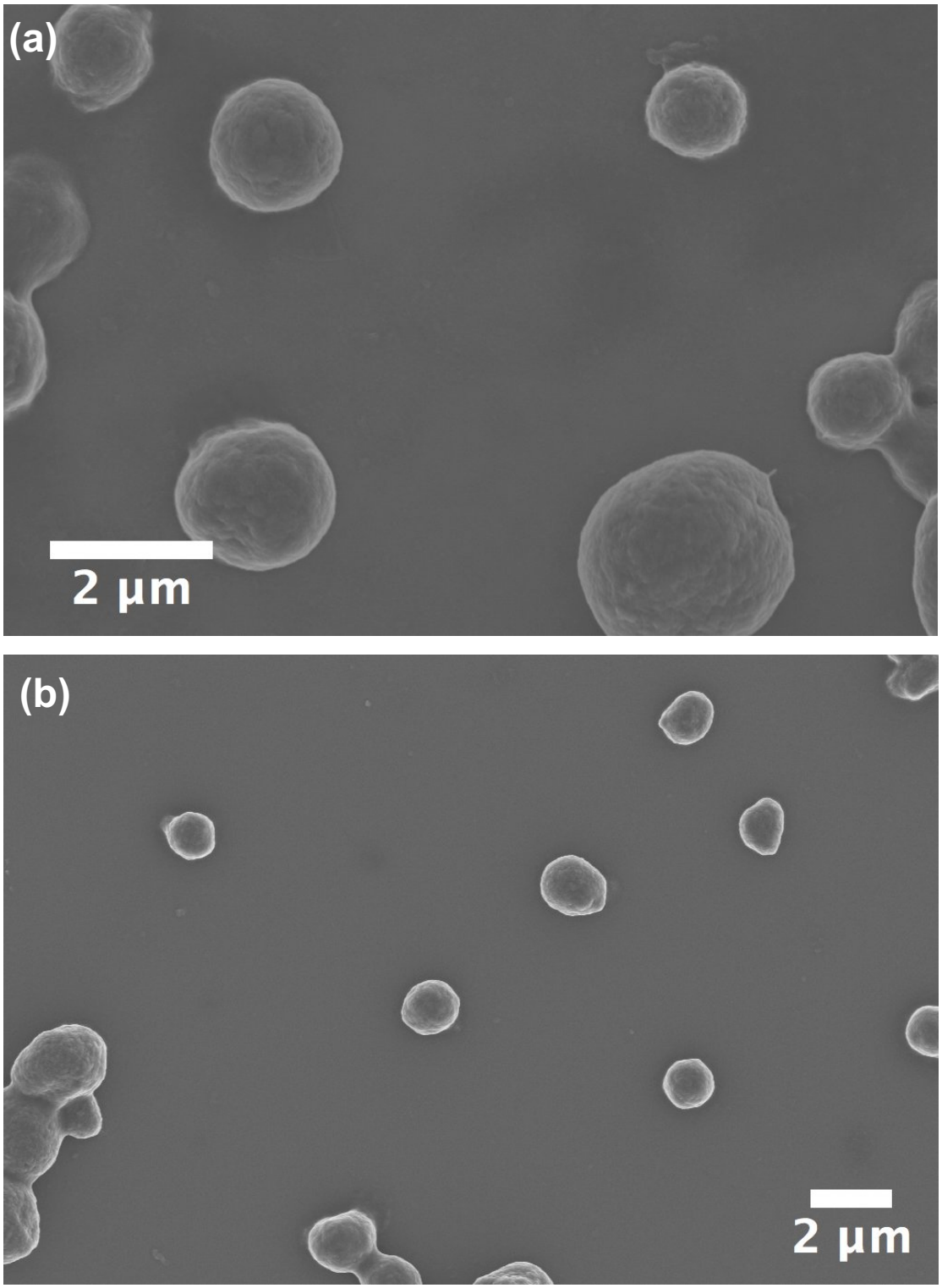

Figure S1. SEM images of several particles of each protein type (a) eADF4(κ16) and (b) eADF4(C16)

S3. Independence of particle mobility with respect to changes in particle size.

The polydispersity of the here presented protein particles is rather large. However, the derived electrokinetic parameters from our analysis are basically independent of the of the protein particles size over a wide range of radii as shown in Figure S2 for various ionic strengths.

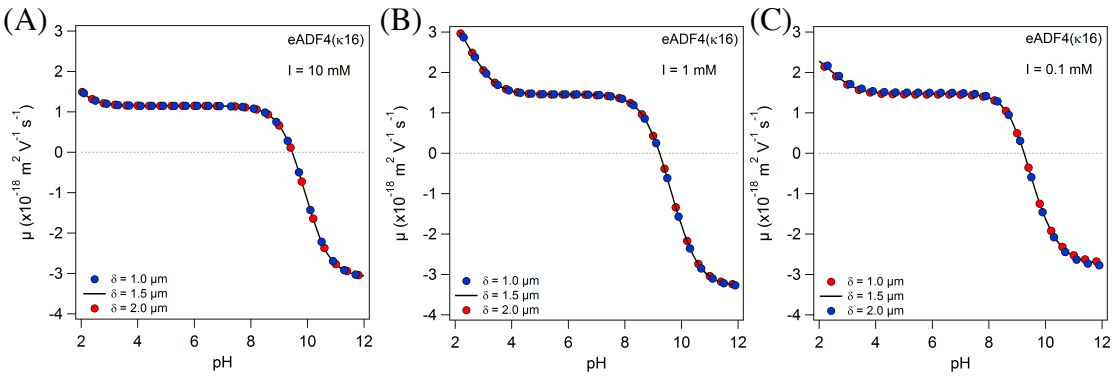

Figure S2. Evidence for the size-independence of eADF4(κ16) electrophoretic mobility in the radius range 1-2 μm at 10 mM (A), 1 mM (B) and 0.1 mM under the conditions as used for studies shown in Figure 3a, Figure 3b, Figure 3c (line (a) therein), respectively, using the Duval-Ohshima's theory.[2] Meaning of symbols and line are specified in the figure with δ the porous particle radius.

References

1. Nelson, D. L.; Cox, M. M. *Lehninger: Principles of Biochemistry*, Palgrave Macmillan, **2012**.

2. Duval, J. F. L.; Ohshima, H. Electrophoresis of diffuse soft particles. *Langmuir* **2006**, *22*, 3533-3546.

5.4 Teilarbeit IV

Structural Insights into Water-Based Spider Silk Protein–Nanoclay Composites with Excellent Gas and Water Vapor Barrier Properties

Autoren: **Elena Doblhofer**, Jasmin Schmid, Martin Rieß, Matthias Daab, Magdalena Suntinger, Christoph Habel, Hendrik Bargel, Christoph Hugenschmidt, Sabine Rosenfeldt, Josef Breu, und Thomas Scheibel

Die Konzeption dieses Projekts oblag mir in Zusammenarbeit mit Jasmin Schmid, Josef Breu und Thomas Scheibel. Das Produktionsverfahren der Barriere-Beschichtungen wurde von mir entwickelt und von Magdalena Suntinger experimentell umgesetzt, dies gilt ebenso für die Analyse der optischen Kennwerte des Materials. Zur Analyse der Barrierebeschichtung wurden Barriere-, PXRD-, PALS und BDS-Messungen von Jasmin Schmid durchgeführt, wobei zur Auswertung der PALS-Messungen Christopher Hugenschmidt zu Rate gezogen wurde. Analysen der Struktur (FTIR-Messungen, sowie FSD-Auswertung), der thermischen Stabilität (TGA und DSC), der chemischen Stabilität, sowie Mechanik-Messungen wurden von mir durchgeführt. Hendrik Bargel fertigte REM-Aufnahmen an, Christoph Habel, Martin Rieß, Mathias Daab und Sabine Rosenfeldt waren für die Charakterisierung des Natriumhektorits und Literaturvergleiche verantwortlich. Das Manuskript wurde von mir verfasst und unter wissenschaftlichen Diskussionen mit Christoph Hugenschmidt, Josef Breu und Thomas Scheibel fertiggestellt.

Der Artikel wurde am 07.09.2016 im Journal *ACS Applied Materials and Interfaces* veröffentlicht.

ACS APPLIED MATERIALS & INTERFACES

Research Article

www.acsami.org

Structural Insights into Water-Based Spider Silk Protein–Nanoclay Composites with Excellent Gas and Water Vapor Barrier Properties

Elena Doblhofer,[†] Jasmin Schmid,[‡] Martin Rieß,[‡] Matthias Daab,[‡] Magdalena Suntinger,[†] Christoph Habel,[‡] Hendrik Bargel,[†] Christoph Hugenschmidt,[∥] Sabine Rosenfeldt,[§] Josef Breu,*[,‡] and Thomas Scheibel*[,†]

[†]Lehrstuhl Biomaterialien, [‡]Lehrstuhl für Anorganische Chemie I, and [§]Lehrstuhl für Physikalische Chemie I, Universität Bayreuth, Universitätsstraße 30, Bayreuth D-95447, Germany

[∥]FRM II und Physik-Department E21, Technische Universität München, James-Franck-Straße 1, Garching D-85748, Germany

Supporting Information

ABSTRACT: Nature reveals a great variety of inorganic–organic composite materials exhibiting good mechanical properties, high thermal and chemical stability, and good barrier properties. One class of natural bio-nanocomposites, e.g. found in mussel shells, comprises protein matrices with layered inorganic fillers. Inspired by such natural bio-nanocomposites, the cationic recombinant spider silk protein eADF4(κ16) was processed together with the synthetic layered silicate sodium hectorite in an all-aqueous setup. Drop-casting of this bio-nanocomposite resulted in a thermally and chemically stable film reflecting a one-dimensional crystal. Surprisingly, this bio-nanocomposite coating was, though produced in an all-aqueous process, completely water insoluble. Analyzing the structural details showed a low inner free volume due to the well-oriented self-assembly/alignment of the spider silk proteins on the nanoclay surface, yielding high oxygen and water vapor barrier properties. The here demonstrated properties in combination with good biocompatibility qualify this new bio-nanocomposite to be used in packaging applications.

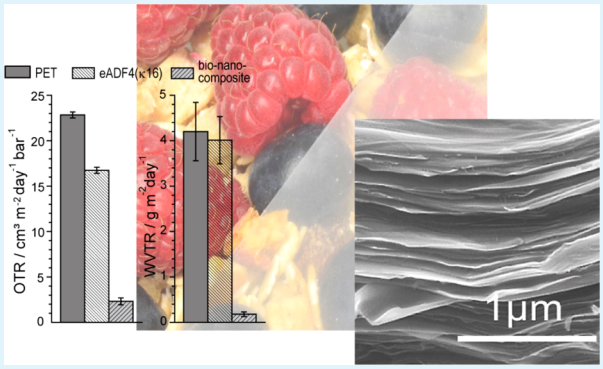

KEYWORDS: *spider silk, layered silicates, bio-nanocomposites, barrier coatings, water-based packaging coatings*

INTRODUCTION

Bio-nanocomposites are materials made of biopolymers and inorganic biocompatible solids with at least one dimension in the nanometer scale.[1] They can be found in nature e.g. in nacre in pearls and shells,[2] ivory,[3] bones,[4] and enamel and dentine in teeth.[5,6] In nature such composite materials show hierarchical arrangements of organic and inorganic components from the nano- to macroscale. In recent years huge efforts have been made to mimic such hierarchical setup in man-made bio-nanocomposites yielding extraordinary material properties.[5] Special focus has been set on the development of bio-nanocomposites displaying good mechanical properties and high thermal stability and acting as gas barrier in combination with biocompatibility and biodegradability.[7,8] Such materials show extraordinary versatility concerning their application, derived from the used variety of biopolymer matrices based on polysaccharides, nucleic acids, or proteins and inorganic particulate fillers such as hydroxyapatite, silica, or layered silicates.[9] Bio-nanocomposites are especially of interest to be used as advanced biomaterials for instance in tissue engineering, artificial bone replacements, and gene therapy, but they can also be applied in controlled drug and pesticide delivery, membranes for food processing, drinking water purification, and food packaging.[10] The possibility of replacing petroleum-derived synthetic composites by naturally abundant and biodegradable materials obtained from renewable sources is one further intriguing aspect.[11,12]

Here, composites made of the cationic recombinant spider silk protein (spidroin) eADF4(κ16) and the nanoclay sodium hectorite (Na-hec) were investigated concerning their hierarchical setup, their structure, and their barrier properties. Spidroins are naturally occurring polymers containing both hydrophobic and hydrophilic as well as charged and uncharged residues and innately fulfill mostly structural features by building load-bearing natural materials.[13] Spidroins combine inherent extraordinary mechanical properties when processed (high elastic modulus and high elongation-to-break) with biocompatibility and biodegradability, qualifying them for a great variety of applications.[14] The latter became increasingly feasible, since recently recombinant spidroins could be successfully produced to overcome shortages of spider-based production.[15] Additionally, the obtained recombinant proteins

Received: July 7, 2016
Accepted: September 7, 2016
Published: September 7, 2016

DOI: 10.1021/acsami.6b08287
ACS Appl. Mater. Interfaces 2016, 8, 25535–25543

provide a series of advantages over the natural ones, like processability into various morphologies (even other than the naturally occurring fibers) and the possibility to modify and adopt the amino acid sequences on a genetic level.[16−18] In terms of bio-nanocomposite production one great advantage is that prior to processing, spidroins are partially intrinsically unstructured in solution and, therefore, can adopt extended molecule conformations and provide maximum van der Waals and electrostatic interactions with other material surfaces, e.g., inorganic fillers.

Layered silicates are most commonly used as nanofillers. Fluorohectorite, as an example, belongs to the 2:1 smectite family and shows a sandwich-like structure comprising two tetrahedral and one octahedral layers with the nominal composition of $[Na_{0.5}]^{inter}[Mg_{2.5}Li_{0.5}]^{oct}[Si_4]^{tet}O_{10}F_2$ (Na-hec).[19] Singular clay nanosheets of 1 nm thickness are tough displaying an in-plane modulus of 150 GPa, while at the same time being highly flexible, and can be squeezed by 30% without breaking.[20,21] Melt-synthesized clay nanosheets, moreover, come in high aspect ratios (>20 000) and with uniform surface charge density qualifying synthetic fluorohectorite as superb fillers in nanocomposite materials. Additionally, such synthetic clays are gently, without mechanical agitation, but nevertheless utterly delaminated into single layers by osmotic swelling when immersed in deionized water, facilitating the incorporation into several matrices.[21]

The aim was to optimize the interplay between the spidroin and the nanoclay in an all-aqueous setup, to find ideal processing conditions, and to generate a material that exceeds the overall properties of other water-based bio-nanocomposites. Therefore, structure, optical, and thermal properties as well as chemical stability of the obtained bio-nanocomposites were investigated after processing. Further, PXRD measurements were conducted to determine the platelet arrangement in the final bio-nanocomposite obtained by self-assembly in a single production step. It could be shown that the concerted self-assembly of spidroins with nanoclay platelets leads to a quite low free inner volume of the bio-nanocomposite film, which in turn yielded a low oxygen permeability and, very surprisingly (since it is a water based system), also a good water vapor barrier.

RESULTS AND DISCUSSION

Bio-nanocomposite Production and Characterization.

Bio-nanocomposite films made of the amphiphilic and cationic recombinant spider silk protein eADF4(κ16) as matrix and the synthetic layered silicate sodium hectorite (Na-hec) as filler were produced in an all-aqueous suspension casting process. Clay synthesis and characterization are described in the Supporting Information. L-Lysine-modified hectorite platelets (Lys-hec), utterly delaminated within deionized water, were compounded with eADF4(κ16) at a weight ratio of 3:2. The modification of the nanoclay with L-lysine was necessary in order to reduce the hydrophilicity of the hectorite (hec) platelets and to adjust the surface energy assuring a better interaction between matrix and filler.[21,22] Drop-casting of the material mixture onto a poly(ethylene terephthalate) (PET) foil and subsequent drying initiated the bio-nanocomposite film formation with a filler content of 60 wt %. The obtained films were free of any processing residuals due to the all-aqueous processing (for experimental details see Materials and Methods section). By the number of drop-casting steps, film thickness could be adjusted manually between 1 μm (2 casting steps) and 30 μm (20 casting steps), displaying a growth of the film thickness of around 1.5 μm per casting step. Additionally, cross sections of the films revealed a highly ordered lamellar structure (Figure 1A), determined by the inherent properties of the

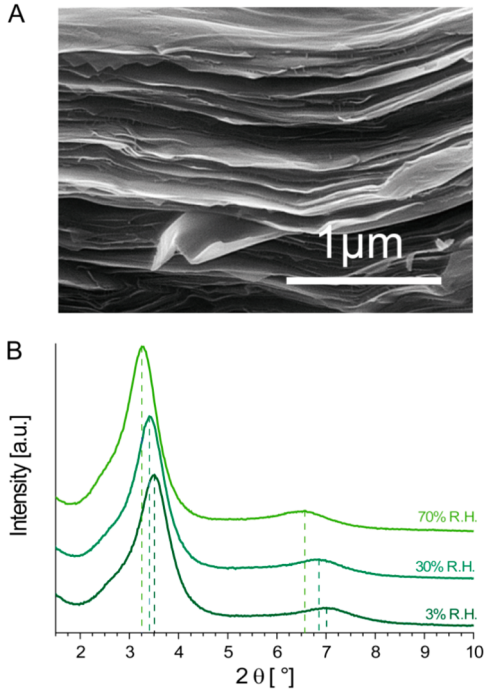

Figure 1. Analysis of spider silk protein−nanoclay composites (A) SEM image of a cross section of the bio-nanocomposite film. (B) Verification of the one-dimensional crystalline restacking of nanoclay within the spider silk matrix using PXRD at 3, 30, and 70% RH indicated limited swelling of the bio-nanocomposite.

nanoclay filler. The high aspect ratio (~20 000) in combination with the uniform thickness of the nanosheets and the high weight proportion of the filler triggered self-assembly into a lamellar structure oriented in parallel to the substrate surface.[23]

Quite surprisingly, powder X-ray diffraction (PXRD, Figure 1B) revealed not only a parallel but also an ordered, equidistant restacking of the nanoplatelets as reflected by a relative sharp interference observed at d = 2.50 nm ($2\theta_{001}$ = 3.5°) for the dry bio-nanocomposite film. Even the second order of the one-dimensional crystal was observed at 1.26 nm ($2\theta_{002}$ = 7.0°). This suggested that the clay nanoplatelets were perfectly uniformly distributed in the spidroin matrix, giving yield to a periodic modulation of the electron density. Consequently, the Coulomb attraction between negatively charged clay nanosheets and the positively charged interlayer species was increased by up to 39% (Madelung constant of a one-dimensional crystal), and a considerable electrostatic pressure compressed the interlayer volume. The 00l reflections observed for the composite resemble an intercalation compound. The d-spacing is, however, much larger than that of typical intercalation compounds, and as expected for a self-assembled structure of filler separated by polymer matrix the d-spacing is less sharply defined, and consequently the reflections are comparatively broader.

Upon compounding with eADF4(κ16), the d-spacing shifted from 1.40 nm for Lys-hec to 2.50 nm in the bio-nanocomposite, indicating that the eADF4(κ16) layer occupied 1.10 nm within the interlayer space.

DOI: 10.1021/acsami.6b08287
ACS Appl. Mater. Interfaces 2016, 8, 25535−25543

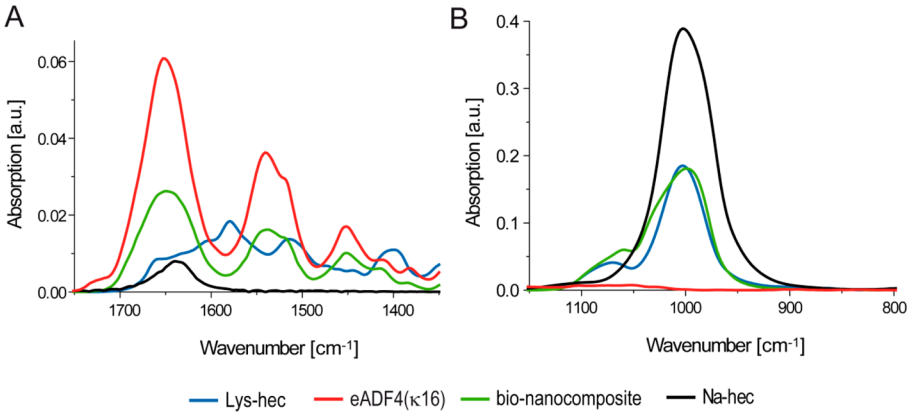

Figure 2. FTIR spectra of eADF4(κ16) film, Na-hec, Lys-hec, and the bio-nanocomposite samples (A) between 1800 and 1300 cm^{-1} for protein structure determination of the amide I and amide II band and (B) between 1200 and 800 cm^{-1} for identification of Na-hec by in-plane (1080 cm^{-1}) and out-of-plane (1003 cm^{-1}) Si−O bond vibration absorption.

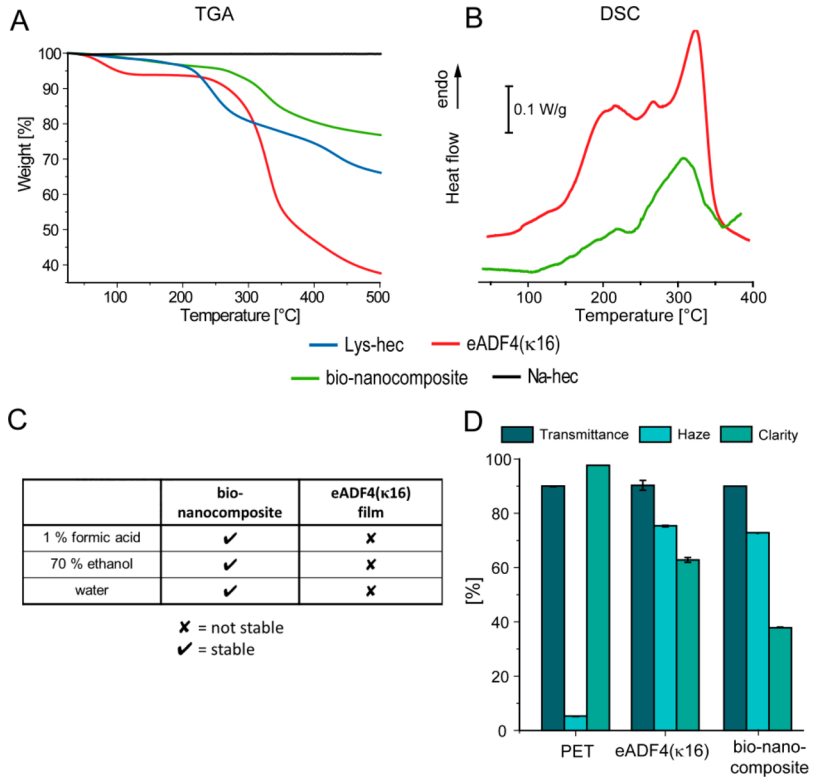

Figure 3. Characterization of material properties of the bio-nanocomposite film in comparison to that of neat eADF4(κ16) films. Analysis of thermal stability of the bio-nanocomposite, Na-hec, Lys-hec, and neat eADF4(κ16) film (A) by thermogravimetric analysis (TGA) in the temperature range from 25 to 500 °C and a heating rate of 5 K/min and (B) by differential scanning calorimetry (DSC) in the temperature range from 40 to 400 °C with a heating rate of 5 K/min. (C) Analysis of chemical stability by incubation of the bio-nanocomposite in comparison to that of neat eADF4(κ16) films in 1% formic acid, 70% ethanol, and water. (D) Optical properties of the bio-nanocomposite on PET foil in comparison to that of a eADF4(κ16) coating on PET foil as well as plain PET regarding transparency, haze, and clarity.

Since the bio-nanocomposite film was cast from an all-aqueous suspension, it was expected to swell heavily when exposed to water vapor. PXRD measurements at various relative humidity (RH) (Figure 1B), quite surprisingly, showed a very limited swelling with increasing RH. The X-ray reflection angle shifted from $2\theta_{001}$ = 3.5° to $2\theta_{001}$ = 3.3°, indicating a rather small increase (0.2 nm) of the interlayer spacing of the bio-nanocomposite from 3% to 70% RH.

FTIR measurements allowed to elucidate the conformational state of eADF4(κ16) in the interlayer spacing. For structural analysis of the protein matrix, peaks in the amide I (1600−1700 cm^{-1}) and amide II (1500−1580 cm^{-1}) regions were examined in greater detail (Figure 2A). These wavenumber regions represent mainly C═O stretching vibrations of the amide backbone (amide I) and N−H bending in combination with C−N asymmetric stretch vibrations (amide II).[24,25] Although lysine in Lys-hec also contains N−H and C−H groups,[26] fortunately its absorption bands did not significantly overlap with eADF4(κ16) absorption bands. Therefore, lysine bands did not hamper structure determination of the protein matrix. FTIR analysis of the composite material showed peaks at 1649 cm^{-1} (amide I) and at 1538 cm^{-1} (amide II) originating from

DOI: 10.1021/acsami.6b08287
ACS Appl. Mater. Interfaces 2016, 8, 25535−25543

A

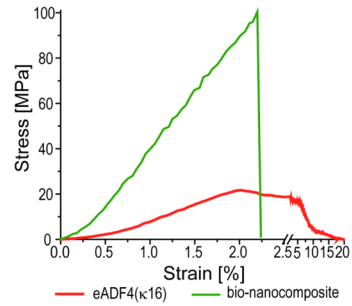

B

	bio-nano composite	eADF4(κ16) film
E-Modulus [MPa]	1682.7 ± 668.7	445.4 ± 296.8
Max. Strength [MPa]	99.9 ± 16.6	27.8 ± 8.2
Max. Strain [%]	2.4 ± 0.2	18.7 ± 6.6
Toughness [MJ/m^3]	1.0 ± 0.2	2.0 ± 0.6

Figure 4. Mechanical properties of the free-standing bio-nanocomposite in comparison to free-standing eADF4(κ16) films: (A) representative example of stress−strain curves obtained at RT and 50% RH by tensile testing; (B) mechanical properties averaged from stress−strain curves; n = 5−12.

random coil structures.[24,25] Calculations using Fourier self-deconvolution (FSD) revealed that 27.6 ± 1.6% of the structural content in the bio-nanocomposite reflected β-sheet conformation (17.6% for neat eADF4(κ16) films).[24,27] The identified structure indicated increased intermolecular interactions between the spidroin molecules in the bio-nanocomposite in contrast to the neat protein film. The observed high β-sheet content provided a basis for good thermal and chemical stability of the material, which is described below.

Besides protein structural determination, FTIR analysis also allowed to identify the presence of hectorite platelets and the interactions with the matrix by absorption bands at wavenumbers between 1000 and 1120 cm^{-1} (Figure 2B). Absorption observed in this region could be attributed to in-plane and out-of-plane vibrations of the Si−O bond in the nanoclay.[28] Lys-hec showed one predominant peak in this region with a maximum at around 1003 cm^{-1} corresponding to the absorption of in-plane Si−O bond vibrations, whereas a shoulder at 1080 cm^{-1} could be attributed to out-of-plane Si−O bond vibration absorptions.[29] In spectra of the bio-nanocomposite, both peaks were present, but each was shifted to a smaller wavenumber indicating electrostatic interactions and the formation of hydrogen bonds between the single platelets and the matrix. This was also confirmed by the development of the FWHM (full width at half-maximum) values of the in-plane Si−O bond vibration peaks, since previous studies of Na-hec have shown an increasing interaction between hectorite layers with increasing FWHM values (FWHM (Na-hec) = 56 cm^{-1}, FWHM (bio-nanocomposite) = 64 cm^{-1}).[29]

Thermal stability of the nanocomposite was analyzed using thermogravimetric analysis (TGA). Since Na-hec does not decompose below 700 °C, the thermal stability of the bio-nanocomposite was determined by the stability of interlayer species. The onset temperatures, as indicated here by the inflection point in the corresponding TGA curves, were found at 226 °C for Lys-hec and 330 °C for neat eADF4(κ16) (Figure 3A). Initial weight losses of 4.4 wt % at temperatures <120 °C could be attributed to the loss of physisorbed water. Because of the dominance of the protein matrix, the decomposition of the bio-nanocomposite was determined by the decomposition of eADF4(κ16) with an onset temperature of 327 °C.

DSC analysis gave a more detailed insight concerning the influence of composite formation on thermal stability of the spidroin material. While the thermal treatment of the bio-nanocomposite showed one distinct maximum at 307 °C (degradation) and a small shoulder at 220 °C (glass transition), eADF4(κ16) induced three peaks (glass transition: 220 °C; bimodal melting/thermal degradation: 267 °C; degradation: 323 °C). Therefore, DSC confirmed the degradation temperatures (maximum heat flow) (Figure 3B) as seen by TGA. Further, the glass transition temperature (T_g) could be determined by the inflection point of the glass transition signal. T_g of eADF4(κ16) films was observed at 174 °C and did not change significantly, upon compounding with the nanoclay. However, the signal of the glass transition of the bio-nanocomposite was reduced from −0.2 g/W (eADF4(κ16)) to −0.07 g/W (bio-nanocomposite). This reduction was higher than expected due to the dilution of eADF4(κ16) with the clay filler. Most likely, this finding can be attributed to an increase of the amount of crystalline β-sheet domains on the expense of the amorphous domains, being in line with FTIR results and previously published T_g values for silk materials with different β-sheet content.[27,30]

Chemical stability of the nanocomposite was tested by incubating the films 7 days in 1% formic acid, 70% ethanol, or water to ensure that the bio-nanocomposite provided a good long-term stability in humid, acidic, and sterilizing environments. The bio-nanocomposite showed good shape stability after incubation in all cases by optical analysis (Figure S3). As a control, pristine, unfilled eADF4(κ16) films were tested but were found to be completely dissolved after 1 day of incubation in all media (Figure 3C). Interestingly, the incorporation of the nanofiller and the applied processing procedure rendered the eADF4(κ16) matrix moisture-resistive without post-treatment as typically necessary for spider silk films[27] due to the protein alignment in the d-spacing of the filler yielding the high β-sheet content as detected by FTIR measurements.

Upon testing the optical properties, coatings of the bio-nanocomposite and neat eADF4(κ16) films revealed only little effect on transmittance (Figure 3D) of the PET support. However, haze, a value for large angle scattering of light causing a milky appearance, and clarity, a value for small-angle scattering of light causing an impairment of image definition, were affected to different extents. Haze increased from 6% for the neat PET substrate to 75% for eADF4(κ16)-coated PET, suggesting that the opaque appearance could be fully attributed to the protein matrix. Compounding did not further affect haze; the value of bio-nanocomposite-coated PET was similar (74%) to that of eADF4(κ16)-coated PET. Clarity was diminished to 63% by the eADF4(κ16) coating and to 38% by the bio-nanocomposite coating.

Besides good thermal and chemical stability, tensile testing of free-standing nanocomposite films revealed good mechanical

DOI: 10.1021/acsami.6b08287
ACS Appl. Mater. Interfaces 2016, 8, 25535−25543

stability. Internalization of hectorite platelets increased the ultimate tensile strength (UTS) in comparison to untreated eADF4(κ16) films (cast from formic acid solution) from 28 ± 8 to 100 ± 16 MPa (Figure 4). While neat eADF4(κ16) films showed a plastic deformation after reaching the relevant UTS value, nanocomposite films ruptured immediately at this point. In contrast to plain protein films, the nanocomposite was not sensitive to variations in relative humidity.

Free Inner-Volume Characteristics. Two positron annihilation techniques—Doppler broadening spectroscopy (DBS) of the annihilation line and positron annihilation lifetime spectroscopy (PALS)—were used to characterize the free volume and the size of (micro)voids in the bio-nanocomposite in greater detail. When implanted into a polymer matrix, positrons thermalize within <10 ps and may either directly annihilate or form positronium (Ps) prior to annihilation. By varying the positron implantation energies from 0.5 to 30 keV, the *S*-parameter was measured as a function of the penetration depth in the nanocomposite as well as in the pure constituents eADF4(κ16) and Na-hec (Figure 5). For very

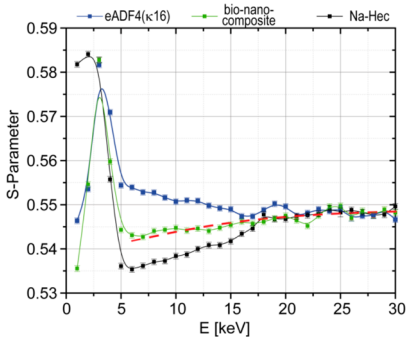

Figure 5. Determination of the *S*-parameter by Doppler broadening spectroscopy (DBS), indicating the decrease of the inner free volume of the bio-nanocomposite coating with increasing positron energy synonymous with increasing penetration depth in comparison to neat eADF4(κ16) films and Na-hec powder (red dashed line: theoretical value by combination of the single bio-nanocomposite components).

low implantation energies (<2 keV) the measured *S*-parameter was attributed to a strong influence of surface effects, e.g., orthopositronium (o-Ps) formation at the surface, and shall not be discussed further. The high *S*-value at 3−4 keV indicated a higher free volume in the near-surface regime in all samples. This surface regime was followed by a steep decrease of the *S*-parameter over the first 250 nm of the bio-nanocomposite film, indicating a quick reduction of the free volume with proceeding sample depth. At high energies (>20 keV) a saturation value was reached, indicating a similar free volume being present in all samples. A pure clay film showed the lowest *S*-parameter, suggesting that there is little if any positronium formation in the silicate platelets. The neat eADF4(κ16) film showed the highest *S*-parameter, indicating the largest free volume of the three samples investigated. The curve for the bio-nanocomposite resided between these two extremes at all penetration depths. Moreover, this curve equaled a weighted superposition of the other curves obtained for the constituents (red dashed line in Figure 5), indicating that the confined matrix in the bio-nanocomposite had a similar free volume as the neat biopolymer. Therefore, the severe confinement (1.1 nm) did not hamper chain packing, and the huge interfacial area did not trigger formation of additional free volume. This advantageous microstructure might be based on the cationic nature of eADF4(κ16) and the Coulomb interaction with the clay platelets which, moreover, is amplified by the Madelung factor due to one-dimensional crystallinity.

The free-volume characteristics of the bio-nanocomposite were additionally probed by PALS at five different implantation energies (1, 2, 4, 8, and 16 keV). In amorphous polymers, the so-called "pick-off" annihilation of long-living o-Ps trapped in nanometer size voids provides information on static and dynamic holes.[31] All spectra were decomposed by fitting three lifetime components, whereby the long lifetime component τ_3 connected with *o*-Ps was interpreted with regard to the mean size of the voids.[32] Most importantly, identical τ_3 values of 1.65 ± 0.03 ns were found for all implantation energies in the bio-nanocomposite. According to the Tao−Eldrup model assuming spherically shaped voids, the observed τ_3 value corresponded to a mean void radius of 2.5 ± 0.1 Å and to a mean volume of about 65.4 ± 7.8 Å^3.[33] Lifetimes and hence void diameter were at the lower end of the typical range for glassy polymers.[34] Together with the slightly increasing slope of the measured *S*-parameter in this energy range, it could be concluded that the mean void size remained essentially the same, but the total free volume, i.e., the concentration of these voids, increased up to a depth of about 4 μm. The uniform nature of the free volume characteristics at larger depths corroborated the homogeneity of the bio-nanocomposite reflecting one-dimensional crystallinity.

A combination of the described characterization methods, including PXRD measurements, FTIR spectroscopy, and DBS/PALS analysis, led to a model of nanocomposite assembly as depicted in Figure 6. Therein, appearance of a textured and one-dimensional crystalline lamellar structure, formation of a densely packed interlayer space with little free volume and small voids, and β-sheet formation are initiated in the final step by self-assembly of the silk protein on the nanoclay surface followed by water evaporation.

Barrier Properties. Because of the huge aspect ratio of the nanoclay platelets and the high filler content, the bio-nanocomposite showed a lamellar structure similar to a wall of bricks with a low free inner volume. Since nanoclay platelets are impermeable for any gases, nanocomposites comprising nanoclay fillers with a brick wall-like structure are conceivable as barrier materials[35] since the presence of the clay layers renders the diffusion path of molecules more tortuous through the composite.[36] To test the barrier properties of the here fabricated bio-nanocomposite, permeation measurements were carried out at 50% RH and at room temperature using 1.5 μm thick bio-nanocomposite coatings on a 100 μm PET foil (Figure 7). In comparison to the uncoated substrate (OTR: 22.83 ± 0.33 cm^3 m^{-2} day^{-1} bar^{-1}; WVTR: 4.20 ± 0.64 g m^{-2} day^{-1}), the oxygen transmission rate (OTR) of bio-nanocomposite-coated PET was reduced by 90% to 2.32 ± 0.38 cm^3 m^{-2} day^{-1} bar^{-1}, while the water vapor transmission rate (WVTR) decreased by 96% to 0.18 ± 0.05 g m^{-2} day^{-1} (Figure 7). In contrast, unfilled eADF4(κ16) coatings had only a minor influence on OTR and no influence on WVTR. In light of the water solubility of neat eADF4(κ16) films and the water-based formulation of the bio-nanocomposite in particular, the large reduction of WVTR was remarkable, and barrier coatings with the detected properties could find application for instance in the field of food packaging.

Comparison with literature values is difficult because test conditions significantly vary and various units are used.

DOI: 10.1021/acsami.6b08287
ACS Appl. Mater. Interfaces 2016, 8, 25535−25543

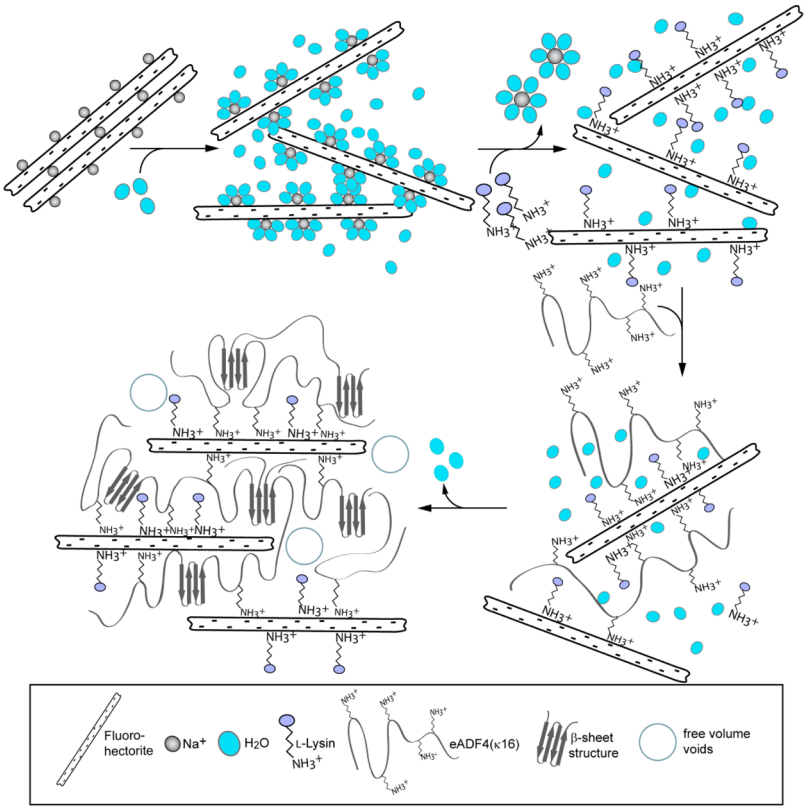

Figure 6. Model of bio-nanocomposite formation: delamination of Na-hec occurs in an aqueous environment; hec is modified by ion exchange of Na^+ against lysine to adjust the platelet's surface energy. After compounding of the cationic eADF4(κ16) with Lys-hec, the bio-nanocomposite assembles upon slow drying, accompanied by β-sheet formation of the protein and simultaneous minimization of the inherent free volume.

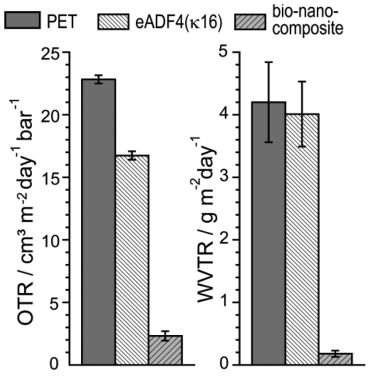

Figure 7. Barrier properties of bio-nanocomposite-coated PET concerning the oxygen (OTR) and the water vapor transmission rate (WVTR) in comparison to that of neat PET and spider silk coated PET ("eADF4(κ16)").

Sometimes pressure differences are not recorded or are simply omitted in the conversions. For applications, absolute transmission rates (OTR and WVTR) are the relevant benchmark values. Transmission rates are, however, largely influenced by the thickness of the barrier coatings and even the transmission rate of the substrate it has been coated on. Consequently, the performance of barrier coatings can only be compared if transmission rates are converted into permeabilities (P) taking coating thickness into account, whereby it is generally assumed that the rate is inversely proportional to the thickness. Moreover, the contribution of the substrate should properly be separated applying a series expansion as suggested by Roberts et al.[37] which requires that the value for the substrate is actually reported.

Generally, in the presence of moisture, the interactions between H_2O molecules and polar groups of water-soluble polymers typically result in plasticization of the polymer chains leading to an increase of permeability not only of water vapor but also of oxygen. For instance, the oxygen permeability of a typical poly(vinyl alcohol) increases by 500% when going from 0% to 55% RH to an absolute OTR for a 1.5 μm thick film of 480 $cm^3\ m^{-2}\ day^{-1}\ bar^{-1}$.[38] Measurements at 0% RH are consequently irrelevant. For instance, the oxygen permeability of a typical poly(vinyl alcohol) (PVOH, 87−89% hydrolysis) film of 6 μm thickness on a 50.8 μm thick PET substrate increases by 500% when going from 0% to 55% RH to an oxygen permeability (OP) of 18.3 $cm^3\ \mu m\ m^{-2}\ day^{-1}$ (presumably bar^{-1}).[38] Water vapor permeability (WVP) is expectedly even higher for PVOH. Chen et al. for instance reported a WVP value of 1469 g μm $m^{-2}\ day^{-1}\ bar^{-1}$ at 50% RH.[39]

The transmission rates featured by the bio-nanocomposite coating correspond to an OP of 3.87 $cm^3\ \mu m\ m^{-2}\ day^{-1}\ bar^{-1}$ and a WVP of 0.28 g μm $m^{-2}\ day^{-1}\ bar^{-1}$. The bio-nanocomposite thus clearly outperforms the most common water-soluble matrix, PVOH, in particular concerning WVP.

We attribute the low sensitivity of the barrier properties to elevated RH for this water-based bio-nanocomposite to the small free volume, the increased β-sheet formation of the silk protein, and the one-dimensional crystallinity.

To transfer the barrier performance of the new spider silk-based bio-nanocomposite onto the shelf life of packed food, a simple calculation was done as an example: packing 450 g of

DOI: 10.1021/acsami.6b08287
ACS Appl. Mater. Interfaces 2016, 8, 25535−25543

dried food (with an initial density of 1 (3% initial moisture content) and a critical moisture content limiting shelf life of 7%) into a rectangular box made of PET with a surface-to-volume ratio of 2.18 and a WVTR of neat PET (4.2 g m^{-2} day^{-1}) and exposure at 25 °C and 75% RH will yield a shelf life of 51 days. Decreasing the WVTR to 0.2 g m^{-2} day^{-1} by coating the substrate with the bio-nanocomposite will prolong this shelf life to 1074 days.[40]

CONCLUSION

Compounding Lys-hec and eADF4(κ16) in an all-aqueous process avoiding toxic additives yielded a new bio-nanocomposite material. Structural characterization using PXRD and FTIR revealed an overall structure that can also be seen as one-dimensional crystal with perfectly delaminated equidistant filler platelets and a matrix with high β-sheet content. While neat (not post-treated) eADF4(κ16) films were chemically unstable, the newly produced bio-nanocomposite revealed a good chemical stability even without post-treatment, usually necessary for stabilizing spider silk materials. Low free volume of the bio-nanocomposite material and a correlated low oxygen and, surprisingly, water vapor permeability qualifies the bio-nanocomposite as a coating for packaging materials used e.g. for food. The bio-nanocomposite is 60-fold more efficient than high performance packaging materials like poly(vinylidene chloride) and 600-fold better than the poly(ethylene terephthalate). In this context, the biodegradability of the bio-nanocomposite (silk as well as clay) will add on to the usability. The unique combination of high oxygen and water vapor barrier properties, processing from aqueous solutions, and sustainability makes this composite highly suitable for new, green, flexible packaging applications.

MATERIALS AND METHODS

Synthesis of Engineered Silk eADF4(κ16). eADF4(κ16) comprising the sequence MASMTGGQQMGRGSM-(GSSAA-AAAAAASGPGGYGPKNQGPSGPGGYGPGGPG)$_{16}$ was produced in *E. coli* BL21 gold (DE3), and the protein was purified using a heat step and ammonium sulfate precipitation as described previously.[16]

Synthesis of $Na_{0.5}$-Fluorohectorite. $Na_{0.5}$-fluorohectorite (Na-hec) with the stoichiometry $[Na_{0.5}][Li_{0.5}Mg_{2.5}][Si_4]O_{10}F_2$ was synthesized via melt synthesis according to an established procedure.[41] The material featured a cation exchange capacity (CEC) of 1.27 mval g^{-1}.

Nanocomposite Preparation. For surface modification of the nanoclay, L-lysine was dissolved in Millipore water at 1 equiv of the CEC of Na-hec, added dropwise to an aqueous suspension of Na-hec (2.5 g L^{-1}), and placed into an overhead shaker overnight.

Lyophilized eADF4(κ16) was resolved in 6 M guanidinium thiocyanate (GdmSCN) and dialyzed against 25 mM Tris/HCl pH 7.5 (Tris-buffer). Samples were dialyzed using a dialysis membrane with a molecular weight cutoff of 6000−8000 Da (Spectrum Laboratories) for 16 h with 3 buffer changes at RT. In a final step, the eADF4(κ16) solution was dialyzed against 25 mM ammonium bicarbonate, which decomposes to carbon dioxide, ammonia, and water upon evaporation and is therefore not interrupting the bio-nanocomposite formation.

Lys-hec was added dropwise to the dissolved spidroin while shaking until an amount of 60 wt % hectorite was reached. The bio-nanocomposite was deposited on PET foils via drop-casting. The obtained films were dried at RT.

Powder X-ray Diffraction (PXRD). PXRD patterns were obtained using nickel-filtered Cu Kα radiation (1.541 87 Å) on a Bragg−Brentano-type diffractometer (Panalytical XPERT-PRO) equipped with an in-situ humidity chamber (Anton Paar) and a humidity generator RH-200 (VTI).

Oxygen Transmission. Oxygen transmission rates were determined on a Mocon OX-TRAN 2/21 M10x instrument with a lower detection limit of 0.0005 cm^3 m^{-2} day^{-1} bar^{-1}. A mixture of 95% nitrogen and 5% hydrogen was used as carrier gas and pure oxygen (>99.95%, Linde Sauerstoff 3.5) as permeant gas. The measurements were conducted at 25 °C and a relative humidity of 50%, applying the standards ASTM D-3985, ASTM F-1927, DIN 53380, JIS K-7126, and ISO CD 15105-2.

Water Vapor Transmission. Water vapor transmission rates were measured at a Mocon PERMATRAN-W model 333 at 25 °C and a relative humidity of 50%. The lower detection limit of the device was 0.05 g m^{-2} day^{-1}.

Transmittance, Clarity, and Haze. The shown graphs are representative of three individual measurements. Transmittance, clarity, and haze of the coatings were measured on a BYK-Gardner Haze-Gard Plus.

Scanning Electron Microscopy (SEM). Film samples were mounted with their cross section facing upright in aluminum slit stubs and wrapped in adhesive silver tape (Scotch; Plano, Germany) to reduce charging. The samples were sputtered with a 2 nm layer of platinum (sputter coater HR208 with MTM20 thickness controller, Cressington, Watford, UK) and analyzed using a LEO 1540 CrossSction SEM (Zeiss, Aalen, Germany) at 5−10 kV.

Thermogravimetric Analysis (TGA). Changes in mass upon heating were assessed by TGA using a SDTA 851e thermogravimetric analyzer (Mettler Toledo, Germany) with a microbalance resolution of 1 mg. Measurements were performed in aluminum oxide pans under a nitrogen atmosphere (50 mL min^{-1}) at a heating rate of 10 °C min^{-1} (from RT to 800 °C).

Differential Scanning Calorimetry (DSC). DSC scans were obtained using a SDTA 821e differential scanning calorimeter (Mettler Toledo, Germany) with a ceramic sensor and a 56-fold Au−AuPd thermocouple pile. Samples (3−4 mg) were sealed hermetically in aluminum pans and heated under purged dry nitrogen gas flow (20 mL min) at 5 °C min^{-1}. In order to evaporate residual solvent, samples were first heated to 110 °C. After 10 min of equilibration they were cooled to 40 °C, and finally, the analysis was started by heating to 400 °C. The shown graphs are representative of two or three individual measurements.

Tensile Testing. Tensile testing was performed using a Bose ElectroForce equipped with a 2.5 or 22 N capacity load cell. A crosshead speed of 0.2 mm min^{-1} was applied, and the gauge length was set to 2 mm. All films were tested in dry state at a relative humidity of 50 ± 2% at 20 °C. Films were cut into strips of 2−3 mm width and 10 mm length. The thickness was individually determined for each sample with a micrometer screw and ranged from 5 to 30 mm. Stress was calculated as force per cross-sectional area. Young's modulus (*E*-modulus) was measured from the initial slopes in the elastic region; tensile strength referred to the average of ultimate stress at failure. Toughness was calculated as the integral below the respective stress−strain curve. The given values in Figure 4B were averaged from up to12 individual samples.

Doppler Broadening Spectroscopy (DBS). Open volume defects and changes of the free volume were analyzed by depth-dependent Doppler-broadening spectroscopy (DBS) using the CDB spectrometer at the neutron-induced positron source Munich (NEPOMUC, FRM II, Germany).[42,43] The incident positron energy was varied from 0.2 to 30 keV, and spectra were measured using a high-purity germanium detector (efficiency 30%) with a resolution of 1.4 at 477.6 keV. The shape of the annihilation photopeak is commonly characterized by the line shape parameter *S*, which is defined as the ratio of a central zone and the integral of the 511 keV photopeak.[44] It is influenced by the annihilation of low momentum and valence electrons and by Ps annihilation. Therefore, the *S*-parameter can be correlated with open volume defects and the free volume.

The Doppler broadening of the 511 keV annihilation line contains information on the electron momentum distribution at the positron annihilation site in the sample. Both the lower probability of core electron annihilation in open volume defects and the annihilation of

DOI: 10.1021/acsami.6b08287
ACS Appl. Mater. Interfaces 2016, 8, 25535−25543

parapositronium (p-Ps) in micropores lead to a narrowing of the annihilation line. Consequently, a rise of the *S*-parameter can be related to an increase of the free volume.[42]

Positron Annihilation Lifetime Spectroscopy (PALS). Positron lifetime measurements were performed at the pulsed low-energy positron system at NEPOMUC.[45] Depth profiles were recorded between 1 and 16 keV positron implantation energy. About 3×10^6 counts were accumulated in each spectrum. Details and limitations of the applied Tao-Eldrup model have recently been discussed.[46]

■ ASSOCIATED CONTENT

Supporting Information

The Supporting Information is available free of charge on the ACS Publications website at DOI: 10.1021/acsami.6b08287.

Clay synthesis and characterization in terms of particle size and particle delamination; setup of chemical stability analysis as an example (PDF)

■ AUTHOR INFORMATION

Corresponding Authors

*(J.B.) Phone +49 (0) 921 55 2530; Fax +49 (0) 921 55 2788; e-mail Josef.Breu@uni-bayreuth.de.

*(T.S.) Phone +49 (0) 921 55 7361; Fax +49 (0) 921 55 7346; e-mail thomas.scheibel@bm.uni-bayreuth.de.

Notes

The authors declare no competing financial interest.

■ ACKNOWLEDGMENTS

The authors thank M. Reiner and T. Gigl for their help with DBS measurements as well as W. Egger for helping with PALS measurements. This work was supported by the SFB840 TP B3 (J.B.) and A8 (T.S.).

■ REFERENCES

(1) Dunlop, J. W. C.; Fratzl, P. Bioinspired Composites: Making a Tooth Mimic. *Nat. Mater.* **2015**, *14* (11), 1082−1083.

(2) Li, X.; Chang, W.-C.; Chao, Y. J.; Wang, R.; Chang, M. Nanoscale Structural and Mechanical Characterization of a Natural Nanocomposite Material: The Shell of Red Abalone. *Nano Lett.* **2004**, *4* (4), 613−617.

(3) Jakubinek, M. B.; Samarasekera, C. J.; White, M. A. Elephant ivory: A Low Thermal Conductivity, High Strength Nanocomposite. *J. Mater. Res.* **2006**, *21* (01), 287−292.

(4) Peterlik, H.; Roschger, P.; Klaushofer, K.; Fratzl, P. From Brittle to Ductile Fracture of Bone. *Nat. Mater.* **2006**, *5* (1), 52−55.

(5) Darder, M.; Aranda, P.; Ruiz-Hitzky, E. Bionanocomposites: A New Concept of Ecological, Bioinspired, and Functional Hybrid Materials. *Adv. Mater.* **2007**, *19* (10), 1309−1319.

(6) Cuy, J. L.; Mann, A. B.; Livi, K. J.; Teaford, M. F.; Weihs, T. P. Nanoindentation Mapping of the Mechanical Properties of Human Molar Tooth Enamel. *Arch. Oral Biol.* **2002**, *47* (4), 281−291.

(7) Alexandre, M.; Dubois, P. Polymer-layered Silicate Nanocomposites: Preparation, Properties and Uses of a New Class of Materials. *Mater. Sci. Eng., R* **2000**, *28* (1−2), 1−63.

(8) Rezwan, K.; Chen, Q. Z.; Blaker, J. J.; Boccaccini, A. R. Biodegradable and Bioactive Porous Polymer/Inorganic Composite Scaffolds for Bone Tissue Engineering. *Biomaterials* **2006**, *27* (18), 3413−3431.

(9) Ruiz-Hitzky, E. R.; Darder, M.; Aranda, P. Functional Biopolymer Nanocomposites Based on Layered Solids. *J. Mater. Chem.* **2005**, *15* (35−36), 3650−3662.

(10) Smith, B. L.; Schaffer, T. E.; Viani, M.; Thompson, J. B.; Frederick, N. A.; Kindt, J.; Belcher, A.; Stucky, G. D.; Morse, D. E.; Hansma, P. K. Molecular Mechanistic Origin of the Toughness of Natural Adhesives, Fibres and Composites. *Nature* **1999**, *399* (6738), 761−763.

(11) Sinharay, S.; Bousmina, M. Biodegradable Polymers and Their Layered Silicate Nano Composites: In Greening the 21st Century Materials World. *Prog. Mater. Sci.* **2005**, *50* (8), 962−1079.

(12) Pandey, J. K.; Kumar, A. P.; Misra, M.; Mohanty, A. K.; Drzal, L. T.; Palsingh, R. Recent Advances in Biodegradable Nanocomposites. *J. Nanosci. Nanotechnol.* **2005**, *5* (4), 497−526.

(13) Dang, Q. Q.; Lu, S. D.; Yu, S.; Sun, P. C.; Yuan, Z. Silk Fibroin/Montmorillonite Nanocomposites: Effect of pH on the Conformational Transition and Clay Dispersion. *Biomacromolecules* **2010**, *11* (7), 1796−1801.

(14) Roemer, L.; Scheibel, T. The Elaborate Structure of Spider Silk − Structure and Function of a Natural High Performance fiber. *Prion* **2008**, *2* (4), 154−161.

(15) Huemmerich, D.; Helsen, C. W.; Quedzuweit, S.; Oschmann, J.; Rudolph, R.; Scheibel, T. Primary Structure Elements of Spider Dragline Silks and Their Contribution to Protein Solubility. *Biochemistry* **2004**, *43* (42), 13604−13612.

(16) Doblhofer, E.; Scheibel, T. Engineering of Recombinant Spider Silk Proteins Allows Defined Uptake and Release of Substances. *J. Pharm. Sci.* **2015**, *104* (3), 988−94.

(17) Spiess, K.; Wohlrab, S.; Scheibel, T. Structural Characterization and Functionalization of Engineered Spider Silk Films. *Soft Matter* **2010**, *6* (17), 4168−4174.

(18) Elsner, M. B.; Herold, H. M.; Muller-Herrmann, S.; Bargel, H.; Scheibel, T. Enhanced Cellular Uptake of Engineered Spider Silk Particles. *Biomater. Sci.* **2015**, *3* (3), 543−551.

(19) Theng, B. K. G. *Formation and Properties of Clay-Polymer Complexes*; Elsevier: Palmerston North, New Zealand, 2012; Vol. *4*.

(20) Kunz, D. A.; Schmid, J.; Feicht, P.; Erath, J.; Fery, A.; Breu, J. Clay-Based Nanocomposite Coating for Flexible Optoelectronics Applying Commercial Polymers. *ACS Nano* **2013**, *7* (5), 4275−4280.

(21) Stöter, M.; Kunz, D. A.; Schmidt, M.; Hirsemann, D.; Kalo, H.; Putz, B.; Senker, J.; Breu, J. Nanoplatelets of Sodium Hectorite Showing Aspect Ratios of approximate to 20 000 and Superior Purity. *Langmuir* **2013**, *29* (4), 1280−1285.

(22) Möller, M. W.; Lunkenbein, T.; Kalo, H.; Schieder, M.; Kunz, D. A.; Breu, J. Barrier Properties of Synthetic Clay with a Kilo-Aspect Ratio. *Adv. Mater.* **2010**, *22* (46), 5245−5249.

(23) Rhim, J.-W.; Park, H.-M.; Ha, C.-S. Bio-nanocomposites for Food Packaging Applications. *Prog. Polym. Sci.* **2013**, *38* (10−11), 1629−1652.

(24) Hu, X.; Kaplan, D.; Cebe, P. Determining Beta-Sheet Crystallinity in Fibrous Proteins by Thermal Analysis and Infrared Spectroscopy. *Macromolecules* **2006**, *39* (18), 6161−6170.

(25) Rabotyagova, O. S.; Cebe, P.; Kaplan, D. L. Role of Polyalanine Domains in beta-Sheet Formation in Spider Silk Block Copolymers. *Macromol. Biosci.* **2010**, *10* (1), 49−59.

(26) Bush, M. F.; Forbes, M. W.; Jockusch, R. A.; Oomens, J.; Polfer, N. C.; Saykally, R. J.; Williams, E. R. Infrared Spectroscopy of Cationized Lysine and Epsilon-N-Methyllysine in the Gas Phase: Effects of Alkali-Metal Ion Size and Proton Affinity on Zwitterion Stability. *J. Phys. Chem. A* **2007**, *111* (32), 7753−7760.

(27) Spiess, K.; Ene, R.; Keenan, C. D.; Senker, J.; Kremer, F.; Scheibel, T. Impact of Initial Solvent on Thermal Stability and Mechanical Properties of Recombinant Spider Silk Films. *J. Mater. Chem.* **2011**, *21* (35), 13594−13604.

(28) Lerot, L.; Low, P. F. Effect of Swelling on Infrared-Absorption Spectrum of Montmorillonite. *Clays Clay Miner.* **1976**, *24* (4), 191−199.

(29) Ijdo, W. L.; Kemnetz, S.; Benderly, D. An Infrared Method to Assess Organoclay Delamnination and Orientation in Organoclay Polymer Nanocomposites. *Polym. Eng. Sci.* **2006**, *46* (8), 1031−1039.

(30) Vasconcelos, A.; Freddi, G.; Cavaco-Paulo, A. Biodegradable Materials Based on Silk Fibroin and Keratin. *Biomacromolecules* **2008**, *9* (4), 1299−1305.

DOI: 10.1021/acsami.6b08287
ACS Appl. Mater. Interfaces 2016, 8, 25535−25543

(31) Merkel, T. C.; Freeman, B. D.; Spontak, R. J.; He, Z.; Pinnau, I.; Meakin, P.; Hill, A. J. Ultrapermeable, Reverse-Selective Nanocomposite Membranes. *Science* **2002**, *296* (5567), 519−522.
(32) Choudalakis, G.; Gotsis, A. D. Free Volume and Mass Transport in Polymer Nanocomposites. *Curr. Opin. Colloid Interface Sci.* **2012**, *17* (3), 132−140.
(33) Herold, C.; Ceeh, H.; Gigl, T.; Reiner, M.; Haumann, M.; Schönweiz, A.; Hugenschmidt, C. Nanometer Size Pores in Ionic Liquid Loaded Silica Gel Characterized by positron Lifetime Spectroscopy. *Phys. Status Solidi A* **2016**, *213* (1), 165−169.
(34) Shantarovich, V. P.; Kevdina, I. B.; Yampolskii, Y. P.; Alentiev, A. Y. Positron Annihilation Lifetime Study of High and Low Free Volume Glassy Polymers: Effects of Free Volume Sizes on the Permeability and Permselectivity. *Macromolecules* **2000**, *33* (20), 7453−7466.
(35) Gusev, A. A.; Lusti, H. R. Rational Design of Nanocomposites for Barrier Applications. *Adv. Mater.* **2001**, *13* (21), 1641−1643.
(36) Cussler, E. L.; Hughes, S. E.; Ward, W. J.; Aris, R. Barrier Membranes. *J. Membr. Sci.* **1988**, *38* (2), 161−174.
(37) Roberts, A. P.; Henry, B. M.; Sutton, A. P.; Grovenor, C. R. M.; Briggs, G. A. D.; Miyamoto, T.; Kano, M.; Tsukahara, Y.; Yanaka, M. Gas Permeation in Silicon-Oxide/Polymer (SiOx/PET) Barrier Films: Role of the Oxide Lattice, Nano-Defects and Macro-Defects. *J. Membr. Sci.* **2002**, *208* (1−2), 75−88.
(38) Grunlan, J. C.; Grigorian, A.; Hamilton, C. B.; Mehrabi, A. R. Effect of Clay Concentration on the Oxygen Permeability and Optical Properties of a Modified Poly(Vinyl Alcohol). *J. Appl. Polym. Sci.* **2004**, *93* (3), 1102−1109.
(39) Mo, C.; Yuan, W.; Lei, W.; Shijiu, Y. Effects of Temperature and Humidity on the Barrier Properties of Biaxially-oriented Polypropylene and Polyvinyl Alcohol Films. *J. Appl. Packag. Res.* **2014**, *6* (1), 40−46.
(40) Wilbey, R. A. Food Packaging and Shelf life: A Practical Guide. *Int. J. Dairy Technol.* **2011**, *64* (4), 598−599.
(41) Breu, J.; Seidl, W.; Stoll, A. J.; Lange, K. G.; Probst, T. U. Charge Homogeneity in Synthetic Fluorohectorite. *Chem. Mater.* **2001**, *13* (11), 4213−4220.
(42) Stadlbauer, M.; Hugenschmidt, C.; Schreckenbach, K. New Design of the CDB-Spectrometer at NEPOMUC for T-Dependent Defect Spectroscopy in Mg. *Appl. Surf. Sci.* **2008**, *255* (1), 136−138.
(43) Hugenschmidt, C.; Löwe, B.; Mayer, J.; Piochacz, C.; Pikart, P.; Repper, R.; Stadlbauer, M.; Schreckenbach, K. Unprecedented Intensity of a Low-Energy Positron Beam. *Nucl. Instrum. Methods Phys. Res., Sect. A* **2008**, *593* (3), 616−618.
(44) Mantl, S.; Triftshauser, W. Direct Evidence for Vacancy Clustering in Electron-Irradiated Copper by Positron-Annihilation. *Phys. Rev. Lett.* **1975**, *34* (25), 1554−1557.
(45) Sperr, P.; Egger, W.; Kogel, G.; Dollinger, G.; Hugenschmidt, C.; Repper, R.; Piochacz, C. Status of the Pulsed Low Energy Positron Beam System (PLEPS) at the Munich Research Reactor FRM-II. *Appl. Surf. Sci.* **2008**, *255* (1), 35−38.
(46) Dlubek, G.; Yu, Y.; Krause-Rehberg, R.; Beichel, W.; Bulut, S.; Pogodina, N.; Krossing, I.; Friedrich, C. Free Volume in Imidazolium Triflimide ([C3MIM][NTf2]) Ionic Liquid from Positron Lifetime: Amorphous, Crystalline, and Liquid States. *J. Chem. Phys.* **2010**, *133* (12), 124502.

DOI: 10.1021/acsami.6b08287
ACS Appl. Mater. Interfaces 2016, 8, 25535−25543

Supporting Information

Structural Insights into Water-Based Spider Silk Protein-Nanoclay Composites with Excellent Gas and Water Vapor Barrier Properties

Elena Doblhofer[a], Jasmin Schmid[b], Martin Rieß[b], Matthias Daab[b], Magdalena Suntinger[a], Christoph Habel[b], Hendrik Bargel[a], Christoph Hugenschmidt[c], Sabine Rosenfeldt[d], Josef Breu[b] and Thomas Scheibel[a]**

[a] Lehrstuhl Biomaterialien, Universität Bayreuth,

Universitätsstraße 30, Universität Bayreuth, Bayreuth D-95447, Germany

[b] Lehrstuhl für Anorganische Chemie I, Universität Bayreuth,

Universitätsstraße 30, Universität Bayreuth, Bayreuth D-95447, Germany

[c] FRM II und Physik-Department E21, Technische Universität München,

James-Franck-Straße 1, Technische Universität München, Garching D-85748, Germany

[d] Lehrstuhl für Physikalische Chemie I, Universität Bayreuth,

Universitätsstraße 30, Universität Bayreuth, Bayreuth D-95447, Germany

Corresponding Author

* Thomas Scheibel, E-mail: thomas.scheibel@bm.uni-bayreuth.de

* Josef Breu, E-mail: Josef.Breu@uni-bayreuth.de

Content:

Clay Synthesis and Characterization

Over the last decade we have developed synthesis protocols that yield platelets with particularly large lateral extensions and homogeneous charge density.[1-3] $Na_{0.5}$-hectorite with the composition $[Na_{0.5}]^{inter}[Mg_{2.5}Li_{0.5}]^{oct}[Si_4]^{tet}O_{10}F_2$ was synthesized by melt synthesis in a closed molybdenum crucible according to a long established procedure.[2] After synthesis the material was annealed for 6 weeks at 1045°C to improve intracrystalline reactivity, charge homogeneity and phase purity as published.[4]

Particle diameters were checked by static light scattering (SLS) of aqueous dispersions using a Retsch Horiba LA-950 SLS instrument (Figure S1). The refractive index of the solid phase was set to a value of 1.5. A measurement routine called "mica in water" supplied by the manufacturer (Horiba) was applied. Mica has similar lateral extensions as the synthetic hectorites studied here. The routine determines transmission rates and optimizes the concentration of the suspensions.

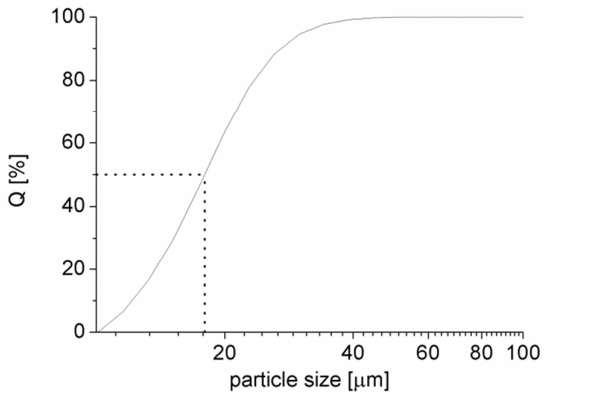

Figure S1. Number weighted particle size distribution as determined by SLS measurement of a $Na_{0.5}$-Hec dispersion in water. The observed median value of 18 μm agrees well with previously published results.[5]

When water is added, the annealed $Na_{0.5}$-hectorite swells osmotically to infinity.[6] The completeness of this repulsive delamination of clay tactoids in the bulk was monitored by small-angle X-ray scattering (SAXS). SAXS data reported here were measured using the system "Double Ganesha AIR" (SAXSLAB, Denmark). The X-ray source of this laboratory-based system is a rotating anode (copper, MicoMax 007HF, Rigaku Corporation, Japan) providing a micro-focused beam. The data are recorded by a position sensitive detector (PILATUS 300K, Dectris). To cover the range of scattering vectors between 0.004-2.0 $Å^{-1}$ different detector positions were used. The measurements were done in 1 mm glass capillaries (Hilgenberg, code 4007610, Germany) at room temperature. The circularly averaged data were normalized to incident beam, sample thickness and measurement time before subtraction of the solvent. The data analysis was performed with the software Scatter (version 2.5).[7]

Complete delamination into single clay layers is evidenced (Figure S2) by firstly the absence of a peak corresponding to a discrete hydration level of clay tactoids. The peak of the two-layer hydrate would be expected at d_{001} = 15.5 Å. Secondly, while the q^{-2}-scaling law of the scattering curve indicates layered objects, the minimum at 8.3 Å confirms a height corresponding single layers of a delaminated material. Thirdly, even at a dilution of 2 wt% the separation of the platelets is only 587 Å, and, consequently, with 20 μm diameter platelets cannot freely rotate but are forced into an approximately parallel arrangement giving rise to week interferences corresponding to the separation of single layers at a given water to clay ratio.

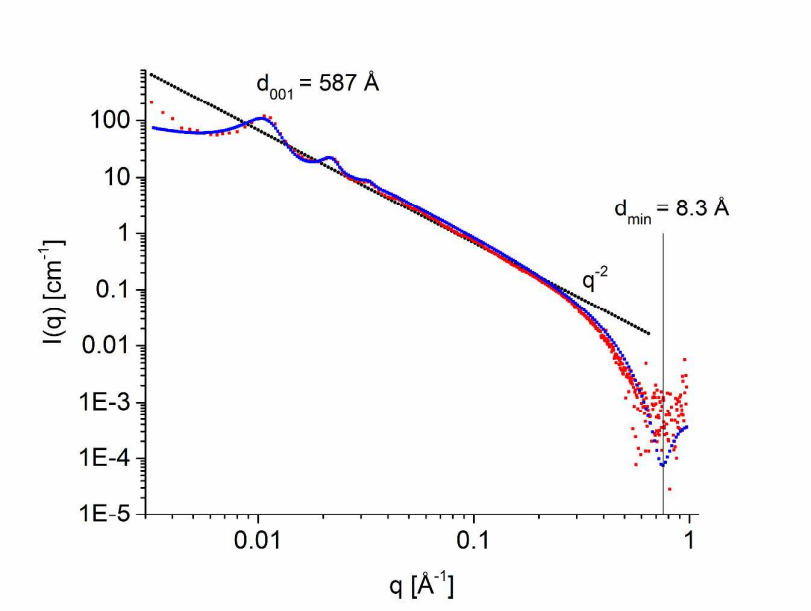

Figure S2. Measured one-dimensional SAXS pattern of a 2 wt% suspension of long-term annealed $Na_{0.5}$-hectorite. The rational 00*l* series illustrates a homogeneous separation of delaminated clay platelets to 587 Å at this water-to-clay ratio.[6]

Chemical Stability of the Bio-Nanocomposite

Chemical stability of freestanding bio-nanocomposite and control films made of eADF4(κ16) was determined by incubation of the samples in various solvents for 120 h and subsequent qualitative optical analysis. As an example, Figure S3 shows the test of chemical stability in Milli-Q-H_2O.

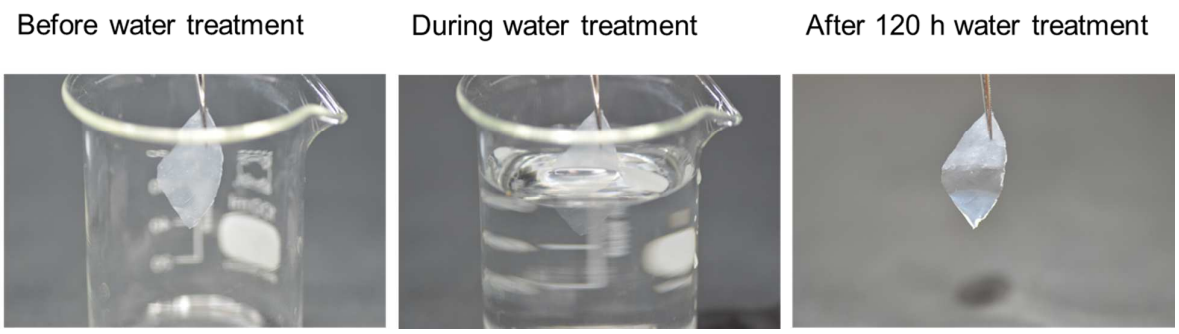

Figure S3. Testing of stability of free standing bio-nanocomposite films in water; within an incubation time of 5 days no significant decomposition was detectable, but the film seemed optically more transparent in the wet state.

Supporting References

1. Kalo, H.; Möller, M. W.; Ziadeh, M.; Dolejs, D.; Breu, J. Large Scale Melt Synthesis in an Open Crucible of Na-Fluorohectorite with Superb Charge Homogeneity and Particle Size. *Appl. Clay Sci.* **2010**, *48*, 39-45.

2. Breu, J.; Seidl, W.; Stoll, A. J.; Lange, K. G.; Probst, T. U. Charge Homogeneity in Synthetic Fluorohectorite. *Chem. Mater.* **2001**, *13*, 4213-4220.

3. Kalo, H.; Moller, M. W.; Kunz, D. A.; Breu, J. How to Maximize the Aspect Ratio of Clay Nanoplatelets. *Nanoscale.* **2012**, *4*, 5633-5639.

4. Stöter, M.; Kunz, D. A.; Schmidt, M.; Hirsemann, D.; Kalo, H.; Putz, B.; Senker, J.; Breu, J. Nanoplatelets of Sodium Hectorite Showing Aspect Ratios of ˜20000 and Superior Purity. *Langmuir.* **2013**, *29*, 1280-1285.

5. Stöter, M.; Kunz, D. A.; Schmidt, M.; Hirsemann, D.; Kalo, H.; Putz, B.; Senker, J.; Breu, J. Nanoplatelets of Sodium Hectorite Showing Aspect Ratios of ˜20000 and Superior Purity. *Langmuir.* **2013**, *29*, 1280-1285.

6. Stöter, M.; Rosenfeldt, S.; Breu, J. Tunable Exfoliation of Synthetic Clays. *Annual Review of Materials Research, Vol 45.* **2015**, *45*, 129-151.

7. Foerster, S.; Fischer, S.; Zielske, K.; Schellbach, C.; Sztucki, M.; Lindner, P.; Perlich, J. Calculation of Scattering-Patterns of Ordered Nano- and Mesoscale Materials. *Adv. Colloid Interface Sci.* **2011**, *163*, 53-83.

5.5 Teilarbeit V

To spin or not to spin: spider silk fibers and more

Autoren: **Elena Doblhofer***, Aniela Heidebrecht* und Thomas Scheibel

Die Konzeption des Artikels wurde von Thomas Scheibel, Aniela Heidebrecht und mir erarbeitet. Das Manuskript wurde von Aniela Heidebrecht und mir zu gleichen Teilen verfasst. Thomas Scheibel war in wissenschaftliche Diskussionen eingebunden und an der Fertigstellung des Manuskripts beteiligt.

Der Artikel wurde am 11.09.2015 im *Journal of Applied Microbiology and Biotechnology* veröffentlicht.

* Gleichberechtigte Co-Autorenschaft

To spin or not to spin: spider silk fibers and more

Elena Doblhofer, Aniela Heidebrecht & Thomas Scheibel

Applied Microbiology and Biotechnology

ISSN 0175-7598

Appl Microbiol Biotechnol
DOI 10.1007/s00253-015-6948-8

Springer

Appl Microbiol Biotechnol
DOI 10.1007/s00253-015-6948-8

MINI-REVIEW

To spin or not to spin: spider silk fibers and more

Elena Doblhofer[1] · **Aniela Heidebrecht**[1] · **Thomas Scheibel**[1,2,3,4,5]

Received: 30 May 2015 / Revised: 16 August 2015 / Accepted: 20 August 2015

Abstract Spider silk fibers have a sophisticated hierarchical structure composed of proteins with highly repetitive sequences. Their extraordinary mechanical properties, defined by a unique combination of strength and extensibility, are superior to most man-made fibers. Therefore, spider silk has fascinated mankind for thousands of years. However, due to their aggressive territorial behavior, farming of spiders is not feasible on a large scale. For this reason, biotechnological approaches were recently developed for the production of recombinant spider silk proteins. These recombinant proteins can be assembled into a variety of morphologies with a great range of properties for technical and medical applications. Here, the different approaches of biotechnological production and the advances in material processing toward various applications will be reviewed.

Elena Doblhofer and Aniela Heidebrecht contributed equally to this work.

✉ Thomas Scheibel
thomas.scheibel@bm.uni-bayreuth.de

[1] Lehrstuhl Biomaterialien, Fakultät für Ingenieurswissenschaften, Universität Bayreuth, 95440 Bayreuth, Germany

[2] Institut für Bio-Makromoleküle (bio-mac), Universität Bayreuth, Universitätsstraße 30, 95440 Bayreuth, Germany

[3] Bayreuther Zentrum für Kolloide und Grenzflächen (BZKG), Universität Bayreuth, Universitätsstraße 30, 95440 Bayreuth, Germany

[4] Bayreuther Zentrum für Molekulare Biowissenschaften (BZMB), Universität Bayreuth, Universitätsstraße 30, 95440 Bayreuth, Germany

[5] Bayreuther Materialzentrum (BayMAT), Universität Bayreuth, Universitätsstraße 30, 95440 Bayreuth, Germany

Keywords Spider silk · Recombinant protein production · Protein morphologies

Introduction

Spider silks represent a class of fibers with a unique combination of strength and flexibility which leads to an outstanding toughness (Gosline et al. 1999). In comparison to one of the strongest man-made fibers, Kevlar, spider silk can absorb three times more energy before breaking (Roemer and Scheibel 2007). Therefore, it is not surprising that ancient Australian aborigines and New Guinean natives utilized spider silk as fishing lines, fishing nets, head gear, and bags (Lewis 1996). Further, until World War II, spider silk was used for crosshairs in optical devices like microscopes, telescopes, and guns because of its extremely small diameters (thickness of 1/40 of a human hair) (Gerritsen 2002; Lewis 1996). By using cobwebs to stanch bleeding wounds, the ancient Greeks unknowingly observed further extraordinary characteristics of this material, like high biocompatibility and low immunogenicity (Altman et al. 2003; Gerritsen 2002; Vollrath et al. 2002). However, the first scientific studies to unravel its biomedical properties were not started until 1710, when it was shown that a spider's web is able to stop bleeding in human wounds and also supports the wound healing (Bon 1710). Two centuries later, Otto G. T. Kiliani investigated spider silk as suture material for surgery (Kiliani 1901).

As illustrated by the long history of spider silk use, the outstanding properties of natural spider silk have been well-known for a long time; however, scientifically, the material attained intensive interest of researchers only in the last decades. The combination of mechanical performance, biodegradability, and ambient processing conditions of the underlying proteins makes spider silk a highly desirable material for

Published online: 11 September 2015

applications from biomaterials to high-performance industrial fibers (Rising 2014; Vollrath and Knight 2001).

Spider silk structure

Female orb weaving spiders can produce up to six different types of silk, with each one produced in a specialized gland that provides the name of the corresponding silk type (Fig. 1). Every silk type has to fulfill a certain task either in the structure of the web, the protection of the offspring, or the wrapping of prey. Additionally, a silk-like glue, produced in a seventh gland, is deposited on the web for prey capture. The most frequently investigated silk type is the dragline silk, used to build frame and radii of an orb web. It also is used as the lifeline of the spider and is therefore easy to obtain by forced silking (Andersen 1970; Blackledge and Hayashi 2006; Denny 1976; Heim et al. 2009; Vollrath 2000). Similar to many biological materials, the outstanding (mechanical) performance of spider silk is based on its hierarchical structure (Brown et al. 2012; Keten and Buehler 2008; Munch et al. 2008; Smith and Scheibel 2013; Sponner et al. 2007). Dragline spider silk fibers exhibit a core-shell structure with proteinaceous fibrils in the core and a three-layered shell of minor ampullate (Mi) silk, glycoproteins, and lipids. While the lipid part of the shell is only loosely attached to the core and does not substantially contribute to the mechanical performance of the fiber, the glyco-layer adheres directly and is a mediator between the fiber and its environment (Sponner et al. 2007). In this context, the shell is thought to be relevant for protection against environmental damage and microbes (Sponner et al. 2007). However, the determinant of the extraordinary mechanical characteristics of spider silk is the proteins which form the core of the fiber. The protein core of dragline silk is composed of two classes of spider silk proteins (spidroins): the highly ordered, hydrophobic spidroin I (Sp1), poor in proline residues, and the less ordered, hydrophilic, proline-rich spidroin II (Sp2), each with a molecular mass of

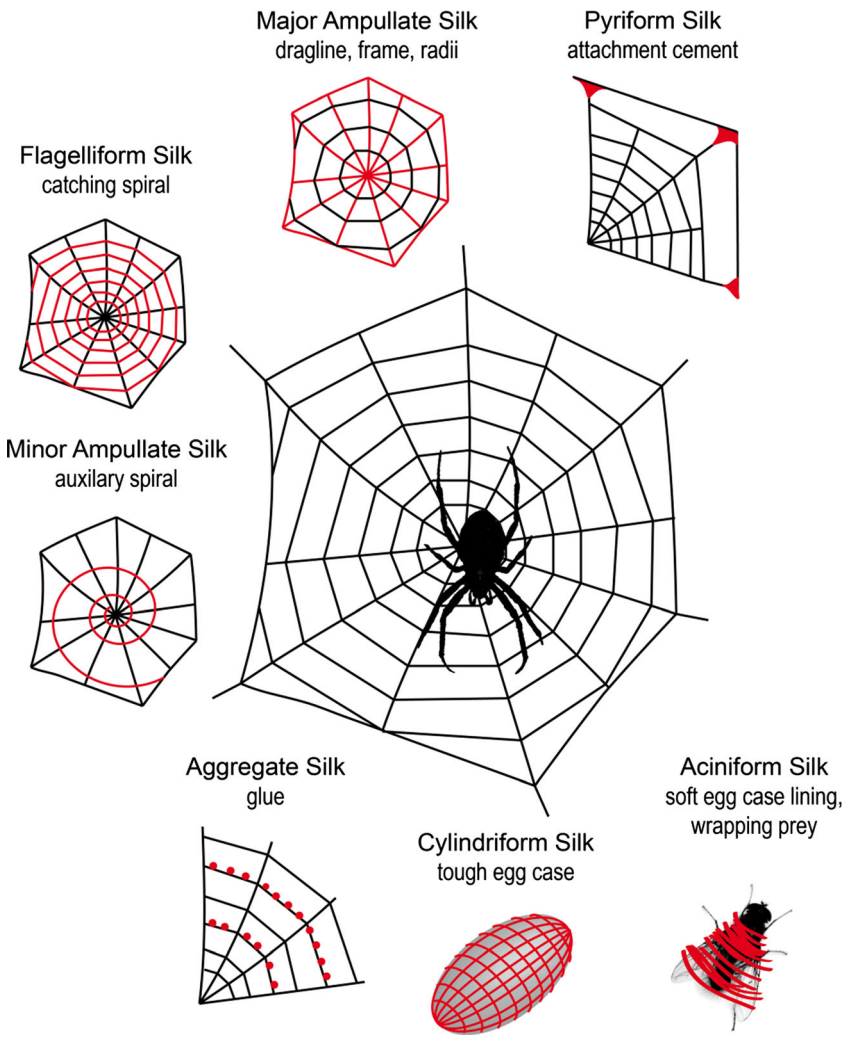

Fig. 1 Schematic overview of the different types of silk produced by female orb weaving spiders (Araneae); each silk type (highlighted in *red*) is tailored for a specific purpose as depicted

around 300 kDa (Heim et al. 2009; Xu and Lewis 1990) (Ayoub et al. 2007; Hinman and Lewis 1992; Xu and Lewis 1990). As they originate from the major ampullate gland, these proteins are also called major ampullate spidroins (MaSp). All MaSps comprise a highly repetitive core domain (up to 100 repeats of highly conserved sequence motifs, with 40 to 200 amino acids each) flanked by short (around 100–150 amino acids each) nonrepetitive (NR) terminal domains (Fig. 2). Upon fiber assembly, the gain and arrangement of secondary structure elements of the spidroins is responsible for the extraordinary mechanical properties of the fiber. Poly-alanine stretches fold into β-sheets, forming hydrophobic crystallites responsible for a high tensile strength (Kummerlen et al. 1996; Lewis 1992; Simmons et al. 1996); 3_1-helices formed by hydrophilic glycine-rich regions (GGX-motif, where X represents tyrosine, leucine, glutamine) are reflecting the elastic part (Kummerlen et al. 1996); and type II β-turns made of proline-rich GPG motifs are important for the reversible extensibility of a spider silk fiber (Hinman and Lewis 1992). While the latter sequence motif is only present in MaSp2, the first two motifs are ubiquitous (Ayoub et al. 2007; Hayashi et al. 1999; Hinman et al. 2000; Hinman and Lewis 1992; van Beek et al. 2002). All these motifs are repeated several dozen times within a single spidroin core domain. The nonrepetitive terminal motifs which flank the core domain have an α-helical secondary structure arranged in a five-helix bundle. These domains are responsible for controlling the storage of the spidroins at high concentrations in the spinning duct (Motriuk-Smith et al. 2005), and they also have an important function during the initiation of fiber formation upon their controlled dimerization and structural arrangement (Challis et al. 2006; Eisoldt et al. 2010, 2011; Hagn et al. 2010, 2011; Hedhammar et al. 2008; Heidebrecht et al. 2015; Huemmerich et al. 2004b; Rising et al. 2006)

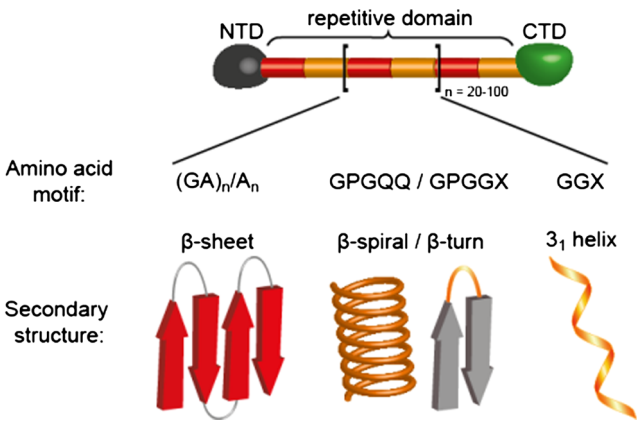

Fig. 2 Schematic structure of major ampullate spidroins including recurring amino acid motifs and the corresponding secondary structure. X: predominantly tyrosine, leucine, glutamine, alanine and serine residues. *NTD* amino-terminal domain, *CTD* carboxy-terminal domain

Biotechnological production of recombinant spider silk proteins

Unfortunately, it is not possible to produce large quantities of spider silk for applications by farming. This is due to the territorial and cannibalistic behavior and lower quality as well as quantity of silk produced by captive spiders (Craig et al. 2000; Fox 1975; Madsen et al. 1999; Vollrath and Knight 1999). Therefore, biotechnological production of the underlying spidroins was pursued to enable applications for spider silks.

Recombinant spidroin production has been conducted using a range of organisms including bacteria (Teule et al. 2009), tobacco plants (Menassa et al. 2004), yeast (Fahnestock and Bedzyk 1997), silk worms (Teule et al. 2012), goats (Steinkraus et al. 2012), insect cells (Huemmerich et al. 2004b), and mammalian cells (Lazaris et al. 2002). Each of these host systems has advantages and disadvantages. To begin with, short fragments of unmodified spider silk genes were expressed in a variety of hosts. It turned out that spider silk genes were unstable or the mRNA folded into undesirable secondary structures. Further, rearrangements, translation pauses, and problems with PCR amplification arose due to the highly repetitive character of the genes and the infidelity of template realignment during primer annealing (Fahnestock and Irwin 1997; Fahnestock et al. 2000). Additionally, host-derived differences in codon usage, problems with expression of repetitive sequences in various hosts, and insufficient Gly- and Ala-tRNA pools led to only limited success concerning the recombinant production of natural spider silk proteins.

To overcome these hurdles, several synthetic genes were designed encoding proteins that resemble the key features of the natural spider silk proteins. Since the gram-negative enterobacterium *Escherichia coli* is relatively simple, has a well-known genetic composition, and has the capability of fast, high-density cultivation, recombinant protein expression in *E. coli* allows for inexpensive, large-scale production (Sørensen and Mortensen 2005). Likewise, several approaches of recombinant spider silk-like protein production were successful in *E. coli* (for an overview, see Heidebrecht and Scheibel 2013).

In addition to *E coli*, yeast or insect cells have been used to express spider silk constructs with the advantage of the latter of being genetically more closely related to spiders. However, the spidroins produced in these systems showed a quite low solubility (Heim et al. 2009; Huemmerich et al. 2004b). Other hosts such as plants and mammalian cells have been used, too, but showed mostly low expression levels (Barr et al. 2004; Hauptmann et al. 2013; Lazaris et al. 2002).

Finally, transgenic animals were tested as hosts to produce recombinant spidroins in secreted body fluids. The presumed advantage of this approach would be the ease of purification

upon secretion into the milk or urine of the respective animal (Heim et al. 2009; Karatzas et al. 1999). However, it turned out that the purification was more difficult than thought due to contamination with animal-based secreted proteins. Given the fact that the generation of transgenic animals is far more complex and time consuming than that of bacteria or yeast, this approach has been rarely used in the past (Heim et al. 2009; Xu et al. 2007). For example, recombinant spider silk-EGFP fusion proteins were produced using BmN cells and larvae of silkworms as a host organism, but the protein yield was low due to the insolubility of the recombinant spider silk proteins (Zhang et al. 2008). In a more successful approach, chimeric proteins containing sequences of spider silk proteins and silkworm fibroin were designed, including either a H-chain promoter (Kuwana et al. 2014; Teule et al. 2012; Zhu et al. 2010) or a sericin promoter (Wen et al. 2010) locating the chimeric silkworm/spider silk proteins in the core or the sericin shell of the fiber. In both cases, silkworms spun fibers with mechanical properties exceeding that of silkworm silk, but they did not reach the properties of natural spider silk (Teule et al. 2012; Wen et al. 2010). Production of designed short spider silk proteins (50 kDa) resembling MaSp1 and MaSp2 of *Nephila clavipes* in goat milk was also successful, while expression of their partial complementary DNA (cDNA) in transgenic mice was not possible likely due to errors in protein synthesis (Perez-Rigueiro et al. 2011; Xu et al. 2007).

Based on the experience throughout the last three decades, *E. coli* has been established as the host system of choice, given the balance of quality of the silk produced with the scalability of the approach.

"To spin": artificial spider silk fibers

Due to the abovementioned, outstanding mechanical and biomedical properties of spider silk fibers, great efforts have been made to employ these fibers in different technical as well as biomedical applications. For instance, functional recovery of nerve defects was successfully performed in rats and sheep by using natural spider silk fibers as a guiding material (Allmeling et al. 2008; Radtke et al. 2011). Further, native spider dragline silk, directly woven onto steel frames, was used as a matrix for three-dimensional skin cell culture (Wendt et al. 2011). Since natural spider silk fibers are not available at large scale as mentioned above (see section "Biotechnological production of recombinant spider silk proteins"), different approaches have been tested to produce artificial spider silk fibers during the last two decades, which will be discussed in greater detail below.

The natural spinning process

In order to successfully establish a man-made spider silk spinning process, it is at first necessary to understand the natural one. Natural spider silk fiber spinning is a highly complex process involving a number of parameters in a highly regulated environment as exemplarily demonstrated in Fig. 3 for the assembly of major ampullate spidroins. Epithelial cells covering the tail and the ampulla of the major ampullate silk gland produce the spidroins and secrete them into the lumen. There, the spidroins are stored in a soluble state at high concentrations (up to 50 % (*w*/*v*)) in the presence of sodium and chloride ions. Analysis of major ampullate silk glands by polarized microscopy revealed a liquid-crystal behavior of the spinning dope (Knight and Vollrath 1999; Viney 1997), whereas in vitro experiments showed micellar-like structures both of which are not mutually exclusive (Eisoldt et al. 2010; Exler et al. 2007; Heidebrecht et al. 2015). The combination of the presence of chaotropic ions (stabilizing soluble protein structures) and a pre-assembly of the spidroins enables their storage at concentrations as found in the ampulla of the spinning gland. From the ampulla, the spinning dope passes into an S-shaped tapered duct, which is lined by a cuticular intima layer. In addition to supporting the duct and protecting the epithelial cells, this layer is hypothesized to function as a hollow fiber dialysis membrane, enabling the dehydration of the spinning dope (Vollrath and Knight 1999). During traveling of the spinning dope through the spinning duct, sodium and chloride ions are replaced by the more kosmotropic potassium and phosphate ions inducing salting-out of the proteins (Knight and Vollrath 2001; Papadopoulos et al. 2007). Additionally, acidification (from pH 7.2 to 5.7; Kronqvist et al. 2014) takes place triggered by carbonic anhydrase (Andersson et al. 2014), which has a contrary structural effect on the terminal domains. Upon acidification, glutamic acid residues of the amino-terminal domain are sequentially protonated, leading to structural rearrangements of the domain enabling dimerization in an antiparallel manner (Rising and Johansson 2015). In contrary to the stabilizing effect of the pH reduction on the amino-terminal domain, the carboxy-terminal one is destabilized upon acidification. In addition to the pH-induced destabilization, the presence of phosphate ions initiates the exposition of hydrophobic areas within the C-terminal domain initiating the parallel alignment of the associated two core domains (Eisoldt et al. 2010, 2012; Hagn et al. 2010). Based on the parallel (carboxy-terminal domains) and antiparallel (amino-terminal domains) orientation of the terminal domains, an endless spidroin network is achieved. Finally, water resorption via the cuticular intima layer and shear stress, resulting from the tapering of the spinning duct and the pulling of the fiber from the spider's abdomen, lead to the final alignment of the spidroins followed by solidification of the fiber (Fig. 3) (Hagn et al. 2011; Hardy et al. 2008).

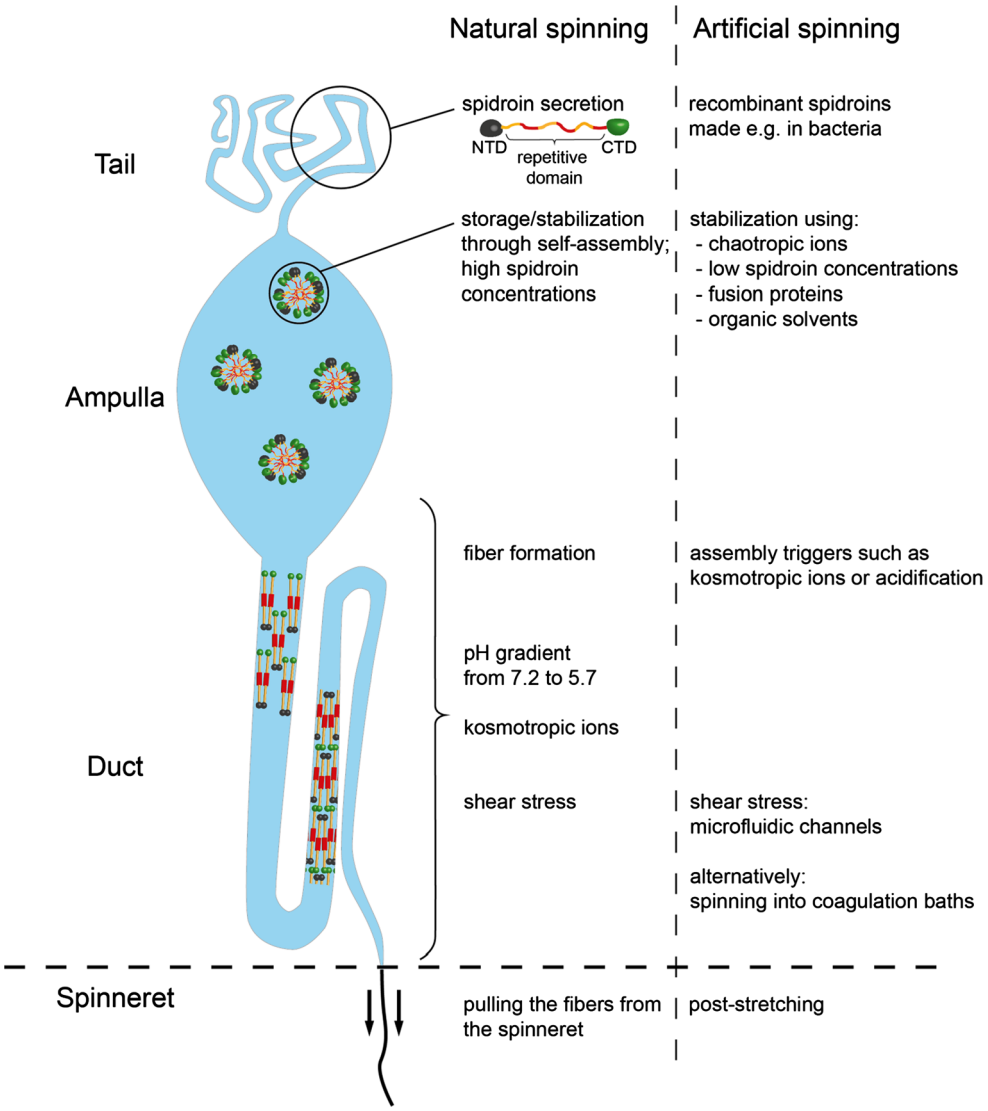

Fig. 3 Overview of natural and artificial spinning processes

Artificial fiber spinning

Commonly used artificial spinning processes are not like the natural silk spinning one. Typical processes out of solution are wet spinning, dry spinning, and electrospinning. In wet spinning, a polymer solution is extruded into a coagulation bath, where the polymer precipitates and the fibers are formed. For dry spinning and electrospinning, the polymers are solvated in an organic solvent and extruded into the air. Whereas fiber formation in dry spinning relies solely on the fast evaporation of the organic solvent, in electrospinning, the polymer solution is extruded into an electrostatic field. This field yields repulsive forces in the extruded solution, leading to eruption of a thin jet that is stretched toward the collector (i.e., counter electrode); as the solvent evaporates, a solid fiber is formed (Greiner and Wendorff 2007; Smit et al. 2005). This fiber is randomly deposited onto the collector, which results in a nonwoven mat (Teo and Ramakrishna 2006). In theory, wet spinning, dry spinning, and electrospinning are suitable methods for spider silk fiber spinning, since organic as well as aqueous spinning dopes can be used. In practice, dry spinning has been shown to be so far not suitable for silk fiber production, since spinning a silk fiber out of an organic solution results in mechanically unstable fibers (unpublished results), while dry spinning from an aqueous solution could not be achieved since this spinning technique relies on a highly volatile solvent for fast fiber formation. Therefore, so far, only wet spinning and electrospinning have been successfully employed for producing artificial spider silk fibers.

Dope preparation

The first step toward the production of artificial spider silk fibers is to solve the spidroins. Therefore, often an organic solvent is used exhibiting strong hydrogen bonding properties in order to guarantee good solvent-protein interactions. A

disadvantage, especially for biomedical applications, of organic spinning solutions is their putative toxicity. However, a high spidroin solubility enables the production of highly concentrated spinning dopes, which simplifies fiber formation (Um et al. 2004). With the objective of high protein solubility, many research groups have used the organic solvent 1,1,1,3,3,3-hexafluoro-2-propanol (HFIP). In HFIP, spidroin concentrations ranging from 10 to 30 % (*w*/*v*) can easily be achieved (Adrianos et al. 2013; An et al. 2011; Brooks et al. 2008; Lin et al. 2013; Teule et al. 2007; Xia et al. 2010), with the highest reported spidroin content of 45–60 % (*w*/*v*) (Albertson et al. 2014). One advantage of HFIP as solvent for spidroins is its volatility. Therefore, HFIP is commonly used for spinning processes which rely on a fast evaporation of the solvent such as electrospinning (Bini et al. 2006; Lang et al. 2013; Stephens et al. 2005; Wong Po Foo et al. 2006; Zhu et al. 2015). In addition to HFIP, formic acid (FA) has been used as an organic solvent of spidroins (Peng et al. 2009).

Seidel et al. (1998, 2000) dissolved dragline silk of *N. clavipes* in HFIP, produced a film out of the reconstituted spidroins, and then solved this film again in HFIP to a concentration of 2.5 % (*w*/*w*) in order to use it as a spinning dope for wet spinning. Dopes made of reconstituted spidroins did not form fibers in the otherwise commonly used methanol and isopropanol coagulation baths, but only in acetone coagulation baths (Seidel et al. 1998).

At first glance, using an organic solvent to gain solutions with a high protein concentration seems to be beneficial for spinning, but good protein-solvent interactions and, therefore, high protein solubility may also prevent protein assembly. Further, if artificial spider silk fibers are to be used for medical applications like suture materials, health risks caused by toxic solvents have to be avoided. Additionally, organic waste disposal in industrial processes is highly regulated and expensive; thus, the application of organic solvents is not favorable for scale-up processes. In order to avoid organic solvents, three approaches have been used to produce highly concentrated aqueous spidroin solutions: (1) spidroin self-assembly in aqueous buffers (Exler et al. 2007; Grip et al. 2009; Heidebrecht et al. 2015; Stark et al. 2007; Teule et al. 2007), (2) concentration of a diluted aqueous spidroin solution (Arcidiacono et al. 2002; Heidebrecht et al. 2015), and (3) direct solvation at high spidroin concentrations (Bogush et al. 2009; Jones et al. 2015). Protein concentrations typically used for spinning fibers out of aqueous solutions range from 10 to 30 % (*w*/*v*) (Arcidiacono et al. 2002; Bogush et al. 2009; Exler et al. 2007; Heidebrecht et al. 2015; Jones et al. 2015; Lazaris et al. 2002), and the highest concentration achieved so far has been 30 % (*w*/*v*) (Bogush et al. 2009). When spidroins are purified by a precipitation step such as salting-out or lyophilization, high spidroin purities are gained, but the spidroins also have to be resolved afterwards.

Heidebrecht et al. (2015) used the strong denaturant guanidinium thiocyanate for spidroin solvation, followed by its removal using dialysis against a 50-mM Tris/HCl buffer (pH 8.0). Additionally, 100 mM NaCl was added to the dialysis buffer in order to stabilize the spidroins in solution. Subsequent dialysis against a phosphate-containing buffer induced a liquid-liquid phase separation of the spidroin solution into a low-density phase and a self-assembled, high-density phase. Such phosphate-induced self-assembly of spidroins in solution resulted in spidroin concentrations ranging between 9 and 11 % (Heidebrecht et al. 2015). Alternatively, spinning dopes were produced by concentrating the protein solution using either ultrafiltration or dialysis against the hygroscopic polyethylene glycol (PEG) (Arcidiacono et al. 2002; Heidebrecht et al. 2015). In this approach, the spidroin molecules are forced into a highly concentrated solution and they cannot self-assemble. However, these spinning dopes are prone to aggregation and are less stable than self-assembled spinning dopes (Heidebrecht et al. 2015). The third approach to achieve highly concentrated aqueous spinning dopes is the direct solvation of spidroins in a medium suitable for spinning. Jones et al. (2015) added a solution containing 0.1 % propionic acid and 10 mM imidazole to spidroins in a glass vial and used sonication and subsequent heating in a microwave oven until complete spidroin solvation (Jones et al. 2015). The spidroin suspension was heated up to 130 °C for more than 48 h, indicating the high energy input that is needed to directly solve a spidroin at high concentration.

Wet spinning

Extrusion of the spinning dope into monohydric alcohols, such as methanol, ethanol, or isopropanol with the exemption of reconstituted spider silks which have to be spun into acetone as mentioned above, initiates fiber formation through dehydration of the spidroins. This technique results in single fibers with a diameter in the micrometer range. An advantage of wet spinning over other techniques such as electrospinning is the rather "slow" fiber formation, which allows a high degree of alignment of the proteins during spinning. This alignment enables the formation of a structural hierarchy necessary to produce fibers with superior mechanical properties. Wet spinning allows the use of different spinning dopes, ranging from inorganic or aqueous solutions to dispersions and liquid crystalline phases, and thus can be used for any polymer/biopolymer. Variation of the spinning dope and the composition of the coagulation bath influence fiber properties, allowing the production of fibers with tunable mechanical properties. One disadvantage of wet spinning is the necessity to remove the solvent or coagulation bath residues after spinning, which requires at least one washing step resulting in a longer and therefore more expensive process compared to dry spinning (Jestin and Poulin 2014).

Besides 100 % of methanol or isopropanol (Adrianos et al. 2013; Albertson et al. 2014; An et al. 2011; Jones et al. 2015; Zhu et al. 2010), mixtures of water with monohydric alcohols are often used as coagulation baths (Arcidiacono et al. 2002; Bogush et al. 2009; Heidebrecht et al. 2015; Lazaris et al. 2002; Teule et al. 2007; Xia et al. 2010). The addition of water to the coagulation bath slows down the coagulation rate of spidroins, and water works as a plasticizer for the fibers, which renders them less brittle and prevents clogging of the spinneret (Lin et al. 2013).

Posttreatment, such as drawing the spun fibers in air or inside a bath, is applied to improve the fibers' mechanical properties. Poststretching of spun fibers has been shown to induce a higher β-sheet content (An et al. 2011) and to align the β-sheet crystals along the thread axis (Heidebrecht et al. 2015). In contrast to the coagulation bath, the poststretching bath needs to contain water because of its plasticizing features for the fibers, which enables the proteins to rearrange and align along the fiber axis. The absence of water results in brittle fibers. An overview of recombinant spider silk fiber wet spinning and posttreatment conditions is given in Table 1.

Electrospinning

Electrospinning of recombinant or reconstituted spider silk protein solutions is possible using an electric field of 4–30 kV with a distance of 2–25 cm between the electrodes (i.e., the capillary tip and the collector) (Bini et al. 2006; Bogush et al. 2009; Lang et al. 2013; Peng et al. 2009; Stephens et al. 2005; Wong Po Foo et al. 2006; Yu et al. 2014; Zhou et al. 2008; Zhu et al. 2015). Parameters influencing the fiber properties (e.g., fiber diameter) of nonwoven mats mostly depend on the properties of the spinning dope, such as the viscosity, surface free energy, protein concentration, and the solvent's intrinsic electrical conductivity and permeability (Greiner et al. 2006). In contrast to wet spinning, electrospinning of comparatively low protein concentrations of 2–6 % (*w*/*v*) (Bini et al. 2006; Leal-Egana et al. 2012; Wong Po Foo et al. 2006; Yu et al. 2014; Zarkoob et al. 2004) also yields fibers, but higher protein concentrations of 10–30 % (*w*/*v*) (Bogush et al. 2009; Lang et al. 2013; Leal-Egana et al. 2012; Peng et al. 2009; Stephens et al. 2005; Zhou et al. 2008; Zhu et al. 2015) are more commonly used. In general, increasing the spidroin concentration in the dope leads to an increased fiber diameter and a reduction of bead formation, the latter being an unwanted side effect of electrospinning (Lang et al. 2013; Leal-Egana et al. 2012). Structural analysis of nonwoven mats electrospun from HFIP using Fourier-transformed infrared spectroscopy (FTIR) with subsequent Fourier self-deconvolution (FSD) revealed a low β-sheet content (~15 %) (Lang et al. 2013). The electric field interacts with the hydrogen bond dipoles of the protein, stabilizing α-helical segments and thus inhibiting β-sheet formation (Stephens et al. 2005). Instead of a solid collector, water- or organic solvent-based coagulation baths can be used to collect the spun micro- and nanofibers. In general, the latter approach has the advantage of including a posttreatment within the spinning process. Yu et al. used a coagulation bath containing 90 % (*v*/*v*) of organic solutions (acetone or methyl alcohol) as a collector; however, SEM images showed inhomogeneous fibers containing many beads (Yu et al. 2014). Posttreatment of electrospun fibers with organic solvents or alcohols is necessary in order to render the spun α-helical fibers water insoluble (i.e., inducing β-sheet formation) (Lang et al. 2013; Leal-Egana et al. 2012; Slotta et al. 2006). Immersing the fibers into alcohol baths resulted in fused intersections of single fibers (Bini et al. 2006), giving the fibers a "molten" appearance. Therefore, instead of immersing the fibers, Leal-Egana et al. (2012) and Lang et al. (2013) exposed them to methanol or ethanol vapor to render the fibers water insoluble with keeping their original morphology.

Other spinning methods

Besides wet spinning and electrospinning, recombinant spider silk fibers were produced using microfluidic devices (Rammensee et al. 2008). Such devices mimic some aspects of the natural spinning process, such as ion exchange, pH change, and elongational flow conditions. Since only low or medium protein concentrations were used, high flow rates were necessary to induce fiber assembly. Shear forces can also be applied by hand-drawing fibers from pre-assembled spidroins out of aqueous solutions (Exler et al. 2007; Teule et al. 2007). The gained fibers show similar properties as those produced by wet spinning. However, several parameters can be fine-tuned within the microfluidic channels which will allow for more sophisticated spinning processes and, therefore, fibers, in the future.

Transgenic silkworms producing silkworm/spider silk composite fibers

One elegant way to "artificially" spin spider silk fibers is to use transgenic, naturally fiber-producing animals. Silkworms are naturally able to produce and spin silk proteins and they can be genetically modified. Transgenic silkworms were engineered to produce silkworm fibroin/spider silk composite fibers with a spider silk content of 0.4 to 5 % (*w*/*w*) (Kuwana et al. 2014; Teule et al. 2012). Importantly, the mechanical properties of silkworm silk (toughness 70 MJ m^{-3}; Gosline et al. 1999) are inferior to those of spider silk (toughness 167 MJ m^{-3}; Heidebrecht et al. 2015), and since the composite material merges the properties of both silks, the mechanical properties of hybrid silkworm/spider silk fibers will always be inferior to those of spider silk. In 2000, Tamura et al. succeeded in a stable germline transformation of the silkworm

Table 1 Overview of wet-spinning conditions used for generating recombinant spider silk fibers

Spinning dope	Max. protein concentration [%]	Coagulation bath	Posttreatment	Source
Aqueous				
160 mM or 1 M urea, 10 mM NaH_2PO_4, 1 mM Tris, 20 mM NaCl, 10 mM or 100 mM glycine, pH 5.0	25 (after ultrafiltration)	MeOH/H_2O mixture	N/A	Arcidiacono et al. (2002)
60 % NaNCS, 20 % acetate solution, mix ratio 8:2 or 10 % LiCl in 90 % formic acid (FA)	30	96 % EtOH	1st draw: 92 % EtOH 2nd draw: 75 % EtOH	Bogush et al. (2009)
50 mM Tris/HCl, pH 8.0 or 50 mM Na-phosphate buffer, pH 7.2	17	IPA/H_2O mixture	IPA/H_2O mixture	Heidebrecht et al. (2015)
0.1 % propionic acid, 10 mM imidazole; microwaved	12	100 % IPA	1st draw: 80 % IPA 2nd draw: 20 % IPA	Jones et al. (2015)
PBS	28	MeOH/H_2O mixture	1st draw: MeOH 2nd draw: H_2O	Lazaris et al. (2002)
Organic				
HFIP (5 % *v*/*v* added to dope prior to spinning)	15	100 % IPA	80 % IPA	Adrianos et al. (2013)
HFIP (evaporation of HFIP prior to spinning)	60	100 % IPA	85 % IPA, 60 °C	Albertson et al. (2014)
HFIP	30	100 % IPA	75 % IPA	An et al. (2011)
HFIP	12	IPA	N/A	Brooks et al. (2008)
HFIP	10	100 mM $ZnCl_2$, 1 mM $FeCl_3$ in H_2O	1st draw: air 2nd draw: 50–70 % EtOH	Lin et al. (2013)
HFIP (addition of 15 % water prior to spinning)	30	90 % IPA	N/A	Teule et al. (2007)
HFIP	15 (10 % silkworm fibroin and 5 % spider silk-like protein)	MeOH	1st: 3 h incubation in MeOH 2nd: drawing in distilled H_2O	Zhu et al. (2010)
HFIP	20	90 % MeOH	90 % MeOH	Xia et al. (2010)

MeOH methanol, *EtOH* ethanol, *IPA* isopropyl alcohol, *PBS* phosphate buffered saline, *HFIP* 1,1,1,3,3,3-hexafluoro-2-propanol, *N/A* not applicable

Bombyx mori using a *piggyBac*-derived vector (Tamura et al. 2000). *PiggyBac* is a transposon discovered in the lepidopteran *Trichoplusia ni* (Cary et al. 1989), and vectors based hereon are able to transpose into *B. mori* chromosomes enabling silkworm transformation with various genes encoding fibrous proteins (Tamura et al. 2000). In general, to create transgenic silkworms producing chimeric silkworm/spider silk, genes were designed encoding synthetic spider silk-like sequences, *B. mori* fibroin sequences as well as a *B. mori* promoter, targeting the foreign protein production to the silk gland. Subsequently, these genes were cloned into a *piggyBac*-based vector which was then injected into *B. mori* eggs. Silk fibroin fibers are composed of three proteins, namely fibroin heavy chain (H-chain), fibroin light chain (L-chain), and fibrohexamerin protein (fhx/P25) (Kojima et al. 2007), and they are covered by a sericin layer (Wen et al. 2010). Just like spidroins, silk fibroins consist of a highly repetitive region which is flanked by nonrepetitive amino- and carboxy-terminal domains. Since the H-chain is believed to be mainly responsible for the mechanical properties of the silk (Kojima et al. 2007), fibroin H-chain genes were modified with spider silk sequences for improved properties (Kuwana et al. 2014; Teule et al. 2012; Zhu et al. 2010). Kuwana et al. (2014) generated three transgenic silkworm strains using a Japanese commercial silkworm strain (C515), two of which contained cDNA of major ampullate spidroins of the spider *Araneus ventricosus*, flanked by the amino- and carboxy-terminal domains of the *B. mori* fibroin H-chain gene. The third strain consisted of a plasmid coding for enhanced green fluorescent protein (EGFP), in order to simplify the analysis of the spun cocoons, subcloned in between the amino- and carboxy-terminal domains of the H-chain gene. After creating transgenic silkworms carrying the modified genes using the *piggyBac*-based vector system, the silkworms produced the modified H-chain/spider silk protein in the silk gland. In the silkworm's gland, the modified H-chain protein dimerized with the fibroin L-chain and was subsequently spun into a cocoon containing the spider dragline protein (Kuwana et al.

2014). Transgenic efficiencies of the strains were 20.0 % for the EGFP-containing strain and 16.7 and 22.6 %, respectively, for the strains containing the spider silk cDNA. Cocoons of the EGFP-transgenic silkworms showed green fluorescence, indicating that the EGFP protein is folded in its functional structure after spinning, suggesting that the spider silk protein may also be present in the cocoon fibers in its natural structure. The maximum amount of the modified H-chain/spider silk protein against the total fibroin was estimated at 0.4–0.6 % (*w*/*w*) (Kuwana et al. 2014) and 2-5 % (*w*/*w*) (Teule et al. 2012).

Alternatively, the sericin promoter has been used to target spider dragline silk proteins toward the outer sericin layer of the silk fiber (Wen et al. 2010). Whereas the breaking strain of the composite fiber was similar to that of natural spider silk fibers, the breaking stress and toughness were increased compared to that of natural silkworm silk, but the average values were still well below those of natural spider silk fibers (Teule et al. 2012). Theoretically, a breaking stress of cocoon silk equal to that of spider dragline silk could be achieved if the spidroin content was raised to 5–8 % (Kuwana et al. 2014), but this has not been shown experimentally, yet.

Properties of reconstituted vs. recombinant fibers

In order to establish processing technologies for gaining biomimetic spider silk fibers, two research groups used reconstituted *Nephila* spp. dragline silk for fiber spinning (Seidel et al. 2000; Shao et al. 2003). The best performing fibers, in terms of mechanical properties, were obtained by drawing the fibers in air after spinning, soaking them in water, and then drawing them in air again. These fibers exhibited a strength of 320 MPa, a Young's modulus of 8 GPa, and an extensibility of 100 % (Seidel et al. 2000). In comparison to natural dragline fibers, these fibers were much more extensible, but had a lower strength. Hand-drawn fibers of reconstituted *Nephila edulis* dragline silk yielded fibers showed natural dragline-like extensibility (10–27 %) and Young's modulus (6 GPa), but a breaking strength (100–140 MPa) that was well below that of the natural dragline fibers (Shao et al. 2003). Generally, achieving man-made fibers with a breaking stress in the regime of natural spider silk fibers seems to be the greatest challenge. Since the amount of natural and, therefore, also reconstituted, spider silk is quite limited due to the facts as mentioned above, the generation of recombinant (i.e., artificial) silk fibers is the only meaningful route toward large-scale applications. In several attempts, extensibility (1.2–302 %) and Young's modulus (0.04–21 GPa) of artificial spider silk fibers have been highly variable, reaching lower as well as higher values in comparison to natural spider silk fibers (24 % and 8 GPa). On the other hand, the strength even of the best performing fibers achieved values far below those of natural spider silk fibers. The highest strength (660 MPa) was achieved by silkworm/spider silk composite fibers, but since these fibers were only extensible up to 19 % (Wen et al. 2010), the toughness was far below that of natural spider silk fibers. In comparison, the highest strength (508 MPa) of recombinant spider silk fibers was achieved by wet spinning of proteins with a molecular weight of 285 kDa containing only amino acid motifs based on the core domain of natural spidroins (Xia et al. 2010). The highest toughness (189 MJ m^{-3}), on the other hand, was observed with fibers wet-spun from a self-assembled aqueous spinning dope of a 134-kDa protein containing all three functional domains: the highly repetitive core domain as well as the helical amino- and carboxy-terminal domains (Heidebrecht et al. 2015).

Tensile testing of electrospun, recombinant fibers also showed, not surprisingly, inferior mechanical properties in comparison to those of natural spider silk fibers (Bogush et al. 2009; Zhu et al. 2015). But in this case, mechanics can be neglected, since electrospun fibers are commonly applied as nonwoven meshes used for biomedical or for filter applications without the need of nature-like mechanical properties. In this context, biocompatibility is the more important feature of spider silks. In general, fibers produced from both reconstituted and recombinant spidroins exhibited good biomedical properties. For instance, fibers electrospun from reconstituted *A. ventricosus* major ampullate spidroins revealed a very low degradation rate and showed a good biocompatibility with PC 12 cells (Yu et al. 2014). Cell attachment and proliferation experiments of BALB/3T3 mouse fibroblasts on nonwoven meshes spun from recombinant spidroins showed cell alignment along individual fibers as well as a protrusion of filopodia/lamellipodia through the interstitial space between the fibers (Leal-Egana et al. 2012). Electrospinning of recombinant spidroins hybridized with the cell binding sequence RGD even induced the differentiation of bone marrow-derived, human mesenchymal stem cells (hMSCs) to osteogenic outcomes (Bini et al. 2006). Also, self-assembled recombinant spidroin fibers implanted subcutaneously in rats did not show any negative systemic or local reactions (Fredriksson et al. 2009), suggesting these fibers to be biocompatible. Additionally, fiber bundles thereof seem to support the formation of vascularized tissue formation, since already 1 week after implantation, new capillaries and fibroblast-like cells formed in the center of such fiber bundles (Fredriksson et al. 2009).

"Not to spin": artificial assembly morphologies

Recombinant spider silk proteins can be processed into more than fibers; other morphologies such as particles, foams, films, or hydrogels can also be fabricated, all of which have a high

application potential (Hardy and Scheibel 2010; Hermanson et al. 2007; Slotta et al. 2008; Spiess et al. 2010a, b). Processing of recombinant spider silk proteins in aqueous solutions can be triggered by changes in the pH value, amount and type of additives (e.g., potassium phosphate, alcohols, or polymers), mechanical shear, or temperature changes. Alternatively, organic solvents such as HFIP or FA can be used; however, the choice of solvent has a significant impact on structure formation. While aqueous processing leads mainly to particle and hydrogel formation, water-soluble films are mainly produced using fast-evaporating organic solvents. Here, posttreatment procedures with agents, like potassium phosphate or monohydric alcohols (methanol, ethanol, isopropanol), are necessary to render the films insoluble in water (Exler et al. 2007; Huemmerich et al. 2004a, b; Lammel et al. 2008; Numata et al. 2010; Rammensee et al. 2008; Rising 2014; Scheibel 2004; Slotta et al. 2007; Spiess et al. 2010b).

Particles

Spidroin particles are produced in a simple, aqueous process by the addition of high concentrations of kosmotropic salts, like potassium phosphate, and fast mixing. This procedure results in solid particles with high β-sheet content, a smooth surface (Hofer et al. 2012; Lammel et al. 2008; Slotta et al. 2008), and particle sizes between 250 nm and 3 μm depending on the mixing intensity, protein concentration, and the concentration of kosmotropic salts (Lammel et al. 2008; Slotta et al. 2008; Spiess et al. 2010a). Using ionic liquids instead of aqueous buffers and high potassium phosphate concentrations to induce phase separation and nucleation in the protein solution or ultrasonication for particle production allowed enhanced size control and a reduced polydispersity index (Elsner et al. 2015; Lucke et al. 2015). eADF4(C16) (engineered *Araneus diadematus* fibroin 4) particles show a brush-like outer layer with protruding protein strands and a thickness of 30–50 nm covering a solid inner core (Helfricht et al. 2013). Importantly, no posttreatment with dehydrating agents is necessary to obtain water-insoluble particles, since the β-sheet content is high after the salting-out process (Slotta et al. 2008). Further, it has been shown that particles made of recombinant spider silk proteins exhibit an extraordinary mechanical stability when analyzed in dry state. In a swollen, hydrated state, these particles exhibited a different mechanical behavior: the elastic modulus was three orders of magnitude lower (E modulus dry, 0.8±0.5 GPa; E modulus hydrated, 2.99±0.90 MPa). Further, when dry, the particles deformed in a plastic response, and when hydrated, they showed a reversible, elastic deformation behavior. In both states, dry and hydrated, the mechanical properties were dependent on the molecular weight of the spidroin: The higher the molecular weight, the better the mechanical stability (Neubauer et al. 2013).

Particles made of recombinant spider silk proteins are suitable for a large variety of applications. Due to their enhanced mechanical properties, these particles can be used, for example, as filler for composite materials. Additionally, due to their favorable properties in a physiological environment (nontoxic, biodegradable, etc.), these particles could be used as carriers of different substances, for example in drug delivery. Silk particles retain their properties for a limited period of time in the human body before they gradually decompose into degradation products which can be eliminated (Altman et al. 2003; George and Abraham 2006; Liu et al. 2005; Müller-Herrmann and Scheibel 2015).

Uptake and release studies of small molecules with model drugs showed that these types of molecular entities can be incorporated either by diffusion or by coprecipitation of both the spidroin and the drug substance. While the latter increased the loading efficiency of the particles, it did not significantly influence the release rate. Importantly, drugs can be only loaded into spidroin particles if there is no electrostatic repulsion. In this context, only positively and neutrally charged drugs can be loaded onto negatively charged spider silk protein particles, such as those made of eADF4(C16) (Blüm and Scheibel 2012; Doblhofer and Scheibel 2015; Lammel et al. 2011). Since protein design allowed the production of positively charged spider silk proteins, particles made thereof were also able to uptake negatively charged small molecules as well as large oligonucleotides (Doblhofer and Scheibel 2015).

One important justification for the use of silk-based drug delivery vehicles is the ability to design the underlying proteins for a specific target, for example uptake by a specific cell type. Previous investigations showed that, in general, negatively charged spider silk particles have a low uptake efficiency by mammalian cells. Therefore, cell penetrating peptides (CPP) as well as an Arg8-TAG or a RGD sequence were engineered to the N- and C-termini of eADF4(C16). The presence of CPP increased the number of incorporated particles in HeLa cells; however, the mechanism behind the increased uptake was surprisingly mainly the particle's surface charge, not the presented surface peptide (Elsner et al. 2015).

Films

The first studies on films made of spider silk proteins were reported in 2002 by Chen et al. where the salt-controlled structural conversion of natural spider silk proteins obtained from the major ampullate gland of *Nephila senegalensis* was investigated (Chen et al. 2002). Films made of recombinant spider silk proteins first gained attention in 2005 where it was shown that these spider silk-like proteins undergo a similar structural conversion from random coil to β-sheet rich. Recombinantly produced engineered spider silk protein films turned out to be

transparent and chemically stable under ambient conditions, depending on their processing (Huemmerich et al. 2006; Slotta et al. 2006; Spiess et al. 2010b). Two major components determine the properties of these films: the molecular structure including the secondary structure and intermolecular as well as intramolecular interactions as well as the macroscopic structure reflecting the material's interface with the environment (Spiess et al. 2010a).

Depending on the solvent, spider silk proteins in solution adopt mainly an α-helical or random coil conformation which is often maintained in as-cast films (Borkner et al. 2014; Slotta et al. 2006). These as-cast films are water soluble, as mentioned above, due to the weak intermolecular interactions of spider silk proteins in an α-helical conformation. Upon conversion of the protein structure toward a β-sheet-rich structure by using agents like kosmotropic salts or alcohols, water vapor, or temperature annealing, films can be rendered chemically more stable and thereby water insoluble (Huemmerich et al. 2006; Slotta et al. 2006; Spiess et al. 2010b). This is an important quality, as most potential applications of recombinant spider silk films involve interaction with a humid environment. Structural control over synthetic recombinant spider silk proteins is also given by the variation of the amino acid sequence toward a higher number of β-sheet forming building blocks, and with the control of the β-sheet portion, mechanical properties can be predetermined (Rabotyagova et al. 2009, 2010). While the terminal domains of spider silk proteins play an important role in the fiber spinning process, no significant influence of the nonrepetitive regions could be observed during the film casting from organic protein solutions. Nevertheless, as-cast films made of recombinant spider silk proteins containing the NR regions are slightly more chemically stable than those without, though there are no disulfide bridges present (Slotta et al. 2006). Besides chemical stability, the β-sheet content also determines the mechanical properties of a film. With increasing β-sheet content, elastic modulus and strength increase, and there is a loss of elasticity. High amounts of β-sheets, therefore, can be correlated with stiffness and brittleness in silk films (Spiess et al. 2010b). However, as the content of β-sheets can be adjusted by the posttreatment conditions upon varying incubation times of the films in alcohols or posttreatment with water/alcohol mixtures at various ratios lead to a varying β-sheet content, this is not a challenge for tailoring films to specific applications (Spiess et al. 2010a). The water content in silk films plays also an important role; due to its softening effect, it can work as a plasticizer. Another possibility to overcome the brittleness of silk films is to add plasticizers like glycerol. It was reported that glycerol can alter the intermolecular interactions of silk proteins in a film and, therefore, is able to enhance the films' elasticity. The addition of 40 % *w*/*w* glycerol to an eADF4(C16) film yielded a 10-fold increased elasticity, but also going along with a 10-fold decrease of the elastic modulus and a slight decrease in strength (Lawrence et al. 2010; Spiess et al. 2010a).

Spider silk protein films can be envisioned for various applications; however, they are especially promising for use in the biomedical field due to their biocompatibility which has been demonstrated in vitro and in vivo (Allmeling et al. 2006, 2008; Gellynck et al. 2008a, b; Hakimi et al. 2010; Vollrath et al. 2002). Conceivable applications are materials for a controlled substance release at a specific site of action in the human body, biomedical sensors, and cell-supporting scaffolds (Hardy et al. 2013; Minoura et al. 1995; Sofia et al. 2001; Vendrely and Scheibel 2007). It is possible, for example, to directly integrate substances (e.g., drugs) into silk films or to load these substances into microparticles that are then embedded in or coated with a silk layer amenable for delayed release (Wang et al. 2007, 2010). Biomedical or biochemical sensors can be fabricated by covalent binding of biologically active compounds to the silk proteins (Lawrence et al. 2008; Spiess et al. 2010b). Cell adhesion on recombinant spider silk protein scaffolds was shown to be very weak (Baoyong et al. 2010); therefore, chemical or genetic coupling of specific functional groups, for example components of the extracellular matrix, and modification of the surface hydrophilicity have been employed to influence the cellular response to a film's surface concerning adhesion, proliferation, and differentiation (Bini et al. 2006; Karageorgiou et al. 2004; Wohlrab et al. 2012a). As mentioned above, the function of silk films can be also partly controlled by the macroscopic structure they adopt. Changing the surface morphology by patterning or partial roughening of a film under different posttreatment conditions can lead to a deviating behavior of cells thereon (Bauer et al. 2013; Borkner et al. 2014). The hydrophilicity of the film surface can easily be affected by the choice of the template for drop-cast films (Wohlrab et al. 2012b). The influence of the template's surface hydrophilicity can be diminished by spin coating of spidroin solutions, since the duration of solvent evaporation determines the rearrangement of silk protein molecules within the films, and their interaction with the underlying substrate and the film properties are in this case determined by the utilized solvent (Metwalli et al. 2007; Wohlrab et al. 2012b). Applications of films made of silk protein in the medical field include coatings for medical devices (Bettinger and Bao 2010; Kim et al. 2010; Zeplin et al. 2014a, b) and skin grafts (Baoyong et al. 2010; Jiang et al. 2007).

In the context of biomedical applications, it is important to mention that recombinant spider silk protein films undergo partial degradation in the presence of wound proteases (~10 %) in a timescale of 15 days, which is in the range of

the initial phase of wound healing (Müller-Herrmann and Scheibel 2015).

Hydrogels

Hydrogels are three-dimensional polymer networks that absorb over 95 % (*w*/*w*) of water (Knight et al. 1998; Lee and Mooney 2001; Rammensee et al. 2006; Schacht and Scheibel 2011; Shin et al. 2003). Their porous structure and mechanical properties make them candidates for applications in tissue engineering, drug delivery, or as functional coatings (Rammensee et al. 2006). The mechanical properties of a specific hydrogel are determined by the properties of its individual constituents, and many different polymers, synthetic and natural ones, have been utilized to form hydrogels. Spidroin hydrogels are built upon self-assembly of nanofibrils by a mechanism of nucleation-aggregation followed by a concentration-dependent gelation in which β-sheet-rich spider silk fibrils become entangled to build a stable three-dimensional network (Hu et al. 2010; Rammensee et al. 2006; Schacht et al. 2015; Schacht and Scheibel 2011; Slotta et al. 2008). Spider silk proteins can be processed into stable hydrogels in a controlled manner by adjusting the protein concentration, pH, temperature, ion composition, and concentration (Jones et al. 2015; Schacht and Scheibel 2011; Vepari and Kaplan 2007). Each of these inputs influences the hydrogel's morphology, mechanical properties, and pore size. In particular, increasing the protein concentration and increasing the addition of chemical crosslinkers lead to an increase in mechanical strength, accompanied by a decrease in pore sizes (Schacht and Scheibel 2011). It has been recently shown that recombinant spidroin hydrogels, like many biopolymer hydrogels, show a viscoelastic behavior with stress changes proportional to the linear increasing strain (Mackintosh et al. 1995). In the special case of eADF4 hydrogels, the elastic behavior dominates over the viscous behavior, with low-viscosity flow behavior, good form stability, and a shear thinning effect, allowing their use as bioink in a biofabrication setup. Eukaryotic cells were embedded within the hydrogel prior to printing with a bioplotter and they survived for at least 7 days after printing. The addition of cells did not considerably influence the print-ability of the spider silk protein gels (Schacht et al. 2015).

Foams and sponges

Foams are defined as material containing small bubbles formed on or in a liquid. To produce foams made of spidroin solutions, gas bubbles remain stable when using a high protein concentration, and the foam is established upon drying. In comparison, sponges are, like foams, three-dimensional porous scaffolds, but differ in their production technique and their mechanical properties. Sponges can be produced by gas foaming, lyophilization, or using porogens. It has been shown for silkworm silk fibroin that porogens like sodium chloride and sugar can be used to produce sponges with defined pore sizes due to silk β-sheet formation around the porogen. Therefore, the pores are the size of the porogen in case of organic protein solutions and 80–90 % of the size of the porogen in aqueous solutions (Kim et al. 2005). As a consequence, it is even possible to produce pore size gradients by stacking porogens with different diameters (Kim et al. 2005; Nazarov et al. 2004; Vepari and Kaplan 2007). Foams and sponges are both qualified for cell culture applications due to the ability of good transportation of nutrients and metabolic waste through the material in combination with a good structural and mechanical stability (Kluge et al. 2008). While a number of studies on silkworm silk fibroin foams and sponges have been published, spider silk protein foams and sponges remain largely unexplored. Widhe et al. showed in 2010 that their recombinant miniature spider silk protein 4RepCT can be processed into foams which stay microscopically stable in a cell culture medium. The surface of these foams showed heterogeneous pores with diameters between 30 and 200 μm. However, in this pore size range, foams lack a characteristic surface topography which influences cell adhesion (Widhe et al. 2010).

Concerning spider silk sponges, Jones et al. developed a method in which hydrogels were frozen in an aqueous medium and subsequently thawed, resulting in a highly elastic, three-dimensional morphology. Such sponges could uptake water to the extent of hydrogels as well as maintain their form upon compression and drying. That is, the effect of dehydration was completely reversible by the addition of water. The high elasticity of these sponges is based on a lower content of stiffening β-sheet crystals and a higher amount of the elastic random coil and helical structures in comparison to other spider silk scaffolds (Jones et al. 2015).

Composite materials including spider silk

Composites provide the opportunity to produce materials with extraordinary properties by complementation of at least two different kinds of materials. In this context, natural as well as recombinant spider silk materials can play a role due to their outstanding mechanical and biocompatible properties. In some studies, naturally spun spider dragline silks were used to assemble composites with inorganic nanoparticles to reinforce the fibers. Recently, it was shown that feeding spiders with carbon nanotubes or graphene dispersions led to carbon-reinforced silk threads (Lepore et al. 2015). Despite that, most approaches to enhance mechanical strength of spider dragline silk were employed after collection of the silk by forced silking. Dragline silk was used as template for the insertion of zinc (Zn), titanium (Ti), and aluminum (Al) by multiple pulsed vapor-phase infiltration (MPI). This treatment

increased the toughness of the spider silk fibers by almost 10-fold and the E moduli of the fibers from 9.7 to 68 GPa, in the best case (Lee et al. 2009).

Spider silk composite production allows not only to increase its mechanical strength but also to extend the range of applications. Dragline silk fibers, for instance, were incubated in chloroauric acid to assemble gold nanoparticles on their surface with the goal of producing water and methanol vapor sensors with a response time of about 10 s and 150-fold change of conductivity. Their supercontraction behavior in the presence of water and methanol vapor led to a change in the distance of the gold nanoparticles and, therefore, altered the electrical conductivity of the fibers (Hardy and Scheibel 2010; Singh et al. 2007). Electrical conductivity was also introduced into spider silk fibers by deposition of amine-functionalized multiwalled carbon nanotubes (MWCNT) onto their surface. In this study, additionally, an increase in mechanical strength was observed for the composite fibers. The combination of properties allowed an extended application of the material in various technical approaches (Steven et al. 2013). The accumulation of calcium carbonate or hydroxyapatite (HAP) on naturally spun fibers enabled producing new scaffolds for bone tissue engineering or building blocks for bone replacement materials (Cao and Mao 2007; Mehta and Hede 2005). In the case of hydroxyapatite deposition, oriented crystal growth was obtained being consistent with the orientation of β-sheet crystals in the silk fibers (Cao and Mao 2007). In another approach, naturally spun spider silk was solubilized in FA for electrospinning. By mixing the resulting protein solution with a poly(D,L-lactic acid) (PDLLA) FA solution and subsequent electrospinning, nonwoven meshes with core-shell structured fibers with a diameter range of about 90–1000 nm were produced. The size of the fibers was tuned by the weight ratio of the two material components in the spinning solution (Zhou et al. 2008).

Recombinant spider silk proteins have been used in blends with polycaprolactone (PCL) and thermoplastic polyurethane (TPU) to cast films with a higher elasticity than nonblended spider silk protein films. Good cell adhesion, proliferation, and the possibility to incorporate drugs in these composite films endorse them as candidates for implant coatings or as scaffolds for tissue engineering (Hardy et al. 2013). Another filler material used in spider silk protein films were carbon nanotubes. Composite films made of recombinant spider silk proteins and single-walled carbon nanotubes led to excellent mechanical properties as a result of the transfer of stress in the matrix to the filler and of the potential for extensive reorganization of the matrix at applied high stress (Blond et al. 2007).

Blended dopes of recombinant spider silk with collagen or gelatin have also been used for electrospinning processes. The resulting composite nonwoven meshes were predominantly used in tissue engineering. Electrospinning of a mixture of spider silk proteins and collagen led to unidirectional, partially crosslinked fiber scaffolds usable in stem cell differentiation and in neural tissue engineering. Collagen-dominant scaffolds were found to provide unique structural, mechanical, and biochemical cues; stem cells were directed to neural differentiation, and the development of long neural filaments along the fibers was facilitated. These neural tissue-like constructs are promising candidates for transplantation in cellular replacement therapies for neurodegenerative disorders such as Alzheimer's or Parkinson's disease (Sridharan et al. 2013; Zhu et al. 2015). Tubular scaffolds made of a blend of recombinant spider silk proteins and gelatins, supported by a polyurethane outer layer, were produced to be used in tissue-engineered vessel grafts (TEVG). The morphological and mechanical characterization of the tubular structures showed strong similarities with the structure of native arteries, both in strength and elasticity. The appearance of RGD sequences in spider silk used for this purpose supported the growth of adult stem cells, yielding a higher cellular content prior to prospective implantation than without the cellular recognition sequence (Zhang et al. 2014).

Modification of recombinant spider silk proteins with specific binding motifs for HAP (Huang et al. 2007), titanium dioxide, germania, and gold could be assembled into various morphologies and provided the control of organic-inorganic interfaces and composite structural features (Belton et al. 2012; Foo et al. 2006; Mieszawska et al. 2010). Silica binding sequences (e.g., R5 from *Cylindrotheka fusiformis*) were used to control silica particle formation and assembly on the surfaces of spider silk films, fibers, and particles. Mineral phase formation, morphology, chemistry, and, therefore, composite properties could be influenced by varying the processing conditions or by sequence alteration. Silica is a critical osteoconductive element, which can be processed under ambient conditions, and has the potential to control the tissue remodeling rate, making this composite a possible scaffold for bone regeneration. Studies with human mesenchymal stem cells (hMSCs) attached to silica/silk films showed upregulation of osteogenic gene markers at high silica contents (Belton et al. 2012; Foo et al. 2006; Mieszawska et al. 2010).

Summary and outlook

Biotechnological production of spider silk proteins and their processing into diverse morphologies (Fig. 4) allow for applications in textile, automotive, and biomedical industries. Concerning the production of artificial spider silk fibers, significant progress has been made in the last years. Since reconstituted spider silk fibers did not show nature-like mechanical properties after spinning, various techniques for biotechnological production (i.e., proteins, transgenic animals, etc.) have been investigated to gain proteins enabling fibers with such features. Regarding the biotechnological production

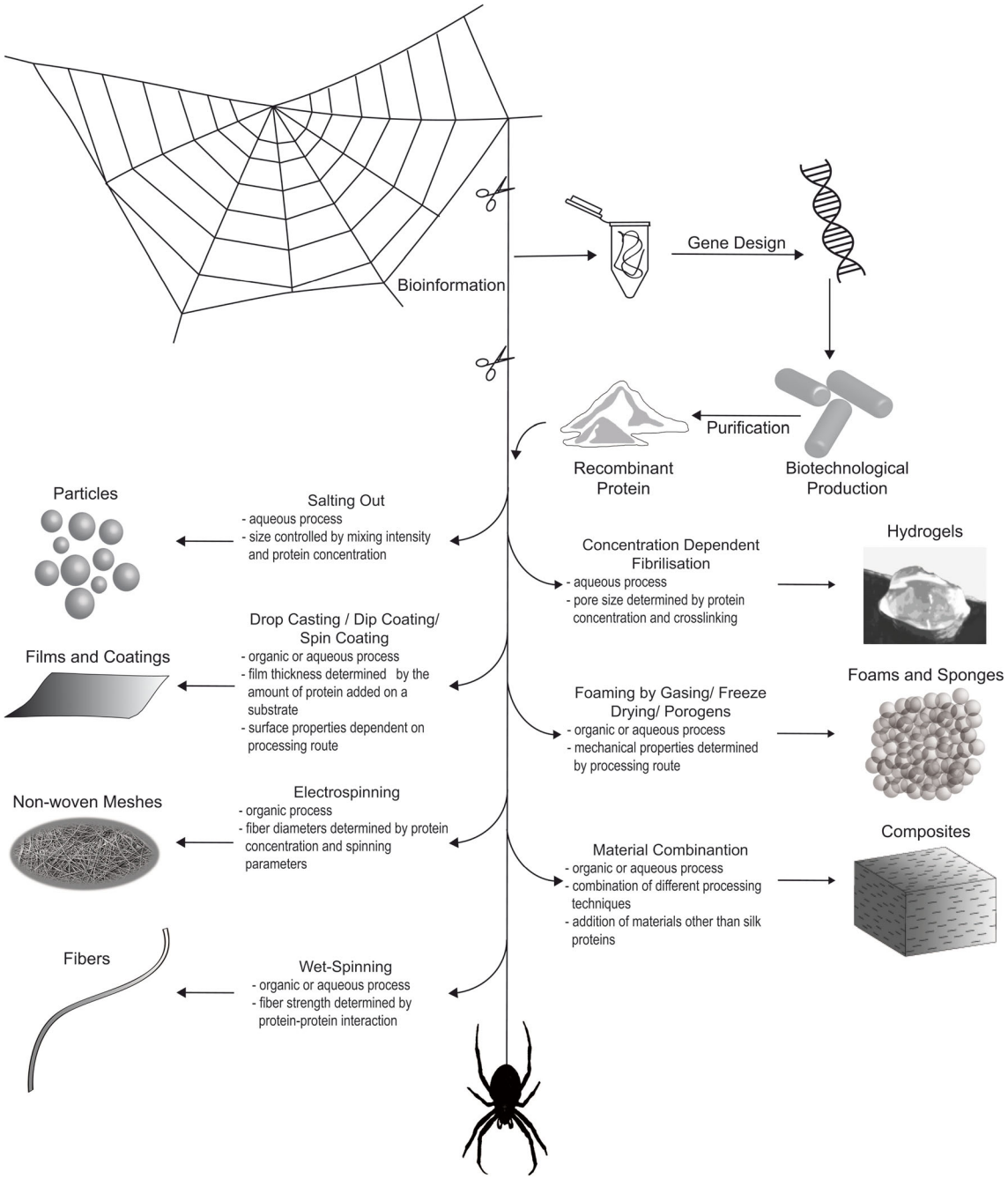

Fig. 4 Design, production, and processing of recombinant spider silk proteins: from identification of the bioinformation given by the natural material produced by a spider, to genetic design of its recombinant counterpart, to possible morphologies

and artificial fiber spinning, great progress was made by analyzing the natural spinning process and the role of the amino- and carboxy-terminal domains. Inclusion of the nonrepetitive terminal domains into the recombinantly produced spider silk proteins and wet spinning these proteins into fibers resulted in a toughness comparable to that of natural fibers. This emphasized the importance of the nonrepetitive terminal domains in the proper alignment of the spidroins, which was neglected in earlier trials. By fine-tuning the composition of the recombinant proteins and the spinning process, artificial spider silk fibers with mechanical properties exceeding those of the natural fibers will be likely possible in the future.

Recombinant production of spider silk proteins does not only offer the option to mimic nature and produce fibers that are similar to their natural counterparts, but it also enables the production of different morphologies. These different structures are biodegradable and biocompatible just like the natural equivalents, but still comprise new properties that lead to

applications in both the medical and the technical field. Particles and films/coatings have already been well-investigated, and this paves the way toward the first applications in drug delivery and cell culture. On the other hand, hydrogels, foams, and sponges require further exploration before they can be used directly in applications. Nevertheless, in all cases, recombinant spider silk protein research tends to explore new tailor-made materials by adapting the morphology's properties to a specific application. The potential of recombinant spider silk proteins in different fields is thereby essentially limitless.

Acknowledgments We kindly thank Elise DeSimone for proofreading the manuscript. A.H. kindly appreciates the financial support by the "Universität Bayern, e.V., Graduiertenförderung nach dem bayerischen Eliteförderungsgesetz." This work was financially supported by DFG grant SFB 840 TP A8 (to T.S.), DFG SCHE 603/4, and the Technologie Allianz Oberfranken (TAO).

Compliance with ethical standards

Conflict of interest The authors declare that they have no competing interests.

Ethics approval This article does not contain any studies with human participants or animals performed by any of the authors.

References

Adrianos SL, Teule F, Hinman MB, Jones JA, Weber WS, Yarger JL, Lewis RV (2013) *Nephila clavipes* flagelliform silk-like GGX motifs contribute to extensibility and spacer motifs contribute to strength in synthetic spider silk fibers. Biomacromolecules 14: 1751–1760. doi:10.1021/bm400125w

Albertson AE, Teule F, Weber W, Yarger JL, Lewis RV (2014) Effects of different post-spin stretching conditions on the mechanical properties of synthetic spider silk fibers. J Mech Behav Biomed Mater 29: 225–234. doi:10.1016/j.jmbbm.2013.09.002

Allmeling C, Jokuszies A, Reimers K, Kall S, Vogt PM (2006) Use of spider silk fibres as an innovative material in a biocompatible artificial nerve conduit. J Cell Mol Med 10:770–777. doi:10.2755/jcmm010.003.18

Allmeling C, Jokuszies A, Reimers K, Kall S, Choi CY, Brandes G, Kasper C, Scheper T, Guggenheim M, Vogt PM (2008) Spider silk fibres in artificial nerve constructs promote peripheral nerve regeneration. Cell Prolif 41:408–420. doi:10.1111/j.1365-2184.2008.00534.x

Altman GH, Diaz F, Jakuba C, Calabro T, Horan RL, Chen J, Lu H, Richmond J, Kaplan DL (2003) Silk-based biomaterials. Biomaterials 24:401–416. doi:10.1016/S0142-9612(02)00353-8

An B, Hinman MB, Holland GP, Yarger JL, Lewis RV (2011) Inducing beta-sheets formation in synthetic spider silk fibers by aqueous post-spin stretching. Biomacromolecules 12:2375–2381. doi:10.1021/bm200463e

Andersen SO (1970) Amino acid composition of spider silks. Comp Biochem Physiol 35:705–711. doi:10.1016/0010-406X(70)90988-6

Andersson M, Chen G, Otikovs M, Landreh M, Nordling K, Kronqvist N, Westermark P, Jornvall H, Knight S, Ridderstrale Y, Holm L, Meng Q, Jaudzems K, Chesler M, Johansson J, Rising A (2014) Carbonic anhydrase generates CO2 and H+ that drive spider silk formation via opposite effects on the terminal domains. PLoS Biol 12:e1001921. doi:10.1371/journal.pbio.1001921

Arcidiacono S, Mello CM, Butler M, Welsh E, Soares JW, Allen A, Ziegler D, Laue T, Chase S (2002) Aqueous processing and fiber spinning of recombinant spider silks. Macromolecules 35:1262–1266. doi:10.1021/Ma011471o

Ayoub NA, Garb JE, Tinghitella RM, Collin MA, Hayashi CY (2007) Blueprint for a high-performance biomaterial: full-length spider dragline silk genes. PLoS ONE 2:e514. doi:10.1371/journal.pone.0000514

Baoyong L, Jian Z, Denglong C, Min L (2010) Evaluation of a new type of wound dressing made from recombinant spider silk protein using rat models. Burns 36:891–896. doi:10.1016/j.burns.2009.12.001

Barr LA, Fahnestock SR, Yang JJ (2004) Production and purification of recombinant DP1B silk-like protein in plants. Mol Breed 13:345–356. doi:10.1016/j.burns.2009.12.001

Bauer F, Wohlrab S, Scheibel T (2013) Controllable cell adhesion, growth and orientation on layered silk protein films. Biomater Sci 1:1244–1249. doi:10.1039/C3bm60114e

Belton DJ, Mieszawska AJ, Currie HA, Kaplan DL, Perry CC (2012) Silk-silica composites from genetically engineered chimeric proteins: materials properties correlate with silica condensation rate and colloidal stability of the proteins in aqueous solution. Langmuir 28:4373–4381. doi:10.1021/La205084z

Bettinger CJ, Bao Z (2010) Biomaterials-based organic electronic devices. Polym Int 59:563–567. doi:10.1002/pi.2827

Bini E, Foo CW, Huang J, Karageorgiou V, Kitchel B, Kaplan DL (2006) RGD-functionalized bioengineered spider dragline silk biomaterial. Biomacromolecules 7:3139–3145. doi:10.1021/bm0607877

Blackledge TA, Hayashi CY (2006) Silken toolkits: biomechanics of silk fibers spun by the orb web spider *Argiope argentata* (Fabricius 1775). J Exp Biol 209:2452–2461. doi:10.1242/jeb.02275

Blond D, McCarthy DN, Blau WJ, Coleman JN (2007) Toughening of artificial silk by incorporation of carbon nanotubes. Biomacromolecules 8:3973–3976. doi:10.1021/Bm700971g

Blüm C, Scheibel T (2012) Control of drug loading and release properties of spider silk sub-microparticles. J Bionanosci 2:67–74. doi:10.1007/s12668-012-0036-7

Bogush VG, Sokolova OS, Davydova LI, Klinov DV, Sidoruk KV, Esipova NG, Neretina TV, Orchanskyi IA, Makeev VY, Tumanyan VG, Shaitan KV, Debabov VG, Kirpichnikov MP (2009) A novel model system for design of biomaterials based on recombinant analogs of spider silk proteins. J Neuroimmune Pharmacol 4:17–27. doi:10.1007/s11481-008-9129-z

Bon M (1710) A discourse upon the usefulness of the silk of spiders. By Monsieur Bon, President of the Court of Accounts, Aydes and Finances, and President of the Royal Society of Sciences at Montpellier. Communicated by the author. Philos Trans R Soc London 27:2–16. doi:10.1098/rstl.1710.0001

Borkner CB, Elsner MB, Scheibel T (2014) Coatings and films made of silk proteins. ACS Appl Mater Interfaces 6:15611–15625. doi:10.1021/Am5008479

Brooks AE, Stricker SM, Joshi SB, Kamerzell TJ, Middaugh CR, Lewis RV (2008) Properties of synthetic spider silk fibers based on *Argiope aurantia* MaSp2. Biomacromolecules 9:1506–1510. doi:10.1021/bm701124p

Brown CP, Harnagea C, Gill HS, Price AJ, Traversa E, Licoccia S, Rosei F (2012) Rough fibrils provide a toughening mechanism in biological fibers. ACS Nano 6:1961–1969. doi:10.1021/nn300130q

Cao B, Mao C (2007) Oriented nucleation of hydroxylapatite crystals on spider dragline silks. Langmuir 23:10701–10705. doi:10.1021/la7014435

Cary LC, Goebel M, Corsaro BG, Wang HG, Rosen E, Fraser MJ (1989) Transposon mutagenesis of baculoviruses: analysis of *Trichoplusia ni* transposon IFP2 insertions within the FP-locus of nuclear

polyhedrosis viruses. Virology 172:156–169. doi:10.1016/0042-6822(89)90117-7

Challis RJ, Goodacre SL, Hewitt GM (2006) Evolution of spider silks: conservation and diversification of the C-terminus. Insect Mol Biol 15:45–56. doi:10.1111/j.1365-2583.2005.00606.x

Chen X, Knight DP, Shao ZZ, Vollrath F (2002) Conformation transition in silk protein films monitored by time-resolved Fourier transform infrared spectroscopy: effect of potassium ions on *Nephila* spidroin films. Biochemistry 41:14944–14950. doi:10.1021/Bi026550m

Craig CL, Riekel C, Herberstein ME, Weber RS, Kaplan D, Pierce NE (2000) Evidence for diet effects on the composition of silk proteins produced by spiders. Mol Biol Evol 17:1904–1913

Denny M (1976) Physical properties of spiders silk and their role in design of orb-webs. J Exp Biol 65:483–506

Doblhofer E, Scheibel T (2015) Engineering of recombinant spider silk proteins allows defined uptake and release of substances. J Pharm Sci 104:988–994. doi:10.1002/jps.24300

Eisoldt L, Hardy JG, Heim M, Scheibel TR (2010) The role of salt and shear on the storage and assembly of spider silk proteins. J Struct Biol 170:413–419. doi:10.1016/j.jsb.2009.12.027

Eisoldt L, Smith A, Scheibel T (2011) Decoding the secrets of spider silk. Mater Today 14:80–86. doi:10.1016/S1369-7021(11)70057-8

Eisoldt L, Thamm C, Scheibel T (2012) The role of terminal domains during storage and assembly of spider silk proteins. Biopolymers 97: 355–361. doi:10.1002/bip.22006

Elsner MB, Herold HM, Muller-Herrmann S, Bargel H, Scheibel T (2015) Enhanced cellular uptake of engineered spider silk particles. Biomater Sci 3:543–551. doi:10.1039/C4bm00401a

Exler JH, Hummerich D, Scheibel T (2007) The amphiphilic properties of spider silks are important for spinning. Angew Chem Int Ed 46: 3559–3562. doi:10.1002/anie.200604718

Fahnestock SR, Bedzyk LA (1997) Production of synthetic spider dragline silk protein in *Pichia pastoris*. Appl Microbiol Biotechnol 47: 33–39

Fahnestock SR, Irwin SL (1997) Synthetic spider dragline silk proteins and their production in *Escherichia coli*. Appl Microbiol Biotechnol 47:23–32

Fahnestock SR, Yao Z, Bedzyk LA (2000) Microbial production of spider silk proteins. Rev Mol Biotechnol 74:105–119. doi:10.1016/S1389-0352(00)00008-8

Foo CWP, Patwardhan SV, Belton DJ, Kitchel B, Anastasiades D, Huang J, Naik RR, Perry CC, Kaplan DL (2006) Novel nanocomposites from spider silk-silica fusion (chimeric) proteins. Proc Natl Acad Sci U S A 103:9428–9433. doi:10.1073/pnas.0601096103

Fox LR (1975) Cannibalism in natural populations. Annu Rev Ecol Syst 6:87–106

Fredriksson C, Hedhammar M, Feinstein R, Nordling K, Kratz G, Johansson J, Huss F, Rising A (2009) Tissue response to subcutaneously implanted recombinant spider silk: an in vivo study. Materials 2:1908–1922. doi:10.3390/Ma2041908

Gellynck K, Verdonk P, Forsyth R, Almqvist KF, Van Nimmen E, Gheysens T, Mertens J, Van Langenhove L, Kiekens P, Verbruggen G (2008a) Biocompatibility and biodegradability of spider egg sac silk. J Mater Sci Mater Med 19:2963–2970. doi:10.1007/s10856-007-3330-0

Gellynck K, Verdonk PCM, Van Nimmen E, Almqvist KF, Gheysens T, Schoukens G, Van Langenhove L, Kiekens P, Mertens J, Verbruggen G (2008b) Silkworm and spider silk scaffolds for chondrocyte support. J Mater Sci Mater Med 19:3399–3409. doi:10.1007/s10856-008-3474-6

George M, Abraham TE (2006) Polyionic hydrocolloids for the intestinal delivery of protein drugs: alginate and chitosan—a review. J Control Release 114:1–14. doi:10.1016/j.jconrel.2006.04.017

Gerritsen VB (2002) The tiptoe of an airbus. Protein Spotlight Swiss Prot 24:1–2

Gosline JM, Guerette PA, Ortlepp CS, Savage KN (1999) The mechanical design of spider silks: from fibroin sequence to mechanical function. J Exp Biol 202:3295–3303

Greiner A, Wendorff JH (2007) Electrospinning: a fascinating method for the preparation of ultrathin fibres. Angew Chem Int Ed 46:5670–5703. doi:10.1002/anie.200604646

Greiner A, Wendorff JH, Yarin AL, Zussman E (2006) Biohybrid nanosystems with polymer nanofibers and nanotubes. Appl Microbiol Biotechnol 71:387–393. doi:10.1007/s00253-006-0356-z

Grip S, Johansson J, Hedhammar M (2009) Engineered disulfides improve mechanical properties of recombinant spider silk. Protein Sci 18:1012–1022. doi:10.1002/Pro.111

Hagn F, Eisoldt L, Hardy JG, Vendrely C, Coles M, Scheibel T, Kessler H (2010) A conserved spider silk domain acts as a molecular switch that controls fibre assembly. Nature 465:239–242. doi:10.1038/Nature08936

Hagn F, Thamm C, Scheibel T, Kessler H (2011) pH-dependent dimerization and salt-dependent stabilization of the N-terminal domain of spider dragline silk—implications for fiber formation. Angew Chem Int Ed 50:310–313. doi:10.1002/anie.201003795

Hakimi O, Gheysens T, Vollrath F, Grahn MF, Knight DP, Vadgama P (2010) Modulation of cell growth on exposure to silkworm and spider silk fibers. J Biomed Mater Res A 92:1366–1372. doi:10.1002/jbm.a.32462

Hardy JG, Scheibel TR (2010) Composite materials based on silk proteins. Prog Polym Sci 35:1093–1115. doi:10.1016/j.progpolymsci.2010.04.005

Hardy JG, Romer LM, Scheibel TR (2008) Polymeric materials based on silk proteins. Polymer 49:4309–4327. doi:10.1016/j.polymer.2008.08.006

Hardy JG, Leal-Egañ A, Scheibel T (2013) Engineered spider silk protein-based composites for drug delivery. Macromol Biosci 13: 1431–1437. doi:10.1002/mabi.201300233

Hauptmann V, Weichert N, Rakhimova M, Conrad U (2013) Spider silks from plants—a challenge to create native-sized spidroins. Biotechnol J 8:1183–1192. doi:10.1002/biot.201300204

Hayashi CY, Shipley NH, Lewis RV (1999) Hypotheses that correlate the sequence, structure, and mechanical properties of spider silk proteins. Int J Biol Macromol 24:271–275. doi:10.1016/S0141-8130(98)00089-0

Hedhammar M, Rising A, Grip S, Martinez AS, Nordling K, Casals C, Stark M, Johansson J (2008) Structural properties of recombinant nonrepetitive and repetitive parts of major ampullate spidroin 1 from *Euprosthenops australis*: implications for fiber formation. Biochemistry 47:3407–3417. doi:10.1021/bi702432y

Heidebrecht A, Scheibel T (2013) Recombinant production of spider silk proteins. Adv Appl Microbiol 82:115–153

Heidebrecht A, Eisoldt L, Diehl J, Schmidt A, Geffers M, Lang G, Scheibel T (2015) Biomimetic fibers made of recombinant spidroins with the same toughness as natural spider silk. Adv Mater 27:2189–2194. doi:10.1002/adma.201404234

Heim M, Keerl D, Scheibel T (2009) Spider silk: from soluble protein to extraordinary fiber. Angew Chem Int Ed 48:3584–3596. doi:10.1002/anie.200803341

Helfricht N, Klug M, Mark A, Kuznetsov V, Blum C, Scheibel T, Papastavrou G (2013) Surface properties of spider silk particles in solution. Biomater Sci 1:1166–1171. doi:10.1039/c3bm60109a

Hermanson KD, Huemmerich D, Scheibel T, Bausch AR (2007) Engineered microcapsules fabricated from reconstituted spider silk. Adv Mater 19:1810–1815. doi:10.1002/adma.200602709

Hinman MB, Lewis RV (1992) Isolation of a clone encoding a second dragline silk fibroin. *Nephila clavipes* dragline silk is a two-protein fiber. J Biol Chem 267:19320–19324

Hinman MB, Jones JA, Lewis RV (2000) Synthetic spider silk: a modular fiber. Trends Biotechnol 18:374–379. doi:10.1016/S0167-7799(00)01481-5

Hofer M, Winter G, Myschik J (2012) Recombinant spider silk particles for controlled delivery of protein drugs. Biomaterials 33:1554–1562. doi:10.1016/j.biomaterials.2011.10.053

Hu X, Lu Q, Sun L, Cebe P, Wang X, Zhang X, Kaplan DL (2010) Biomaterials from ultrasonication-induced silk fibroin-hyaluronic acid hydrogels. Biomacromolecules 11:3178–3188. doi:10.1021/bm1010504

Huang J, Wong C, George A, Kaplan DL (2007) The effect of genetically engineered spider silk-dentin matrix protein 1 chimeric protein on hydroxyapatite nucleation. Biomaterials 28:2358–2367. doi:10.1016/j.biomaterials.2006.11.021

Huemmerich D, Helsen CW, Quedzuweit S, Oschmann J, Rudolph R, Scheibel T (2004a) Primary structure elements of spider dragline silks and their contribution to protein solubility. Biochemistry 43:13604–13612. doi:10.1021/Bi048983q

Huemmerich D, Scheibel T, Vollrath F, Cohen S, Gat U, Ittah S (2004b) Novel assembly properties of recombinant spider dragline silk proteins. Curr Biol 14:2070–2074. doi:10.1016/j.cub.2004.11.005

Huemmerich D, Slotta U, Scheibel T (2006) Processing and modification of films made from recombinant spider silk proteins. Appl Phys A Mater Sci Process 82:219–222. doi:10.1007/s00339-005-3428-5

Jestin S, Poulin P (2014) Chapter 6—wet spinning of CNT-based fibers. In: Yin Z, Schulz MJ, Shanov VN (eds) Nanotube superfiber materials. William Andrew Publishing, Boston, pp 167–209. doi:10.1016/B978-1-4557-7863-8.00006-2

Jiang C, Wang X, Gunawidjaja R, Lin YH, Gupta MK, Kaplan DL, Naik RR, Tsukruk VV (2007) Mechanical properties of robust ultrathin silk fibroin films. Adv Funct Mater 17:2229–2237. doi:10.1002/adfm.200601136

Jones JA, Harris TI, Tucker CL, Berg KR, Christy SY, Day BA, Gaztambide DA, Needham NJ, Ruben AL, Oliveira PF, Decker RE, Lewis RV (2015) More than just fibers: an aqueous method for the production of innovative recombinant spider silk protein materials. Biomacromolecules 16:1418–1425. doi:10.1021/acs.biomac.5b00226

Karageorgiou V, Meinel L, Hofmann S, Malhotra A, Volloch V, Kaplan D (2004) Bone morphogenetic protein-2 decorated silk fibroin films induce osteogenic differentiation of human bone marrow stromal cells. J Biomed Mater Res A 71A:528–537. doi:10.1002/jbm.a.30186

Karatzas CN, Turner JD, Karatzas A-L (1999) Production of biofilaments in transgenic animals. Canada Patent

Keten S, Buehler MJ (2008) Geometric confinement governs the rupture strength of H-bond assemblies at a critical length scale. Nano Lett 8:743–748. doi:10.1021/nl0731670

Kiliani OG (1901) II. On traumatic keloid of the median nerve, with observations upon the absorption of silk sutures. Ann Surg 33:13

Kim U-J, Park J, Joo Kim H, Wada M, Kaplan DL (2005) Three-dimensional aqueous-derived biomaterial scaffolds from silk fibroin. Biomaterials 26:2775–2785. doi:10.1016/j.biomaterials.2004.07.044

Kim D-H, Viventi J, Amsden JJ, Xiao J, Vigeland L, Kim Y-S, Blanco JA, Panilaitis B, Frechette ES, Contreras D, Kaplan DL, Omenetto FG, Huang Y, Hwang K-C, Zakin MR, Litt B, Rogers JA (2010) Dissolvable films of silk fibroin for ultrathin conformal bio-integrated electronics. Nat Mater 9:511–517. doi:10.1038/nmat2745

Kluge JA, Rabotyagova O, Leisk GG, Kaplan DL (2008) Spider silks and their applications. Trends Biotechnol 26:244–251. doi:10.1016/j.tibtech.2008.02.006

Knight DP, Vollrath F (1999) Liquid crystals and flow elongation in a spider's silk production line. Proc R Soc London, Ser B 266:519–523. doi:10.1098/rspb.1999.0667

Knight DP, Vollrath F (2001) Changes in element composition along the spinning duct in a *Nephila* spider. Naturwissenschaften 88:179–182

Knight DP, Nash L, Hu XW, Haffegee J, Ho MW (1998) In vitro formation by reverse dialysis of collagen gels containing highly oriented arrays of fibrils. J Biomed Mater Res 41:185–191. doi:10.1002/(sici)1097-4636(199808)41:2<185::aid-jbm2>3.0.co;2-e

Kojima K, Kuwana Y, Sezutsu H, Kobayashi I, Uchino K, Tamura T, Tamada Y (2007) A new method for the modification of fibroin heavy chain protein in the transgenic silkworm. Biosci Biotechnol Biochem 71:2943–2951. doi:10.1271/bbb.70353

Kronqvist N, Otikovs M, Chmyrov V, Chen G, Andersson M, Nordling K, Landreh M, Sarr M, Jornvall H, Wennmalm S, Widengren J, Meng Q, Rising A, Otzen D, Knight SD, Jaudzems K, Johansson J (2014) Sequential pH-driven dimerization and stabilization of the N-terminal domain enables rapid spider silk formation. Nat Commun 5:3254. doi:10.1038/ncomms4254

Kummerlen J, vanBeek JD, Vollrath F, Meier BH (1996) Local structure in spider dragline silk investigated by two-dimensional spin-diffusion nuclear magnetic resonance. Macromolecules 29:2920–2928

Kuwana Y, Sezutsu H, Nakajima K, Tamada Y, Kojima K (2014) High-toughness silk produced by a transgenic silkworm expressing spider (*Araneus ventricosus*) dragline silk protein. PLoS ONE 9:e105325. doi:10.1371/journal.pone.0105325

Lammel A, Schwab M, Slotta U, Winter G, Scheibel T (2008) Processing conditions for the formation of spider silk microspheres. ChemSusChem 1:413–416. doi:10.1002/cssc.200800030

Lammel A, Schwab M, Hofer M, Winter G, Scheibel T (2011) Recombinant spider silk particles as drug delivery vehicles. Biomaterials 32:2233–2240. doi:10.1016/j.biomaterials.2010.11.060

Lang G, Jokisch S, Scheibel T (2013) Air filter devices including nonwoven meshes of electrospun recombinant spider silk proteins. J Vis Exp e50492 doi:10.3791/50492

Lawrence BD, Cronin-Golomb M, Georgakoudi I, Kaplan DL, Omenetto FG (2008) Bioactive silk protein biomaterial systems for optical devices. Biomacromolecules 9:1214–1220. doi:10.1021/Bm701235f

Lawrence BD, Wharram S, Kluge JA, Leisk GG, Omenetto FG, Rosenblatt MI, Kaplan DL (2010) Effect of hydration on silk film material properties. Macromol Biosci 10:393–403. doi:10.1002/mabi.200900294

Lazaris A, Arcidiacono S, Huang Y, Zhou JF, Duguay F, Chretien N, Welsh EA, Soares JW, Karatzas CN (2002) Spider silk fibers spun from soluble recombinant silk produced in mammalian cells. Science 295:472–476. doi:10.1126/science.1065780

Leal-Egana A, Lang G, Mauerer C, Wickinghoff J, Weber M, Geimer S, Scheibel T (2012) Interactions of fibroblasts with different morphologies made of an engineered spider silk protein. Adv Eng Mater 14:B67–B75. doi:10.1002/adem.201180072

Lee KY, Mooney DJ (2001) Hydrogels for tissue engineering. Chem Rev 101:1869–1879. doi:10.1021/cr000108x

Lee S-M, Pippel E, Gösele U, Dresbach C, Qin Y, Chandran CV, Bräuniger T, Hause G, Knez M (2009) Greatly increased toughness of infiltrated spider silk. Science 324:488–492. doi:10.1126/science.1168162

Lepore E, Bonaccorso F, Bruna M, Bosia F, Taioli S, Garberoglio G, Ferrari A, Pugno NM (2015) Silk reinforced with graphene or carbon nanotubes spun by spiders. arXiv preprint arXiv:150406751

Lewis RV (1992) Spider silk: the unraveling of a mystery. Acc Chem Res 25:392–398. doi:10.1021/ar00021a002

Lewis R (1996) Unraveling the weave of spider silk. Bioscience 46:636–638

Lin Z, Deng Q, Liu XY, Yang D (2013) Engineered large spider eggcase silk protein for strong artificial fibers. Adv Mater 25:1216–1220. doi:10.1002/adma.201204357

Liu X, Sun Q, Wang H, Zhang L, Wang JY (2005) Microspheres of corn protein, zein, for an ivermectin drug delivery system. Biomaterials 26:109–115. doi:10.1016/j.biomaterials.2004.02.013

Lucke M, Winter G, Engert J (2015) The effect of steam sterilization on recombinant spider silk particles. Int J Pharm 481:125–131. doi:10.1016/j.ijpharm.2015.01.024

Mackintosh FC, Kas J, Janmey PA (1995) Elasticity of semiflexible biopolymer networks. Phys Rev Lett 75:4425–4428

Madsen B, Shao ZZ, Vollrath F (1999) Variability in the mechanical properties of spider silks on three levels: interspecific, intraspecific and intraindividual. Int J Biol Macromol 24:301–306

Mehta N, Hede S (2005) Spider silk calcite composite. Hypothesis 3:21. doi:10.1021/nn204506d

Menassa R, Hong Z, Karatzas CN, Lazaris A, Richman A, Brandle J (2004) Spider dragline silk proteins in transgenic tobacco leaves: accumulation and field production. Plant Biotechnol J 2:431–438. doi:10.1111/j.1467-7652.2004.00087.x

Metwalli E, Slotta U, Darko C, Roth SV, Scheibel T, Papadakis CM (2007) Structural changes of thin films from recombinant spider silk proteins upon post-treatment. Appl Phys A Mater Sci Process 89:655–661. doi:10.1007/s00339-007-4265-5

Mieszawska AJ, Fourligas N, Georgakoudi I, Ouhib NM, Belton DJ, Perry CC, Kaplan DL (2010) Osteoinductive silk-silica composite biomaterials for bone regeneration. Biomaterials 31:8902–8910. doi:10.1016/j.biomaterials.2010.07.109

Minoura N, Aiba S, Gotoh Y, Tsukada M, Imai Y (1995) Attachment and growth of cultured fibroblast cells on silk protein matrices. J Biomed Mater Res 29:1215–1221

Motriuk-Smith D, Smith A, Hayashi CY, Lewis RV (2005) Analysis of the conserved N-terminal domains in major ampullate spider silk proteins. Biomacromolecules 6:3152–3159. doi:10.1021/bm050472b

Müller-Herrmann S, Scheibel T (2015) Enzymatic degradation of films, particles, and nonwoven meshes made of a recombinant spider silk protein. ACS Biomater Sci Eng 1:247–259. doi:10.1021/ab500147u

Munch E, Launey ME, Alsem DH, Saiz E, Tomsia AP, Ritchie RO (2008) Tough, bio-inspired hybrid materials. Science 322:1516–1520. doi:10.1126/science.1164865

Nazarov R, Jin H-J, Kaplan DL (2004) Porous 3-D scaffolds from regenerated silk fibroin. Biomacromolecules 5:718–726. doi:10.1021/bm034327e

Neubauer MP, Blum C, Agostini E, Engert J, Scheibel T, Fery A (2013) Micromechanical characterization of spider silk particles. Biomater Sci 1:1160–1165. doi:10.1039/c3bm60108k

Numata K, Hamasaki J, Subramanian B, Kaplan DL (2010) Gene delivery mediated by recombinant silk proteins containing cationic and cell binding motifs. J Control Release 146:136–143. doi:10.1016/j.jconrel.2010.05.006

Papadopoulos P, Solter J, Kremer F (2007) Structure-property relationships in major ampullate spider silk as deduced from polarized FTIR spectroscopy. Eur Phys J E: Soft Matter Biol Phys 24:193–199. doi:10.1140/epje/i2007-10229-9

Peng H, Zhou S, Jiang J, Guo T, Zheng X, Yu X (2009) Pressure-induced crystal memory effect of spider silk proteins. J Phys Chem B 113:4636–4641. doi:10.1021/jp811461b

Perez-Rigueiro J, Elices M, Guinea GV, Plaza GR, Karatzas C, Riekel C, Agullo-Rueda F, Daza R (2011) Bioinspired fibers follow the track of natural spider silk. Macromolecules 44:1166–1176. doi:10.1021/ma102291m

Rabotyagova OS, Cebe P, Kaplan DL (2009) Self-assembly of genetically engineered spider silk block copolymers. Biomacromolecules 10:229–236. doi:10.1021/bm800930x

Rabotyagova OS, Cebe P, Kaplan DL (2010) Role of polyalanine domains in beta-sheet formation in spider silk block copolymers. Macromol Biosci 10:49–59. doi:10.1002/mabi.200900203

Radtke C, Allmeling C, Waldmann K-H, Reimers K, Thies K, Schenk HC, Hillmer A, Guggenheim M, Brandes G, Vogt PM (2011) Spider silk constructs enhance axonal regeneration and remyelination in long nerve defects in sheep. PLoS ONE 6:e16990. doi:10.1371/journal.pone.0016990

Rammensee S, Huemmerich D, Hermanson KD, Scheibel T, Bausch AR (2006) Rheological characterization of hydrogels formed by recombinantly produced spider silk. Appl Phys A Mater Sci Process 82:261–264. doi:10.1007/s00339-005-3431-x

Rammensee S, Slotta U, Scheibel T, Bausch AR (2008) Assembly mechanism of recombinant spider silk proteins. Proc Natl Acad Sci U S A 105:6590–6595. doi:10.1073/pnas.0709246105

Rising A (2014) Controlled assembly: a prerequisite for the use of recombinant spider silk in regenerative medicine? Acta Biomater 10:1627–1631. doi:10.1016/j.actbio.2013.09.030

Rising A, Johansson J (2015) Toward spinning artificial spider silk. Nat Chem Biol 11:309–315. doi:10.1038/nchembio.1789

Rising A, Hjalm G, Engstrom W, Johansson J (2006) N-terminal nonrepetitive domain common to dragline, flagelliform, and cylindriform spider silk proteins. Biomacromolecules 7:3120–3124. doi:10.1021/bm060693x

Roemer L, Scheibel T (2007) Basis for new material—spider silk protein. Chem Unserer Zeit 41:306–314

Schacht K, Scheibel T (2011) Controlled hydrogel formation of a recombinant spider silk protein. Biomacromolecules 12:2488–2495. doi:10.1021/bm200154k

Schacht K, Jüngst T, Schweinlin M, Ewald A, Groll J, Scheibel T (2015) Biofabrication of cell-loaded 3D spider silk constructs. Angew Chem Int Ed 54:2816–2820. doi:10.1002/anie.201409846

Scheibel T (2004) Spider silks: recombinant synthesis, assembly, spinning, and engineering of synthetic proteins. Microb Cell Factories 3:14. doi:10.1186/1475-2859-3-14

Seidel A, Liivak O, Jelinski LW (1998) Artificial spinning of spider silk. Macromolecules 31:6733–6736. doi:10.1021/Ma9808880

Seidel A, Liivak O, Calve S, Adaska J, Ji GD, Yang ZT, Grubb D, Zax DB, Jelinski LW (2000) Regenerated spider silk: processing, properties, and structure. Macromolecules 33:775–780. doi:10.1021/Ma990893j

Shao ZZ, Vollrath F, Yang Y, Thogersen HC (2003) Structure and behavior of regenerated spider silk. Macromolecules 36:1157–1161. doi:10.1021/Ma0214660

Shin H, Jo S, Mikos AG (2003) Biomimetic materials for tissue engineering. Biomaterials 24:4353–4364

Simmons AH, Michal CA, Jelinski LW (1996) Molecular orientation and two-component nature of the crystalline fraction of spider dragline silk. Science 271:84–87

Singh A, Hede S, Sastry M (2007) Spider silk as an active scaffold in the assembly of gold nanoparticles and application of the gold–silk bioconjugate in vapor sensing. Small 3:466–473. doi:10.1002/smll.200600413

Slotta U, Tammer M, Kremer F, Koelsch P, Scheibel T (2006) Structural analysis of spider silk films. Supramol Chem 18:465–471. doi:10.1080/10610270600832042

Slotta U, Hess S, Spiess K, Stromer T, Serpell L, Scheibel T (2007) Spider silk and amyloid fibrils: a structural comparison. Macromol Biosci 7:183–188. doi:10.1002/mabi.200600201

Slotta UK, Rammensee S, Gorb S, Scheibel T (2008) An engineered spider silk protein forms microspheres. Angew Chem Int Ed 47:4592–4594. doi:10.1002/anie.200800683

Smit E, Buttner U, Sanderson RD (2005) Continuous yarns from electrospun fibers. Polymer 46:2419–2423. doi:10.1016/j.polymer.2005.02.002

Smith A, Scheibel T (2013) Basis for new material—spider silk protein. In: Fratzl P, Dunlop J, Weinkamer R (eds) Materials design inspired by nature: function through inner architecture. RSC smart materials,

vol 4. RSC Publishing, Cambridge, pp 256–281. doi:10.1039/9781849737555-00256

Sofia S, McCarthy MB, Gronowicz G, Kaplan DL (2001) Functionalized silk-based biomaterials for bone formation. J Biomed Mater Res 54: 139–148. doi:10.1002/1097-4636(200101)54:1<139

Sørensen HP, Mortensen KK (2005) Advanced genetic strategies for recombinant protein expression in *Escherichia coli*. J Biotechnol 115: 113–128. doi:10.1016/j.jbiotec.2004.08.004

Spiess K, Lammel A, Scheibel T (2010a) Recombinant spider silk proteins for applications in biomaterials. Macromol Biosci 10:998–1007. doi:10.1002/mabi.201000071

Spiess K, Wohlrab S, Scheibel T (2010b) Structural characterization and functionalization of engineered spider silk films. Soft Matter 6: 4168–4174. doi:10.1039/b927267d

Sponner A, Vater W, Monajembashi S, Unger E, Grosse F, Weisshart K (2007) Composition and hierarchical organisation of a spider silk. PLoS ONE 2:e998. doi:10.1371/journal.pone.0000998

Sridharan I, Kim T, Strakova Z, Wang R (2013) Matrix-specified differentiation of human decidua parietalis placental stem cells. Biochem Biophys Res Commun 437:489–495. doi:10.1016/j.bbrc.2013.07.002

Stark M, Grip S, Rising A, Hedhammar M, Engstrom W, Hjalm G, Johansson J (2007) Macroscopic fibers self-assembled from recombinant miniature spider silk proteins. Biomacromolecules 8:1695–1701. doi:10.1021/Bm070049y

Steinkraus HB, Rothfuss H, Jones JA, Dissen E, Shefferly E, Lewis RV (2012) The absence of detectable fetal microchimerism in nontransgenic goats (*Capra aegagrus hircus*) bearing transgenic offspring. J Anim Sci 90:481–488. doi:10.2527/jas.2011-4034

Stephens JS, Fahnestock SR, Farmer RS, Kiick KL, Chase DB, Rabolt JF (2005) Effects of electrospinning and solution casting protocols on the secondary structure of a genetically engineered dragline spider silk analogue investigated via Fourier transform Raman spectroscopy. Biomacromolecules 6:1405–1413. doi:10.1021/Bm049296h

Steven E, Saleh WR, Lebedev V, Acquah SFA, Laukhin V, Alamo RG, Brooks JS (2013) Carbon nanotubes on a spider silk scaffold. Nat Commun 4:2435. doi:10.1038/ncomms3435

Tamura T, Thibert C, Royer C, Kanda T, Abraham E, Kamba M, Komoto N, Thomas JL, Mauchamp B, Chavancy G, Shirk P, Fraser M, Prudhomme JC, Couble P (2000) Germline transformation of the silkworm *Bombyx mori* L. using a *piggyBac* transposon-derived vector. Nat Biotechnol 18:81–84. doi:10.1038/71978

Teo WE, Ramakrishna S (2006) A review on electrospinning design and nanofibre assemblies. Nanotechnology 17:R89–R106. doi:10.1088/0957-4484/17/14/R01

Teule F, Furin WA, Cooper AR, Duncan JR, Lewis RV (2007) Modifications of spider silk sequences in an attempt to control the mechanical properties of the synthetic fibers. J Mater Sci 42:8974–8985. doi:10.1007/s10853-007-1642-6

Teule F, Cooper AR, Furin WA, Bittencourt D, Rech EL, Brooks A, Lewis RV (2009) A protocol for the production of recombinant spider silk-like proteins for artificial fiber spinning. Nat Protoc 4: 341–355. doi:10.1038/nprot.2008.250

Teule F, Miao YG, Sohn BH, Kim YS, Hull JJ, Fraser MJ, Lewis RV, Jarvis DL (2012) Silkworms transformed with chimeric silkworm/spider silk genes spin composite silk fibers with improved mechanical properties. Proc Natl Acad Sci U S A 109:923–928. doi:10.1073/pnas.1109420109

Um IC, Ki CS, Kweon H, Lee KG, Ihm DW, Park YH (2004) Wet spinning of silk polymer. II. Effect of drawing on the structural characteristics and properties of filament. Int J Biol Macromol 34: 107–119. doi:10.1016/j.ijbiomac.2004.03.011

van Beek JD, Hess S, Vollrath F, Meier BH (2002) The molecular structure of spider dragline silk: folding and orientation of the protein backbone. Proc Natl Acad Sci U S A 99:10266–10271. doi:10.1073/pnas.152162299

Vendrely C, Scheibel T (2007) Biotechnological production of spider-silk proteins enables new applications. Macromol Biosci 7:401–409. doi:10.1002/mabi.200600255

Vepari C, Kaplan DL (2007) Silk as a biomaterial. Prog Polym Sci 32: 991–1007. doi:10.1016/j.progpolymsci.2007.05.013

Viney C (1997) Natural silks: archetypal supramolecular assembly of polymer fibres. Supramol Sci 4:75–81

Vollrath F (2000) Strength and structure of spiders' silks. J Biotechnol 74: 67–83. doi:10.1016/S1389-0352(00)00006-4

Vollrath F, Knight DP (1999) Structure and function of the silk production pathway in the spider *Nephila edulis*. Int J Biol Macromol 24:243–249. doi:10.1016/S0141-8130(98)00095-6

Vollrath F, Knight DP (2001) Liquid crystalline spinning of spider silk. Nature 410:541–548. doi:10.1038/35069000

Vollrath F, Barth P, Basedow A, Engstrom W, List H (2002) Local tolerance to spider silks and protein polymers in vivo. In vivo 16:229–234

Wang X, Wenk E, Matsumoto A, Meinel L, Li C, Kaplan DL (2007) Silk microspheres for encapsulation and controlled release. J Control Release 117:360–370. doi:10.1016/j.jconrel.2006.11.021

Wang X, Yucel T, Lu Q, Hu X, Kaplan DL (2010) Silk nanospheres and microspheres from silk/PVA blend films for drug delivery. Biomaterials 31:1025–1035. doi:10.1016/j.biomaterials.2009.11.002

Wen HX, Lan XQ, Zhang YS, Zhao TF, Wang YJ, Kajiura Z, Nakagaki M (2010) Transgenic silkworms (*Bombyx mori*) produce recombinant spider dragline silk in cocoons. Mol Biol Rep 37:1815–1821. doi:10.1007/s11033-009-9615-2

Wendt H, Hillmer A, Reimers K, Kuhbier JW, Schafer-Nolte F, Allmeling C, Kasper C, Vogt PM (2011) Artificial skin—culturing of different skin cell lines for generating an artificial skin substitute on cross-weaved spider silk fibres. PLoS ONE 6:e21833. doi:10.1371/journal.pone.0021833

Widhe M, Bysell H, Nystedt S, Schenning I, Malmsten M, Johansson J, Rising A, Hedhammar M (2010) Recombinant spider silk as matrices for cell culture. Biomaterials 31:9575–9585. doi:10.1016/j.biomaterials.2010.08.061

Wohlrab S, Müller S, Schmidt A, Neubauer S, Kessler H, Leal-Egaña A, Scheibel T (2012a) Cell adhesion and proliferation on RGD-modified recombinant spider silk proteins. Biomaterials 33:6650–6659. doi:10.1016/j.biomaterials.2012.05.069

Wohlrab S, Spieß K, Scheibel T (2012b) Varying surface hydrophobicities of coatings made of recombinant spider silk proteins. J Mater Chem 22:22050–22054. doi:10.1039/C2JM35075K

Wong Po Foo C, Patwardhan SV, Belton DJ, Kitchel B, Anastasiades D, Huang J, Naik RR, Perry CC, Kaplan DL (2006) Novel nanocomposites from spider silk-silica fusion (chimeric) proteins. Proc Natl Acad Sci U S A 103:9428–9433. doi:10.1073/pnas.0601096103

Xia X-X, Qian Z-G, Ki CS, Park YH, Kaplan DL, Lee SY (2010) Native-sized recombinant spider silk protein produced in metabolically engineered *Escherichia coli* results in a strong fiber. Proc Natl Acad Sci U S A 107:14059–14063. doi:10.1073/pnas.1003366107

Xu M, Lewis RV (1990) Structure of a protein superfiber: spider dragline silk. Proc Natl Acad Sci 87:7120–7124

Xu HT, Fan BL, Yu SY, Huang YH, Zhao ZH, Lian ZX, Dai YP, Wang LL, Liu ZL, Fei J, Li N (2007) Construct synthetic gene encoding artificial spider dragline silk protein and its expression in milk of transgenic mice. Anim Biotechnol 18:1–12. doi:10.1080/10495390601091024

Yu Q, Xu S, Zhang H, Gu L, Xu Y, Ko F (2014) Structure-property relationship of regenerated spider silk protein nano/microfibrous scaffold fabricated by electrospinning. J Biomed Mater Res Part A 102:3828–3837. doi:10.1002/jbm.a.35051

Zarkoob S, Eby RK, Reneker DH, Hudson SD, Ertley D, Adams WW (2004) Structure and morphology of electrospun silk nanofibers. Polymer 45:3973–3977. doi:10.1016/j.polymer.2003.10.102

Zeplin PH, Berninger AK, Maksimovikj NC, van Gelder P, Scheibel T, Walles H (2014a) Verbesserung der Biokompatibilität von Silikonimplantaten durch Spinnenseidenbeschichtung: Immunhistochemische Untersuchungen zum Einfluss auf die Kapselbildung. Handchir Mikrochir Plast Chir 46:336–341. doi:10.1055/s-0034-1395558

Zeplin PH, Maksimovikj NC, Jordan MC, Nickel J, Lang G, Leimer AH, Römer L, Scheibel T (2014b) Spider silk coatings as a bioshield to reduce periprosthetic fibrous capsule formation. Adv Funct Mater 24:2658–2666. doi:10.1002/adfm.201302813

Zhang Y, Hu J, Miao Y, Zhao A, Zhao T, Wu D, Liang L, Miikura A, Shiomi K, Kajiura Z, Nakagaki M (2008) Expression of EGFP-spider dragline silk fusion protein in BmN cells and larvae of silkworm showed the solubility is primary limit for dragline proteins yield. Mol Biol Rep 35:329–335. doi:10.1007/s11033-007-9090-6

Zhang C-Y, Zhang D-C, Chen D, M L (2014) A bilayered scaffold based on RGD recombinant spider silk proteins for small diameter tissue engineering. Polym Compos. doi:10.1002/pc.23208

Zhou S, Peng H, Yu X, Zheng X, Cui W, Zhang Z, Li X, Wang J, Weng J, Jia W, Li F (2008) Preparation and characterization of a novel electrospun spider silk fibroin/poly(D, L-lactide) composite fiber. J Phys Chem B 112:11209–11216. doi:10.1021/jp800913k

Zhu ZH, Kikuchi Y, Kojima K, Tamura T, Kuwabara N, Nakamura T, Asakura T (2010) Mechanical properties of regenerated *Bombyx mori* silk fibers and recombinant silk fibers produced by transgenic silkworms. J Biomater Sci Polym Ed 21:395–412. doi:10.1163/156856209x423126

Zhu B, Li W, Lewis RV, Segre CU, Wang R (2015) E-spun composite fibers of collagen and dragline silk protein: fiber mechanics, biocompatibility, and application in stem cell differentiation. Biomacromolecules 16:202–213. doi:10.1021/bm501403f

6 Publikationsliste

I. **E. Doblhofer**, T. Scheibel. Engineering of Recombinant Spider Silk Proteins Allows Defined Uptake and Release of Substances. *Journal of Pharmaceutical Sciences*, 2015, 104 (3): 988-94 DOI 10.1002/jps.24300.

II. M. B. Schierling*, **E. Doblhofer***, T. Scheibel. Cellular uptake of drug loaded spider silk particles. *Biomaterials Science*, 2016, 110*(*4): 1515-1523 DOI 10.1039/C6BM00435K. (*Gleichberechtigte Erstautorenschaft).

III. N. Helfricht, **E. Doblhofer**, J.F.L. Duval, T. Scheibel and G. Papastavrou. Colloidal Properties of Recombinant Spider Silk Protein Particles. *Journal of Physical Chemistry C*, 2016, 120(32): 18015–18027 **DOI** 10.1021/acs.jpcc.6b03957.

IV. **E. Doblhofer** *et al.*. Structural Insights into Water-Based Spider Silk Protein–Nanoclay Composites with Excellent Gas and Water Vapor Barrier Properties. *ACS Applied Materials and Interfaces,* 2016, 8(38): 25535-43. DOI 10.1021/acsami.6b08287

V. **E. Doblhofer***, A. Heidebrecht *and T. Scheibel. To spin or not to spin: spider silk fibers and more. *Journal of Applied Microbiology and Biotechnology*, 2015, 99 (22): 9361-80, DOI 10.1007/s00253-015-6948-8 (*Gleichberechtigte Erstautorenschaft).

VI. N. Helfricht, **E. Doblhofer**, V. Bieber, P. Lommes, V. Sieber, T. Scheibel and G. Papastavrou. Probing the adhesion properties of alginate hydrogels: a new approach towards the preparation of soft colloidal probes for direct force measurements. *Soft Matter*, 2017 13(3): 578-589, DOI 10.1039/c6sm02326f.

DANKSAGUNG

An dieser Stelle möchte ich die Gelegenheit nutzen den Menschen zu danken, die in den letzten Jahren einen großen Beitrag zum Gelingen der vorliegenden Arbeit geleistet haben.

Zuallererst gilt dieser Dank meinem Doktorvater Prof. Dr. Thomas Scheibel zum einen für die Bereitstellung einer sehr interessanten, vielseitigen, spannenden und weit gefassten Themenstellung, bei deren Bearbeitung er mich mit ausführlichen Diskussionen unterstützte und mit großem Vertrauen in meine Arbeit (auch wenn mir dieses ab und an verloren ging) immer wieder ermutigte die einzelnen Projekte voranzutreiben. Zum anderen möchte ich ihm hier für die zahlreichen Erfahrungen danken, die ich bei meiner Arbeit am Lehrstuhl Biomaterialien, sowie auf diversen Konferenzbesuchen und Wissenschaftsreisen sammeln konnte.

In diesem Zusammenhang danke ich auch meinen Kollaborationspartnern Prof. Dr. Josef Breu und Jasmin Schmid (Lehrstuhl für Anorganische Chemie I), Prof. Dr. Georg Papastavrou und Nicolas Helfricht (Lehrstuhl Physikalische Chemie II), sowie Prof. Markus Linder (PhD) und Katri Kurppa (*Technical Institute Finland VTT*) für die gute Zusammenarbeit, die fruchtbaren Diskussionen und die Möglichkeit eine große Vielfalt an Materialien, Methoden und Denkweisen kennen zu lernen.

Besonders danke ich Prof. Markus Linder (PhD) und dem *Technical Institute Finland VTT* für die Ermöglichung und die Finanzierung eines Gastaufenthaltes in Espoo/Helsinki und die wunderbare Zeit die ich dort verbringen durfte.

Außerdem danke ich folgenden Personen für die erfolgreiche Zusammenarbeit:

- Ute Kuhn für ihre Hilfe bezüglich DSC- und TGA-Messungen.
- Dr. Hendrik Bargel für zahlreiche REM-Aufnahmen
- Andreas Schmidt und Johannes Diehl für die Herstellung der Spinnenseidenproteine in großen Mengen.
- Dr. Martin Humenik und Andreas Schmidt für die Durchführung von MALDI-TOF Analysen.

Eva Möller und Andreas Schmidt danke ich zudem für die zahlreichen Tätigkeiten und die Unterstützung im Laboralltag am Standort FAN, sowie dem Sekretariat für jegliche Hilfe in bürokratischen Fragen.

Ein großes Dankeschön geht auch an alle BioMatler, die in den letzten Jahren für eine angenehme Arbeitsatmosphäre gesorgt haben, mir mit vielen Tipps und Tricks im Laboralltag und in wissenschaftlichen Diskussionen zur Seite standen und sich durch diverse Gespräche in Kaffeepausen, auf genialen Weihnachtsfeiern und Sommerfesten unvergesslich gemacht haben. Daraus möchte ich drei Menschen besonders hervorheben: Heike, Joschi und Chris! Sie waren vor allem in der Endphase meiner Dissertation wichtige Komplizen im täglichen Kampf gegen meine Ungeduld und ohne sie hätte ich wohl nicht so lange durchgehalten… Es war mir eine Ehre!!!

Ich danke meinem Bruder Philipp für seine geschwisterliche Unterstützung und zahlreiche „Spinnereien“, die mir immer wieder ein Lachen ins Gesicht gezaubert haben.

Mein größter Dank gilt jedoch den Menschen, denen ich mein ganzes Dasein verdanke: Meinen Eltern! Elfriede und Egon Doblhofer haben mir durch ihren beispiellosen Rückhalt und ihren Glauben an mich und mein Können den Mut gegeben neue Wege zu beschreiten und an mich selbst zu glauben. Sie mussten durch meine Wahl der Ausbildung sehr oft auf mich verzichten und sind dennoch jeden einzelnen Schritt mit mir gegangen.

(EIDESSTATTLICHE) VERSICHERUNGEN UND ERKLÄRUNGEN

(§ 8 S. 2 Nr. 6 PromO)

Hiermit erkläre ich mich damit einverstanden, dass die elektronische Fassung meiner Dissertation unter Wahrung meiner Urheberrechte und des Datenschutzes einer gesonderten Überprüfung hinsichtlich der eigenständigen Anfertigung der Dissertation unterzogen werden kann.

(§ 8 S. 2 Nr. 8 PromO)

Hiermit erkläre ich eidesstattlich, dass ich die Dissertation selbständig verfasst und keine anderen als die von mir angegebenen Quellen und Hilfsmittel benutzt habe.

(§ 8 S. 2 Nr. 9 PromO)

Ich habe die Dissertation nicht bereits zur Erlangung eines akademischen Grades anderweitig eingereicht und habe auch nicht bereits diese oder eine gleichartige Doktorprüfung endgültig nicht bestanden.

(§ 8 S. 2 Nr. 10 PromO)

Hiermit erkläre ich, dass ich keine Hilfe von gewerbliche Promotionsberatern bzw. -vermittlern in Anspruch genommen habe und auch künftig nicht nehmen werde.

Bayreuth, 16.06.2017